

# **Regulation of reabsorption process in kidney by neuraminidase 1: implications in nephrosialidosis.**

Ikhui Kho

Faculty of Medicine  
Department of Anatomy and Cell Biology  
McGill University, Montreal  
Quebec, Canada  
November 2023

A thesis submitted to McGill University in partial fulfilment of the requirements of the degree of  
Doctor of Philosophy

©Ikhui Kho 2023

## Contents

<b>LIST OF FIGURES</b> .....	4
<b>LIST OF TABLES</b> .....	5
<b>LIST OF ABBREVIATIONS</b> .....	6
<b>ABSTRACT</b> .....	9
<b>RÉSUMÉ</b> .....	11
<b>ACKNOWLEDGEMENT</b> .....	13
<b>CONTRIBUTION TO ORIGINAL KNOWLEDGE</b> .....	14
<b>CONTRIBUTION OF AUTHOR</b> .....	15
1 Introduction and literature review .....	17
1.1 Lysosomes .....	17
1.1.1 Lysosomal degradation pathway .....	18
1.1.2 Lysosomal biogenesis .....	19
1.2 Lysosomal storage diseases .....	20
1.2.1 Neuropathic lysosomal storage disorders .....	22
1.2.2 Nephropathic lysosomal storage disorders .....	24
1.3 Sialidosis .....	26
1.4 Treatment of lysosomal storage diseases .....	32
1.5 Glycoconjugates .....	35
1.5.1 Lectins .....	38
1.5.2 Microbial lectins .....	38
1.5.3 Animal lectins .....	39
1.6 Sialic acids .....	40
1.6.1 Synthesis of sialic acids .....	41
1.6.2 Function of sialic acids .....	42
1.6.3 Polysialic acid .....	43
1.7 Neuraminidases .....	43
1.7.1 Neuraminidase 1 .....	44
1.7.2 Neuraminidase 2 .....	45
1.7.3 Neuraminidase 3 .....	45
1.7.4 Neuraminidase 4 .....	46
1.8 Renal pathology in nephrosialidosis and chronic kidney diseases .....	46
1.8.1 Glomerulopathy .....	47
1.8.2 Tubulopathy .....	49
1.9 Rationale and objective .....	53

1.10	References.....	55
2	Severe kidney dysfunction in sialidosis mice reveals a novel role for neuraminidase 1 in reabsorption. ....	67
2.1	Introduction.....	67
2.2	Results .....	69
2.2.1	Systemic pathology of <i>Neu1<sup>ΔEx3</sup></i> and <i>Neu1<sup>Cx3cr1ΔEx3</sup></i> mice.....	69
2.2.2	<i>Neu1<sup>ΔEx3</sup></i> and <i>Neu1<sup>Cx3cr1ΔEx3</sup></i> mice show deficiency of NEU1 activity and increased lysosomal biogenesis in tissues.....	72
2.2.3	<i>Neu1<sup>ΔEx3</sup></i> and <i>Neu1<sup>Cx3cr1ΔEx3</sup></i> mice show prominent tubuloglomerular pathology. ....	75
2.2.4	Glycomic profiling reveals protein hypersialylation in <i>Neu1<sup>ΔEx3</sup></i> mice kidneys. ....	82
2.2.5	Aberrant glycosylation and trafficking of endocytic receptor megalin in kidney cells of <i>Neu1<sup>ΔEx3</sup></i> mice.....	87
2.3	Methods .....	91
2.4	Discussion .....	92
2.5	References.....	97
2.6	Supplementary data .....	101
2.7	Supplementary materials .....	147
	Link between chapter 2 and chapter 3 .....	157
3	Allogenic HSPC transplantation of <i>Neu1<sup>ΔEx3</sup></i> mice .....	158
3.1	Introduction.....	158
3.2	Materials and method .....	161
3.3	Result.....	164
3.3.1	<i>Neu1<sup>ΔEx3</sup></i> mice show high engraftment after allogenic HSPC translocation. ....	164
3.3.2	Transplanted <i>Neu1<sup>ΔEx3</sup></i> mouse shows improvement of behavior deficits. ....	165
3.3.3	<i>Neu1<sup>ΔEx3</sup></i> mouse transplanted with HSPC shows reduced lysosomal biogenesis in multiple tissues compared with untreated mice.....	167
3.3.4	Reduction of lysosomal storage and protein hypersialylation and rescue of Megalin receptor level and localization in the kidney of HSPC transplanted <i>Neu1<sup>ΔEx3</sup></i> mouse. ....	169
3.3.5	Improvement of CNS pathology in HSPC transplanted <i>Neu1<sup>ΔEx3</sup></i> mouse.....	172
3.4	Discussion .....	174
3.5	References.....	177
3.6	Supplementary data .....	3-2
4	General discussion .....	144
	Conclusion.....	146
	Master references list.....	147

## LIST OF FIGURES

<b>Figure 1.1: Multiple pathways are involved in lysosomal protein delivery and lysosomal fusion (7).</b> .....	18
<b>Figure 1.2: Type II sialidosis patient at 4 years old with severe edema and ascites (77).</b> .....	27
<b>Figure 1.3: N-glycan synthesis in humans consists of three final structures of high-mannose, hybrid and complex N-glycans (135).</b> .....	37
<b>Figure 1.4: The sialome presented at different levels of complexity (167).</b> .....	41
<b>Figure 1.5: Podocyte, glomerular basement membrane and endothelial cells makes up the glomerular filtration barrier in the glomerulus (249).</b> .....	48
<b>Figure 1.6: Ultrastructure of S1, S2 and S3 of segment proximal tubules (260)</b> .....	50
<b>Figure 2.1: Pathophysiology of Neu1<sup>ΔEx3</sup> and Neu1<sup>Cx3er1ΔEx3</sup> mice.</b> .....	71
<b>Figure 2.2: Neu1<sup>ΔEx3</sup> and Neu1<sup>Cx3er1ΔEx3</sup> homozygous mice show deficiency of NEU1 activity and increased lysosomal biogenesis in kidney tissues.</b> .....	74
<b>Figure 2.3: Light microscope images of cortical and medullary regions of kidney from WT, Neu1<sup>ΔEx3</sup>, and Neu1<sup>Cx3er1ΔEx3</sup> mice stained with H&amp;E (A, B), Masson's Trichrome (C) and toluidine blue (D).</b> .....	77
<b>Figure 2.4: Pathological changes in glomerular and tubular cells in Neu1<sup>ΔEx3</sup> and Neu1<sup>Cx3er1ΔEx3</sup> mice.</b> .....	81
<b>Figure 2.5: Abnormal protein glycosylation in Neu1<sup>ΔEx3</sup> kidney tissues.</b> .....	83
<b>Figure 2.6: MALDI TOF MS analysis of mouse kidney proteins shows changes in the profile of N-glycans.</b> .....	86
<b>Figure 2.7: Aberrant glycosylation of megalin affects its abundance and trafficking in the kidney of Neu1<sup>ΔEx3</sup> mice.</b> .....	90
<b>Figure 3.1: Flow cytometry reveals high % of CD45.1+ myeloid cells in the blood of transplanted Neu1<sup>ΔEx3</sup> suggesting effective HSPC engraftment.</b> .....	165
<b>Figure 3.2: Corrected locomotion in HSPC transplanted Neu1<sup>ΔEx3</sup> mouse.</b> .....	166
<b>Figure 3.3: HSPC transplanted Neu1<sup>ΔEx3</sup> mouse show partial normalization of increased lysosomal biogenesis in visceral organs.</b> .....	168
<b>Figure 3.4: WT HSPC transplantation of Neu1<sup>ΔEx3</sup> mouse partially improved pathological alterations in proximal convoluted tubules.</b> .....	170
<b>Figure 3.5: Lysosomal storage and neuroinflammation are not reduced in the brain cortex of HSPC transplanted Neu1<sup>ΔEx3</sup> mouse.</b> .....	173

## LIST OF TABLES

<b>Table 1.1: Defects in lysosomal membrane proteins and the associated disorder (20).....</b>	<b>20</b>
<b>Table 1.2: Cases of type II sialidosis (nephrosialidosis).....</b>	<b>29</b>
<b>Table 2.1: Major N-linked sialylated glycans are abnormally abundant in Neu1<sup>ΔEx3</sup> mouse kidney tissues.....</b>	<b>86</b>
<b>Table 3.1: HSPC transplantation of Neu1<sup>ΔEx3</sup> mice. ....</b>	<b>164</b>

## LIST OF ABBREVIATIONS

Adaptor protein (AP)  
Adeno-associated virus (AAV)  
Alpha-synuclein ( $\alpha$ -synuclein).  
Asparagine (Asn)  
basic helix-loop-helix- leucine zipper (bHLH-Zip)  
Beta-hexosaminidase A (HEXA)  
Blood brain barrier (BBB)  
Brush border (BB)  
CD2-associated (CD2AP)  
Chaperone mediated autophagy (CMA)  
chaperone-mediated autophagy (CMA)  
Chronic kidney diseases (CKDs)  
CMP sialic acid synthase (CMAS)  
CMP-Neu5Ac hydroxylase (CMAH)  
Concanavalin A (ConA)  
Coordinated Lysosomal Expression and Regulation (CLEAR)  
Cubilin (Cubn)  
Cytidine monophosphate (CMP)  
Damage-associated molecular patterns (DAMPs)  
Diabetic kidney diseases (DKD)  
Distal convoluted tubule (DCT)  
early endosomes (EEs)  
Endosomal sorting complex required for transport (ESCRT)  
Enzyme replacement therapy (ERT)  
Extracellular matrix (ECM)  
Fc receptors for immunoglobulin G (Fc $\gamma$ R)  
GalNAc transferase (GALNTs)  
Gaucher disease (GD)  
Glucocerebrosidase (GCase)  
Glucocerebroside (GlcCer)  
Glucosylsphingosine (GlcSph)  
Glycosphingolipid (GSL)  
GM2 activator protein (GM2AP)  
Golgi localized  $\gamma$ -ear containing ARF-binding protein (GGA)  
Haemagglutinin (HA)  
Haemolytic Uremic syndrome (HUS)  
heat shock 70kDa protein 8 (HSPA8/HSC70)  
heat shock 70kDa protein 8 (HSPA8/HSC70)  
Hematopoietic stem progenitor cell (HSPC)  
Hematopoietic stem/progenitor cell transplantation (HSCT)  
Insulin receptor (IR)  
Ischemia reperfusion injury (IRI)  
Light protein 1 light chain 3 (LC3)  
Lipopolysaccharide (LPS)  
Low density lipoprotein-related protein 2 (LRP2)  
Low molecular weight proteinuria (LMWP)  
Lysosomal storage diseases (LSD)  
Maackia amurensis agglutinin (MAA I and II)  
Maackia Amurensis lectin II (MALII)

mannose-6-phosphate (M6P)  
mannose-6-phosphate receptors (M6PR)  
mechanistic target of rapamycin complex 1 (mTORC1)  
Megalin (*Lrp-2*)  
Mesangial cells (MC)  
Metachromatic Leukodystrophy (MLD)  
microphthalmia family (MiT family)  
mucopolysaccharidoses (MPS)  
Multivesicular bodies (MVBs)  
Myelin associate glycoprotein (MAG)  
N-acetylgalactosamine (GalNAc)  
N-acetylglucosamine (GlcNAc)  
N-acetylglucosamine 2-epimerase/N-acetylmannosamine kinase (GNE)  
N-acetylmannosamine (ManNAc)  
N-Acetylmannosamine (ManNAc)  
N-acetylneuraminic acid synthase (NANS)  
N-acetylneuraminic acid (Neu5Ac)  
Neu5Ac-9-P-phosphatase (NANP)  
Neural cell adhesion molecule (NCAM)  
Neuraminidase 1 (NEU1)  
Neuraminidase 2 (NEU2)  
Neuraminidase 3 (NEU3)  
Neuraminidase 4 (NEU4)  
Neurofibrillary tangles (NFTs)  
Neuropilin (NRP2)  
N-Glycolylneuraminic acid (Neu5Gc)  
Non-small cell lung cancer (NSCLC)  
Peanut Agglutinin (PNA)  
Peptide N-glycosidase F (PNGaseF)  
phosphoinositide 3-kinase (PI3K)  
Phosphoinositide 3-kinase (PI3K)  
Polysialyltransferases (PolySTs)  
Prostaglandin E2 receptor EP2 M  
Protective protein/cathepsin A (CTSA)  
Proximal convoluted tubules (PCT)  
Proximal renal tubules (PRT)  
Pyruvate by N-acetylneuraminic acid pyruvate lyase (NPL)  
Retinol binding protein (RBP)  
Ricinus communis agglutinin (RCA-1 and II)  
Ricinus Communis Agglutinin (RCA-1)  
Sambucus nigra agglutinin (SNA)  
Sambucus Nigra lectin (SNA)  
S-carbohydrate recognition domains (S-CRD)  
Sialic acids (Sia)  
Slit diaphragm (SD)  
Sodium/glucose cotransporter 2 (*Sglt2*)  
Solute carrier family 22 member 12 (*Slc22a12*, Urate anion exchanger 1)  
Solute carrier family 22 member 2 (*Slc22a2*, Organic cation transporter 2)  
Solute carrier family 22 member 6 (*Slc22a6*, kidney-specific organic transport protein 1)  
Synaptic cell adhesion molecule (SynCAM)

Transcription Factor EB (TFEB)  
Transcription Factor EB (TFEB)  
Trans-Golgi Network (TGN)  
Transmission electron microscopy (TEM)  
Ubiquitin (Ub)  
UDP-GlcNAc 2-epimerase/ManNAc kinase (GNE)  
Unilateral ureteric obstruction (UUO)  
Uridine diphosphate N-acetylglucosamine (UDP-GlcNAc)  
Urinary-albumin-creatinine ratio (UACR)  
vacuolar H<sup>+</sup> ATPase (V-ATPase)  
Vitamin D binding protein (DBP)  
 $\gamma$ -ear containing ARF-binding protein (GGA)

## ABSTRACT

Sialidosis is an ultra-rare multisystemic lysosomal disease caused by mutations in the gene encoding for Neuraminidase 1 (NEU1) that cleaves terminal sialic acid residues from glycan chains of glycoproteins. NEU1 deficiency results in intracellular accumulation of sialoglycoconjugates in all tissues leading to multisystemic dysfunction. No specific therapy for sialidosis is currently available. In human patients, the severe Type II form of sialidosis, caused by reduction of the NEU1 activity to <5% of normal, manifests with severe symptoms. A subset of these patients develops nephrosialidosis, a progressive glomerular nephropathy with unresolved pathophysiological mechanism leading to a kidney failure. To study the mechanism underlying the disease, we studied a constitutive Neu1 knockout (*Neu1<sup>ΔEx3</sup>*) mouse model that showed progressive kidney dysfunction matching the clinical manifestations of nephrosialidosis patients.

The first aim of this thesis was to elucidate the underlying mechanism of kidney dysfunction in *Neu1<sup>ΔEx3</sup>* mouse model. Our study showed that highest NEU1 levels are found in kidney with males showing about 2-fold higher enzyme activity compared to females. Phenotypes of the *Neu1<sup>ΔEx3</sup>* mice includes organomegaly, urinary retention, loss of nephrons, renal fibrosis, and progressive albuminuria. Lifespan was decreased to 17 weeks in male and 25 weeks in female mice. Lectin staining of kidney tissues revealed a drastic increase in glycoprotein sialylation in glomeruli and in proximal and distal renal tubules. Analysis of N-linked glycans by mass spectrometry revealed increased abundance of N-linked glycoforms bearing sialylated species in *Neu1<sup>ΔEx3</sup>* kidney with males showing higher levels than females. One of the abnormally sialylated proteins was an endocytic reabsorption receptor megalin, normally prominently expressed in proximal convoluted tubules. Megalin levels were severely reduced in *Neu1<sup>ΔEx3</sup>* mice and the pool of megalin bearing O-linked glycans with terminal galactose residues which is essential for protein targeting and activity was reduced to below detection levels. Using confocal microscopy, we showed the receptors directed to the lysosomes for degradation instead of being returned to the apical plasma membrane. Proteomics analysis further revealed reduction of other endocytic receptors and solute-carriers suggesting that NEU1 plays an essential role by regulating reabsorption process.

The second aim of my thesis is to test a therapeutic approach to rescue NEU1 deficiency in by transplantation of wild-type hematopoietic stem progenitor cells (HSPC) into sialidosis mouse model. Macrophages derived from the donor HSPC expressing normal levels of NEU1 engraft in peripheral organs, catabolizing sialoglycoconjugates accumulated in cells and tissues. Engraftment rate, biochemical and histological characterization were performed to determine response to the HSPC transplantation,

showed amelioration of brain and kidney (urinary retention) pathology. The transplanted sialidosis mice also demonstrated increased life span, reduced levels of storage materials and improved behavior post-treatment.

## RÉSUMÉ

La sialidose est une maladie lysosomale multisystémique très rare causée par des mutations dans le gène codant pour la neuraminidase 1 (NEU1) qui clive les résidus d'acide sialique terminaux des chaînes glycaniques des glycoprotéines. Le déficit en NEU1 entraîne une accumulation intracellulaire de sialoglycoconjugués dans tous les tissus, ce qui provoque un dysfonctionnement multisystémique. Il n'existe actuellement aucune thérapie spécifique pour la sialidose. Chez les patients humains, la forme sévère de type II de la sialidose, causée par une réduction de l'activité de NEU1 à <5% de la normale, se manifeste par des symptômes graves. Un sous-ensemble de ces patients développe une néphrosialidose, une néphropathie glomérulaire progressive dont le mécanisme physiopathologique n'est pas élucidé et qui conduit à une insuffisance rénale. Afin d'étudier le mécanisme sous-jacent à la maladie, nous avons étudié un modèle de souris knock-out constitutif de Neu1 (Neu1 $\Delta$ Ex3) qui a montré un dysfonctionnement progressif des reins correspondant aux manifestations cliniques des patients atteints de néphrosialidose.

Le premier objectif de cette thèse était d'élucider le mécanisme sous-jacent du dysfonctionnement rénal dans le modèle de souris Neu1 $\Delta$ Ex3. Notre étude a montré que les niveaux les plus élevés de NEU1 se trouvent dans les reins, les mâles présentant une activité enzymatique environ deux fois plus élevée que les femelles. Les phénotypes des souris Neu1 $\Delta$ Ex3 comprennent l'organomégalie, la rétention urinaire, la perte de néphrons, la fibrose rénale et l'albuminurie progressive. L'espérance de vie a été réduite à 17 semaines chez les souris mâles et à 25 semaines chez les souris femelles. La coloration des tissus rénaux par les lectines a révélé une augmentation considérable de la sialylation des glycoprotéines dans les glomérules et dans les tubules rénaux proximaux et distaux. L'analyse des glycanes liés à l'azote par spectrométrie de masse a révélé une abondance accrue des glycoformes liés à l'azote portant des espèces sialylées dans les reins Neu1 $\Delta$ Ex3, les mâles présentant des niveaux plus élevés que les femelles. L'une des protéines anormalement sialylées était un récepteur de réabsorption endocytaire, la mégaline, normalement exprimée de façon proéminente dans les tubules contournés proximaux. Les niveaux de mégaline étaient sévèrement réduits chez les souris Neu1 $\Delta$ Ex3mice et le pool de mégaline portant des glycanes liés en O avec des résidus de galactose terminaux, qui est essentiel pour le ciblage et l'activité de la protéine, était réduit à des niveaux inférieurs à ceux de la détection. En utilisant la microscopie confocale, nous avons montré que les récepteurs étaient dirigés vers les lysosomes pour être dégradés au lieu d'être renvoyés vers la membrane plasmique apicale. L'analyse protéomique a également révélé une

réduction des autres récepteurs endocytiques et des transporteurs de soluté, ce qui suggère que NEU1 joue un rôle essentiel en régulant le processus de réabsorption.

Le deuxième objectif de ma thèse est de tester une approche thérapeutique pour remédier à la déficience en NEU1 par la transplantation de cellules souches hématopoïétiques progénitrices (HSPC) de type sauvage dans le modèle murin de la sialidose. Les macrophages dérivés des HSPC du donneur exprimant des niveaux normaux de NEU1 se greffent dans les organes périphériques, catabolisant les sialoglycoconjugués accumulés dans les cellules et les tissus. Le taux de greffe, la caractérisation biochimique et histologique ont été effectués pour déterminer la réponse à la transplantation de HSPC, montrant une amélioration de la pathologie cérébrale et rénale (rétention urinaire). Les souris transplantées atteintes de sialidose ont également montré une augmentation de leur durée de vie, une réduction des niveaux de matériaux de stockage et une amélioration de leur comportement après le traitement.

## ACKNOWLEDGEMENT

I would like to express my deepest gratitude to my supervisor, Prof. Alexey V. Pshezhetsky, for his continuous support throughout my Ph.D. journey. For his willingness to lend his insights and expertise to guide me through this challenging pursuit. I thank you for being patient and providing me with opportunities to grow as a professional and for seeing this degree through to its successful end.

I am also grateful to my co-supervisor, Prof. Carlos Morales, for his constructive feedback that has been offered so generously and consistently throughout my candidature. I would also like to thank my committee meeting members, Dr. Graziella Di Cristo, Dr. Phillippe Campeau, and Dr. Khanh Huy Bui for their valuable time and input in helping guide me through my research direction.

To all my lab members, I extend my utmost appreciation for their constant support and encouragement, and countless laboratory discussions that have never failed to provide me with new perspectives.

I would also like to extend my gratitude to my collaborators, Dr. Mathieu Lemaire for his valuable insight on nephrology, Irene Londono for helping with histology, Dr. Pierre Thibault and Eric Bonneil for proteomics analysis, Jeannie Mui for assisting with TEM, without which this work would never have been possible. I would also like to thank Dr. Elke Küster-Schöck for her support with microscopy, Ines Boufaied for assisting with flow cytometry, and the personnel from the CHU Sainte-Justine animal facility, special thanks to Veronique for her valuable help and dedicated care.

To my family, I am always grateful for their patience and understanding in my constant educational pursuit. It should be the last one, at least for the moment. My greatest appreciation to my parents, for their trust and unconditional support so that I would be able to accomplish what I set out to do, and my sisters for always being there even when I'm running my mouth.

## CONTRIBUTION TO ORIGINAL KNOWLEDGE

In this doctoral thesis, I characterized the pathophysiology of *Neu1<sup>ΔEx3</sup>* and *Neu1<sup>Cx3cr1ΔEx3</sup>* mice model, first to establish the biomarkers for the disease, then to test a new treatment approach. The *Neu1<sup>ΔEx3</sup>* and *Neu1<sup>Cx3cr1ΔEx3</sup>* mice were previously generated in our laboratory (Pan *et al.* 2017) but their pathological phenotype was not characterized. Hence, I described the systemic dysfunction of both mouse models, focusing in-depth on the study of progressive renal pathology.

I measured the enzyme activities in different tissues to characterize the levels of different neuraminidases (NEU1-NEU4) using specific assays (Guo *et al.* 2018). I described the systemic pathology exhibited in both mice models including organomegaly, short lifespan, slow growth and smaller body mass, infertility, skeletal malformation and renal pathology. I studied the histopathological changes in the kidney by staining sections with H&E, Masson's Trichrome and toluidine blue of the glomeruli and renal tubular sections. Using transmission electron microscopy, I showed accumulation and ultrastructural changes in the podocytes, glomeruli, proximal tubules and distal renal tubules. I also documented the changes in kidney proteins by proteomics and alteration of protein glycosylation in the kidneys using lectin staining and confocal microscopy. My results revealed the mis-trafficking of hypersialylated endocytic receptor megalin to the lysosomes instead of the epithelial surface in the proximal renal tubules. Together these results provided evidence that renal dysfunction in the nephrosialidosis is a result of aberrant changes in renal protein glycosylation.

I also conducted of allogenic transplant of WT HSPC in *Neu1<sup>ΔEx3</sup>* mouse. This pilot study laid a foundation for the future development of a therapy for sialidosis with LV-modified HPSC transplant that will be conducted in our laboratory. For the first time, in the *Neu1<sup>ΔEx3</sup>* mouse model, I demonstrated engraftment of donor HSPC and showed the rescue of increased lysosomal biogenesis in peripheral tissues. Using confocal microscopy, I showed the normalization of lysosomal storage markers, levels of activated macrophages and megalin in the kidneys and partial rescue of brain pathology through the normalization of exploratory behavior of a transplanted *Neu1<sup>ΔEx3</sup>* mouse. Even though the HSPC transplant did not result in a complete amelioration of pathology, our pilot study provides preliminary evidence that allogenic engraftment is promising in the *Neu1<sup>ΔEx3</sup>* sialidosis mouse model.

## CONTRIBUTION OF AUTHOR

During my doctoral candidature, I participated in the following publications and studies:

1. **Kho, I.**, Demina, E. P., Pan, X., Londono, I., Cairo, C. W., Sturiale, L., Palmigiano, A., Messina, A., Garozzo, D., Ung, R. V., Mac-Way, F., Bonneil, É., Thibault, P., Lemaire, M., Morales, C. R., & Pshezhetsky, A. V. (2023). Severe kidney dysfunction in sialidosis mice reveals an essential role for neuraminidase 1 in reabsorption. *JCI insight*, 8(20), e166470. <https://doi.org/10.1172/jci.insight.166470>

Contribution of author:

**Ikhui Kho**: Experimental design, protocol writing and validation, data curation, statistical analyses, writing (draft, review and editing), genotyped mice and maintained colonies, documented survival and mouse behavior, performed enzyme activities in mouse tissues, collected and processed mouse organs, blood and urine for analyses, processed tissues for proteomics and MALDI-TOF, performed IHC, TEM and western blot, performed qPCR, performed micro-CT imaging.

Ekaterina Demina: Maintain *Neu1<sup>Cx3cr1ΔEx3</sup>* mouse colony, generate *Neu1<sup>Cx3cr1ΔEx3</sup>* mouse survival curve and collected *Neu1<sup>Cx3cr1ΔEx3</sup>* organ weights.

Xuefang Pan: Made *Neu1<sup>ΔEx3</sup>* mouse model.

Irene Londono: Performed micro-CT and bone analysis.

Lucia Sturiale, Angelo Palmigiano and Domenico Garozzo: Performed MALDI-TOF analysis.

Roth-visal Ung and Fabrice Mac-way: Performed bone histology and analysis.

Eric Bonneil and Pierre Thibault: Performed proteomic analysis.

2. Allogenic transplant of WT HSPC in *Neu1<sup>ΔEx3</sup>* mouse.

Contribution of author:

**Ikhui Kho**: Harvested and isolated WT HSPC for transplant, performed cell culture, performed myeloablative regimen with daily injection of busulfan, performed tail vein injection of HSPCs, daily health assessment on mice, collected mandibular blood for flow cytometry analysis, performed Open Field and Y-maze behavior test and analysis, collected tissues and bone marrow for enzyme activities, IHC, confocal imaging and analysis.

3. Da Silva, A., Dort, J., Orfi, Z., Pan, X., Huang, S., **Kho, I.**, Heckel, E., Muscarnera, G., van Vliet, P. P., Sturiale, L., Messina, A., Romeo, D. A., van Karnebeek, C. D. M., Wen, X. Y., Hinek, A., Molina, T., Andelfinger, G., Ellezam, B., Yamanaka, Y., Olivos, H. J., ... Pshezhetsky, A. V. (2023). *N*-acetylneuraminidase controls sialylation of muscle glycoproteins essential for muscle regeneration and function. *Science advances*.

Contribution of author:

**Ikhui Kho**: Collected and processed mouse tissues, prepared samples for TEM, conducted TEM imaging and analyses.

# 1 Introduction and literature review

## 1.1 Lysosomes

Lysosomes are enclosed organelles that contain more than 50 different acid hydrolases that are capable of breaking down proteins, carbohydrates, lipids, and nucleic acids (1). Lysosomal enzymes have the highest catalytic activity at pH 4.5-5.0 and a similar pH is maintained in the lysosomal lumen by an action of a tightly regulated vacuolar H<sup>+</sup> ATPase (V-ATPase) and Cl<sup>-</sup>/H<sup>+</sup> antiporter present at the lysosomal membrane (2).

Soluble and lysosomal membrane proteins are synthesized in the endoplasmic reticulum (ER) and transported along the biosynthetic pathway of the Golgi apparatus and the trans-Golgi network (TGN), ending at the lysosomes (1). Along the way, post-translational modification of newly synthesized soluble proteins is initiated in the ER by the addition of sugars which aid in protein folding and sorting (3). Upon arrival at the Golgi, soluble lysosomal enzymes have an additional modification on mannose sugars forming mannose-6-phosphate (M6P) tags essential for their trafficking. This modification is generated by the sequential action of two enzymes, N-acetylglucosaminyl-1-phosphotransferase (GlcNac-1-phosphotransferase) and N-acetylglucosamine-1-phosphodiester  $\alpha$  N-acetylglucosaminidase (uncovering enzyme, UCE) (3). The M6P-tagged enzymes are recognized by two M6P-specific receptors (MPR), the cation-dependent (CD) receptor and the cation-independent (CI) receptor, which help to package acid hydrolases into vesicles that are targeted to fuse with endosomes and mature lysosomes (4). Alternative transport for soluble lysosomal enzymes and non-enzymatic proteins is mediated by M6P-independent sorting receptors sortilin and LIMP-2 (3). Some lysosomal proteins that are poorly mannose-6-phosphorylated are transported through these receptors, for example, beta-glucocerebrosidase GBA is targeted by LIMP-2, while cathepsins D and H are mainly targeted to the lysosomes through the sortilin-mediated pathway (5).

Transmembrane proteins are not modified with M6P tags but rather contain amino-acid sequence-based sorting signals in the cytosolic tails or loops to facilitate lysosomal targeting and endocytosis. These sorting signals are either tyrosine-based sorting signals with NPXY and YXX $\emptyset$  motifs or dileucine-based signals with DXXLL and [DE]XXXL[LI] motifs (6). These trafficking signals are recognized by adaptor protein (AP) complexes, clathrin, Dab2, and Golgi localized  $\gamma$ -ear containing ARF-binding protein (GGA) (6).

### 1.1.1 Lysosomal degradation pathway

Lysosomes play a central role in cellular catabolism where macromolecules at the plasma membrane are internalized and sorted to the endosomes-autophagosome-lysosomal pathway for degradation (Figure 1.1) (7). The early endosomes act as sorting centers where changes in pH from neutral to acidic allow the dissociation of ligands and their delivery to the lysosome, while the receptors are recycled back to the plasma membrane (8). When the early endosomes evolve into the late endosome, also called multivesicular bodies (MVBs), substrates are taken up into intra-lysosomal vesicles for degradation with the help of the endosomal sorting complex required for transport (ESCRT) machinery (8).

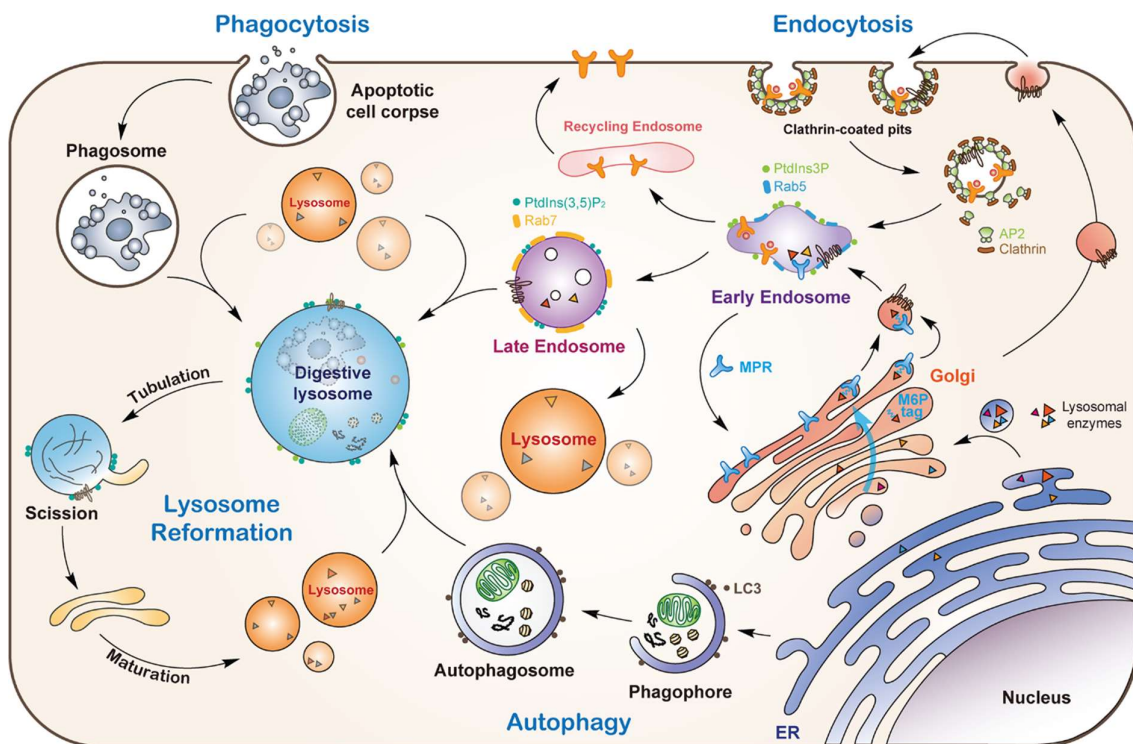


**Figure 1.1: Multiple pathways are involved in lysosomal protein delivery and lysosomal fusion (7). [Reproduced with permission from the publisher]**

Autophagy or “self-eating” is a process in which non-functional cytoplasmic proteins or organelles are utilized by the cell. Autophagy is induced by starvation and is essential in maintaining cellular homeostasis by targeting intracellular cytosolic components for lysosomal degradation. Autophagy has been classified into three different distinct forms, macroautophagy, chaperone-mediated autophagy (CMA), and microautophagy, which all end in lysosomal degradation (9). In macroautophagy, a double membrane autophagosome forms and engulfs cytoplasmic material to be delivered and degraded in the lysosomes (10). The process is

initiated by the formation of autophagosome through two major complexes, the ULK1 complex and the phosphoinositide 3-kinase (PI3K) complex (10). Protein light chain 3 (LC3) and P62/SQSTM1 (P62) are membrane proteins generated early in the process of autophagosome formation. Both are also substrates for autophagic degradation and thus are indicators of autophagic flux (11). Microautophagy involves the direct uptake of cargo through the lysosomal membrane for degradation while CMA is a highly distinct process that does not use membranous structure to sequester protein but instead involves chaperone proteins that target protein substrates with KFERQ amino acid sequence motif (9). This pentapeptide motif is recognized by heat shock 70kDa protein 8 (HSPA8/HSC70), which then unfolds the substrates and delivers them directly across the lysosomal membrane into the lysosome (9).

### 1.1.2 Lysosomal biogenesis

Lysosomal biogenesis is an essential function of cellular homeostasis that is maintained by a coordinated network of lysosomal proteins and transcriptional factors. Genes encoding lysosomal proteins or proteins involved in lysosomal biogenesis have in common a 10-base E-box-like palindromic sequence (GTCACGTGAC) called the Coordinated Lysosomal Expression and Regulation (CLEAR) element that is recognized by transcriptional factors to promote the expression of lysosomal and autophagy genes to increase lysosome size and numbers to meet the need for catabolism (12). In mammalian cells, members of the microphthalmia family (MiT family) such as Transcription Factor EB (TFEB), TFE3, and TFEC that belong to basic helix-loop-helix-leucine zipper (bHLH-Zip) transcription factors bind to CLEAR element to activate lysosomal gene expression, promoting lysosomal biogenesis (13).

The regulation of TFEB is dependent on the mechanistic target of rapamycin (mTOR)-mediate phosphorylation that is stimulated by the nutrient content of the cell. Under nutrient-rich conditions, TFEB is inactive and largely sequestered at the lysosomal membrane due to phosphorylation at the ser142 and ser211 serine residue on the TFEB protein by mechanistic target of rapamycin complex 1 (mTORC1) (13). Upon inhibition of mTORC1, TFEB is dephosphorylated and rapidly translocated to the nucleus where it activates the transcription of target lysosomal and autophagy genes. However, mTOR-independent activation of lysosomal biogenesis also exists, for example in lysosomal storage diseases hyperactivation of mTOR coincides with increased TFEB nuclear translocation (14, 15).

## 1.2 Lysosomal storage diseases

Lysosomal storage diseases (LSD) are a group of inborn errors of metabolism characterized by the gradual accumulation of substrates due to dysfunctional lysosomal catabolism. LSD belong to a group of orphan diseases due to their rare occurrence (from 1:20,000 to 1:2,000,000 live births). However, although LSD are rare individually, their combined prevalence is 1 in 7000 live births (16), so they represent an essential health problem. Most LSD are inherited in an autosomal recessive manner except for three LSD, Fabry disease, Danon disease, and Hunter syndrome which are X-linked recessive (17).

LSD can be categorized depending on the type of primary substrate storage into glycoproteinoses (also known as oligosaccharidoses), sphingolipidoses, mucopolysaccharidoses (MPS), glycogenoses, and lipidoses (17). Although, in general, LSD present with a broad spectrum of clinical manifestations, their severity and pathogenesis can vary depending on the age of onset (18). More importantly, the different types of mutation affect protein structure and function to a different degree, for example, mutation at the surface of NEU1 enzyme results in failure to integrate into the multienzyme complex with  $\beta$ -galactosidase and cathepsin A (CTSA), causing it to degrade instantly, while other mutations affect positions of the active center residues causing a partial reduction of the enzyme activity (19).

**Table 1.1: Defects in lysosomal membrane proteins and the associated disorder (20).**

[Adopted and modified with permission from publisher]

Disease	Clinical pathology	Protein	Function
Action myoclonus-renal failure syndrome	myoclonic epilepsy associated with renal failure	LIMP2 (SCARB2)	Transport of $\beta$ -GC to lysosomes, lysosomal biogenesis, and sorting of vesicles to apical membranes
Cobalmin F-type disease	Developmental delay, stomatitis, glossitis, seizures and minimal methylmalonic aciduria	LMBRD1	Lysosomal export of cobalmin

Cystinosis	Pathology of kidney, eye, liver, muscles, pancreas, brain, and white blood cells, as well as diabetes, hypothyroidism, and end-stage kidney failure	Cystinosin	Lysosomal H <sup>+</sup> and l-cysteine symport
Danon disease	X-linked vacuolar cardiomyopathy, myopathy, and variable mental retardation	LAMP2	Chaperone-mediated autophagy, macroautophagy, lysosomal fusion and motility
Niemann–Pick type C	Hepatosplenomegaly, thrombocytopenia, ataxia, dysarthria, dysphagia, dystonia, dementia, and seizures	NPC1	Lysosomal lipid and cholesterol export
Mucopolipidosis type IV	Autosomal recessive genetic disorder with delayed psychomotor development and ocular aberrations	MCOLN1	Lysosomal cation (Na <sup>+</sup> , K <sup>+</sup> , Ca <sup>2+</sup> , Fe <sup>2+</sup> and H <sup>+</sup> ) channel
Mucopolysaccharidosis type IIIC	Autosomal recessive genetic disorder with delayed psychomotor development and ocular aberrations	HGSNAT	Transfer of cytosolic acetyl-CoA to luminal α-glucosamine residues of heparan sulphate
Malignant infantile osteopetrosis	Anaemia, thrombocytopenia, granulo-cytopenia,	CIC7	H <sup>+</sup> and anion (Cl <sup>-</sup> ) antiport

		blindness, deafness, fractures, and infections		
Neuronal lipofuscinosis (late infantile)	ceroid	Ataxia and seizures with rapid mental deterioration	CLN7 (also known as MFSD8)	Transport of sugars, drugs, inorganic and organic cations, and other metabolites
Neuronal lipofuscinosis (juvenile)	ceroid	Early progressive vision loss, seizures and ataxia or clumsiness	CLN3	Membrane transport
Salla disease		Nystagmus, hypotonia, cognitive impairment and reduced muscle tone and strength	Sialin	H <sup>+</sup> and sugar symport (resulting in the export of sialic acids and acidic hexoses) and asparagine and glutamine import.

While most LSD are caused by the deficiency of acid hydrolases, there are exceptions. For example, the deficiency of GM2 activator protein (GM2AP) – a small non-enzymatic protein necessary for degradation of GM2-ganglioside by lysosomal beta-hexosaminidase A (HEXA) (21), a mutation in either protein causes GM2 gangliosidosis (22). Non-enzymatic lysosomal proteins involved in the trafficking of substrates to and off the lysosome, such as lysosomal membrane channels and transporters are also necessary to maintain the catabolic function of lysosomes (Table 1.1) (20).

### 1.2.1 Neuropathic lysosomal storage disorders

Most (two-thirds) of LSD are neuropathic, with accumulated substrates affecting the central nervous system (CNS) and visceral organs. However, neurological symptoms such as cognitive development delay or behavioral abnormalities is often not evident at an early stage of the disease since it manifests slower than systemic pathology, which often results in misdiagnosis. For example, adult-onset Krabbe with progressive neuropathy (demyelination) can be first diagnosed as ataxia with mild gait impairment (23). Other neurological features reported in LSD encompasses behavioral changes, motor weakness, seizures, and extra-pyramidal motor signs (17). There are traits shared with adult neurodegenerative disorders such as Parkinson's

disease (PD) and Alzheimer's diseases (AD). For example, AD shows evidence of impaired autophagy and lysosomal dysfunction in neuronal cells while accumulation of beta-amyloid-(A $\beta$ ) plaques and intracellular neurofibrillary tangles (NFTs) in the brain (24) are also seen in MPS III (25) and sialidosis (26). Amyloid precursor protein was proposed to be a substrate of neuraminidase 1 (NEU1) and cerebral injection of adenoviral vectors encoding NEU1 in the established AD mouse model reduced beta-amyloid plaques (26). Additionally, mutations in the *GBA* gene which encodes for glucocerebrosidase (GCase), which is deficient in Gaucher disease, is also a major genetic risk factor for PD (27-30). Meanwhile in PD, the loss of GCase activity results in the accumulation of glucocerebroside (GlcCer), glucosylsphingosine (GlcSph) and alpha-synuclein ( $\alpha$ -synuclein). While Gaucher disease patients present astrogliosis and neuronal loss in brain regions including the hippocampus, calcarine cortex (layer 4b) and cerebral cortex (layers 3 and 5), which are some key characteristics of neurodegenerative diseases (27).

In neurological LSD, the accumulation of substrates triggers the activation and mobilization of microglial cells (microgliosis) and astrocytes (astrogliosis) leading to persistent neuroinflammation and neurodegeneration. In the brain, gangliosides (GM1, GD1a, GD1b, and GT1b) are abundantly found on neurons and are essential for myelination, neurogenesis, differentiation and maturation of neurons (31). As such, impaired catabolic processing of gangliosides leads to neurologic disorders for example, *Neu3/Neu4* double-deficient mouse model shows storage of GM3 ganglioside in microglia, neurons and vascular pericytes, micro-astrogliosis in the cortex and CA1 area of hippocampus with memory deficits in aged mice (32). Similar neuropathological findings were reported in a sialidosis patient which showed the presence of membrane-bound vacuoles in the Purkinje cells and zebra bodies in the neurons of the spinal cord indicative of storage, and loss of Purkinje cells and the degeneration of inner granular layer of the cerebellar cortex (33).

Neuroinflammation which drives the production of cytokines with immunomodulation properties has been proven to drive neurogenesis. For example, immune-deficient mice were found with impaired neurogenesis of hippocampal neurons which is essential for cognitive learning, and priming with activated T-cells shapes microglial neuroprotective behavior for neural cell survival and renewal (34). However, prolonged inflammatory responses are detrimental to the brain by perpetuating the inflammatory cycle which ultimately leads to neurodegeneration. For example, a mouse model with selective ablation of CD11b prevented monocyte and macrophage recruitment to the site of the injured sciatic nerve and resulted in

failed peripheral nerve graft regeneration (35). Two main categories of cells in the brain consist of neurons and glial cells. Glial cells, which include astrocytes, oligodendrocytes and microglia modulate immune response in the CNS by producing cytokines that can impact memory, cognition and behavior (36). These activated microglia and astrocytes secrete elevated levels of proinflammatory cytokines such as IL-1 $\beta$ , TNF- $\alpha$ , and IL-6 (37). These proinflammatory cytokines act in an autocrine/paracrine manner to activate neighboring glial cells, inducing cell death and damage to the blood-brain-barrier (BBB) in LSD such as Gaucher disease (38), Niemann Pick disease (39), and other neurodegenerative disorders such as AD (40) and progressive loss of dopaminergic neurons in PD (41). More importantly, the activation of inflammatory response is not exclusive to the brain but can also be detected in peripheral organs. For example, in Fabry's disease the accumulation of glycosphingolipid Gb3 in various organs including the brain, heart, liver, spleen and kidneys leads to massive mobilization of leucocytes and secretion of proinflammatory cytokines causing system tissue damage in visceral organs (42).

#### 1.2.2 Nephropathic lysosomal storage disorders

Some LSD that manifest kidney involvement, most notably Fabry's disease and cystinosis, both involve the accumulation of substrate in the lysosomes of renal cells followed by tissue inflammation and interstitial fibrosis which eventually leads to kidney failure. In cystinosis, the lack of cysteine-specific lysosomal transporter protein results in the accumulation of amino acid cystine in the kidneys with or low molecular weight proteinuria (LMWP) (43). One of the clinical presentations of cystinosis is excessive urinary excretion of low molecular weight proteins, whereas, in normal kidneys, LMWP are capable of passing through the glomerular filtration barrier which restricts proteins of 65 kDa or larger, but allows small proteins such as lysozyme, or  $\beta$ -microglobulin and vitamin D binding protein to pass through the filter (44). LMWP that passes through the glomerular filtration barrier to the proximal convoluted tubules (PCT) are immediately recovered by endocytic receptors, megalin and cubilin, that are found on the epithelial cells of PCT and delivered to the lysosomes for degradation. However, generalized defect of the PCT leads to malabsorption of metabolites. For example renal Fanconi syndrome where a generalized defect of the proximal renal tubules (PRT) causes altered reabsorption mechanisms that leads to excessive loss of solutes and essential metabolites in urine (45). On the other hand, changes in the lysosomal-mediated delivery pathway disrupt renal function. In Dent's disease, the loss of function of CLC-5, a chloride channel, result in the failure of the early endosome to acidify correctly (46). While the loss of

CLC-5 also directly impacts receptor-mediated endocytosis and trafficking to the lysosomes resulting in decreased uptake of ligands and elevated levels of urinary LWMP (47).

The PRT are responsible for up to 80% of the reabsorption of glomerular filtrate in the kidneys (48), and are therefore susceptible to injury from aging, oxidative stress and nephrotoxic substances. Autophagy protects renal cells from injury and cell death by mediating cellular clearance and cellular homeostasis, and changes to the degradative pathway, affecting renal physiological function. This suggests a connection between endosomal trafficking, lysosomal storage and impaired autophagy in kidney dysfunction. Patients with SCARB2 deficiency and *Scarb2* deficient mice demonstrated similar pathology of tubular proteinuria from the failure of the endosome-lysosomes fusion (49). Deficiency of LIMP-2 (also called CD63 in mice) is a lysosomal membrane protein responsible for the transport of GCCase and the deficiency of this protein changes water balances in the kidneys of mice, leading to increased urinary flow and reduced urine osmolality (50). In nephropathic LSD, the progressive accumulation of substrates in cells and tissues disrupts the structural integrity of the kidney. In Fabry's disease for example, deficiency of  $\alpha$ -galactosidase results in glycosphingolipids accumulation in the podocytes, mesangial cells and parietal cells of the glomerulus, as well as in the proximal and distal tubular cells (51). This accumulation causes glomerular sclerosis and tubulointerstitial fibrosis, proteinuria and eventually results in renal failure (52). Furthermore, there are shared traits between nephropathic LSD and other chronic kidney diseases (CKD). For example accumulation of damaged lysosomes and insufficient autophagy are found in the podocytes (53) and PRT (54) of diabetic nephropathy animal models. While, restoring the autophagy function leads to the recovery of damaged podocytes and proximal tubular defects in diabetic kidney failure patients (55).

The PRT contain a large population of mitochondria to accommodate the energy expensive process of reabsorption (48), and impaired mitophagy and mitochondrial biogenesis can negatively impact kidney function. For example, autophagy block is reported in the PRT of cystinosis patients with accumulation of P62 and LC3II and reduced number of mitochondria (56, 57) Likewise, impaired autophagic flux was reported in the podocytes and mesangial cells of Fabry's patients, with increased mitochondria-containing autophagosome in fibroblasts (58). Mitophagy facilitates mitochondria turnover by removing damaged mitochondria which can act as damage-associated molecular patterns (DAMPs), triggering immune responses by recruiting macrophages, dendritic cells and neutrophils that produce pro-inflammatory cytokines TNF- $\alpha$ , IL-6 and IL-1 $\beta$  and causes tissue injury (59). Nephropathic cystinosis which

presents with generalized proximal tubular dysfunction also reveals impaired mitophagy and increased apoptosis in renal proximal tubular cells (57).

Extracellular matrix (ECM) remodeling in the kidney is an essential response to injury, and one of the early signs that frequently occurs in the glomeruli and tubulointerstitial spaces. ECM provides structural scaffolding (60) and regulates cellular functions such as activation of cell proliferation and immunological reaction via TGF- $\beta$ 1 signaling (61). However, excessive matrix formation disrupts the renal architecture and reduces blood supply causing kidney failure. In injured kidneys, glomerular fibrosis is promoted by excessive collagen production by podocytes and endothelial cells lining the glomerular basement membrane (GBM) (62) and parietal epithelial cells lining the Bowman's capsule (63), leading to impaired filtration. Due to the excessive protein load that passes the glomerular filtration barrier, injured PRT also undergoes adaptive dedifferentiation, promoting epithelial-to-mesenchymal cell transition by losing epithelial cell markers E-cadherin and gaining vimentin (64). For example, the loss of tight junction protein ZO1 in PRT epithelia of nephropathic Fabry's mouse model (65), decreased cell differentiation genes *Slc5a2* and *Slc34a1* and increased dedifferentiation marker (Foxm1, Sox9 and Vimentin) (66). This transition occurs alongside the loss of the brush border structures and polarity of PRT cells after which they migrate, proliferate and differentiate into new functional nephrons. However, after repeated injury and recovery, maladaptive dedifferentiation occurs where cell cycle progression of epithelial cells is arrested at G2/M checkpoint (64), following which fibrotic cytokines and growth factors such as TGF- $\beta$ 1, HER2 and FGF2 are secreted to induced myofibroblast differentiation and ECM production (67, 68). Therefore, ECM remodeling and renal structural changes are demonstrated in different kidney diseases, for example, thinning of the GBM in Alport's disease (69) and thickening of the GBM and Bowman's capsule in diabetic nephropathy (63). On the other hand, lysosomal cysteine cathepsins are shown to participate in ECM remodeling including processing of inflammatory cytokines which contributes to disease progression in the kidney (70), heart (71), and liver (72). In the kidney for example, cathepsin D inhibition leads to increased collagen III and IV degradation in the kidney cortex of unilateral ureteric obstruction (UUO) and ischemia reperfusion injury (IRI) CKD mouse models (73).

### 1.3 Sialidosis

Sialidosis is an ultrarare (prevalence of 1 per 5,000,000 live births) neuropathic LSD caused by a defect in the neuraminidase 1 (*NEU1*) gene (OMIM #256550). The deficiency of this lysosomal enzyme causes intracellular accumulation of sialylated proteins. Currently, there are

more than forty mutations identified in sialidosis patients (74, 75). These mutations are classified by nomenclature of missense, insertions and splice-sites mutations and do not affect NEU1 mRNA synthesis and stability. These NEU1 protein variants can be categorized based on their molecular and biochemical properties for example, the enzyme is functional but does not localize to lysosomes or non-functional enzyme located in the lysosomes, (75, 76).

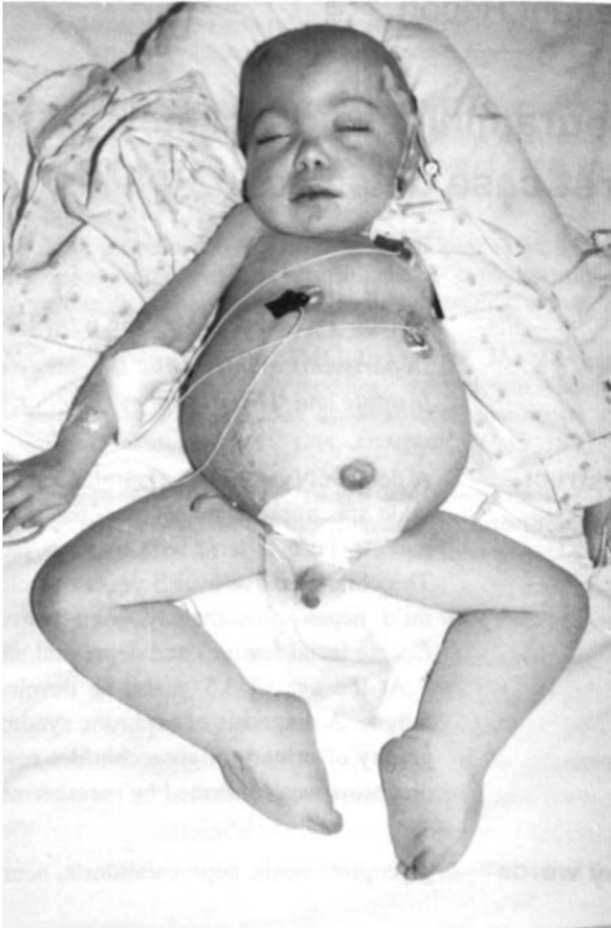


**Figure 1.2: Type II sialidosis patient at 4 years old with severe edema and ascites (77). [Reproduced with permission from the publisher]**

Sialidosis is divided into two subtypes with different ages of onset and severity. Sialidosis Type I manifests as a milder, late-onset disease where the patients suffer from myoclonus, progressive vision failure and mild cognitive impairment. Type II sialidosis (also known as early-onset or congenital/infantile/juvenile form) is a more severe dysmorphic form of the disease (78, 79). Patients with type II sialidosis display abnormal somatic features (Figure 1.2), dysostosis multiplex, ascites, visceromegaly and severely impaired intellectual function (79). A subtype of the type II sialidosis presenting with a severe nephrotic syndrome is described as

nephrosialidosis (Table 1.2) (80). Kidney biopsy in these patients revealed severely vacuolated glomerular and tubular epithelial cells with electron dense lining on the inner lining of the membrane (80). Due to the rarity of this condition, very few cases have been described (81), and while the pathophysiology of nephrosialidosis remains mainly unexplained, however, excessive proteinuria suggest pathology beyond glomerular defects (77). When compared to controls, the urine of patients is enriched not only with albumin (a marker of glomerular dysfunction), but urine oligosaccharide profile with total sialic acid was six times the normal value (10371  $\mu\text{mol/g}$  creatinine) (82).

**Table 1.2: Cases of type II sialidosis (nephrosialidosis).**

**\*Denoting sibling pair described in the same publication.**

Gender	Age of onset	Renal pathology (sialyloligosaccharide)	CNS pathology (motor and cognitive)	Systemic/peripheral pathology	Author
Male	At birth	Proteinuria (4g per 24 h), 13.1 nmol/mg neuraminic acid in urine (13-fold increase)	Poor motor development (unable to roll over)	Ascites, bilateral testicular hydroceles, hepatosplenomegaly, skeletal dysostosis	Aylsworth <i>et al.</i> (1980) (79)
Female	8-month	Free sialic acid at 6220 nmol/mg (normal range 156-789) and bound sialic acid at 3370 nmol/mg creatinine (normal range 154-842 nmol/mg creatinine); Died of nephropathy at 9-years old	Normal EEG and EMG; Cognitive impairment (language comprehension at 5-6 years old level at 9-years old)	Dysostosis multiplex, coarse facial features, lens opacities, hepatosplenomegaly	Kelly <i>et al.</i> (1977) (83); Follow-up study Roth <i>et al.</i> (1988) (84)
Female*	At birth	Proteinuria (4.6 g per 24 h), free sialic acid 6575 nmol/mg creatinine (normal range 32-254 nmol/mg), bound sialic acid 846 nmol/mg creatinine (normal range 12-390 nmol/mg),	severe psychomotor retardation	Dyspnoea, recurrent respiratory infections, and hepatosplenomegaly, decreased muscle tone, hearing loss	Sperl <i>et al.</i> (1990) (85)

Male*	At birth	proteinuria (60 mg/dl), free sialic acid 2716 nmol/mg creatinine (normal range 32-254 nmol/mg), bound sialic acid 647 nmol/mg creatinine (normal range 12-390 nmol/mg),	Not determined due to death at 3-months	Tachypnoea and dyspnoea occurred and hepatosplenomegaly, umbilical hernia, clubfeet and massive oedema, moderate hydrocephalus	
Male	12-year-old	Sialic acid in urine (not measured)	Mental retardation, nystagmus, myoclonus, cerebral seizures	Skeletal dysostosis, hearing loss, cherry-red macular spot,	Spranger <i>et al.</i> (1977) (86)
Female	At birth	No mucopolysaccharide in urine	Motor retardation, sensorineural deafness	Marked hepatosplenomegaly, bilateral congenital dislocation of hips and bilateral inguinal hernia,	Laver <i>et al.</i> (1983) (87)
Male	At birth	Free sialic acid 2238 nmol/mg creatinine (normal range 18-50 nmol/mg), bound sialic acid 1296 nmol/mg creatinine (normal range 162-390 nmol/mg),	Mental and motor retardation	Dyspnea, hypertrophic cardiomyopathy, cardiomegaly, hepatomegaly,	Paschke <i>et al.</i> (1986) (88)
Female	At birth	Proteinuria (0.8 g/24 h), presence of sialyloligosaccharide (not measured)	Not present	limb oedema, liver and spleen enlargement,	Schiff <i>et al.</i> (2005) (89)

				dysmorphic features, dysostosis multiplex,	
Male	2-year-old	Bilaterally swollen kidneys, proteinuria (5.28 g per 24 h), sialyloligosaccharide not reported	Not determined due to death at 2.5-years old	Malnutrition, systemic organ failure	Chen <i>et al.</i> (2011)(80)
Female*	33 <sup>st</sup> week of gestation	Not determined	Not determined due to death at 87 days after birth	Hydrops fetalis, subcutaneous edema, pleural effusion, ascites, hepatosplenomegaly	Itoh <i>et al.</i> (2002) (90)
Male*	21 <sup>st</sup> week of gestation	Not determined	Not determined due to artificial abortion at 21 <sup>st</sup> week of gestation	slight generalized subcutaneous edema, mild pleural effusion, ascites, and mild hepatosplenomegaly	

As with most LSD, sialidosis is a multisystemic disease and both type I and type II patients show CNS pathology. Although type I sialidosis reported minimal cognitive impairment, however neurophysiological signs such as seizures and loss of consciousness are documented in most patients (6 of 13 patients) (91). Abnormal electroencephalography (EEG) showed frequent and slow-wave polyspike in sialidosis type I patients (92) which are characteristic of myoclonic epilepsy (93). Such chronic seizures are commonly seen in neurological disorders such as epilepsy, which impairs the long-term potentiation of pyramidal neurons in the hippocampus leading to reduced cognitive function (94). In type II sialidosis, seizures, myoclonus and ataxia are commonly seen at a young age, with the earliest diagnosed at age  $10.4 \pm 5.3$  years regardless of gender (91). However, there is a debate as to whether the loss of motor control is of neurological or musculoskeletal causes. For example, osteonecrosis has been described in type I sialidosis (95) and skeletal dysplasia in type II sialidosis (77). With NEU1 described with roles in mediating skeletal muscle differentiation and regeneration (96). More importantly, some type I patients presented with progressive motor difficulties and no

neurodegeneration in the brain and spinal cord. Neuropsychological assessment showed average attention span, verbal fluency and memory skills (97). However, being a progressive disease, brain atrophy becomes more evident with age (98). Case studies on type I patients showed compromised white matter tract, diffuse brain atrophy and other somatic phenotype such as ophthalmic pathology such as macular degeneration and cherry-red spots (98-100). As white matter helps modulate the action potential distribution and is essential in relaying communication signals between brain regions, changes in white matter are predictors of cerebral atrophy and cognitive decline (101). The ophthalmic phenotype likely extends beyond the eye impairment and comes from a combination of optic atrophy, white matter loss and neuronal degeneration of the calcarine cortex, the primary visual cortex in the brain (102). Decreased visual acuity and cortical blindness was also reported in galactosialidosis patients, with cortical neurons filled with lipofuscin granules and degenerated neurons in the calcarine cortex, while the neurons in the brain stem, midbrain, cerebellum and spinal cord showing accumulation of substrates (103). Sialidosis type I patients showed no abnormalities in the neurons in the substantia nigra, cerebellum and brainstem (104), which are brain regions that control fine motor movement and balance (105). In type II sialidosis, a common neuropathology is the occurrence of hydrocephalus caused by the accumulation of cerebrospinal fluids in the ventricle of the brain, isolated ascites and hydrops fetalis (77). Furthermore, extensive storage was found in the epithelial cells of the choroid plexus and endothelial cells of the ependymal layer in murine models of sialidosis while vacuolated neurons and activated microglial cells were also detected throughout the parenchyma of the brain (106).

Interestingly sialidosis type II patients show also defects in hematopoiesis and the presence of foamy cells and vacuolated lymphocytes in the bone marrow (79, 82, 107). A routine blood test for an eight-month-old type II patient detected anemia and thrombocytopenia with low hemoglobin (Hb 8.2 g/dl; normal range for 8 months old infant is 9.5-14 g/dl) and platelets (73000/ $\mu$ L; normal range is 250,000-450,000/ $\mu$ L), hypoalbuminemia (29 g/L; normal range is 34-54 g/L) (82).

#### 1.4 Treatment of lysosomal storage diseases

Over the past two decades, different approaches have been introduced for the treatment of LSD. Among the options currently used in clinical practice, the most broadly used is enzyme replacement therapy (ERT), such as Gaucher disease (GD) (108), Fabry disease (109), mucopolysaccharidosis I, II, IVA and VI (110), and Pompe's disease patients (111). ERT

involves an infusion of the recombinant enzymes produced by cultured human or mammalian cells to restore enzyme deficiency and catabolize accumulated substrates. However, the availability of enzymes varies in different tissues due to the half-life of recombinant enzyme. For example, rhPPCA ERT in galactosialidosis mouse model demonstrated half-life between 10-23 hours of enzymes in the liver, spleen, kidney, and lung tissue, while less penetrable tissues like the brain and heart have basal expression levels of CTSA (112). After long-term treatment of 8 weeks, CTSA in the kidney and brain saw an increase of 19% and 14% respectively with normalization of NEU1 activity (112). A limitation of ERT is that the systemic infusion is unable to treat neuropathic LSD due to the presence of the blood-brain barrier (BBB) (113). However, there exists a narrow developmental window where the BBB is permeable between embryonic day 13.5 to 15.5 (E13.5-E15.5) (114). Hence, in utero ERT is ideal for LSD diagnosed prenatally and corrects pathology before irreversible organ damage. LSD with prenatal manifestations like Infantile-onset Pompe's disease present with hypertrophic cardiomyopathy have a poor outlook at birth and typically die by 2 years of age. However, with in utero administration of  $\alpha$ -glucosidase alfa (20 mg per kg of estimated fetal weight) through the umbilical vein, infants have a normal cardiac and motor function and are meeting developmental milestones (115). Another clinically approved method is substrate reduction therapy (SRT), where lysosomal storage of undigested substrates is prevented by inhibiting the enzymes involved in their biosynthesis. The inhibitor of glucosylceramide synthase, Miglustat is used for the treatment of both GM1 gangliosidosis (116) and non-neuropathic Gaucher patients (117).

Hematopoietic stem/progenitor cell (HSPC) transplantation from healthy donors to LSD patients corrects the enzyme defect in hematopoietic stem cells (HSC) which then differentiates into lymphoid and myeloid lineages. These cells then migrate to various organs and correct the stored substrates through secretion of the enzyme and cross-correction of other tissue cells. Importantly, donor-derived monocytes are also capable of crossing the BBB and differentiating into microglial cells, thus ameliorating neuropathology (118, 119). This approach is currently the treatment of choice for neuropathic disorder patients. However, allogeneic transplantation carries with it a high risk of immune rejection and a matching donor is not always possible due to the demands for early intervention in LSD (120). Besides, this approach did not show efficacy for LSD (including MPSIII), where the defective enzyme is secreted at a low level or is unable to diffuse between cells. Although, direct delivery of gene therapy to the brain has shown good efficacy in MPS IIIB mouse and MPS I dog (121, 122). However, diffusion of the

adeno-associated virus (AAV) vector, which is commonly used in these protocols, is limited to near the site of injection (121, 123). Beside the potential immune rejection, the long-term consequences of stereotaxic injection of AAV are not well studied. Autologous lentivirus (LV)-mediated gene correction of HSPC followed by their transplantation, can treat neurological LSD by soluble enzymes secreted in exosomes from HSPC-derived brain microglia and macrophages (119, 124-128). In neuropathic LSD, cytokines and chemokines generated from activated macrophages/microglia and astrocytes, stimulate trans-endothelial migration of monocytes from the blood into the parenchyma to sites of damage, where they secrete cytotoxic pro-inflammatory cytokines, leading to further damage and cell death. However, gene-corrected HPSC-derived macrophages gain the ability to cross-correct other cells in the CNS and catabolize stored substrates. This approach improves or completely treats the diseases in several LSD models including the MPS IIIA mouse (124). For example, Metachromatic Leukodystrophy (MLD) clinical trials showed prevention of disease onset in patients pre-symptomatic at the time of treatment (126, 128). As a result, HSPC-LV therapy for infantile MLD patients (Libmeldy™) has been approved for clinical use in Europe. Clinical trials for presymptomatic MPSIIIA patients are currently in progress in the Manchester Hospital, UK, where the first treated patients showed a supraphysiologic SGSH activity in leukocytes and plasma, as well as >90% reduction of HS levels in biological fluids over the baseline, and the early neurocognitive data are strongly suggestive of neurological correction (Dr. S. Johns, WORLD Symposium on LSD, Orlando, Feb. 2023). Unfortunately, the treatment comes with a high cost (€2,000,000 per patient with Libmeldy™) estimated to over-stretch the public healthcare system. Besides, treated MLD patients continued to decline and die despite showing normal levels of the therapeutic enzyme. HSPC transplantation has been also performed for cystinosis patients who without the regular use of cysteamine show an average life expectancy of 28 years and suffer from neuromuscular, renal complications and intestinal damage (129). In the murine model of cystinosis treatment with genetically modified autologous HSPC reduced cystine content in all studied tissues and improved renal function (130). This demonstrated that gene-modified HSPC carrying a normal, healthy copy of the gene allows for supraphysiologic expression of enzymes that could treat nephropathic LSD.

Treatment for sialidosis is not currently available for human patients. However, it has been attempted in animal models of the disease with variable outcomes. ERT with a recombinant NEU1 enzyme purified from insect cells was attempted in an animal model of sialidosis but resulted in severe immune response after 2 weeks of treatment (131). In contrast,

galactosialidosis (CTSA KO) mice that received short-term dual ERT of CTSA and NEU1 showed complete recovery in visceral organs, but not of the brain and only with minor correction in the kidneys (132). In addition to general limitations of ERT, such as a need for frequent life-long infusions and lack of tissue specificity, there are additional constraints for NEU1 which requires CTSA for stabilizing its enzymatic function and targeting to the lysosomes. This limits the ability of the NEU1 enzyme to reach different organs and hence limited efficacy to correct the pathology. To overcome these issues, gene therapy with AAV9-mediated overexpression of CTSA was tested in a sialidosis type I mouse model and found increased CTSA and NEU1 enzyme activity in the liver, bone marrow, kidney, spleen, heart, lung and muscle but not in the brain (133). Moreover, kidney histopathology showed minor correction, with lysosomal storage in the glomeruli and sialylated oligosaccharides in the urine (133).

Allogenic hematopoietic cell transplantation (HCT) was attempted in a female sialidosis type I patient with myoclonus ataxia, seizures, and rapid loss of motor control, who was also walker-dependent by 20 years of age (97). Despite high levels of hematopoietic engraftment of CD15<sup>+</sup> (68%) and CD3<sup>+</sup> (>90%) which was sustained for eleven years post-HCT, cognitive function and motor control rapidly deteriorated from three years post-HCT (97). In another report, an allogenic bone marrow transplant was performed on a 9-month-old, type II female sialidosis patient who presented with edema, hepatosplenomegaly, hypotonia, dysostosis multiplex and urinary oligosaccharidosis with progressive kidney dysfunction (89). Following renal failure, a cadaver kidney transplant was performed seven years post-HCT, but at 11-years-old her general condition had deteriorated with psychomotor retardation (89). On the other hand, bone marrow transplantation in a sialidosis mouse model was also attempted and found consistent short-term engraftment (10 days post-transplant) but decreased 16 days post-transplant (134), suggesting an association in NEU1 deficiency in bone marrow retention. There were decreased levels of VCAM-1 in *Neu1* deficiency mouse bone marrow extracellular fluid which is needed for homing and retention of bone marrow cells (134).

## 1.5 Glycoconjugates

Glycoconjugates are molecules containing glycan chains of varying sequences that are linked to lipids or proteins forming glycoproteins and glycolipids. In eukaryotic cells, glycoconjugates are mainly found on the outer surface and the inner surface of organelles of the endo-lysosomal pathway. These glycoconjugates can also be secreted. The N-linked glycans are formed by the attachment of N-acetylglucosamine (GlcNAc) to the nitrogen atom of asparagine (Asn) residue

of the Asn-X-Ser/Thr motif and generally contain a core glycan of two GlcNAc and three mannose residues (135). N-linked glycans are highly conserved in all eukaryotes. Their synthesis involves the production of a dolichol-linked lipid precursor and the transfer of the glycan bloc to the peptide with subsequent processing and modification of the glycans followed by folding and trafficking of the formed glycoprotein (Figure 1.3) (135). Three major types of glycans are high mannose, complex and hybrid oligosaccharide (Figure 1.3) (136), which are additionally modified through galactosylation, mannosylation, fucosylation and sialylation to form these final structures.

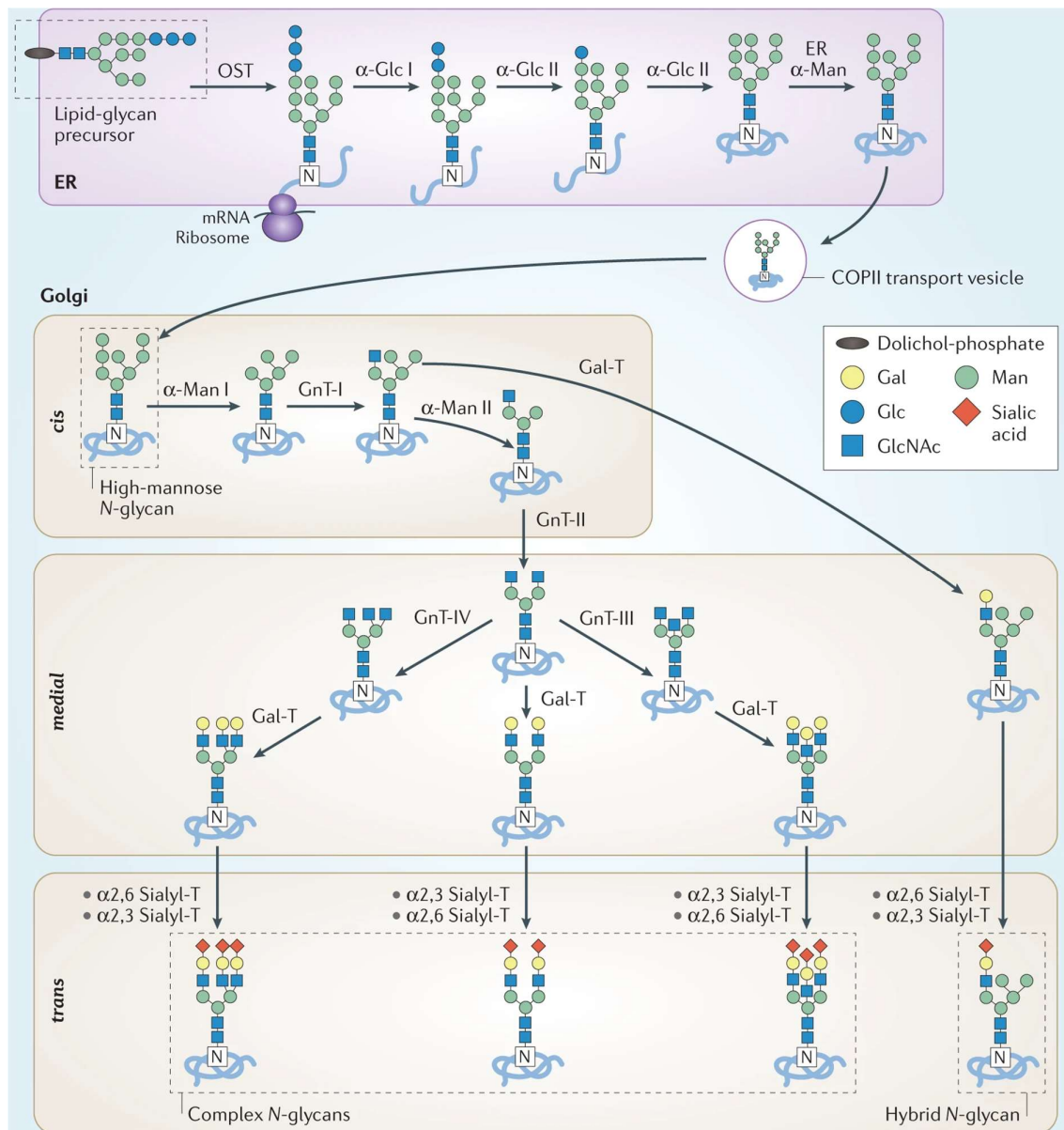


**Figure 1.3: N-glycan synthesis in humans consists of three final structures of high-mannose, hybrid and complex N-glycans (135). [Reproduced with permission from the publisher]**

In contrast, O-glycans are more diverse in terms of their length, composition and position in glycoproteins, although the biosynthesis is simpler than N-linked glycans and does not require the lipid precursor for transfer to protein. O-glycans were first identified and studied in mucins, one of the major secretory and extracellular proteins on endothelial surfaces of intestine and lung alveoli (135). The synthesis of O-glycan was initiated with the addition of a monosaccharide GlcNAc or N-acetylgalactosamine (GalNAc) attached to the oxygen atom of

Ser/Thr residues. GalNAc-linked glycans, also known as mucin type O-glycans consist of six major basic core structures designated core 1-4 attached to the terminal GalNAc (Tn) and sialyl-Tn antigen (137). In mammalian tissues, synthesis of mucin-type O-glycans begins with a single GalNAc residue attached to Ser/Thr residues initiated by GalNAc transferase (GALNTs), which is then extended in the Golgi with galactose, fucose or sialic acids by different glycosyltransferase (136). Unlike mucin-type O-glycans, O-GlcNAc linkage is dynamically added and removed by O-GlcNAc transferases (OGTs) and O-GlcNAcases (OGAs) (137, 138).

Meanwhile, glycolipids are formed by the attachment of sugars to a lipid component such as glycerol, polyisoprenyl pyrophosphate, fatty acid ester or sphingolipids (139). Glycosphingolipids (GSLs) in mammalian tissues include membrane phospholipids sphingomyelin and sphingosine-1-phosphate and are essential in the regulation of cell proliferation and cell differentiation of neurons (140).

#### 1.5.1 Lectins

Lectins were isolated from plants that recognize and bind to specific carbohydrate residues. These lectins are classified based on the binding specificity and used as a tool to probe for glycans structures on tissues and cells to characterize glycoconjugates. Some examples of plant lectins include R-type lectins (isolated from *Ricinus communis*) that recognize Gal and GalNAc structures and L-type lectins (from leguminous plants) that bind to mannose (141). L-type lectins such as Concanavalin A (ConA), a lectin isolated from Jack bean seeds were used as determinants of the human ABO blood group due to their haemagglutinin properties (142). Furthermore, R-type lectins such as *Ricinus communis* agglutinin (RCA-1 and II), *Sambucus nigra* agglutinin (SNA) and *Maackia amurensis* agglutinin (MAA I and II) contain a carbohydrate recognition domain (CRD) and are used in the diagnosis of cancer (143).

#### 1.5.2 Microbial lectins

Lectins play a role in modulating immune response during host-pathogen interaction. Immune responses are first initiated by lectin-glycan interaction on immune cells which triggers a signaling cascade that activates or suppresses the inflammatory responses. For example, haemagglutinin (HA) is a sialic acid-binding lectin found in human influenza virus A that exclusively targets  $\alpha$ -Neu5Ac-(2-3)-Gal of human tracheal cells (144). Other than viral glycan-binding protein, bacterial glycan-binding protein known as adhesin is present on the surface of the fimbriae or pili of microorganisms to attach to host cells. For example, the Hsa adhesin of

*Streptococcus gordonii* DL1 binds strongly to the terminal sialic acid of the host glycoprotein and contributes to the pathogenicity of oral infection (145). While, bacterial toxin such as Shiga toxins (Stx1 and Stx2) produced by *Escherichia coli* are capable of binding to glycolipid Gb3 in host cells causing Haemolytic Uremic syndrome (HUS) (146).

### 1.5.3 Animal lectins

Animal lectins are differentiated into C-, P-, S- and I-type lectins, each with their specific function. For example, C-type lectins (selectins) are a family of calcium-dependent glycan-binding lectins and are described in bacterial adhesion and pathogen recognition (147). The selectin members consist of P-selectin, E-selectin and L-selectin and are expressed on activated platelets, endothelial cells and leucocytes respectively (148). Selectins share a common ligand with Lewis antigens, a series of carbohydrates with  $\alpha$ 2-3 linked sialic acid attached to fucosylated core structure, such as sialyl Lewis x (sLe<sup>x</sup>) (NeuAc  $\alpha$ 2-3 Gal  $\beta$ 1-4 [Fuc  $\alpha$ 1-3] GlcNAc) and sialyl Lewis a (sLe<sup>a</sup>) (Neu5Ac  $\alpha$ 2-3 Gal  $\beta$ 1-4 [Fuc  $\alpha$ 1-4] GlcNAc) (149). Furthermore, these Lewis antigens are expressed on the surface of cancer cells and facilitate tumor progression and metastasis by interacting with selectins on endothelium, for example, in non-small cell lung cancer (NSCLC) (150), breast cancer (151) and colorectal cancer (152).

Lectins are essential in the regulation of protein synthesis and trafficking. Beginning with the synthesis of new proteins in the ER, resident lectin chaperones calreticulin and calnexin in the ER ensure the proper folding of N-glycosylated proteins (153). Glucosidase I/II trimmed terminal glucose residues off proteins which exposes the monoglucosylated form that binds to the P-domain of calreticulin or calnexin to promote protein folding and maturation. P-type lectin MPR specifically recognizes M6P signals and facilitates the intracellular transport of lysosomal enzymes from the Golgi to lysosomes (154).

S-lectins are characterized by their S-carbohydrate recognition domains (S-CRD) with two  $\beta$ -sheets folded into a sandwich structure with multiple glycan-binding sites specific to  $\beta$ -galactosides (155). The S-type lectin is also known as galectin, where CRD of different galectin have diverse amino acid sequences allowing for the recognition and binding of different glycans (156). For example, galectin-3 drives oligodendrocyte differentiation while galectin-1 and -3 are involved in the activation of astrocytes and microglia (157).

Lastly, the I-type lectins possess an immunoglobulin (Ig)-like domain that recognizes specific sialic acid. These I-type lectins are also otherwise known as sialic acid-binding immunoglobulin or siglecs that are expressed by cells of the immune system. They are divided

into two categories based on sequence similarity and evolutionary conservation, one subset includes sialoadhesin (Siglecs-1), CD22 (Siglecs-2), myelin associate glycoprotein (MAG, Siglecs 4) and CD33 (Siglecs-3) (158). Siglecs are expressed on specific cell types, namely Siglec-1 are found on tissue macrophages and circulating monocytes (159), Siglec-2 is expressed on B-cells (160), and MAG/Siglec-4 is found on glial cells (161), while Siglec-3 are more widely found in lymphoid cells such as T cell and Natural-killer (NK) cells (162). Siglecs are essential in the regulation of immune response, for example, siglecs-2 found on B-cells are responsible for the B cell fate in response to antigen stimulation. For instance, Siglec-2 deficient mice not only show reduced B-cell in the bone marrow due to induced apoptosis and therefore reduced survival, but also impaired T-cell independent immune response (160). Moreover, cancers with altered sialic acids are known to evade recognition by immune cells. For example, hypersialylated cancer cells are primed for recognition by siglecs on T-cells, however, once bound to Siglec-3, -7 and -9, cancer sialoglycans interfere with cytotoxic T cells and NK cells to prevent activation and eradication (163, 164).

## 1.6 Sialic acids

Sialic acids (Sia) are a family of negatively charged, nine-carbon acidic sugars that are present at the terminal ends of glycan chains of glycoproteins and glycolipids at the cell surface and on secreted proteins (165). These sialylated glycoconjugates form a diverse surface glycan coat, known as glycocalyx, that can be visualized as an electron dense layer on the surface of organelles and plasma membrane (166). This complex cell surface structure was also described as a “sialome”, which can be separated into five distinct levels. The first level consists of core sialic acid structures which are attached by different Sia linkages (second level) to the underlying glycan chains (third level), forming the different glycan classes (fourth level), finally appearing as distinct organization of sugar patches on the surface of the membrane (level 5) (Figure 1.4) (167).

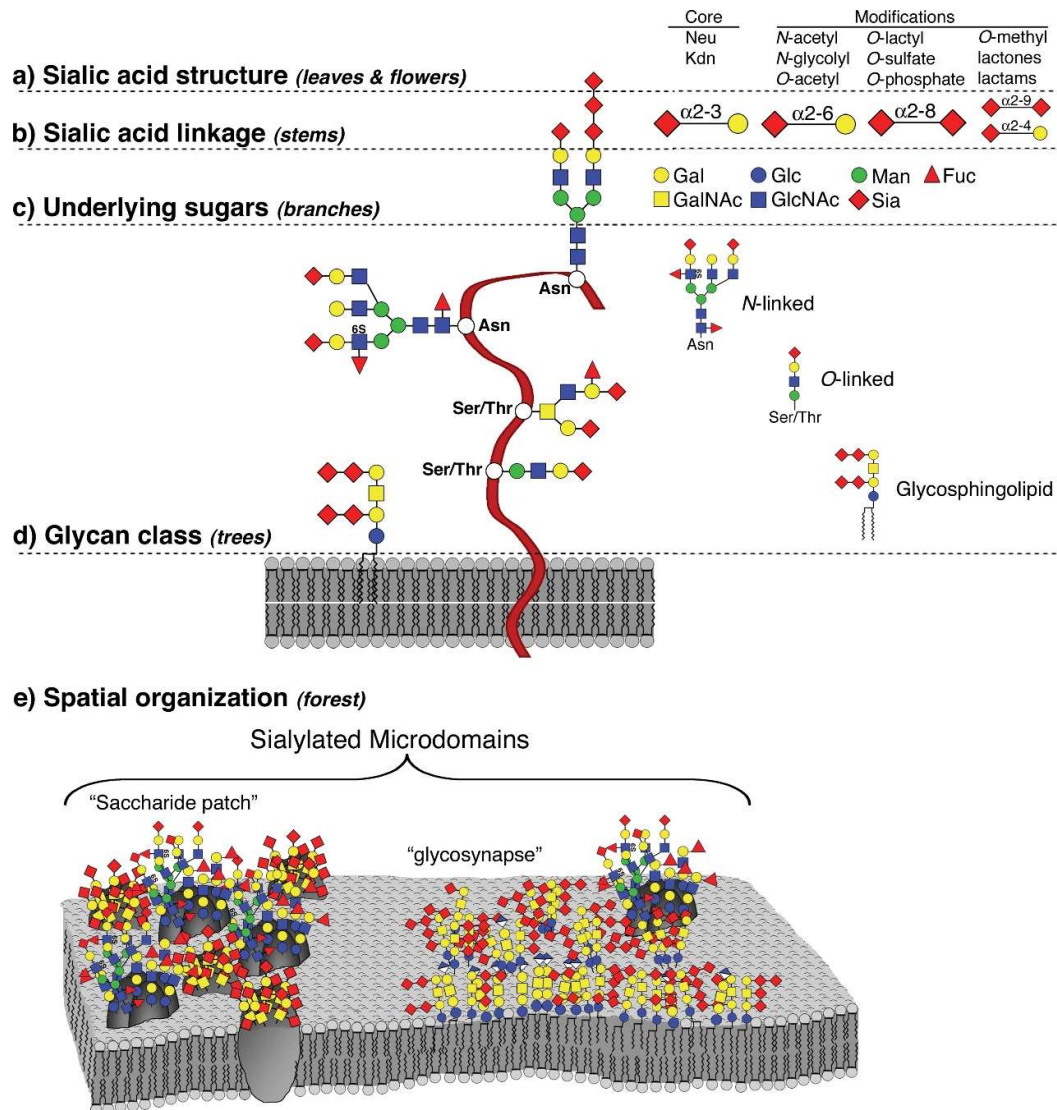


**Figure 1.4: The sialome presented at different levels of complexity (167). [Reproduced with permission from the publisher]**

### 1.6.1 Synthesis of sialic acids

Sia biosynthesis is derived from glucose metabolism. First, uridine diphosphate N-acetylglucosamine (UDP-GlcNAc), a precursor for Neu5Ac, is produced from glucose. Then, the bifunctional enzyme UDP-GlcNAc 2-epimerase/ManNAc kinase (GNE) converts UDP-GlcNAc into N-Acetylmannosamine (ManNAc) and further to ManNAc-6-phosphate. Subsequently, the N-acetylneuraminate synthase (NANS) is required to convert ManNAc-6-phosphate into Neu5Ac-9-phosphate that is dephosphorylated by Neu5Ac-9-P-phosphatase (NANP) to produce Neu5Ac. Neu5Ac is conjugated with cytidine monophosphate (CMP) by the CMP sialic acid synthase (CMAS) in the nucleus before its transport into the Golgi

apparatus through SLC35A1, a CMP-sialic acid transporter whose cytosolic level regulates Sia synthesis by inhibiting GNE enzyme via a negative feedback loop. In the Golgi, 20 sialyltransferase isoenzymes link sialic acid to glycans. Sia is cleaved from sialoglycans either at the cell surface or in the endolysosomal compartment through the action of sialidases (neuraminidases) represented in mammals by four isoenzymes (NEU1-NEU4). Then the lysosomal pool of Sia is relocated to the cytosol by sialin transporter (SLC17A5) followed either by recycling of Sia in the biosynthesis, or by its degradation into ManNAc and pyruvate by the NPL (168-170).

### 1.6.2 Function of sialic acids

Of the fifty structurally different sialic acids found in nature, the three most abundant ones are N-acetylneuraminic acid (Neu5Ac), N-glycolylneuraminic acid (Neu5Gc) and O-acetylated derivatives of neuraminic acids (149). Two main types of sialic acid found in mammalian tissues are Neu5Ac and Neu5GC. The conversion of CMP-Neu5Ac into CMP-Neu5Gc by cytosolic CMP-Neu5Ac hydroxylase (CMAH) was thought to be the major source of this metabolite in animal tissues (171), with genetic evidence that Neu5Gc is directly used for the synthesis of CMP-Neu5Gc. Neu5Gc is not produced in humans due to a genetic variant that inactivates the *CMAH* gene (172). However, Neu5Gc has been found in glycoconjugates on the cell surface of human tissues (173, 174) and is likely derived from the consumption of animal products, such as red meat and milk (175-178). However, trace amounts of Neu5Gc cause the production of autoreactive antibodies resulting in chronic inflammation (179, 180).

Sialic acids are the outermost monosaccharide units of glycan chains in glycoproteins and glycolipids and are involved in cell-cell communication, cell migration and adhesion. Sia serves as recognition sites by lectins but can also shield receptors from selectins and Siglecs which play major roles in infection and disease progression (181). Hence, sialic acids are used by bacterial, pathogen and cancer cells to escape the host immune response (182). Sialic acids on the cell surface are recognized by Siglecs-expressing cells which respond by inhibiting immune cell activation. Whereas the desialylation of receptors activates the immune response for the removal of protein aggregates or pathogens. For example, in the CNS, immune-activated microglia increase their surface desialylation which stimulates phagocytosis (183). Sialic acid present on the surface of cells helps maintain the structural integrity and function, for example, desialylation of pulmonary endothelium disrupts the cell-cell and cell-matrix adhesions contributing to the dysfunction of endothelial barrier integrity (184). In the kidneys,

sialic acid is found on all cell surfaces throughout the renal structures especially the podocytes and GBM which forms the filtration barrier (185).

### 1.6.3 Polysialic acid

Polysialic acid (PSA) is a long polymer of  $\alpha$ 2,8-linked Sia that is found on N- and O-linked glycoproteins such as Neural cell adhesion molecule (NCAM) and Synaptic cell adhesion molecule (SynCAM) in the CNS (186). Synthesis of PSA is mediated by ST8SIA2 and ST8SIA4 polysialyltransferases (PolySTs) with elongation of the sialic acid chain added on by  $\alpha$ 2-3 or  $\alpha$ 2-6 to the penultimate sugar (187). Due to their bulky conformation and being electronegatively charged, PSA only acts as a spacer between cells. In neurons, PSA-NCAM facilitates adhesion, signaling and transportation of synaptic vesicles, and is necessary for maintaining synaptic plasticity (188, 189). Hence, the dysregulation of PSA synthesis has been associated with neurodegenerative diseases such as AD and PD (190, 191). In addition, PSA has an immune modulatory function, for example, polysialylated neuropilin (NRP2) of dendritic cells helps the migration and maturation of dendritic cells and facilitates the proliferation of active T-lymphocytes (192). Similarly, innate immunity in the CNS is facilitated by resident microglia that generates anti-inflammatory and immunosuppressive signals to maintain homeostasis. For example, traumatic brain injury-induced activation leads to the accumulation of PSA in microglia which is secreted in its fully activated state, while the introduction of exogenous PSA inhibits this response (193).

### 1.7 Neuraminidases

The enzymatic removal of terminal sialic acid from glycan chains is catalyzed by neuraminidases. There are four neuraminidases in mammalian tissues which have different tissue expression profiles and subcellular localization (194). NEU1 is located on the plasma membrane and in the lysosomes (195), NEU2 in the cytosol (196), and NEU3 in the lysosome and plasma membrane (197), while NEU4 is found in the lysosome and mitochondria (198). These enzymes have diverse but overlapping substrate specificity (199), with NEU1 active against sialylated glycopeptides and oligosaccharides, NEU3 preferring substrates with a hydrophobic aglycone such as gangliosides (200), while NEU2 and NEU4 show a broader substrate specificity and are active against oligosaccharides, glycoproteins and gangliosides (201, 202). These enzymes also discriminate against different Sia linkages, with NEU1 and NEU3 preferring  $\alpha$ 2,6- Sia linkages over  $\alpha$ 2,3- Sia linkages, NEU2 having no activity towards  $\alpha$ 2,6- Sia linkages, NEU3 hydrolyses  $\alpha$ 2,8, and NEU1 and NEU4 cleaves  $\alpha$ 4,8- Sia (194, 199, 201, 203).

### 1.7.1 Neuraminidase 1

The *NEU1* gene encoding human neuraminidase 1 is located on chromosome 6 (6p21) in proximity to the Human Leucocyte Antigen (*HLA*) gene (204). Murine *Neu1* is similarly mapped to the mouse major histocompatibility complex locus on the mouse chromosome 17 (205). NEU1 is expressed in all tissues with the highest expression in the kidneys and at varying levels in other tissues and organs of animal models (106), which was similarly confirmed by northern blot of *NEU1*, *NEU3* and *NEU4* in human tissues (198). In mammalian tissues, NEU1 is found in the lysosomes in a multienzyme complex together with a carboxypeptidase, CTSA and  $\beta$ -galactosidase (74). It was reported that NEU1 is poorly mannose-6-phosphorylated, with CTSA necessary for transport to the lysosomes (74). In contrast, CTSA was also reported to act as a molecular chaperone by stabilizing the enzymatically active conformation of NEU1 and protecting it from lysosomal degradation (74, 206). The genetic deficiency of NEU1 enzyme causes sialidosis, while the genetic deficiency of CTSA causes the secondary deficiency of NEU1 and  $\beta$ -galactosidase and the lysosomal storage disease galactosialidosis (207). As NEU1 prefers sialylated oligosaccharides and glycopeptides, these metabolites are found stored in cells and secreted in the urine of sialidosis patients (208, 209). Accumulation of gangliosides GM3 and GD3 was also reported in visceral organs (but not in the brain) of sialidosis patients, however, these lipids could represent secondary storage materials (210).

In addition, NEU1 is involved with the cell signaling on the plasma membrane, for example, the desialylation and activation of the insulin receptor kinase (IRK) on the cell surface (211, 212). It was reported that NEU1-deficient mice placed on high-fat diet developed hyperglycemia and insulin resistance. NEU1 also has immunomodulatory roles through the desialylation of Fc receptors for immunoglobulin G (Fc $\gamma$ R). For example, a mouse model with NEU1 deficiency showed hypersialylation of Fc $\gamma$ R and reduced phagocytic capacity of macrophages and dendritic cells (213). Moreover, suppression of NEU1 in macrophages reduced phagocytosis of bacteria and IL-1b, IL-6 and TNF- $\alpha$  cytokine production, while differentiation of circulating monocytes into macrophages triggered an increase of endogenous *Neu1* mRNA by 5-fold (214). Similar findings reported the activation of T-lymphocytes and immune cell recruitment dependent on NEU1, where partial deficiency of NEU1 in SM/J mice results in the accumulation of surface Sia on T-lymphocytes and impaired immune response (215). Further reports found that increased NEU1 but not NEU3 levels were found in activated T-cells, while inhibition of NEU1 in T-cells reduces IFN- $\gamma$  (216), a cytokine necessary for the activation of macrophage. Similarly, under LPS-induced inflammatory response, NEU1

formed a complex with Toll-like receptor 4 (TLR4) on naïve macrophage with the secretion of pro-inflammatory cytokines (217), while seeing reduced Sia in brain glycoproteins and increased *Neu1* mRNA expression in the cerebral cortex (218).

#### 1.7.2 Neuraminidase 2

NEU2 was first identified in the cytosolic fraction of rat skeletal muscle (219). Biochemical characterization of this enzyme revealed that it strongly prefers alpha 2-3 sialyl linkages over 2-6 or 2-8 sialyl linkages and is active at pH 6.5-8.0 (220). The human *NEU2* encodes two exons and is mapped to chromosome 2q37.1 (221). NEU2 is active against a broad range of substrates, with several studies reporting its role in lipid metabolism and muscle fiber differentiation. For example, a *Neu2* knockout mouse model found an accumulation of sialylated glycoconjugates in the liver and lipids in the muscles (222). This enzyme also has immunomodulatory role, for example, hypersialylation of cancer cells is used as a mechanism to evade the immune system accompanied by low cytosolic NEU2 levels. Additionally, overexpression of NEU2 was found with upregulation of autophagy-related proteins and desialylation of Atg5, which enhances autophagosome formation and induces apoptosis of ovarian cancer cells (223).

#### 1.7.3 Neuraminidase 3

Human *NEU3* has four exons and maps to 11q13.5 with the highest expression levels found in skeletal muscle and testis (224). Human NEU3 levels are abundantly found in the pancreas, liver, heart, thymus and brain, but expressed at low levels in the kidney, lung, placenta and digestive organs (224). NEU3 enzyme prefers substrates with hydrophobic aglycones such as gangliosides GD3, GM3, GD1a and GD1b, and in the presence of GM2 activator protein, it also hydrolyses GM1 and GM2 gangliosides (225). However, no alterations in the ganglioside composition except for the increase in GM3 were found in the brain of *Neu3* knockout and *Neu3/Neu4* double knockout mice, suggesting that this ganglioside is the only biological glycolipid substrate of NEU3 enzyme (32). NEU3 enzyme is found in endosomal structures and on the cell surface as a peripheral membrane protein (197), where it modulates cell-surface biological processes. For example, NEU3 expression in Neuro2a, a neuroblast cell line induces neurite arborization (226). Other than the brain, GM3 ganglioside accumulation in adipocytes interferes with insulin receptor (IR) while simultaneously triggering TNF- $\alpha$ , which further suppresses IR and confers insulin resistance in type 2 diabetes (227, 228).

#### 1.7.4 Neuraminidase 4

*NEU4* gene is composed of four exons and maps to chromosome 2 (198). Human NEU4 has two isoforms, a short form with an M6P-tag targeted to the lysosomes (198), and a long form with an additional mitochondrial-targeting sequence at the N-terminus (229). NEU4 are expressed in a tissue-specific manner, with the short form predominantly in the liver and colon, while both isoforms were found in the kidney, brain and muscle (229). This enzyme has a broad substrate specificity against glycoproteins, oligosaccharides, sialylated glycolipids and artificial substrate 4-MU-NANA (198). Similarly, murine NEU4 has two isoforms, NEU4a and NEU4b, with NEU4b having a high enzymatic activity against GD3 while NEU4a is effective against PSA-NCAM (230). The expression of murine *Neu4* is the highest in the brain, where the levels rapidly increase from E18 to P49, suggesting a role in brain development (230). As NEU4 and NEU1 share many of the same substrates, it is expected that NEU4 would be able to substitute for NEU1 in the catabolism of sialylated glycoconjugates. For example, transfected NEU4 showed proper trafficking to the lysosomal compartment and cleared the accumulated substrates in the fibroblast of sialidosis patients (198). Similarly, a NEU4 deficient mouse model demonstrated a marked accumulation of gangliosides storage in the lung, spleen and brain, but an absence of pathology in the liver and kidney (231). Whereas, a double deficient *Neu4<sup>-/-</sup>/HexA<sup>-/-</sup>* mouse model with severe neuropathology, demonstrated epileptic seizures and rapid neuronal loss which was not exhibited by single knockout *HexA<sup>-/-</sup>* and *Neu4<sup>-/-</sup>* siblings, suggesting the contribution of another sialidase to the metabolic bypass (32, 232).

#### 1.8 Renal pathology in nephrosialidosis and chronic kidney diseases

In kidneys, sialic acids are enriched at the membranes of the glomerular endothelial cells and at the basement membrane, which supports the glomerular filtration barrier by maintaining structural integrity (185, 233). Aberrant glomerular sialylation caused by genetic or environmental factors is linked to multiple kidney diseases. For example, glomerular hyposialylation is observed in severe pneumococcal infections (234), as well as in ~50% of patients with a sialic acid transporter defect (235).

Induced kidney damage in animal models showed similar renal pathology, for example, mice exposed to pneumococcal neuraminidase (NanA) (236), puromycin amino nucleoside (PAN) (237) and polylysine (238). Kidney pathology in mouse models with PAN-induced damage resulted in the effacement of podocyte foot processes and proteinuria (185, 237). Meanwhile, mice with disrupted sialic acid metabolism such as *Cmas* (239), *Clgalt1* (240), *ST3GAL1* (241,

242) and *Gne* (243), share the same glomerular pathology. In mouse models with the genetic deficiency in N-acetylglucosamine 2-epimerase/N-acetylmannosamine kinase (GNE), the key enzyme of sialic acid synthesis, showed hyposialylation of the glomerular glycoproteins nephrin and podocalyxin (244). Meanwhile, treatment of *Gne*-deficient mice with the sialic acid precursor, ManNAc, improved the sialylation of glomerular glycoproteins and ameliorated glomerulopathy (244). Several murine models of CKD with significant changes in sialylation of kidney proteins also observed reduced renal functions, for example, albuminuria and proximal tubule alterations (245).

A subset of type II patients exhibited severe nephrotic syndrome, which was described as nephrosialidosis (79, 83). Some pathological alterations in the glomeruli of nephrosialidosis patients include effacement of podocyte foot processes and the vacuolization of podocytes (80). These vacuoles contain accumulations of sialoglycoconjugates with  $\alpha$ -linked mannose, and *N*-acetylgalactosamine residues (246, 247), which were also released in the urine of sialidosis patients (80, 91) and *Neu1*-null mice (106).

The importance of protein glycosylation is highlighted by the existence of multiple diseases caused by aberrant glycosylation, which include congenital disorders, immunity and cancer (reviewed by Reily et al. 2019 (135)). Several diseases associated with the onset and progression of renal dysfunction are also connected with changes in protein glycosylation. O-glycosylation and N-glycosylation both contribute to sustaining glomerular function. For example, glycosylation of membrane proteins nephrin and podocalyxin is crucial for maintaining podocyte structure and function (135). Meanwhile, increased O-glycosylation of IgA1 in IgA nephropathy result in elevated levels of nephritogenic immune complex deposits in the mesangial cells leading to glomerular injury (248).

### 1.8.1 Glomerulopathy

CKD results in the gradual failure of kidney function which eventually leads to end-stage renal disease (ESRD). Major contributors to CKD are diabetic kidney diseases (DKD), inherited genetic diseases and autoimmune diseases. The shared traits of all CKD are poor filtration of the blood and excessive fluid and waste retention in the body and proteinuria. At early stages, CKD are diagnosed through measurements of the glomerular filtration rate (eGFR) and urinary-creatinine-albumin ratio (UACR) which assess the kidney filtration function.

### 1.8.1.1 Glomerular basement membrane

The nephron is the main blood filtration unit of the kidneys and consists of the glomerulus and a network of renal tubules that facilitate the reabsorption and concentration of filtrate before urine excretion. In the glomerulus, the filtration barrier is composed of three layers, the endothelial cells of the inner capillary layer, the GBM and the epithelial cells at the outermost layer (Figure 1.5) (249). Glomerulopathy, a generalized dysfunction of the glomerulus due to injury or dysfunction of the glomerular filtration barrier, podocytes, or the endothelium, eventually leads to proteinuria. Glomerulopathy can be categorized as glomerulonephritis, characterized by an inflammation of the glomeruli or glomerulosclerosis with the scarring of the glomeruli. Etiology of glomerulopathy can vary but results in similar pathological changes such as a structural thickening of the GBM, mesangial expansion, reduced podocyte counts and effaced podocyte foot processes such as seen in DKD patients (250, 251).

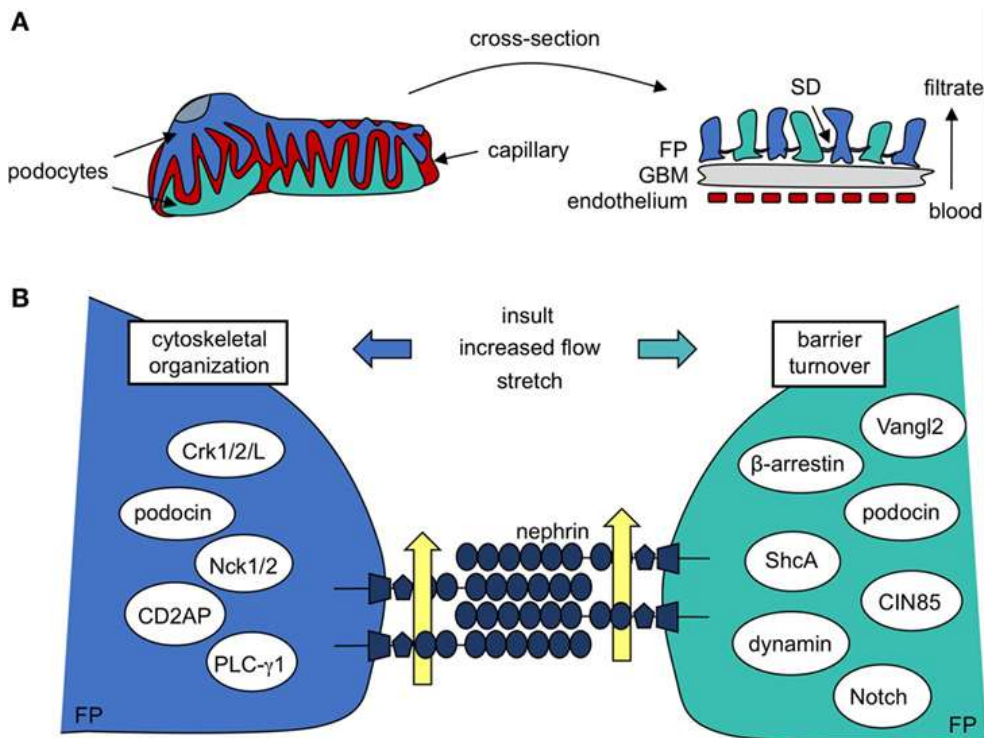


**Figure 1.5: Podocyte, glomerular basement membrane and endothelial cells makes up the glomerular filtration barrier in the glomerulus (249). [Reproduced with permission from the publisher]**

### 1.8.1.2 Podocytes

The podocytes are highly specialized epithelial cells that wrap around the glomerular capillary, with interdigitation of the foot processes of adjacent podocytes forming a slit diaphragm (SD)

that serves as a filtration sieve to retain large molecules and proteins (Figure 1.5). Membrane proteins such as nephrin and podocin are found solely in podocytes and are an integral part of the adhesion and endothelial scaffolding for structural maintenance of SD of interdigitating podocyte foot processes (249, 252). Other proteins such as TRPC6, CD2-associated (CD2AP) and podocalyxin are also essential for SD maintenance (44, 249) and podocyte morphogenesis (253). For example, in animal model with nephrin deficiency, diabetic nephropathy and FSGS patients, all found the loss-of-function of these membrane proteins resulting in podocyte injury (254).

#### *1.8.1.3 Mesangial cells*

Mesangial cells (MC) are specialized cells located in the mesangium of the glomerulus and attached to the GBM, and make up 30-40% of the glomerular cell population (255). They facilitate the capillary flow by altering ultrafiltration surface area through their contractile properties, clearing the glomerulus of protein aggregates and immune complexes with phagocytic and scavenging functions. Although the exact mechanism of how mesangial expansion causes kidney dysfunction is unknown, elevated inflammatory markers and renal fibrosis at the latter stages of CKD are detected by kidney biopsy and used to reliably distinguish between different causes of glomerulosclerosis. For example, in IgA nephropathy, deposits of immunoglobulins in the mesangium and expansion of mesangial cells are followed by excessive ECM synthesis and increased expression of inflammatory cytokines and growth factors (256). In the glomerulus, the glycocalyx layer consists of a network of glycoproteins, GAGs and proteoglycans with a net negative charge behaving as a charge-selective barrier. Different types of proteoglycans have been described and their involvement in filtration processes documented. For example, Agrin, type XVIII collagen and perlecan are prominently featured on the GBM, and heparan sulfate on podocytes maintains the SD of interdigitating podocyte foot processes (135, 257). Importantly, heparan sulfate loss was detected in chronic kidney diseases such as lupus nephritis and diabetic nephropathy (257).

#### *1.8.2 Tubulopathy*

Tubulopathy refers to inherited or acquired damage to the kidney renal tubules that disrupt their normal function. The proximal renal tubules are divided into three segments (S1, S2 and S3). The first segment (S1) consisting of the PCT is located after the glomeruli and gradually transitions to S2 and S3. These different segments of the proximal tubules have distinct ultra-structure profiles describing different brush border lengths, cell height and cytoplasmic density (Figure 1.6). The PCT is responsible for reabsorption of amino acids, glucose and the majority

of solute, where only 1% of the filter load is excreted in the urine (258). Additionally, the PCT also maintains the acid-base balance of the body through regulating  $\text{NaCl}$  and  $\text{NaHCO}_3$  transport (259).

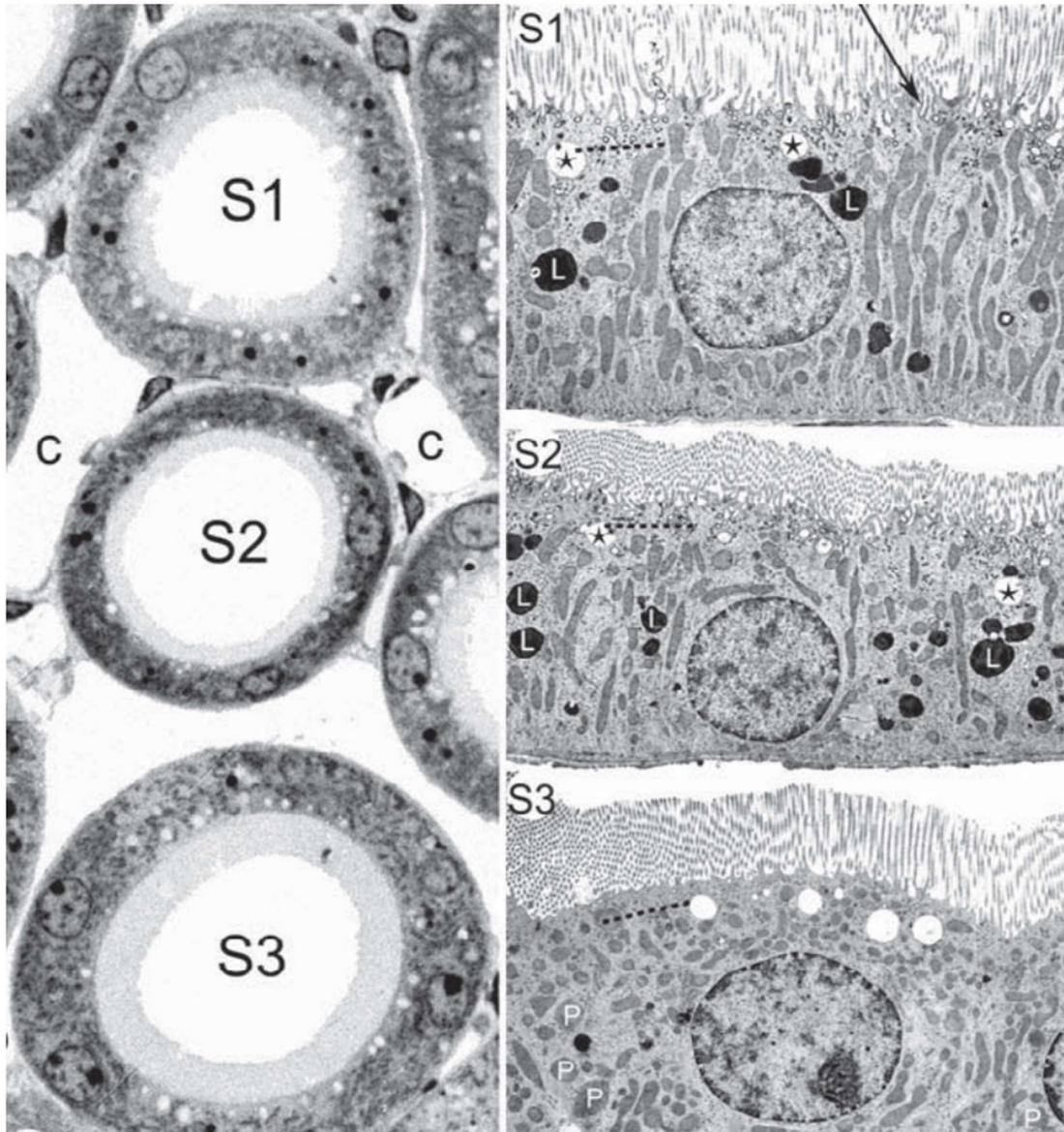


**Figure 1.6: Ultrastructure of S1, S2 and S3 of segment proximal tubules (260). [Reproduced with permission from the publisher]**

Differences in the outer diameter of proximal renal tubule cells describing brush border length, cell height and cytoplasmic density.

C= peritubular capillaries, \* = endosomes, L = lysosomes, P = peroxisomes

### *1.8.2.1 Proximal renal tubules*

In the event of glomerular damage causing the leakage of proteins and metabolites into the filtrate, these macromolecules are recovered by endocytic receptors present at the apical surface of the PRT. Megalin and cubilin are endocytic receptors ubiquitously expressed throughout all epithelial tissues including the brain, but they are prominently expressed at the PRT epithelia (261). Megalin, also known as low-density lipoprotein-related protein 2 (LRP2) and cubilin have many shared ligands and are considered to be scavenger receptors that facilitate the clearance of proteins including albumin, vitamin D binding protein (DBP), retinol-binding protein (RBP), lipoproteins, hormones and enzymes (261), some of which are LMWPs. For example, megalin genetic deficiency is found in Donnai-Barrow syndrome (also known as Faciooculoacousticorenal syndrome) which presents with proteinuria and excessive excretion of DBP and RBP in the urine (262).

Renal Fanconi syndrome consists of a group of disorders with generalized dysfunction of the PRT resulting in tubular proteinuria. This group of disorders displays defects in the endo-lysosomal pathways, including dysfunctional endocytic receptors, impaired endosomes and intracellular trafficking of receptors (263). As megalin is ubiquitously expressed in epithelial cells of multiple tissues, the disease also manifests with neuroanatomical changes of the forebrain and olfactory bulb, holoprosencephaly, microphthalmia and craniofacial dysmorphology (262, 264).

Features such as aminoaciduria and glycosuria are commonly seen in renal Fanconi syndrome due to the dysfunctional solute carrier of  $\text{Na}^+$  and  $\text{K}^+$  ATPase pump present on the apical surface of the proximal renal tubules. For example, a mutation in the proximal tubular sodium-phosphate transporter NaPi-IIa causes retention of the transporter in the cytoplasm instead of localizing on the plasma membrane (265). However, the secondary cause includes solute-carrier cotransporter mutation in inherited systemic diseases such as cystinosis (266).

### *1.8.2.2 Distal convoluted tubules*

The distal convoluted tubules are a short segment that lies downstream of the macula densa but before the collecting tubules. Its roles include modulating sodium chloride reabsorption, potassium secretion, calcium and magnesium handling. Although most of the absorption of  $\text{Na}^+$  and  $\text{Cl}^-$  and  $\text{K}^+$  secretion is handled by the PRT, distal tubules share this function (267). Because salt handling in the kidney directly regulates blood pressure, dysfunction in this segment results in hypertension (268). This salt-losing tubulopathy is commonly represented

in Gitelman syndrome, which is clinically diagnosed by having both hypomagnesemia and hypocalciuria as a result of loss of *SLC12A3* and *TRPM6*, encoding the receptors for NaCl and MgCl respectively in the distal convoluted tubule (269).

## 1.9 Rationale and objective

There is much we still need to understand about the pathophysiology of sialidosis to determine the underlying mechanism of renal pathology in nephrosialidosis patients. As sialidosis is an ultrarare disease with a combined prevalence of 1 per 5,000,000 live births with less than a hundred nephrosialidosis cases reported to date, animal models have become an essential tool for studying this disease. Our laboratory generated a mouse model of type II sialidosis (*Neu1<sup>ΔEx3</sup>* strain), developed by Pan *et al.* (2017) and characterized by Kho *et al.* in the current work (2023) which closely recapitulates the clinical symptoms reported in patients. The clinical phenotypes include a drastically shortened life span, loss of weight and smaller body size. The *Neu1<sup>ΔEx3</sup>* mouse model showed a full deficiency of NEU1 enzyme activity in all tissues, organomegaly, neuroinflammation, skeletal deformation and progressive renal dysfunction. Signs of urinary retention were observed as early as 4 months in males and 6 months in females, with increased albuminuria and decreased endocytic receptors on the epithelial cells surface of the proximal renal tubules.

Previous work identified severe pathological alterations in the glomeruli of nephrosialidosis patients, such as vacuolization of podocytes and effacement of the pedicels (80). These vacuoles also contained substrates with terminal sialic acid,  $\alpha$ -linked mannose, and N-acetylgalactosamine residues (246, 247), with sialylated oligosaccharides found in the urine of sialidosis patients (80, 91) and *Neu1*-null mice (106). This suggests the presence of a glomerular dysfunction in addition to tubular dysfunction resulting in poor reabsorption of solutes. Previous work has also demonstrated that NEU1 is present in lysosomes and on the cell surface, where it readily desialylates protein targets (201, 270). The nephropathic phenotype in mouse models and sialidosis patients suggests a glycosylation-dependent defects in both the glomeruli and proximal renal tubules. Therefore we hypothesize is that endocytic receptors that are present on the epithelial surface of the proximal renal tubule are targets of NEU1.

Therapeutic approaches such as AAV gene therapy and short-term ERT have been tested in animal models of sialidosis type I and galactosialidosis, but failed due to a poor expression of the enzymes in tissues and inability to penetrate organs such as the brain and kidneys (133). Alternatively, HSPC transplantation where HSPC-derived progeny cells replenish the resident macrophage population in different tissues following a myeloablative regimen. Published research has shown the distribution of HSPC progeny cells can vary vastly in different tissues,

(271). As such, our second hypothesis is that the HSPC-derived macrophages will migrate to the kidney to replace the resident macrophages, correct hypersialylation, reduce lysosomal accumulation and ameliorate renal dysfunction (272). We expect to see reduced levels of lysosomal biogenesis and inflammation and normalization of endocytic receptor at the apical surface of the PRT. Additionally, HSPC-derived macrophages and microglia are expected to cross the BBB to the brain to correct neuroinflammation and neurodegeneration (271). To prove the hypothesis, two specific objectives of my doctoral research project were defined as the study of glycosylation in the protein trafficking in the proximal renal tubules and its contribution to the progression of kidney dysfunction (Chapter 2, Kho *et al.*, 2023) and testing efficacy of allogenic HSPC transplantation to rescue renal dysfunction and neuroinflammation in sialidosis type II mouse model (Chapter 3).

## 1.10 References

1. Alberts B, et al., *Molecular Biology of the Cell 5th edition*. 2008, Garland Science: New York.
2. Ishida, Y., et al., *A model of lysosomal pH regulation*. J Gen Physiol, 2013. **141**(6): p. 705-20.
3. Braulke, T. and J.S. Bonifacino, *Sorting of lysosomal proteins*. Biochim Biophys Acta, 2009. **1793**(4): p. 605-14.
4. Alberts, B., et al., *Molecular Biology of the Cell*. 5th edition ed. 2008.
5. Canuel, M., et al., *Sortilin mediates the lysosomal targeting of cathepsins D and H*. Biochem Biophys Res Commun, 2008. **373**(2): p. 292-7.
6. Bonifacino, J.S. and L.M. Traub, *Signals for sorting of transmembrane proteins to endosomes and lysosomes*. Annu Rev Biochem, 2003. **72**: p. 395-447.
7. Yang, C. and X. Wang, *Lysosome biogenesis: Regulation and functions*. J Cell Biol, 2021. **220**(6).
8. Hu, Y.B., et al., *The endosomal-lysosomal system: from acidification and cargo sorting to neurodegeneration*. Transl Neurodegener, 2015. **4**: p. 18.
9. Parzych, K.R. and D.J. Klionsky, *An overview of autophagy: morphology, mechanism, and regulation*. Antioxid Redox Signal, 2014. **20**(3): p. 460-73.
10. Hurley, J.H. and L.N. Young, *Mechanisms of Autophagy Initiation*. Annu Rev Biochem, 2017. **86**: p. 225-244.
11. Runwal, G., et al., *LC3-positive structures are prominent in autophagy-deficient cells*. Sci Rep, 2019. **9**(1): p. 10147.
12. Zhang, W., et al., *Regulation of TFEB activity and its potential as a therapeutic target against kidney diseases*. Cell Death Discov, 2020. **6**: p. 32.
13. Napolitano, G. and A. Ballabio, *TFEB at a glance*. J Cell Sci, 2016. **129**(13): p. 2475-81.
14. Palmieri, M., et al., *mTORC1-independent TFEB activation via Akt inhibition promotes cellular clearance in neurodegenerative storage diseases*. Nat Commun, 2017. **8**: p. 14338.
15. Brown, R.A., et al., *mTOR hyperactivity mediates lysosomal dysfunction in Gaucher's disease iPSC-neuronal cells*. Dis Model Mech, 2019. **12**(10).
16. Meikle, P.J., et al., *Prevalence of lysosomal storage disorders*. JAMA, 1999. **281**(3): p. 249-54.
17. Pastores, G.M. and G.H. Maegawa, *Clinical neurogenetics: neuropathic lysosomal storage disorders*. Neurol Clin, 2013. **31**(4): p. 1051-71.
18. Sun, A., *Lysosomal storage disease overview*. Ann Transl Med, 2018. **6**(24): p. 476.
19. Lukong, K.E., et al., *Characterization of the sialidase molecular defects in sialidosis patients suggests the structural organization of the lysosomal multienzyme complex*. Hum Mol Genet, 2000. **9**(7): p. 1075-85.
20. Saftig, P. and J. Klumperman, *Lysosome biogenesis and lysosomal membrane proteins: trafficking meets function*. Nat Rev Mol Cell Biol, 2009. **10**(9): p. 623-35.
21. Sandhoff, K. and K. Harzer, *Gangliosides and gangliosidoses: principles of molecular and metabolic pathogenesis*. J Neurosci, 2013. **33**(25): p. 10195-208.
22. Liu, Y., et al., *Mouse model of GM2 activator deficiency manifests cerebellar pathology and motor impairment*. Proc Natl Acad Sci U S A, 1997. **94**(15): p. 8138-43.
23. Duraes, J., E. Salsano, and M.D.C. Macario, *Adult-Onset Krabbe Disease: The Importance of a Systematic Approach to Brain MRI Findings*. Neurol Clin Pract, 2021. **11**(1): p. e15-e17.
24. Orr, M.E. and S. Oddo, *Autophagic/lysosomal dysfunction in Alzheimer's disease*. Alzheimers Res Ther, 2013. **5**(5): p. 53.
25. Ohmi, K., et al., *Sanfilippo syndrome type B, a lysosomal storage disease, is also a tauopathy*. Proc Natl Acad Sci U S A, 2009. **106**(20): p. 8332-7.
26. Annunziata, I., et al., *Lysosomal NEU1 deficiency affects amyloid precursor protein levels and amyloid-beta secretion via deregulated lysosomal exocytosis*. Nat Commun, 2013. **4**: p. 2734.
27. Wong, K., et al., *Neuropathology provides clues to the pathophysiology of Gaucher disease*. Mol Genet Metab, 2004. **82**(3): p. 192-207.

28. Cullen, V., et al., *Acid beta-glucosidase mutants linked to Gaucher disease, Parkinson disease, and Lewy body dementia alter alpha-synuclein processing*. *Ann Neurol*, 2011. **69**(6): p. 940-53.
29. Sidransky, E., et al., *Multicenter analysis of glucocerebrosidase mutations in Parkinson's disease*. *N Engl J Med*, 2009. **361**(17): p. 1651-61.
30. Clark, L.N., et al., *Mutations in the glucocerebrosidase gene are associated with early-onset Parkinson disease*. *Neurology*, 2007. **69**(12): p. 1270-7.
31. Schnaar, R.L., R. Gerardy-Schahn, and H. Hildebrandt, *Sialic acids in the brain: gangliosides and polysialic acid in nervous system development, stability, disease, and regeneration*. *Physiol Rev*, 2014. **94**(2): p. 461-518.
32. Pan, X., et al., *Neuraminidases 3 and 4 regulate neuronal function by catabolizing brain gangliosides*. *FASEB J*, 2017. **31**(8): p. 3467-3483.
33. Yamano, T., et al., *Pathological study on a severe sialidosis (alpha-neuraminidase deficiency)*. *Acta Neuropathol*, 1986. **71**(3-4): p. 278-84.
34. Ziv, Y., et al., *Immune cells contribute to the maintenance of neurogenesis and spatial learning abilities in adulthood*. *Nat Neurosci*, 2006. **9**(2): p. 268-75.
35. Barrette, B., et al., *Requirement of myeloid cells for axon regeneration*. *J Neurosci*, 2008. **28**(38): p. 9363-76.
36. Leon-Rodriguez, A., et al., *Anxiety-like behavior and microglial activation in the amygdala after acute neuroinflammation induced by microbial neuraminidase*. *Sci Rep*, 2022. **12**(1): p. 11581.
37. Choi, S.S., et al., *Human astrocytes: secretome profiles of cytokines and chemokines*. *PLoS One*, 2014. **9**(4): p. e92325.
38. Vitner, E.B., et al., *Contribution of brain inflammation to neuronal cell death in neuronopathic forms of Gaucher's disease*. *Brain*, 2012. **135**(Pt 6): p. 1724-35.
39. Van Hoecke, L., et al., *Involvement of the Choroid Plexus in the Pathogenesis of Niemann-Pick Disease Type C*. *Front Cell Neurosci*, 2021. **15**: p. 757482.
40. Versele, R., et al., *TNF-alpha and IL-1beta Modulate Blood-Brain Barrier Permeability and Decrease Amyloid-beta Peptide Efflux in a Human Blood-Brain Barrier Model*. *Int J Mol Sci*, 2022. **23**(18).
41. Tansey, M.G., et al., *Inflammation and immune dysfunction in Parkinson disease*. *Nat Rev Immunol*, 2022. **22**(11): p. 657-673.
42. Rozenfeld, P. and S. Feriozzi, *Contribution of inflammatory pathways to Fabry disease pathogenesis*. *Mol Genet Metab*, 2017. **122**(3): p. 19-27.
43. Trauner, D.A., et al., *Neurological impairment in nephropathic cystinosis: motor coordination deficits*. *Pediatr Nephrol*, 2010. **25**(10): p. 2061-6.
44. Zhang, A. and S. Huang, *Progress in pathogenesis of proteinuria*. *Int J Nephrol*, 2012. **2012**: p. 314251.
45. Klootwijk, E.D., et al., *Renal Fanconi syndrome: taking a proximal look at the nephron*. *Nephrol Dial Transplant*, 2015. **30**(9): p. 1456-60.
46. Hara-Chikuma, M., et al., *Impaired acidification in early endosomes of CIC-5 deficient proximal tubule*. *Biochem Biophys Res Commun*, 2005. **329**(3): p. 941-6.
47. Christensen, E.I., et al., *Loss of chloride channel CIC-5 impairs endocytosis by defective trafficking of megalin and cubilin in kidney proximal tubules*. *Proc Natl Acad Sci U S A*, 2003. **100**(14): p. 8472-7.
48. Bhargava, P. and R.G. Schnellmann, *Mitochondrial energetics in the kidney*. *Nat Rev Nephrol*, 2017. **13**(10): p. 629-646.
49. Desmond, M.J., et al., *Tubular proteinuria in mice and humans lacking the intrinsic lysosomal protein SCARB2/Limp-2*. *Am J Physiol Renal Physiol*, 2011. **300**(6): p. F1437-47.
50. Schroder, J., et al., *Deficiency of the tetraspanin CD63 associated with kidney pathology but normal lysosomal function*. *Mol Cell Biol*, 2009. **29**(4): p. 1083-94.

51. Christensen, E.I., et al., *Distribution of alpha-galactosidase A in normal human kidney and renal accumulation and distribution of recombinant alpha-galactosidase A in Fabry mice*. J Am Soc Nephrol, 2007. **18**(3): p. 698-706.
52. Valbuena, C., et al., *Kidney biopsy findings in heterozygous Fabry disease females with early nephropathy*. Virchows Arch, 2008. **453**(4): p. 329-38.
53. Tagawa, A., et al., *Impaired Podocyte Autophagy Exacerbates Proteinuria in Diabetic Nephropathy*. Diabetes, 2016. **65**(3): p. 755-67.
54. Yamahara, K., et al., *Obesity-mediated autophagy insufficiency exacerbates proteinuria-induced tubulointerstitial lesions*. J Am Soc Nephrol, 2013. **24**(11): p. 1769-81.
55. Liu, W.J., et al., *Lysosome restoration to activate podocyte autophagy: a new therapeutic strategy for diabetic kidney disease*. Cell Death Dis, 2019. **10**(11): p. 806.
56. Sansanwal, P. and M.M. Sarwal, *p62/SQSTM1 prominently accumulates in renal proximal tubules in nephropathic cystinosis*. Pediatr Nephrol, 2012. **27**(11): p. 2137-2144.
57. Sansanwal, P., et al., *Mitochondrial autophagy promotes cellular injury in nephropathic cystinosis*. J Am Soc Nephrol, 2010. **21**(2): p. 272-83.
58. Chévrier, M., et al., *Autophagosome maturation is impaired in Fabry disease*. Autophagy, 2010. **6**(5): p. 589-99.
59. Zhang, Q., et al., *Circulating mitochondrial DAMPs cause inflammatory responses to injury*. Nature, 2010. **464**(7285): p. 104-107.
60. Bulow, R.D. and P. Boor, *Extracellular Matrix in Kidney Fibrosis: More Than Just a Scaffold*. J Histochem Cytochem, 2019. **67**(9): p. 643-661.
61. Isaka, Y., *Targeting TGF-beta Signaling in Kidney Fibrosis*. Int J Mol Sci, 2018. **19**(9).
62. Abrahamson, D.R., et al., *Cellular origins of type IV collagen networks in developing glomeruli*. J Am Soc Nephrol, 2009. **20**(7): p. 1471-9.
63. Holderied, A., et al., *Glomerular parietal epithelial cell activation induces collagen secretion and thickening of Bowman's capsule in diabetes*. Lab Invest, 2015. **95**(3): p. 273-82.
64. Canaud, G. and J.V. Bonventre, *Cell cycle arrest and the evolution of chronic kidney disease from acute kidney injury*. Nephrol Dial Transplant, 2015. **30**(4): p. 575-83.
65. Raggi, C., et al., *Dedifferentiation and aberrations of the endolysosomal compartment characterize the early stage of nephropathic cystinosis*. Hum Mol Genet, 2014. **23**(9): p. 2266-78.
66. Berquez, M., et al., *Lysosomal cystine export regulates mTORC1 signaling to guide kidney epithelial cell fate specialization*. Nat Commun, 2023. **14**(1): p. 3994.
67. Iwano, M., et al., *Evidence that fibroblasts derive from epithelium during tissue fibrosis*. J Clin Invest, 2002. **110**(3): p. 341-50.
68. Huang, R., P. Fu, and L. Ma, *Kidney fibrosis: from mechanisms to therapeutic medicines*. Signal Transduct Target Ther, 2023. **8**(1): p. 129.
69. Wickman, L., et al., *Podocyte Depletion in Thin GBM and Alport Syndrome*. PLoS One, 2016. **11**(5): p. e0155255.
70. Cocchiari, P., et al., *The Multifaceted Role of the Lysosomal Protease Cathepsins in Kidney Disease*. Front Cell Dev Biol, 2017. **5**: p. 114.
71. Petermann, I., et al., *Lysosomal, cytoskeletal, and metabolic alterations in cardiomyopathy of cathepsin L knockout mice*. FASEB J, 2006. **20**(8): p. 1266-8.
72. Moles, A., et al., *Cathepsins B and D drive hepatic stellate cell proliferation and promote their fibrogenic potential*. Hepatology, 2009. **49**(4): p. 1297-307.
73. Fox, C., et al., *Inhibition of lysosomal protease cathepsin D reduces renal fibrosis in murine chronic kidney disease*. Sci Rep, 2016. **6**: p. 20101.
74. Bonten, E.J., et al., *Heterodimerization of the sialidase NEU1 with the chaperone protective protein/cathepsin A prevents its premature oligomerization*. J Biol Chem, 2009. **284**(41): p. 28430-28441.

75. Seyrantepe, V., et al., *Molecular pathology of NEU1 gene in sialidosis*. Hum Mutat, 2003. **22**(5): p. 343-52.
76. d'Azzo, A., E. Machado, and I. Annunziata, *Pathogenesis, Emerging therapeutic targets and Treatment in Sialidosis*. Expert Opin Orphan Drugs, 2015. **3**(5): p. 491-504.
77. Tylki-Szymanska, A., A. Ługowska, and B. Czartoryska, *Neuraminidase deficiency presenting as a nephrosialidosis: The first case detected in Poland*. Pediatrics International, 1996. **38**(5): p. 529-532.
78. Arora, V., et al., *Sialidosis type II: Expansion of phenotypic spectrum and identification of a common mutation in seven patients*. Mol Genet Metab Rep, 2020. **22**: p. 100561.
79. Aylsworth, A.S., et al., *A severe infantile sialidosis: clinical, biochemical, and microscopic features*. J Pediatr, 1980. **96**(4): p. 662-8.
80. Chen, W., et al., *Histological studies of renal biopsy in a boy with nephrosialidosis*. Ultrastruct Pathol, 2011. **35**(4): p. 168-71.
81. Maroofian, R., et al., *Parental Whole-Exome Sequencing Enables Sialidosis Type II Diagnosis due to an NEU1 Missense Mutation as an Underlying Cause of Nephrotic Syndrome in the Child*. Kidney Int Rep, 2018. **3**(6): p. 1454-1463.
82. Tazi, K., et al., *Ascites in infantile onset type II Sialidosis*. JIMD Rep, 2022. **63**(4): p. 316-321.
83. Kelly, T.E. and G. Graetz, *Isolated acid neuraminidase deficiency: a distinct lysosomal storage disease*. Am J Med Genet, 1977. **1**(1): p. 31-46.
84. Roth, K.S., et al., *Acid alpha-neuraminidase deficiency: a nephropathic phenotype?* Clin Genet, 1988. **34**(3): p. 185-94.
85. Sperl, W., et al., *Nephrosis in two siblings with infantile sialic acid storage disease*. Eur J Pediatr, 1990. **149**(7): p. 477-82.
86. Sphranger, J., J. Gehler, and M. Cantz, *Mucopolipidosis I--a sialidosis*. Am J Med Genet, 1977. **1**(1): p. 21-9.
87. Laver, J., et al., *Infantile lethal neuraminidase deficiency (sialidosis)*. Clin Genet, 1983. **23**(2): p. 97-101.
88. Paschke, E., et al., *Infantile type of sialic acid storage disease with sialuria*. Clin Genet, 1986. **29**(5): p. 417-24.
89. Schiff, M., et al., *Long-term follow-up of metachronous marrow-kidney transplantation in severe type II sialidosis: what does success mean?* Nephrol Dial Transplant, 2005. **20**(11): p. 2563-5.
90. Itoh, K., et al., *Novel missense mutations in the human lysosomal sialidase gene in sialidosis patients and prediction of structural alterations of mutant enzymes*. J Hum Genet, 2002. **47**(1): p. 29-37.
91. Lowden, J.A. and J.S. O'Brien, *Sialidosis: a review of human neuraminidase deficiency*. Am J Hum Genet, 1979. **31**(1): p. 1-18.
92. Lv, R.J., et al., *Clinical and genetic characteristics of type I sialidosis patients in mainland China*. Ann Clin Transl Neurol, 2020. **7**(6): p. 911-923.
93. Emmady, P.D. and A.C. Anilkumar, *EEG Abnormal Waveforms*, in StatPearls. 2023: Treasure Island (FL).
94. Loughman, A., S.C. Bowden, and W.J. D'Souza, *A comprehensive assessment of cognitive function in the common genetic generalized epilepsy syndromes*. Eur J Neurol, 2017. **24**(3): p. 453-460.
95. Urbanski, G., et al., *A Case of Type I Sialidosis With Osteonecrosis Revealing a New Mutation in NEU1*. Journal of Inborn Errors of Metabolism and Screening, 2014. **2**: p. 2326409814543468.
96. Neves Jde, C., et al., *Neuraminidase-1 mediates skeletal muscle regeneration*. Biochim Biophys Acta, 2015. **1852**(9): p. 1755-64.
97. Gupta, A.O., et al., *Hematopoietic cell transplantation for sialidosis type I*. Mol Genet Metab Rep, 2022. **30**: p. 100832.

98. Sekijima, Y., et al., *Clinical and serial MRI findings of a sialidosis type I patient with a novel missense mutation in the NEU1 gene*. Intern Med, 2013. **52**(1): p. 119-24.
99. Lu, C.S., et al., *Cortical damage in the posterior visual pathway in patients with sialidosis type 1*. Brain Imaging Behav, 2017. **11**(1): p. 214-223.
100. Palmeri, S., et al., *Type I sialidosis: a clinical, biochemical and neuroradiological study*. Eur Neurol, 2000. **43**(2): p. 88-94.
101. Palaniyappan, L., et al., *Combined white matter imaging suggests myelination defects in visual processing regions in schizophrenia*. Neuropsychopharmacology, 2013. **38**(9): p. 1808-15.
102. Raz, N. and N. Levin, *Cortical and white matter mapping in the visual system-more than meets the eye: on the importance of functional imaging to understand visual system pathologies*. Front Integr Neurosci, 2014. **8**: p. 68.
103. Amano, N., et al., *Neuropathological findings of an autopsy case of adult beta-galactosidase and neuraminidase deficiency*. Acta Neuropathol, 1983. **61**(3-4): p. 283-90.
104. Mohammad, A.N., et al., *Type 1 sialidosis presenting with ataxia, seizures and myoclonus with no visual involvement*. Mol Genet Metab Rep, 2018. **15**: p. 11-14.
105. Delgado-Zabalza, L., et al., *Targeting parvalbumin-expressing neurons in the substantia nigra pars reticulata restores motor function in parkinsonian mice*. Cell Rep, 2023. **42**(10): p. 113287.
106. de Geest, N., et al., *Systemic and neurologic abnormalities distinguish the lysosomal disorders sialidosis and galactosialidosis in mice*. Hum Mol Genet, 2002. **11**(12): p. 1455-64.
107. Kanaka, C., et al., *Mucocutaneous bleeding, a rare but severe complication in nephrosialidosis*. Eur J Pediatr, 1994. **153**(9): p. 703-4.
108. Andrade-Campos, M., et al., *Diagnosis features of pediatric Gaucher disease patients in the era of enzymatic therapy, a national-base study from the Spanish Registry of Gaucher Disease*. Orphanet J Rare Dis, 2017. **12**(1): p. 84.
109. Lee, C.L., et al., *Fabry Disease and the Effectiveness of Enzyme Replacement Therapy (ERT) in Left Ventricular Hypertrophy (LVH) Improvement: A Review and Meta-Analysis*. Int J Med Sci, 2022. **19**(1): p. 126-131.
110. Concolino, D., F. Deodato, and R. Parini, *Enzyme replacement therapy: efficacy and limitations*. Ital J Pediatr, 2018. **44**(Suppl 2): p. 120.
111. Ditters, I.A.M., et al., *Home-based enzyme replacement therapy in children and adults with Pompe disease; a prospective study*. Orphanet J Rare Dis, 2023. **18**(1): p. 108.
112. Cadaoas, J., et al., *Galactosialidosis: preclinical enzyme replacement therapy in a mouse model of the disease, a proof of concept*. Mol Ther Methods Clin Dev, 2021. **20**: p. 191-203.
113. Sahin, O., et al., *Mucopolysaccharidoses and the blood-brain barrier*. Fluids Barriers CNS, 2022. **19**(1): p. 76.
114. Ben-Zvi, A., et al., *Mfsd2a is critical for the formation and function of the blood-brain barrier*. Nature, 2014. **509**(7501): p. 507-11.
115. Cohen, J.L., et al., *In Utero Enzyme-Replacement Therapy for Infantile-Onset Pompe's Disease*. N Engl J Med, 2022. **387**(23): p. 2150-2158.
116. Fischetto, R., et al., *Substrate reduction therapy with Miglustat in pediatric patients with GM1 type 2 gangliosidosis delays neurological involvement: A multicenter experience*. Mol Genet Genomic Med, 2020. **8**(10): p. e1371.
117. Cox, T., et al., *Novel oral treatment of Gaucher's disease with N-butyldeoxynojirimycin (OGT 918) to decrease substrate biosynthesis*. Lancet, 2000. **355**(9214): p. 1481-5.
118. Krivit, W., et al., *Microglia: the effector cell for reconstitution of the central nervous system following bone marrow transplantation for lysosomal and peroxisomal storage diseases*. Cell Transplant, 1995. **4**(4): p. 385-92.

119. Biffi, A., et al., *Correction of metachromatic leukodystrophy in the mouse model by transplantation of genetically modified hematopoietic stem cells*. J Clin Invest, 2004. **113**(8): p. 1118-29.
120. Masouridi-Levrat, S., F. Simonetta, and Y. Chalandon, *Immunological Basis of Bone Marrow Failure after Allogenic Hematopoietic Stem Cell Transplantation*. Front Immunol, 2016. **7**: p. 362.
121. Cressant, A., et al., *Improved behavior and neuropathology in the mouse model of Sanfilippo type IIIB disease after adeno-associated virus-mediated gene transfer in the striatum*. J Neurosci, 2004. **24**(45): p. 10229-39.
122. Ciron, C., et al., *Gene therapy of the brain in the dog model of Hurler's syndrome*. Ann Neurol, 2006. **60**(2): p. 204-13.
123. Markakis, E.A., et al., *Comparative transduction efficiency of AAV vector serotypes 1-6 in the substantia nigra and striatum of the primate brain*. Mol Ther, 2010. **18**(3): p. 588-93.
124. Sergijenko, A., et al., *Myeloid/Microglial driven autologous hematopoietic stem cell gene therapy corrects a neuronopathic lysosomal disease*. Mol Ther, 2013. **21**(10): p. 1938-49.
125. Wilkinson, F.L., et al., *Busulfan conditioning enhances engraftment of hematopoietic donor-derived cells in the brain compared with irradiation*. Mol Ther, 2013. **21**(4): p. 868-76.
126. Biffi, A., et al., *Lentiviral hematopoietic stem cell gene therapy benefits metachromatic leukodystrophy*. Science, 2013. **341**(6148): p. 1233158.
127. Capotondo, A., et al., *Brain conditioning is instrumental for successful microglia reconstitution following hematopoietic stem cell transplantation*. Proc Natl Acad Sci U S A, 2012. **109**(37): p. 15018-23.
128. Sessa, M., et al., *Lentiviral haemopoietic stem-cell gene therapy in early-onset metachromatic leukodystrophy: an ad-hoc analysis of a non-randomised, open-label, phase 1/2 trial*. Lancet, 2016. **388**(10043): p. 476-87.
129. Cherqui, S., *Cysteamine therapy: a treatment for cystinosis, not a cure*. Kidney Int, 2012. **81**(2): p. 127-9.
130. Harrison, F., et al., *Hematopoietic stem cell gene therapy for the multisystemic lysosomal storage disorder cystinosis*. Mol Ther, 2013. **21**(2): p. 433-44.
131. Wang, D., et al., *Short-term, high dose enzyme replacement therapy in sialidosis mice*. Mol Genet Metab, 2005. **85**(3): p. 181-9.
132. Bonten, E.J., et al., *Targeting macrophages with baculovirus-produced lysosomal enzymes: implications for enzyme replacement therapy of the glycoprotein storage disorder galactosialidosis*. FASEB J, 2004. **18**(9): p. 971-3.
133. Bonten, E.J., et al., *Chaperone-mediated gene therapy with recombinant AAV-PPCA in a new mouse model of type I sialidosis*. Biochim Biophys Acta, 2013. **1832**(10): p. 1784-92.
134. Yogalingam, G., et al., *Neuraminidase 1 Is a Negative Regulator of Lysosomal Exocytosis*. Developmental Cell, 2008. **15**(1): p. 74-86.
135. Reily, C., et al., *Glycosylation in health and disease*. Nat Rev Nephrol, 2019. **15**(6): p. 346-366.
136. Stanley P, M.K., Lewis NE, et al. N-Glycans., *Essentials of Glycobiology 4th edition*, in *Essentials of Glycobiology*, A. Varki, et al., Editors. 2022: Cold Spring Harbor (NY).
137. Zachara NE, A.Y., Boyce M, et al., *Essentials of Glycobiology, Fourth Edition*, in *Essentials of Glycobiology*, A. Varki, et al., Editors. 2022: Cold Spring Harbor (NY).
138. Hart, G.W., M.P. Housley, and C. Slawson, *Cycling of O-linked beta-N-acetylglucosamine on nucleocytoplasmic proteins*. Nature, 2007. **446**(7139): p. 1017-22.
139. Shivatare, S.S., V.S. Shivatare, and C.H. Wong, *Glycoconjugates: Synthesis, Functional Studies, and Therapeutic Developments*. Chem Rev, 2022. **122**(20): p. 15603-15671.
140. Jung, J.U., et al., *The roles of glycosphingolipids in the proliferation and neural differentiation of mouse embryonic stem cells*. Exp Mol Med, 2009. **41**(12): p. 935-45.
141. Cummings RD, S.R., Ozeki Y., *Essentials of Glycobiology, Fourth Edition*, in *Essentials of Glycobiology*, A. Varki, et al., Editors. 2022: Cold Spring Harbor (NY).

142. Sharon, N. and H. Lis, *History of lectins: from hemagglutinins to biological recognition molecules*. *Glycobiology*, 2004. **14**(11): p. 53R-62R.
143. Islam, M.K., et al., *Lectins as potential tools for cancer biomarker discovery from extracellular vesicles*. *Biomarker Research*, 2023. **11**(1): p. 85.
144. Suzuki, Y., *Sialobiology of influenza: molecular mechanism of host range variation of influenza viruses*. *Biol Pharm Bull*, 2005. **28**(3): p. 399-408.
145. Ishikawa, Y., et al., *Expression and diversity of the sialic acid-binding adhesin and its homologs associated with oral streptococcal infection*. *Microbiol Immunol*, 2022. **66**(2): p. 59-66.
146. Gallegos, K.M., et al., *Shiga toxin binding to glycolipids and glycans*. *PLoS One*, 2012. **7**(2): p. e30368.
147. Brown, G.D., J.A. Willment, and L. Whitehead, *C-type lectins in immunity and homeostasis*. *Nat Rev Immunol*, 2018. **18**(6): p. 374-389.
148. Smith, B.A.H. and C.R. Bertozzi, *Author Correction: The clinical impact of glycobiology: targeting selectins, Siglecs and mammalian glycans*. *Nat Rev Drug Discov*, 2021. **20**(3): p. 244.
149. Stanley P, W.M., Lauc G, et al., *Essentials of Glycobiology, Fourth Edition*, in *Essentials of Glycobiology*, A. Varki, et al., Editors. 2022: Cold Spring Harbor (NY).
150. Ferreira, I.G., et al., *Carcinoembryonic antigen is a sialyl Lewis x/a carrier and an E-selectin ligand in non-small cell lung cancer*. *Int J Oncol*, 2019. **55**(5): p. 1033-1048.
151. Julien, S., et al., *Selectin ligand sialyl-Lewis x antigen drives metastasis of hormone-dependent breast cancers*. *Cancer Res*, 2011. **71**(24): p. 7683-93.
152. Dall'Olio, F., M. Pucci, and N. Malagolini, *The Cancer-Associated Antigens Sialyl Lewis(a/x) and Sd(a): Two Opposite Faces of Terminal Glycosylation*. *Cancers (Basel)*, 2021. **13**(21).
153. Kozlov, G. and K. Gehring, *Calnexin cycle - structural features of the ER chaperone system*. *FEBS J*, 2020. **287**(20): p. 4322-4340.
154. Varki, A. and S. Kornfeld, *P-type Lectins*, in *Essentials of Glycobiology*, A. Varki, et al., Editors. 2009: Cold Spring Harbor (NY).
155. Lobsanov, Y.D., et al., *X-ray crystal structure of the human dimeric S-Lac lectin, L-14-II, in complex with lactose at 2.9-Å resolution*. *J Biol Chem*, 1993. **268**(36): p. 27034-8.
156. Nio-Kobayashi, J. and T. Itabashi, *Galectins and Their Ligand Glycoconjugates in the Central Nervous System Under Physiological and Pathological Conditions*. *Front Neuroanat*, 2021. **15**: p. 767330.
157. Pasquini, L.A., et al., *Galectin-3 drives oligodendrocyte differentiation to control myelin integrity and function*. *Cell Death Differ*, 2011. **18**(11): p. 1746-56.
158. Varki, A. and T. Angata, *Siglecs--the major subfamily of I-type lectins*. *Glycobiology*, 2006. **16**(1): p. 1R-27R.
159. York, M.R., et al., *A macrophage marker, Siglec-1, is increased on circulating monocytes in patients with systemic sclerosis and induced by type I interferons and toll-like receptor agonists*. *Arthritis Rheum*, 2007. **56**(3): p. 1010-20.
160. Nitschke, L., et al., *CD22 is a negative regulator of B-cell receptor signalling*. *Curr Biol*, 1997. **7**(2): p. 133-43.
161. Sun, J., et al., *Myelin-associated glycoprotein (Siglec-4) expression is progressively and selectively decreased in the brains of mice lacking complex gangliosides*. *Glycobiology*, 2004. **14**(9): p. 851-7.
162. Hernandez-Caselles, T., et al., *A study of CD33 (SIGLEC-3) antigen expression and function on activated human T and NK cells: two isoforms of CD33 are generated by alternative splicing*. *J Leukoc Biol*, 2006. **79**(1): p. 46-58.
163. Stanczak, M.A., et al., *Self-associated molecular patterns mediate cancer immune evasion by engaging Siglecs on T cells*. *J Clin Invest*, 2018. **128**(11): p. 4912-4923.

164. Hudak, J.E., S.M. Canham, and C.R. Bertozzi, *Glycocalyx engineering reveals a Siglec-based mechanism for NK cell immunoevasion*. Nat Chem Biol, 2014. **10**(1): p. 69-75.
165. Varki, A., *Glycan-based interactions involving vertebrate sialic-acid-recognizing proteins*. Nature, 2007. **446**(7139): p. 1023-9.
166. Rabelink, T.J. and D. de Zeeuw, *The glycocalyx--linking albuminuria with renal and cardiovascular disease*. Nat Rev Nephrol, 2015. **11**(11): p. 667-76.
167. Cohen, M. and A. Varki, *The sialome--far more than the sum of its parts*. OMICS, 2010. **14**(4): p. 455-64.
168. Moons, S.J., et al., *Sialic acid glycoengineering using N-acetylmannosamine and sialic acid analogs*. Glycobiology, 2019. **29**(6): p. 433-445.
169. Freeze, H.H., G.W. Hart, and R.L. Schnaar, *Glycosylation Precursors*, in *Essentials of Glycobiology*, A. Varki, et al., Editors. 2015, Cold Spring Harbor Laboratory Press

Copyright 2015-2017 by The Consortium of Glycobiology Editors, La Jolla, California. All rights reserved.: Cold Spring Harbor (NY). p. 51-63.

170. Varki, A., R.L. Schnaar, and R. Schauer, *Sialic Acids and Other Nonulosonic Acids*, in *Essentials of Glycobiology*, A. Varki, et al., Editors. 2015, Cold Spring Harbor Laboratory Press

Copyright 2015-2017 by The Consortium of Glycobiology Editors, La Jolla, California. All rights reserved.: Cold Spring Harbor (NY). p. 179-95.

171. Kwon, D.N., et al., *CMP-Neu5Ac Hydroxylase Null Mice as a Model for Studying Metabolic Disorders Caused by the Evolutionary Loss of Neu5Gc in Humans*. Biomed Res Int, 2015. **2015**: p. 830315.
172. Varki, A., *Loss of N-glycolylneuraminic acid in humans: Mechanisms, consequences, and implications for hominid evolution*. Am J Phys Anthropol, 2001. **Suppl 33**(Suppl): p. 54-69.
173. Domon, B. and C.E. Costello, *A systematic nomenclature for carbohydrate fragmentations in FAB-MS/MS spectra of glycoconjugates*. Glycoconjugate Journal, 1988. **5**(4): p. 397-409.
174. Stephenson, R.O., Y. Yamanaka, and J. Rossant, *Disorganized epithelial polarity and excess trophectoderm cell fate in preimplantation embryos lacking E-cadherin*. Development, 2010. **137**(20): p. 3383-91.
175. Bergfeld, A.K., et al., *Metabolism of vertebrate amino sugars with N-glycolyl groups: elucidating the intracellular fate of the non-human sialic acid N-glycolylneuraminic acid*. J Biol Chem, 2012. **287**(34): p. 28865-81.
176. Akhavan, A., et al., *SEA domain proteolysis determines the functional composition of dystroglycan*. Faseb j, 2008. **22**(2): p. 612-21.
177. Knibbs, R.N., et al., *Characterization of the carbohydrate binding specificity of the leucoagglutinating lectin from Maackia amurensis. Comparison with other sialic acid-specific lectins*. J Biol Chem, 1991. **266**(1): p. 83-8.
178. Shibuya, N., et al., *The elderberry (Sambucus nigra L.) bark lectin recognizes the Neu5Ac(alpha 2-6)Gal/GalNAc sequence*. J Biol Chem, 1987. **262**(4): p. 1596-601.
179. Bashir, S., et al., *Presentation Mode of Glycans Affect Recognition of Human Serum anti-Neu5Gc IgG Antibodies*. Bioconjug Chem, 2019. **30**(1): p. 161-168.
180. Tangvoranuntakul, P., et al., *Human uptake and incorporation of an immunogenic nonhuman dietary sialic acid*. Proc Natl Acad Sci U S A, 2003. **100**(21): p. 12045-50.
181. Varki, A., *Sialic acids in human health and disease*. Trends Mol Med, 2008. **14**(8): p. 351-60.
182. Jennings, M.P., C.J. Day, and J.M. Atack, *How bacteria utilize sialic acid during interactions with the host: snip, snatch, dispatch, match and attach*. Microbiology (Reading), 2022. **168**(3).
183. Allendorf, D.H., M. Puigdemívol, and G.C. Brown, *Activated microglia desialylate their surface, stimulating complement receptor 3-mediated phagocytosis of neurons*. Glia, 2020. **68**(5): p. 989-998.

184. Cioffi, D.L., et al., *Terminal sialic acids are an important determinant of pulmonary endothelial barrier integrity*. Am J Physiol Lung Cell Mol Physiol, 2012. **302**(10): p. L1067-77.
185. Charest, P.M. and J. Roth, *Localization of sialic acid in kidney glomeruli: regionalization in the podocyte plasma membrane and loss in experimental nephrosis*. Proc Natl Acad Sci U S A, 1985. **82**(24): p. 8508-12.
186. Werneburg, S., et al., *Polysialic acid modification of the synaptic cell adhesion molecule SynCAM 1 in human embryonic stem cell-derived oligodendrocyte precursor cells*. Stem Cell Res, 2015. **14**(3): p. 339-46.
187. Mori, A., et al., *Different properties of polysialic acids synthesized by the polysialyltransferases ST8SIA2 and ST8SIA4*. Glycobiology, 2017. **27**(9): p. 834-846.
188. Quartu, M., et al., *Polysialylated-neural cell adhesion molecule (PSA-NCAM) in the human trigeminal ganglion and brainstem at prenatal and adult ages*. BMC Neurosci, 2008. **9**: p. 108.
189. El Maarouf, A. and U. Rutishauser, *Removal of polysialic acid induces aberrant pathways, synaptic vesicle distribution, and terminal arborization of retinotectal axons*. J Comp Neurol, 2003. **460**(2): p. 203-11.
190. Mikkonen, M., et al., *Hippocampal plasticity in Alzheimer's disease: changes in highly polysialylated NCAM immunoreactivity in the hippocampal formation*. Eur J Neurosci, 1999. **11**(5): p. 1754-64.
191. Murray, H.C., et al., *Distribution of PSA-NCAM in normal, Alzheimer's and Parkinson's disease human brain*. Neuroscience, 2016. **330**: p. 359-75.
192. Curreli, S., et al., *Polysialylated neuropilin-2 is expressed on the surface of human dendritic cells and modulates dendritic cell-T lymphocyte interactions*. J Biol Chem, 2007. **282**(42): p. 30346-56.
193. Thiesler, H., J. Beimdiek, and H. Hildebrandt, *Polysialic acid and Siglec-E orchestrate negative feedback regulation of microglia activation*. Cell Mol Life Sci, 2021. **78**(4): p. 1637-1653.
194. Miyagi, T. and K. Yamaguchi, *Mammalian sialidases: physiological and pathological roles in cellular functions*. Glycobiology, 2012. **22**(7): p. 880-96.
195. Lukong, K.E., et al., *Intracellular distribution of lysosomal sialidase is controlled by the internalization signal in its cytoplasmic tail*. J Biol Chem, 2001. **276**(49): p. 46172-81.
196. Miyagi, T. and S. Tsuiki, *Rat-liver lysosomal sialidase. Solubilization, substrate specificity and comparison with the cytosolic sialidase*. Eur J Biochem, 1984. **141**(1): p. 75-81.
197. Zanchetti, G., et al., *Sialidase NEU3 is a peripheral membrane protein localized on the cell surface and in endosomal structures*. Biochem J, 2007. **408**(2): p. 211-9.
198. Seyrantepe, V., et al., *Neu4, a novel human lysosomal lumen sialidase, confers normal phenotype to sialidosis and galactosialidosis cells*. J Biol Chem, 2004. **279**(35): p. 37021-9.
199. Smutova, V., et al., *Structural basis for substrate specificity of mammalian neuraminidases*. PLoS One, 2014. **9**(9): p. e106320.
200. Sandbhor, M.S., et al., *Substrate recognition of the membrane-associated sialidase NEU3 requires a hydrophobic aglycone*. Biochemistry, 2011. **50**(32): p. 6753-62.
201. Pshezhetsky, A.V. and M. Ashmarina, *Keeping it trim: roles of neuraminidases in CNS function*. Glycoconj J, 2018. **35**(4): p. 375-386.
202. Li, Y., et al., *Identifying selective inhibitors against the human cytosolic sialidase NEU2 by substrate specificity studies*. Mol Biosyst, 2011. **7**(4): p. 1060-72.
203. Davies, L.R., et al., *Metabolism of vertebrate amino sugars with N-glycolyl groups: resistance of alpha2-8-linked N-glycolylneuraminic acid to enzymatic cleavage*. J Biol Chem, 2012. **287**(34): p. 28917-31.
204. Pshezhetsky, A.V., et al., *Cloning, expression and chromosomal mapping of human lysosomal sialidase and characterization of mutations in sialidosis*. Nat Genet, 1997. **15**(3): p. 316-20.
205. Carrillo, M.B., et al., *Cloning and characterization of a sialidase from the murine histocompatibility-2 complex: low levels of mRNA and a single amino acid mutation are*

- responsible for reduced sialidase activity in mice carrying the *Neu1a* allele. *Glycobiology*, 1997. **7**(7): p. 975-86.
206. Vinogradova, M.V., et al., *Molecular mechanism of lysosomal sialidase deficiency in galactosialidosis involves its rapid degradation*. *Biochem J*, 1998. **330** ( Pt 2)(Pt 2): p. 641-50.
  207. Annunziata, I. and A. d'Azzo, *Galactosialidosis: historic aspects and overview of investigated and emerging treatment options*. *Expert Opin Orphan Drugs*, 2017. **5**(2): p. 131-141.
  208. Takahashi, Y., et al., *Urinary oligosaccharide excretion and severity of galactosialidosis and sialidosis*. *Clin Chim Acta*, 1991. **203**(2-3): p. 199-210.
  209. Oheda, Y., et al., *Elimination of abnormal sialylglycoproteins in fibroblasts with sialidosis and galactosialidosis by normal gene transfer and enzyme replacement*. *Glycobiology*, 2006. **16**(4): p. 271-80.
  210. Ulrich-Bott, B., et al., *Lysosomal sialidase deficiency: increased ganglioside content in autopsy tissues of a sialidosis patient*. *Enzyme*, 1987. **38**(1-4): p. 262-6.
  211. Dridi, L., et al., *Positive regulation of insulin signaling by neuraminidase 1*. *Diabetes*, 2013. **62**(7): p. 2338-46.
  212. Fougerat, A., et al., *Neuraminidase 1 activates insulin receptor and reverses insulin resistance in obese mice*. *Mol Metab*, 2018. **12**: p. 76-88.
  213. Seyrantepe, V., et al., *Regulation of phagocytosis in macrophages by neuraminidase 1*. *J Biol Chem*, 2010. **285**(1): p. 206-15.
  214. Liang, F., et al., *Monocyte differentiation up-regulates the expression of the lysosomal sialidase, Neu1, and triggers its targeting to the plasma membrane via major histocompatibility complex class II-positive compartments*. *J Biol Chem*, 2006. **281**(37): p. 27526-38.
  215. Rottier, R.J., E. Bonten, and A. d'Azzo, *A point mutation in the neu-1 locus causes the neuraminidase defect in the SM/J mouse*. *Hum Mol Genet*, 1998. **7**(2): p. 313-21.
  216. Nan, X., I. Carubelli, and N.M. Stamatou, *Sialidase expression in activated human T lymphocytes influences production of IFN-gamma*. *J Leukoc Biol*, 2007. **81**(1): p. 284-96.
  217. Amith, S.R., et al., *Dependence of pathogen molecule-induced toll-like receptor activation and cell function on Neu1 sialidase*. *Glycoconj J*, 2009. **26**(9): p. 1197-212.
  218. Demina, E.P., et al., *Persistent reduction in sialylation of cerebral glycoproteins following postnatal inflammatory exposure*. *J Neuroinflammation*, 2018. **15**(1): p. 336.
  219. Miyagi, T., et al., *Molecular cloning and expression of cDNA encoding rat skeletal muscle cytosolic sialidase*. *J Biol Chem*, 1993. **268**(35): p. 26435-40.
  220. Miyagi, T. and S. Tsuiki, *Purification and characterization of cytosolic sialidase from rat liver*. *J Biol Chem*, 1985. **260**(11): p. 6710-6.
  221. Monti, E., et al., *Cloning and characterization of NEU2, a human gene homologous to rodent soluble sialidases*. *Genomics*, 1999. **57**(1): p. 137-43.
  222. Oh, M., et al., *Defect in cytosolic Neu2 sialidase abrogates lipid metabolism and impairs muscle function in vivo*. *Sci Rep*, 2022. **12**(1): p. 3216.
  223. Satyavarapu, E.M., S. Nath, and C. Mandal, *Desialylation of Atg5 by sialidase (Neu2) enhances autophagosome formation to induce anchorage-dependent cell death in ovarian cancer cells*. *Cell Death Discov*, 2021. **7**(1): p. 26.
  224. Wada, T., et al., *Cloning, expression, and chromosomal mapping of a human ganglioside sialidase*. *Biochem Biophys Res Commun*, 1999. **261**(1): p. 21-7.
  225. Li, S.C., et al., *Degradation of G(M1) and G(M2) by mammalian sialidases*. *Biochem J*, 2001. **360**(Pt 1): p. 233-7.
  226. Hasegawa, T., et al., *Molecular cloning of mouse ganglioside sialidase and its increased expression in Neuro2a cell differentiation*. *J Biol Chem*, 2000. **275**(11): p. 8007-15.
  227. Tagami, S., et al., *Ganglioside GM3 Participates in the Pathological Conditions of Insulin Resistance\**. *Journal of Biological Chemistry*, 2002. **277**(5): p. 3085-3092.

228. Kabayama, K., et al., *Dissociation of the insulin receptor and caveolin-1 complex by ganglioside GM3 in the state of insulin resistance*. Proceedings of the National Academy of Sciences, 2007. **104**(34): p. 13678-13683.
229. Yamaguchi, K., et al., *Evidence for mitochondrial localization of a novel human sialidase (NEU4)*. Biochem J, 2005. **390**(Pt 1): p. 85-93.
230. Shiozaki, K., et al., *Developmental change of sialidase neu4 expression in murine brain and its involvement in the regulation of neuronal cell differentiation*. J Biol Chem, 2009. **284**(32): p. 21157-64.
231. Seyrantepe, V., et al., *Mice deficient in Neu4 sialidase exhibit abnormal ganglioside catabolism and lysosomal storage*. Hum Mol Genet, 2008. **17**(11): p. 1556-68.
232. Seyrantepe, V., et al., *Mice doubly-deficient in lysosomal hexosaminidase A and neuraminidase 4 show epileptic crises and rapid neuronal loss*. PLoS Genet, 2010. **6**(9): p. e1001118.
233. Mohos, S.C. and L. Skoza, *Glomerular sialoprotein*. Science, 1969. **164**(3887): p. 1519-21.
234. Klein, P.J., et al., *Thomsen-Friedenreich antigen in haemolytic-uraemic syndrome*. Lancet, 1977. **2**(8046): p. 1024-5.
235. Lemyre, E., et al., *Clinical spectrum of infantile free sialic acid storage disease*. Am J Med Genet, 1999. **82**(5): p. 385-91.
236. Coats, M.T., et al., *Exposure of Thomsen-Friedenreich antigen in Streptococcus pneumoniae infection is dependent on pneumococcal neuraminidase A*. Microb Pathog, 2011. **50**(6): p. 343-9.
237. Pawluczyk, I.Z., et al., *Sialic acid supplementation ameliorates puromycin aminonucleoside nephrosis in rats*. Lab Invest, 2015. **95**(9): p. 1019-28.
238. Firth, J.D., *Effect of polycations on the function of the isolated perfused rat kidney*. Clin Sci (Lond), 1990. **79**(6): p. 591-8.
239. Niculovic, K.M., et al., *Podocyte-Specific Sialylation-Deficient Mice Serve as a Model for Human FSGS*. J Am Soc Nephrol, 2019. **30**(6): p. 1021-1035.
240. Alexander, W.S., et al., *Thrombocytopenia and kidney disease in mice with a mutation in the C1galt1 gene*. Proc Natl Acad Sci U S A, 2006. **103**(44): p. 16442-7.
241. MacArthur, D.G., et al., *Guidelines for investigating causality of sequence variants in human disease*. Nature, 2014. **508**(7497): p. 469-76.
242. Martin, L.T., et al., *Genetically altered mice with different sialyltransferase deficiencies show tissue-specific alterations in sialylation and sialic acid 9-O-acetylation*. J Biol Chem, 2002. **277**(36): p. 32930-8.
243. Galeano, B., et al., *Mutation in the key enzyme of sialic acid biosynthesis causes severe glomerular proteinuria and is rescued by N-acetylmannosamine*. J Clin Invest, 2007. **117**(6): p. 1585-94.
244. Kakani, S., et al., *The Gne M712T mouse as a model for human glomerulopathy*. Am J Pathol, 2012. **180**(4): p. 1431-40.
245. Yu, A., et al., *Changes in the Expression of Renal Brush Border Membrane N-Glycome in Model Rats with Chronic Kidney Diseases*. Biomolecules, 2021. **11**(11).
246. Kashtan, C.E., et al., *Proteinuria in a child with sialidosis: case report and histological studies*. Pediatr Nephrol, 1989. **3**(2): p. 166-74.
247. Toyooka, K., et al., *Nephrosialidosis: ultrastructural and lectin histochemical study*. Acta Neuropathol, 1993. **86**(2): p. 198-205.
248. Novak, J., et al., *Aberrant Glycosylation of the IgA1 Molecule in IgA Nephropathy*. Semin Nephrol, 2018. **38**(5): p. 461-476.
249. Martin, C.E. and N. Jones, *Nephrin Signaling in the Podocyte: An Updated View of Signal Regulation at the Slit Diaphragm and Beyond*. Front Endocrinol (Lausanne), 2018. **9**: p. 302.

250. Thomas, H.Y. and A.N. Ford Versypt, *Pathophysiology of mesangial expansion in diabetic nephropathy: mesangial structure, glomerular biomechanics, and biochemical signaling and regulation*. J Biol Eng, 2022. **16**(1): p. 19.
251. Weil, E.J., et al., *Podocyte detachment and reduced glomerular capillary endothelial fenestration promote kidney disease in type 2 diabetic nephropathy*. Kidney Int, 2012. **82**(9): p. 1010-7.
252. Ohmori, T., et al., *Impaired NEPHRIN localization in kidney organoids derived from nephrotic patient iPS cells*. Sci Rep, 2021. **11**(1): p. 3982.
253. Refaeli, I., et al., *Distinct Functional Requirements for Podocalyxin in Immature and Mature Podocytes Reveal Mechanisms of Human Kidney Disease*. Sci Rep, 2020. **10**(1): p. 9419.
254. Li, X., et al., *Nephrin Preserves Podocyte Viability and Glomerular Structure and Function in Adult Kidneys*. J Am Soc Nephrol, 2015. **26**(10): p. 2361-77.
255. Olivetti, G., et al., *Morphometry of the renal corpuscle during normal postnatal growth and compensatory hypertrophy. A light microscope study*. J Cell Biol, 1977. **75**(2 Pt 1): p. 573-85.
256. Ebefors, K., et al., *Mesangial cells from patients with IgA nephropathy have increased susceptibility to galactose-deficient IgA1*. BMC Nephrol, 2016. **17**: p. 40.
257. Borza, D.B., *Glomerular basement membrane heparan sulfate in health and disease: A regulator of local complement activation*. Matrix Biol, 2017. **57-58**: p. 299-310.
258. Zhuo, J.L. and X.C. Li, *Proximal nephron*. Compr Physiol, 2013. **3**(3): p. 1079-123.
259. Curthoys, N.P. and O.W. Moe, *Proximal tubule function and response to acidosis*. Clin J Am Soc Nephrol, 2014. **9**(9): p. 1627-38.
260. Kriz, W. and B. Kaissling, *CHAPTER 20 - Structural Organization of the Mammalian Kidney, in Seldin and Giebisch's The Kidney (Fourth Edition)*, R.J. Alpern and S.C. Hebert, Editors. 2008, Academic Press: San Diego. p. 479-563.
261. Christensen, E.I. and H. Birn, *Megalin and cubilin: multifunctional endocytic receptors*. Nat Rev Mol Cell Biol, 2002. **3**(4): p. 256-66.
262. Kantarci, S., et al., *Mutations in LRP2, which encodes the multiligand receptor megalin, cause Donnai-Barrow and facio-oculo-acoustico-renal syndromes*. Nat Genet, 2007. **39**(8): p. 957-9.
263. Norden, A.G., et al., *Lysosomal enzymuria is a feature of hereditary Fanconi syndrome and is related to elevated CI-mannose-6-P-receptor excretion*. Nephrol Dial Transplant, 2008. **23**(9): p. 2795-803.
264. Willnow, T.E., et al., *Defective forebrain development in mice lacking gp330/megalin*. Proc Natl Acad Sci U S A, 1996. **93**(16): p. 8460-4.
265. Magen, D., et al., *A loss-of-function mutation in NaPi-IIa and renal Fanconi's syndrome*. N Engl J Med, 2010. **362**(12): p. 1102-9.
266. Haque, S.K., G. Ariceta, and D. Batlle, *Proximal renal tubular acidosis: a not so rare disorder of multiple etiologies*. Nephrol Dial Transplant, 2012. **27**(12): p. 4273-87.
267. Castaneda-Bueno, M., D.H. Ellison, and G. Gamba, *Molecular mechanisms for the modulation of blood pressure and potassium homeostasis by the distal convoluted tubule*. EMBO Mol Med, 2022. **14**(2): p. e14273.
268. McCormick, J.A. and D.H. Ellison, *Distal convoluted tubule*. Compr Physiol, 2015. **5**(1): p. 45-98.
269. Knoers, N.V. and E.N. Levtchenko, *Gitelman syndrome*. Orphanet J Rare Dis, 2008. **3**: p. 22.
270. Pshezhetsky, A.V. and A. Hinek, *Where catabolism meets signalling: neuraminidase 1 as a modulator of cell receptors*. Glycoconj J, 2011. **28**(7): p. 441-52.
271. Peterson, C.W., et al., *Autologous, Gene-Modified Hematopoietic Stem and Progenitor Cells Repopulate the Central Nervous System with Distinct Clonal Variants*. Stem Cell Reports, 2019. **13**(1): p. 91-104.
272. Syres, K., et al., *Successful treatment of the murine model of cystinosis using bone marrow cell transplantation*. Blood, 2009. **114**(12): p. 2542-52.

## 2 Severe kidney dysfunction in sialidosis mice reveals a novel role for neuraminidase 1 in reabsorption.

### 2.1 Introduction

Sialic acids are found attached to the terminal ends of glycoproteins and glycolipids on the surface of all mammalian cells, forming a glycocalyx that functions as a barrier and mediates cell-cell interaction (135, 181). In kidneys, sialic acids are remarkably enriched at the membranes of the glomerular endothelial cells and at the basement membrane, supporting the glomerular filtration barrier and maintaining cellular structural integrity (185, 233). Aberrant glomerular sialylation caused by genetic or environmental factors is linked to multiple kidney diseases. For example, glomerular hyposialylation is observed in severe pneumococcal infections (234), as well as in ~50% of patients with a sialic acid transporter defect (235).

A similar pathology is described in multiple animal models of kidney disease, including mice exposed to pneumococcal neuraminidase (NanA) (236), puromycin amino nucleoside (237) or polylysine (238), or in mice with genetic defects that disrupt sialic acid metabolism (e.g., *Cmas* (239), *CIgalt1* (240), *ST3GAL1* (241, 242) or *Gne* (243)). Specifically, glomerular hyposialylation in the animal models of kidney damage, induced by puromycin amino nucleoside (PAN), results in effacement of podocyte foot processes and proteinuria (185, 237). Glomerulopathy is also observed in mouse models of the genetic deficiency in N-acetylglucosamine 2-epimerase/N-acetylmannosamine kinase (GNE), the key enzyme of sialic acid synthesis (244). Treatment of *Gne*-deficient mice with sialic acid precursor, ManNAc, ameliorates hyposialylation, reduces albuminuria and partially restores glomerular architecture (244). Significant differences in sialylation of kidney proteins were also observed in several rodent models of chronic kidney diseases (CKD) (245).

On the other hand, kidney pathology is also associated with a deficiency of neuraminidase 1 (NEU1) which cleaves terminal sialic acids from glycan chains in glycoproteins. A genome-wide association study based on samples from over 1 million individuals revealed a significant association ( $P < 10^{-14}$ ) between a G > A variant in the 3' UTR of the *NEU1* gene and decreased glomerular filtration rate (273), later replicated ( $P < 10^{-36}$ ) by an independent study (274). The G > A variant is present in all populations sampled in Genome Aggregation Database (gnomAD) with allele frequencies ranging from 3 to 16%, however, its functional impact is unclear.

Pathogenic genetic *NEU1* variants cause sialidosis (Online Mendelian Inheritance in Man (OMIM) #256550), a rare autosomal recessive disease with a prevalence of less than

1/1,000,000 live births. NEU1 deficiency blocks catabolism of sialylated glycoproteins and oligosaccharides and results in progressive lysosomal accumulation and urinary excretion of sialylated oligosaccharides and glycopeptides, eventually leading to multisystemic dysfunction (75, 91).

Sialidosis is divided into two subtypes with different onset age and severity. Type I manifests as a relatively mild, late-onset disease with patients suffering from myoclonus, progressive vision failure and mild cognitive impairment (91). Type II is an early-onset, infantile/juvenile form, in which patients display abnormal somatic features, hepatosplenomegaly and substantially impaired intellectual and adaptive functioning (79). A subset of type II patients, presenting with a severe nephrotic syndrome, is described as nephrosialidosis (79, 83). Previous work identified severe pathological alterations in the glomeruli of nephrosialidosis patients, including diffused fusion of podocyte foot processes and vacuolization of podocytes (80). These vacuoles accumulate glycoconjugates containing terminal sialic acid,  $\alpha$ -linked mannose, and *N*-acetylgalactosamine residues (246, 247). These glycoconjugates are also released by podocytes in the urine ultrafiltrate, resulting in a drastically increased concentration of sialylated oligosaccharides in the urine of sialidosis patients (80, 91) and *Neu1*-null mice (106).

Notably, the glomerular lesions alone do not fully explain the pathophysiology of nephrosialidosis. When compared to controls, the urine of patients is enriched not only with albumin (a marker of glomerular dysfunction), but also with low molecular weight proteins and soluble metabolites (79, 83) that are freely filtered at the glomeruli and reabsorbed at the proximal tubule. Previous work has established that in addition to lysosomes, NEU1 is present on the cell surface, where it desialylates multiple protein targets, and that NEU1 deficiency results in dramatic hypersialylation of membrane proteins (201, 270). Integrating all these findings, we hypothesized that the pathological kidney phenotype observed in mice and humans with NEU1 deficiency is complex and implicates hypersialylation-dependent defects in both glomeruli and proximal tubules.

In the current work, we demonstrate that NEU1 deficiency in constitutive *Neu1* <sup>$\Delta$ Ex3</sup> and novel conditional phagocyte specific *Neu1*<sup>Cx3cr1 $\Delta$ Ex3</sup> knockout (KO) mice results in hypersialylation of endocytic receptor megalin, which disrupts its normal targeting to the tubular apical membranes and impairs protein reabsorption processes in the proximal tubules.

## 2.2 Results

### 2.2.1 Systemic pathology of *Neu1<sup>ΔEx3</sup>* and *Neu1<sup>Cx3cr1ΔEx3</sup>* mice

Recent studies revealed that DAM (Disease-Associated Microglia) phagocytic cells play an essential role in the pathology of lysosomal storage diseases including sialidosis (reviewed in (275)). To assess the contribution of NEU1-deficient phagocytic cells to systemic pathology in sialidosis, we have generated a phagocyte-specific conditional *Neu1* KO (*Neu1<sup>Cx3cr1ΔEx3</sup>*) and compared it with previously described constitutive *Neu1* KO mouse (*Neu1<sup>ΔEx3</sup>*) (32). *Neu1<sup>Cx3cr1ΔEx3</sup>* mice were generated by producing a *Neu1<sup>loxPEX3</sup>* strain with the *Neu1* exon 3, flanked with the loxP sites, and crossing it with the mouse, expressing the Cre recombinase under the control of the *Cx3cr1* (chemokine C-X3-C motif receptor 1) gene promoter (Supplementary figure S2-1). This resulted in the deletion of exon 3 in all *Cx3cr1*-expressing cells (Supplementary figure S2-1).

Homozygous *Neu1<sup>Cx3cr1ΔEx3</sup>* mice showed normal appearance and general behavior indistinguishable from that of WT or heterozygous animals until the age of 20 weeks. Mice were fertile and produced normal litter sizes. Neurological assessment (gait, posture, avoidance response, righting reflex, inverted wire screen test) conducted on the group of ten *Neu1<sup>Cx3cr1ΔEx3</sup>* and WT mice at the age of 8 weeks did not reveal signs of overt neuromuscular pathology.

Heterozygous *Neu1<sup>ΔEx3</sup>* breeding pairs also produced average litters (3-8 pups), and homozygous *Neu1<sup>ΔEx3</sup>* mice were born at an expected Mendelian frequency of ~20%. They however showed slower growth and smaller size than their heterozygous or WT littermates resembling the previously described phenotype (106). Male *Neu1<sup>ΔEx3</sup>* mice were sterile, while female *Neu1<sup>ΔEx3</sup>*, crossed with heterozygous males, could infrequently produce a small-size (1-2 pups) first litter, but never the second litter.

The weight of male *Neu1<sup>ΔEx3</sup>* mice was reduced by about 30%, and female *Neu1<sup>ΔEx3</sup>* mice by about 20%, as compared with age- and sex-matched WT mice (Figure 2.1A). At the age of 4 months, *Neu1<sup>ΔEx3</sup>* mice were visibly smaller than their heterozygous and WT littermates (Figure 2.1B). In contrast, *Neu1<sup>Cx3cr1ΔEx3</sup>* mice of both sexes showed no significant difference in weight (Figure 2.1A) or size from their WT littermates.

Starting from 4 weeks, both male and female *Neu1<sup>ΔEx3</sup>* mice appeared physically unwell, displaying a hunched posture, mobility issues and slower response to touch. Abnormal motor movements and gait clumsy were also noted. *Neu1<sup>ΔEx3</sup>* mice also showed hydrocephalus (5% of mice), dental malocclusion, and a tendency to develop rectal prolapse seen in ~55% of mice (Supplementary figure S2-2). With age, homozygous mice of both strains developed a severely

distended bladder filled with urine (Supplementary figure S2-2) and had to be euthanized. Other causes for euthanasia included asthenia, severe weight loss, and hydrocephalus. *Neu1<sup>ΔEx3</sup>* male mice had the shortest median lifespan (18.3 weeks), followed by female *Neu1<sup>ΔEx3</sup>* mice (24.9 weeks), male *Neu1<sup>Cx3cr1ΔEx3</sup>* mice (27 weeks) and female *Neu1<sup>Cx3cr1ΔEx3</sup>* mice (56 weeks) (Figure 2.1C). Pathological examination revealed enlargement of liver, kidneys and spleen, and reduced intraabdominal fat in *Neu1<sup>ΔEx3</sup>* compared to WT mice (Figure 8D; Supplementary figure S2-2). *Neu1<sup>Cx3cr1ΔEx3</sup>* mice showed a similar trend; however, due to a large variability, a significant weight increase was observed only for kidneys of female *Neu1<sup>Cx3cr1ΔEx3x</sup>* and spleens of male *Neu1<sup>Cx3cr1ΔEx3</sup>* mice (Figure 2.1D).

Since bone abnormalities, represent a frequent clinical feature in sialidosis patients, we conducted a micro-CT scan of the *Neu1<sup>ΔEx3</sup>* mice tibia which detected increased mineral density of the trabecular bone while mineral content and density in the cortical diaphysis bone was reduced (Figure 2.1E). A reconstructed 3-dimensional image of the spine also showed thick and flattened spinous process of the cervical vertebra and short transverse process of the thoracic vertebra (Figure 2.1F). Despite being smaller in size and weight, the KO mice showed increased primary and secondary spongiosa bone volume, while the growth plate thickness seemed not to differ from those in WT (Figure 2.1G and supplementary table S2-1).

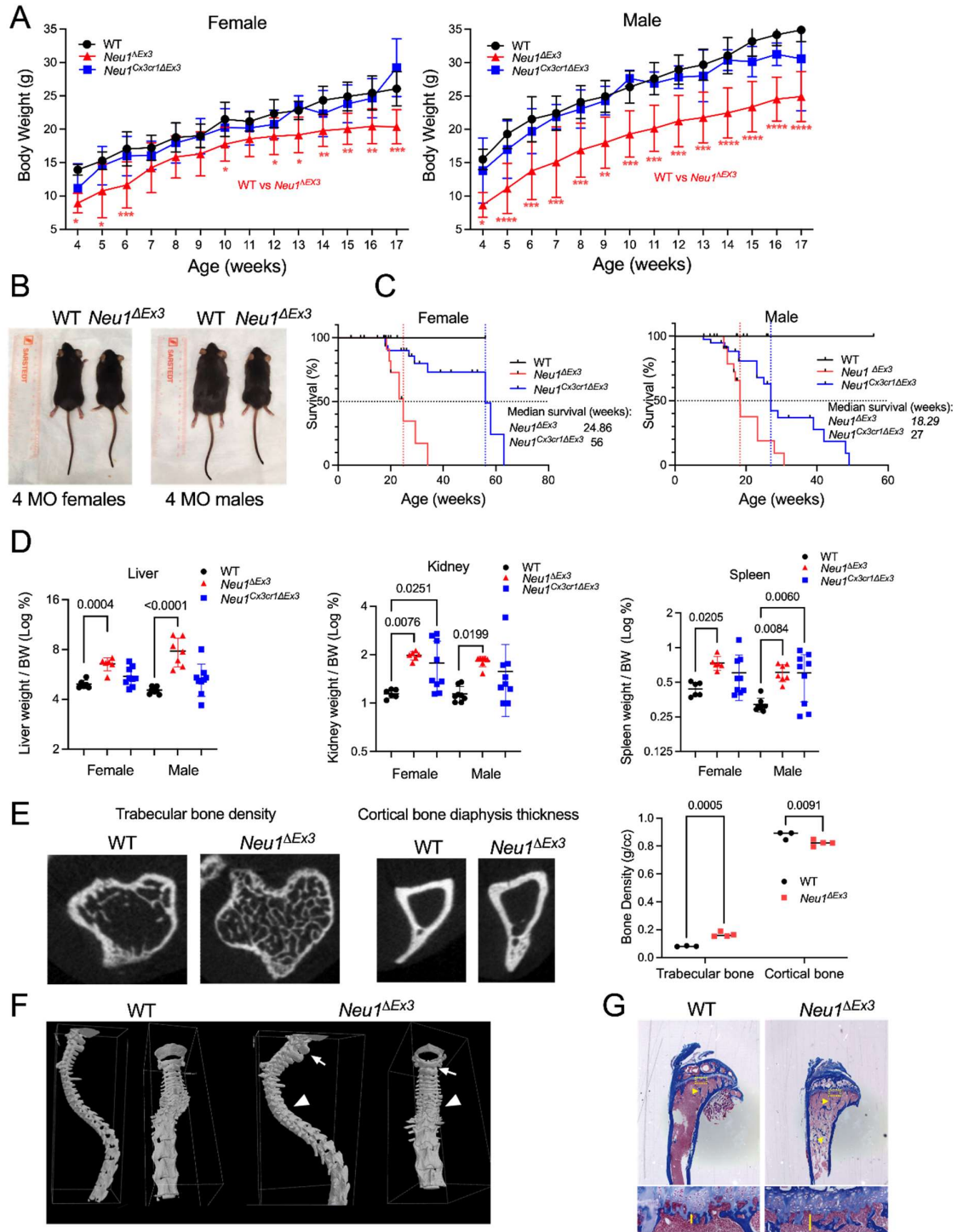


**Figure 2.1: Pathophysiology of *Neu1 $\Delta$ Ex3* and *Neu1Cx3cr1 $\Delta$ Ex3* mice.**

(A) Male and female *Neu1 $\Delta$ Ex3* mice have a significantly reduced body mass compared to WT mice of the same age. Body mass was measured weekly, from 4 to 17 weeks of age. P values were calculated using 2-way ANOVA with a Bonferroni post hoc test. (B) Representative

images of 4-month-old *Neu1<sup>ΔEx3</sup>* mice and their sex-matched WT littermates. (C) Kaplan-Meier plots showing the survival of *Neu1<sup>ΔEx3</sup>* and *Neu1<sup>Cx3cr1ΔEx3</sup>* mice and their WT counterparts. (D) *Neu1<sup>ΔEx3</sup>* mice present with visceromegaly of the kidney, liver and spleen in both males and females. *Neu1<sup>Cx3cr1ΔEx3</sup>* mice present a similar trend with significant differences from WT littermates, observed for spleens of males and kidneys of females. P values were calculated using one-way ANOVA with a Dunnett post hoc test. (E-G) Bone abnormalities in 4-month-old *Neu1<sup>ΔEx3</sup>* mice. (E) Micro-CT scan of tibia showed increased mineral density of the trabecular bone and reduced mineral content and density in the cortical diaphysis bone in *Neu1<sup>ΔEx3</sup>* compared to the WT mice. (F) A reconstructed 3D image of the spine showed thick and flattened spinous process (white arrow) of the cervical vertebra and short transverse process of the thoracic vertebra (white arrowhead). (G) Histology analysis reveals increased primary spongiosa (squares and vertical lines) and trabecular bone (arrows) in the *Neu1<sup>ΔEx3</sup>* mice.

#### 2.2.2 *Neu1<sup>ΔEx3</sup>* and *Neu1<sup>Cx3cr1ΔEx3</sup>* mice show deficiency of NEU1 activity and increased lysosomal biogenesis in tissues.

Total acidic neuraminidase (NEU1, NEU3 and NEU4 together), specific NEU1, total β-hexosaminidase and acidic β-galactosidase enzyme activities were measured with fluorogenic 4-methylumbelliferyl substrates in the homogenates of kidney, liver, spleen, lungs, and brain of WT, *Neu1<sup>ΔEx3</sup>* and *Neu1<sup>Cx3cr1ΔEx3</sup>* mice. NEU1 enzymatic activity, measured in the presence of a specific NEU3/NEU4 inhibitor C9-4BPT-DANA (276), was below detection limit in tissues of *Neu1<sup>ΔEx3</sup>* mice (Figure 2.2A). Surprisingly, *Neu1<sup>Cx3cr1ΔEx3</sup>* mice also showed similarly reduced NEU1 activity levels in all studied tissues except for the brain, where the activity was reduced to ~30-50% of normal and liver (~20% of normal, Figure 2.2A). By comparing levels of total neuraminidase and NEU1 activity, we conclude that NEU1 is the major (>90%) source of neuraminidase activity in the kidney. NEU1 is a relatively minor component in the spleen (<20% of total), as well as in the brain, lungs and liver (~30% of total neuraminidase activity). Notably, mRNA levels for *Neu2-Neu4* isoenzymes were similar in the kidney of *Neu1<sup>ΔEx3</sup>* and WT mice, indicating that genetic depletion of *Neu1* did not cause changes in the expression of other neuraminidases (Figure 2.2B).

Activities of non-targeted lysosomal glycosidases (β-hexosaminidases A and B, and β-galactosidase) showed a significant increase in all tissues of *Neu1<sup>ΔEx3</sup>* mice except for the liver, where total β-hexosaminidase activity showed a trend for an increase (Figure 2.2C and D). These effects are expected and result from lysosomal storage and elevated lysosomal

biogenesis. Lysosomal  $\beta$ -galactosidase and  $\beta$ -hexosaminidase enzyme activities were significantly increased in kidney, lungs, spleen and brain of *Neu1<sup>Cx3cr1 $\Delta$ Ex3</sup>* female mice. Lysosomal  $\beta$ -galactosidase activity was also significantly increased in the spleen of male *Neu1<sup>Cx3cr1 $\Delta$ Ex3</sup>* mice, while lysosomal  $\beta$ -hexosaminidase activity was elevated in their kidney. In the other tissues of male *Neu1<sup>Cx3cr1 $\Delta$ Ex3</sup>* mice, both enzymes showed only a trend for increased activity due to wider variations between individual mice (Figure 2.2C and D). Drastically increased levels of lysosome-associated membrane protein 1 (LAMP1) in the tissues of both *Neu1 $\Delta$ Ex3* and *Neu1<sup>Cx3cr1 $\Delta$ Ex3</sup>* mice, revealed by immunochemistry (Supplementary figure S2-3), were also suggestive of increased lysosomal biogenesis.

To evaluate this further, we conducted a non-targeted proteomic analysis of kidney tissues of 3 male and 3 female 4-month-old mice *Neu1 $\Delta$ Ex3* and WT mice. Prior to the tryptic digestion, protein samples were treated or not with PNGaseF to reveal peptides potentially bearing N-linked glycan chains. The immunoblot analysis of untreated and PNGaseF-treated protein extracts, using anti-LAMP-1 antibodies (Supplementary figure S2-4) revealed that in the treated samples from both WT and *Neu1 $\Delta$ Ex3* mice LAMP-1 immunoreactive band showed a positive electrophoretic mobility shift corresponding to a difference in size of  $-25$  kDa as compared with untreated samples, consistent with a removal of N-linked glycan chains (277). The same analysis also confirmed a  $\sim 5$ -fold increase in LAMP-1 band intensity (Supplementary figure S2-4). The LC-MS/MS analysis identified 1841 proteins in the kidney extracts ( $\text{FDR} \leq 1\%$ ). 101 proteins were absent or reduced in female and 75 in male *Neu1 $\Delta$ Ex3* mice, whereas 150 proteins were increased or present only in female and 243 in male *Neu1 $\Delta$ Ex3* mice compared to WT (Supplementary figure S2-4, Supplementary table S2-3). These proteins were classified according to their biological function and linked to a particular metabolic or signaling pathway using automated GO (gene ontology terms) annotation (Supplementary figure S2-4) (278). The group with the major increase in the kidney of *Neu1 $\Delta$ Ex3* mice contained lysosomal soluble and membrane proteins (25% of increased proteins in female and 16% in male mice, 101 proteins in total, Figure 2.2E, Supplementary figure S2-4 and Supplementary table S2-3) consistent with induced lysosomal biogenesis. To test this further, we have analyzed levels and localization of Transcription Factor EB (TFEB) protein, the master regulator of lysosomal genes expression (reviewed in (279)) by immunofluorescent microscopy (Figure 2.2F). These experiments revealed significantly increased levels of TFEB in the nuclei of endothelial cells of proximal tubules, the phenomenon reported for multiple tissues with lysosomal storage and known to cause increased expression of the lysosomal genes.

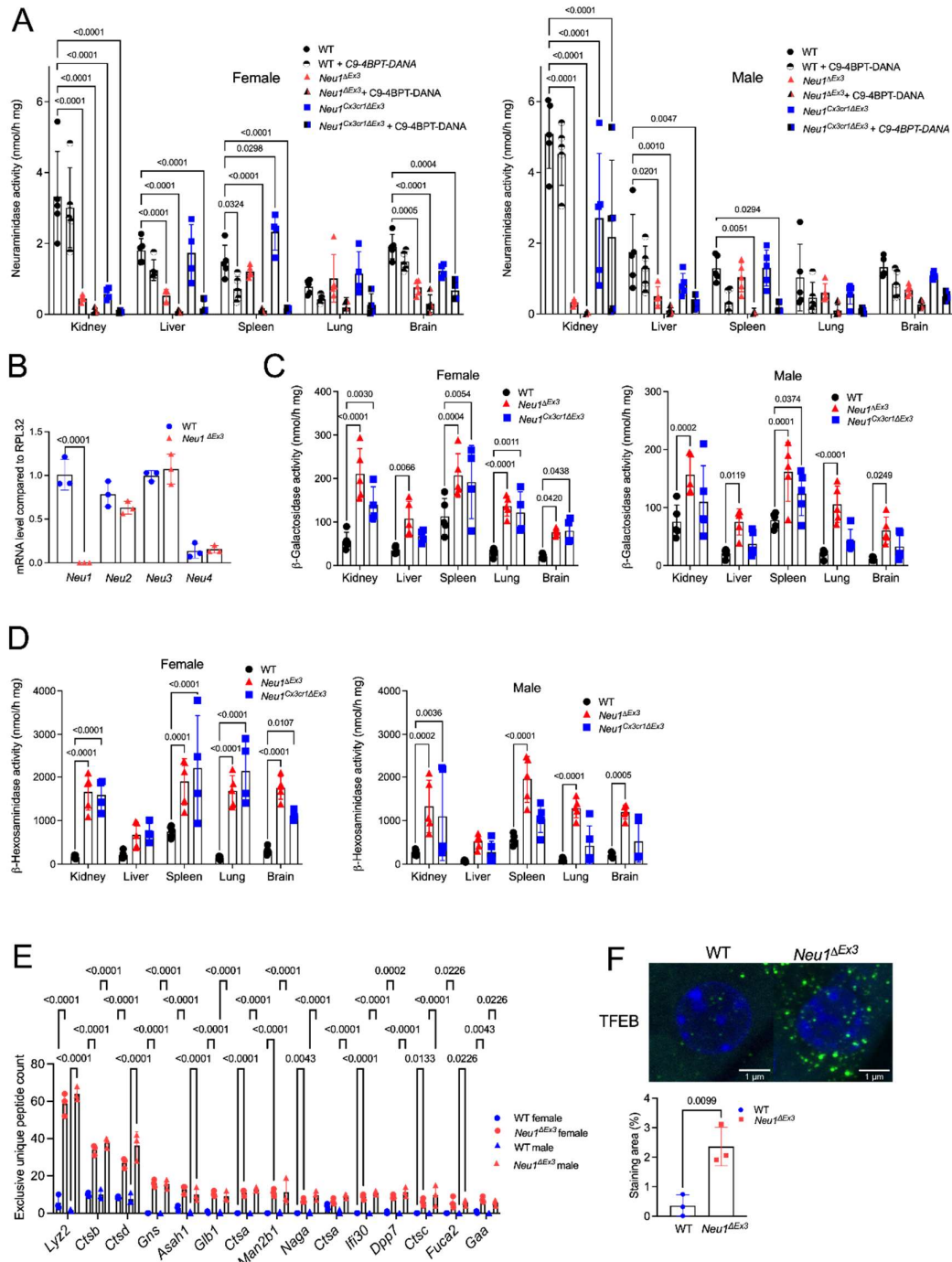


**Figure 2.2:** *Neu1<sup>ΔEx3</sup>* and *Neu1<sup>Cx3cr1ΔEx3</sup>* homozygous mice show deficiency of NEU1 activity and increased lysosomal biogenesis in kidney tissues.

(A) Total neuraminidase and NEU1 enzyme activity were measured in the tissue homogenates of 4-month-old WT, *Neu1<sup>ΔEx3</sup>* and *Neu1<sup>Cx3cr1ΔEx3</sup>* homozygous male and female mice, using flurogenic substrate, 4-MU NANA, in the absence and in the presence of the NEU3/NEU4 inhibitor, C9-4BPT-DANA. Residual NEU1 activity was reduced to below detection levels in

all studied tissues, except for the brain, where the NEU1 activity was reduced in *Neu1<sup>ΔEx3</sup>* but not in *Neu1<sup>Cx3cr1ΔEx3</sup>* mice. P values were calculated using one-way ANOVA with Dunnett post hoc test. **(B)** mRNA levels of *Neu1*, *Neu2*, *Neu3* and *Neu4* were measured in the kidneys of 3 mice per genotype using quantitative RT-PCR. **(C, D)** Elevated levels of lysosomal β-galactosidase and β-hexosaminidase activities, characteristic of increased lysosomal biogenesis, were found in all studied tissues of *Neu1<sup>ΔEx3</sup>* mice as well as in the kidney, spleen, lungs and brain of female *Neu1<sup>Cx3cr1ΔEx3</sup>* mice and show a trend towards an increase in the tissues of males. P values were calculated using one-way ANOVA with Tukey post hoc test. All graphs show individual data, means and SD of experiments performed using tissues from 5 mice per genotype. **(E)** Increased levels of lysosomal proteins in kidney of *Neu1<sup>ΔEx3</sup>* mice. Bar graph shows exclusive unique peptide counts for 15 most abundant lysosomal proteins. Proteomic analyses were performed using kidney protein extracts from 3 mice per sex per genotype. P-values for the exclusive unique peptide counts were calculated using 2-way ANOVA with Sidak post hoc test. **(F)** Immunohistochemical analysis shows increased TFEB levels (green) in the nuclei of endothelial cells in proximal tubules of *Neu1<sup>ΔEx3</sup>* mice. DAPI (blue) was used as nuclear counterstain. Bar graph shows quantification (individual data, means and SD, n=3) of TFEB/DAPI labeled areas by ImageJ software. P values were calculated by unpaired t test.

### 2.2.3 *Neu1<sup>ΔEx3</sup>* and *Neu1<sup>Cx3cr1ΔEx3</sup>* mice show prominent tubuloglomerular pathology.

Our further analysis was focused on kidney pathology to provide insights into the mechanism underlying kidney dysfunction in nephrosialidosis patients. We first conducted light microscopy examination of sagittal H&E-stained kidney sections, which showed several pathological changes in kidneys of both *Neu1<sup>ΔEx3</sup>* and *Neu1<sup>Cx3cr1ΔEx3</sup>* mice: deformed tubules, vacuolized endothelial cells, and condensed glomeruli (Figure 2.3A). However, we did not observe bilateral hydronephrosis or other signs of acute kidney injury that would be expected to result from urinary retention, occurring in both *Neu1<sup>ΔEx3</sup>* and *Neu1<sup>Cx3cr1ΔEx3</sup>* strains. The analysis also revealed a significant (by a factor of 60-70%) reduction in the number of glomeruli in *Neu1*-null mice (Figure 2.3B). Surprisingly, this dramatic change was not accompanied by a drastic decline of renal function since serum creatinine levels were similar. We reasoned that our calculations were likely biased because *Neu1<sup>ΔEx3</sup>* mice are smaller than their WT littermates, while they have larger kidneys. This latter phenomenon is largely due to the presence of storage materials throughout the kidneys, which increases kidney size without parallel scaling of the number of glomeruli. Thus, we, first, approximated of the overall number of glomeruli for each kidney (by multiplying the average number of glomeruli by the kidney

weight); then, we adjusted for discrepant body sizes by dividing this value by the mouse body weight at sacrifice. After these normalizations, the number of glomeruli was only mildly reduced in *Neu1*-null mice (WT  $1.00\pm 0.061$ ; *Neu1* <sup>$\Delta$ Ex3</sup>  $0.796\pm 0.053$ ;  $p=0.034$ ) but not in the conditional KO strain. Also, Masson's Trichrome staining detected mild-to-moderate collagen deposition in the tubulointerstitial areas and parietal epithelium of the Bowman's capsule indicative of renal fibrosis (Figure 2.3C).

To identify specific structural abnormalities, we studied semithin kidney sections, stained with toluidine blue, by high-resolution light microscopy, as well as thin sections, contrasted with uranyl acetate, by transmission electron microscopy (TEM). Toluidine blue-stained sections showed a severe buildup of lysosomal vacuoles in the intraglomerular region and in the epithelial cells of proximal and distal tubule in *Neu1* <sup>$\Delta$ Ex3</sup> mice, which was not detected in the WT controls (Figure 2.3D). In *Neu1*<sup>*Cx3cr1* $\Delta$ Ex3</sup> mice, glomerular cells were similarly affected; however, in contrast to *Neu1* <sup>$\Delta$ Ex3</sup> mice, only the distal convoluted tubules showed moderate accumulation of lysosomal vacuoles, while the proximal convoluted tubules and loop of Henle in the medulla showed no signs of vacuolization (Figure 2.3D).

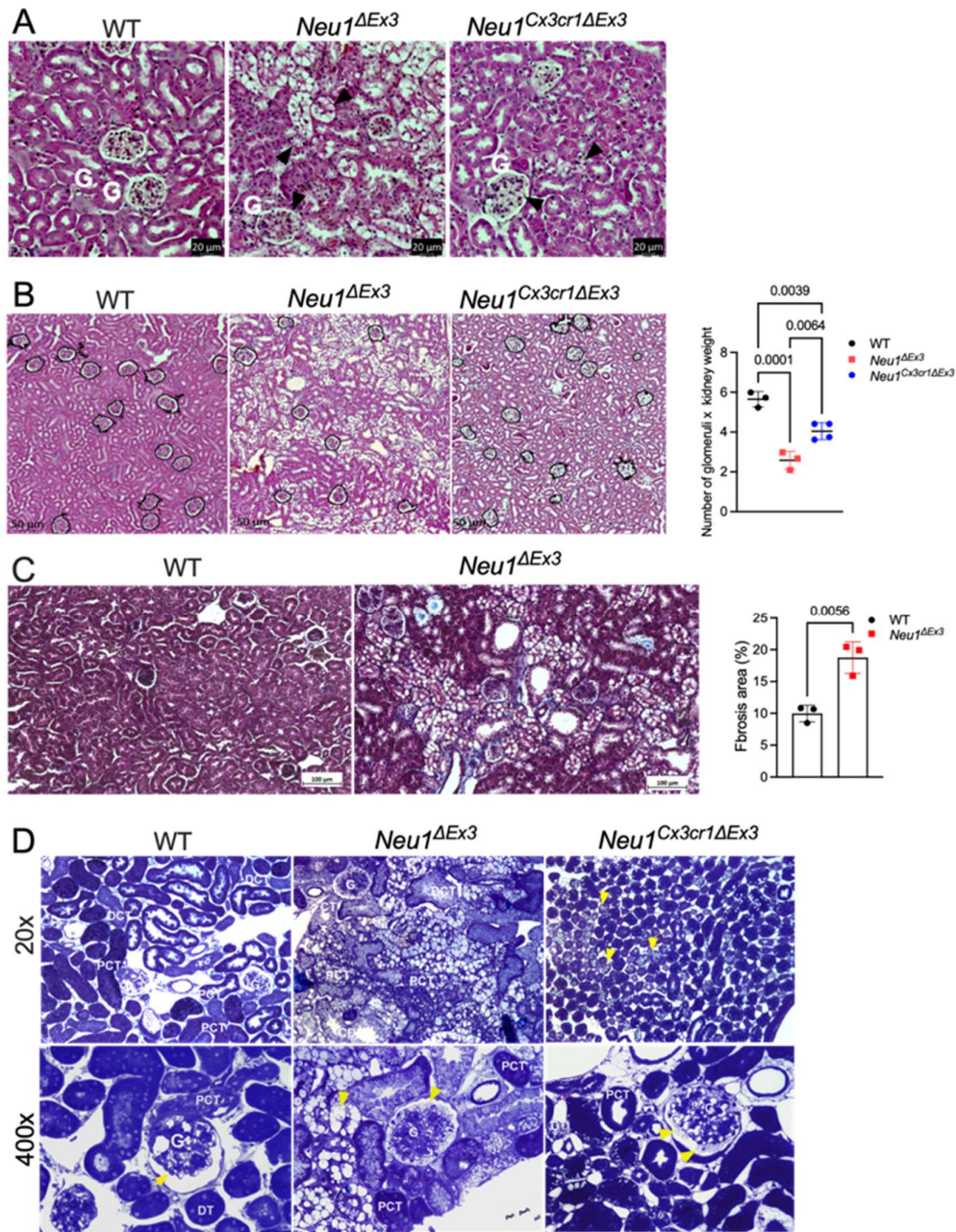


**Figure 2.3: Light microscope images of cortical and medullary regions of kidney from WT, *Neu1 $\Delta$ Ex3*, and *Neu1Cx3cr1 $\Delta$ Ex3* mice stained with H&E (A, B), Masson's Trichrome (C) and toluidine blue (D).**

(A) Normal glomeruli (G) and renal tubular structures are observed in the kidneys of WT mice. In *Neu1 $\Delta$ Ex3* kidney, severe accumulation of storage materials is present in the glomerular cells, and in surrounding tubules (black arrowheads) leading to morphological changes. Deformed tubules with vacuolized epithelial cells, are also present in the kidney of *Neu1Cx3cr1 $\Delta$ Ex3* mice. (B) A significant loss of nephrons was observed in the kidney cortex of 4-month-old *Neu1 $\Delta$ Ex3*

mice. Panels show representative images with nephrons circled, and the graph shows individual values (number of nephrons/regions of interest selected at the same positions from the cortex and multiplied by the kidney weight to account for kidney enlargement occurring in *Neu1*-deficient mice due to lysosomal storage), means and SD obtained from 3 WT, 3 *Neu1<sup>ΔEx3</sup>*, and 4 *Neu1<sup>Cx3cr1ΔEx3</sup>* male and female mice. P values were calculated using one-way ANOVA with Tukey post hoc test. **(C)** Masson's Trichrome staining reveals collagen deposits (blue) in the tubulointerstitial areas and parietal epithelium of the Bowman's capsule in *Neu1<sup>ΔEx3</sup>* mouse characteristic of renal fibrosis. **(D)** WT mouse kidney have normal morphology and do not present buildup of lysosomal vacuoles in intraglomerular cells (G), proximal tubular cells (PT), distal tubular cells (DT), and cells of collecting ducts (CD). Conversely, the kidney of *Neu1<sup>ΔEx3</sup>* mice show a prominent accumulation of vacuoles in intraglomerular cells (G), and, presumably, podocytes (yellow arrow). The epithelial cells of DT and CD exhibit a prominent accumulation of vacuoles. In *Neu1<sup>Cx3cr1ΔEx3</sup>* mice, both the cortex and medulla were mildly affected. In the cortex, both intraglomerular and DT cells show a moderate accumulation of lysosomal vacuoles. In the medulla, the descending portions of the loop of Henle are normal. PT, proximal convoluted tubule; DT, distal convoluted tubule; CD, collecting duct.

Further examination of kidney cortices by TEM confirmed the existence of severe structural defects in the renal tubules and glomeruli. In *Neu1<sup>ΔEx3</sup>* mice, the proximal convoluted tubule (PCT), identified by the presence of the brush border (BB), displayed numerous lysosomal vacuoles containing multilamellated structures (Figure 2.4A). The PCT of *Neu1<sup>Cx3cr1ΔEx3</sup>* mice displayed mitochondria with fragmented cristae and vacuoles with multilamellar structures adjacent to the brush border. However, in contrast to the PCT of *Neu1<sup>ΔEx3</sup>* mice, no enlarged lysosomes were observed in the PCT of *Neu1<sup>Cx3cr1ΔEx3</sup>* mice. Distal convoluted tubules (DCT) in the *Neu1<sup>ΔEx3</sup>* mice showed multiple electron lucent lysosomes with multivesicular bodies (Figure 2.4A). The mitochondria in the DCT of *Neu1<sup>ΔEx3</sup>* mice were pleomorphic, small and disorganized with absent cristae, while in the *Neu1<sup>Cx3cr1ΔEx3</sup>* mice, numerous mitochondria were detached from the basolateral membrane.

Severe pathological changes were also detected in the glomeruli of *Neu1<sup>ΔEx3</sup>* mice, which had multiple lysosomes located throughout the cell body of podocytes, mesangial cells and glomerular parietal epithelial cells (Figure 2.4B). In the *Neu1<sup>Cx3cr1ΔEx3</sup>* kidney, most glomeruli appeared healthy, but some showed a pathology similar to that seen in the *Neu1<sup>ΔEx3</sup>* mice, with vacuolation of the mesangial cells and podocytes. At higher magnification, multivesicular bodies and some osmiophilic structures, resembling lipid or protein aggregates, were detected

in the lysosomal compartments of *Neu1<sup>ΔEx3</sup>* podocytes. In contrast, *Neu1<sup>Cx3cr1ΔEx3</sup>* podocytes exhibited multiple clear, fused vacuoles. In both *Neu1<sup>ΔEx3</sup>* and *Neu1<sup>Cx3cr1ΔEx3</sup>* glomeruli, the filtration slits between podocyte foot processes (pedicels) displayed effacement that was absent in WT kidneys (Figure 2.4B). Glomerular endothelial cells appeared grossly normal, with normal fenestrations.

Since the presence of pleomorphic mitochondria and vacuoles with the content resembling secondary storage materials of protein and lipid nature in glomerular and tubular cells was consistent with an autophagy block, we have analyzed kidney tissues for the presence of puncta positive for autophagosome proteins P62 and LC3 (Figure 2.4C). While in the tissues of WT mice both proteins were not detected, consistent with normal autophagy flux, in the endothelial cells of proximal tubules of *Neu1<sup>ΔEx3</sup>* mice, we observed coarse LC3-positive and P62-positive puncta indicative of autophagy block caused by inability of autophagosomes to fuse with lysosomes (280). The increased LC3 and P62 levels were confirmed by immunoblotting of total kidney proteins (Figure 2.4D). Both immunofluorescent microscopy and immunoblot experiments also revealed increased levels of phosphorylated (S240/S244) S6 ribosomal protein, the substrate of mTORC1, a key regulator of autophagy and lysosome biogenesis (Figure 2.4C and D). This indicated that mTORC1 activity against this substrate was increased in kidney of *Neu1<sup>ΔEx3</sup>* mice and, specifically, in the cells of proximal tubules.

Since tissue infiltration with immune cells was previously reported for sialidosis patients, kidney tissues were examined by immunohistochemistry for the presence of CD68-positive macrophages. Our results demonstrated that the kidneys of both *Neu1<sup>ΔEx3</sup>* and *Neu1<sup>Cx3cr1ΔEx3</sup>* mice exhibited high numbers of CD68-positive cells, whereas none were detectable in WT controls (Supplementary figure S2-3). Importantly, in mice of both strains, macrophages showed an “ameba-like” morphology that is typical for activated cells.

The extent of kidney tissue abnormalities in *Neu1<sup>ΔEx3</sup>* and *Neu1<sup>Cx3cr1ΔEx3</sup>* mice revealed by light microscopy and TEM suggested that it would likely be accompanied by abnormalities in kidney function(s). To verify if proteinuria was present, urine samples, collected from 4-month-old WT, *Neu1<sup>ΔEx3</sup>* and *Neu1<sup>Cx3cr1ΔEx3</sup>* mice using metabolic cages, were analyzed by SDS-PAGE. The gels showed a prominent protein 65 kDa band, characteristic of albumin, in the urine of *Neu1<sup>ΔEx3</sup>* mice. This band was absent in the urine of age and sex-matching WT and *Neu1<sup>Cx3cr1ΔEx3</sup>* mice (Supplementary figure S2-5). Analysis with a urine dipstick also revealed increased protein and glucose levels, and reduction of pH in the urine of *Neu1<sup>ΔEx3</sup>* mice (Supplementary figure S2-5). At the same time, the specific gravity of urine of *Neu1<sup>ΔEx3</sup>* and

*Neu1<sup>Cx3cr1ΔEx3</sup>* mice was in the normal range (1.030, similar to that of WT mice), indicating that these mice do not develop a urinary concentrating defect with polyuria (Supplementary S2-5). To test whether glucosuria was associated with glycemia, we measured blood glucose levels in 4-month-old, fasted mice of both strains and detected elevated glucose levels in *Neu1<sup>ΔEx3</sup>* mice, and in male, but not in female *Neu1<sup>Cx3cr1ΔEx3</sup>* mice (Supplementary figure S2-5). Finally, ELISA test confirmed increased urine albumin levels and increased Urine Albumin-to-Creatinine Ratio (UACR) levels in 4-month-old *Neu1<sup>ΔEx3</sup>* and 5-month-old *Neu1<sup>Cx3cr1ΔEx3</sup>* mice (Supplementary figure S2-5).

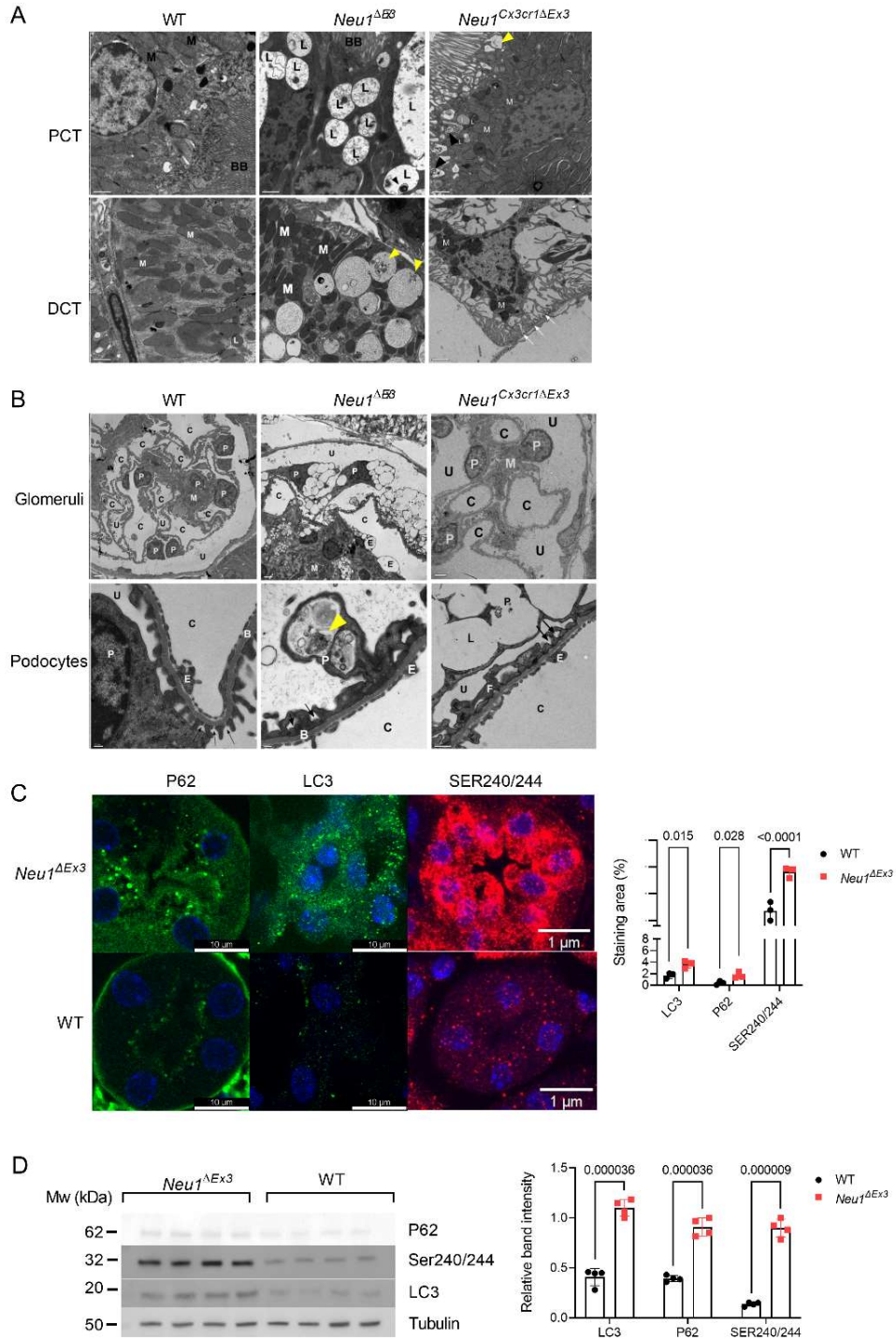


**Figure 2.4: Pathological changes in glomerular and tubular cells in *Neu1*<sup>ΔEx3</sup> and *Neu1*<sup>Cx3cr1ΔEx3</sup> mice.**

(A) Kidney of *Neu1*<sup>ΔEx3</sup> mice contain numerous enlarged electron-lucent lysosomes (L) filled with multilamellar structures (black arrowhead) in the proximal convoluted tubule (PCT), and

multivesicular bodies (yellow arrowheads) in the lysosomal compartments of the distal convoluted tubules (DCT). Small irregularly shaped mitochondria with fragmented cristae (M) are found throughout the PCT and DCT of *Neu1<sup>ΔEx3</sup>* and *Neu1<sup>Cx3cr1ΔEx3</sup>* mice. In the DCT of *Neu1<sup>Cx3cr1ΔEx3</sup>* mice, mitochondria are dissociated from the distorted basolateral plasma membrane (white arrows). **(B)** In the glomeruli of *Neu1<sup>ΔEx3</sup>* mice, the podocytes (P) and mesangial cells (M) are severely vacuolated. Higher magnification of podocytes shows multivesicular structures and osmiophilic deposits (yellow arrowhead). The podocyte foot processes (F), form a discontinuous lining for the inner aspect of the WT glomerular basement membrane, are widely effaced in both *Neu1<sup>ΔEx3</sup>* and *Neu1<sup>Cx3cr1ΔEx3</sup>* mice (black arrows). C identifies capillaries, U, urinary space and E, endothelium. All transmission electron microscopy panels show representative images taken for 3 WT, 3 *Neu1<sup>ΔEx3</sup>* and 2 *Neu1<sup>Cx3cr1ΔEx3</sup>* mice. Size bars equal 1 μm in **(A)**, 2 μm in glomeruli and 0.2 μm in high magnification images of podocytes **(B)**. **(C)** Endothelial cells of the proximal convoluted renal tubules in *Neu1<sup>ΔEx3</sup>* mice reveal accumulation of P62<sup>+</sup> and LC3<sup>+</sup> puncta, consistent with impaired autophagy, and increased phosphorylation (Ser240/244) of S6 ribosomal protein substrate of mTORC1. Graph shows relative areas stained with antibodies against P62, LC3 and Ser240/244 S6 quantified with ImageJ. Individual values, means and SD are shown (n=3). P values were calculated with multiple unpaired t-tests. **(D)** Immunoblotting of kidney proteins confirms increase in P62, LC3 and Ser240/244 levels. Graph shows bands intensities, quantified with ImageJ software and normalized to the intensities of tubulin immunoreactive bands. Individual values, means and SD are shown (n=3). P values were calculated with multiple unpaired t-tests.

#### 2.2.4 Glycomic profiling reveals protein hypersialylation in *Neu1<sup>ΔEx3</sup>* mice kidneys.

To test whether NEU1 deficiency altered protein sialylation in kidney tissues, we stained kidney sections with fluorescently labeled *Sambucus nigra* lectin (SNA) that binds preferentially to sialic acids attached to terminal galactose in  $\alpha$ -2,6 and, to a lesser degree,  $\alpha$ -2,3 position. We also used *Maackia amurensis* lectin 2-4 (MAL-II), specific for  $\alpha$ -2,3 linked Sia residues, *Arachis hypogaea* (peanut) agglutinin (PNA), specific for terminal  $\beta$ -galactose residues in O-linked glycans, and *Ricinus Communis* Agglutinin I (RCA-1) specific for terminal  $\beta$ -galactose residues in N-linked glycans. The labeling with SNA and MAL-II was drastically increased throughout the kidney and specifically in the proximal renal tubules of *Neu1<sup>ΔEx3</sup>* compared with WT mice (Figure 2.5A and B). In contrast, labeling with RCA-1, usually exposed in complex glycans after neuraminidase treatment was reduced, while PNA

labeling showed a non-significant trend towards reduction (Figure 2.5A and B). Treatment of kidney tissues with exogenous pan-specific *Arthrobacter ureafaciens* sialidase increases PNA and RCA-1 labeling and reduces MAL-II and SNA labeling in the proximal convoluted renal tubules of both *Neu1<sup>ΔEx3</sup>* and WT mice, confirming specificity of the assay (Figure 2.5D). These results, suggesting hypersialylation of kidney tissues in *Neu1<sup>ΔEx3</sup>* mice, were partially confirmed by lectin blotting, indicating that multiple proteins extracted from *Neu1<sup>ΔEx3</sup>* mice kidneys had increased affinity to SNA and decreased affinity to PNA (Figure 2.5D). Intensity of MAL-II or RCA-1 labeling of total kidney proteins was not significantly different for WT and *Neu1<sup>ΔEx3</sup>* mice.

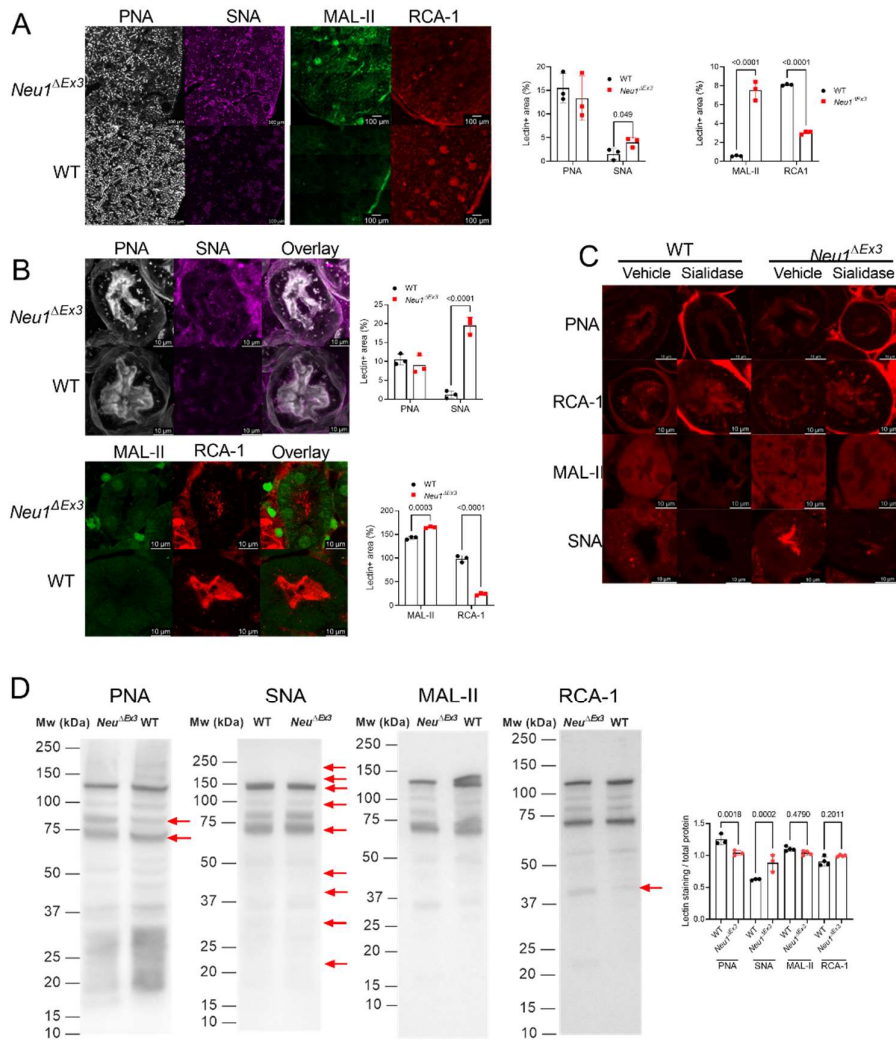


**Figure 2.5: Abnormal protein glycosylation in *Neu1<sup>ΔEx3</sup>* kidney tissues.**

(A) Kidney cortex sections of *Neu1<sup>ΔEx3</sup>* mice show elevated labeling with SNA (purple) and MAL-II (green) lectins, and reduced labeling with RCA-1 (red) lectin. PNA labeling (white)

shows a non-significant trend towards a decrease. **(B)** SNA (purple) and MAL-II (green) labeling is drastically increased in the proximal convoluted renal tubules of *Neu1<sup>ΔEx3</sup>* mice, RCA-1 labeling (red) shows a decrease and PNA labeling (white) a non-significant trend towards a decrease. **(C)** Treatment of kidney tissues with exogenous pan-specific bacterial *Arthrobacter ureafaciens* sialidase increases PNA and RCA-1 labeling and reduces MAL-II and SNA labeling in the proximal convoluted renal tubules of both *Neu1<sup>ΔEx3</sup>* and WT mice, confirming specificity of the assay. Cryopreserved 15 μm thick kidney sections treated (Sialidase) or not (Vehicle) with bacterial sialidase were stained with cy5-labeled SNA (magenta), cy3-labeled PNA (white), Rhodamine-labeled RCA-1 (red) or FITC-labeled MAL-II (green) lectins. Images were taken with Leica confocal microscope SP8-DLS. Scale bars equal 100 μm **(A)** and 10 μm **(B, C)**. Graphs show lectin-positive areas (individual values, means and SD, n=3). Quantifications were performed by ImageJ software, and P values were calculated using multiple t-tests.

**(D)** Lectin blotting of kidney proteins shows changes in glycosylation of proteins in tissues of *Neu1<sup>ΔEx3</sup>* mice compared to WT mice. Panels show images of representative lectin blots. Red arrows mark protein bands with decreased affinity for PNA and increased affinity for SNA. Graphs show combined intensities (individual values, means and SD) of protein bands stained with lectins and normalized by combined intensities of Ponceau staining. Quantifications were performed by ImageJ software, and P values were calculated using a t-test.

To confirm the results of lectin staining and to compare structures of protein N-glycans in WT and NEU1-deficient mice, we analyzed the N-glycome of kidney tissues from 4-month-old WT and *Neu1<sup>ΔEx3</sup>* mice. First line of MALDI-TOF MS examination revealed the occurrence of sialylated glycans in tissues of *Neu1<sup>ΔEx3</sup>* mice that were absent in WT counterparts (Supplementary figure S2-6A and B, Supplementary Table S2-2). These species, most likely, represent free oligosaccharides stored in the lysosomes of kidney tissues and/or secreted in the urine of *Neu1* KO mice, since their corresponding human analogs were frequently identified in the urine of sialidosis patients (281). Besides, the major structure at *m/z* 2607.2, analyzed by MALDI-TOF MS/MS (Supplementary figure S2-6C), showed the presence of a single GlcNAc at the reducing glycan end, instead of the chitobiose disaccharide GlcNAc-GlcNAc, which is expected to be found in N-linked glycans.

Thus, kidney protein pellets were additionally washed with ddH<sub>2</sub>O to remove soluble free oligosaccharides (further studied separately by MS and MS/MS, Table S2-2), and the N-glycome analyses were repeated. MALDI-TOF MS profiles of permethylated N-glycans of

proteins from WT mice (Figure 2.6A) were essentially similar to the profiles from unwashed tissues. They presented three major peaks at  $m/z$  2837.5, 3460.8 and 4084.1 corresponding to bisected, core-fucosylated N-glycan structures bearing two, three and four antennae, respectively, each terminated with a Lewis-X epitope, as verified by MALDI MS/MS fragmentation analysis. Minor peaks corresponded to paucimannose, oligomannose and core-fucosylated bisected structures, latter being predominantly terminated with galactose. Sialylated glycoforms were found in traces and were assigned at lower molecular weight to biantennary structures bearing Neu5Gc or Neu5Ac (e.g.  $m/z$  2605.3, 2635.3, 2852.4 and 2966.4), and over  $m/z$  4000 to bisected structures whose antennae were mainly terminated with Lewis-X motifs or Neu5Gc (e.g.  $m/z$  4127.0 and 4301.2). The relative intensities of N-linked glycans were changed in *Neu1<sup>ΔEx3</sup>* compared to WT mice (Figure 2.6B). In particular, we observed a drastic accumulation of paucimannose and oligomannose structures and occurrence/increase of sialylated, not bisected complex N-glycans bearing Neu5Ac (Figure 2.6B, underlined  $m/z$  values e.g. 2156, 2431.2, 2605.3, 2635.3, 2966.4, 3054.5, and 3415.6). Importantly, MALDI MS profiles obtained from male and female *Neu1<sup>ΔEx3</sup>* mice were clearly distinguishable, with males showing an intense peak at  $m/z$  2852.4 (corresponding to a biantennary disialo-glycoform bearing one Neu5Gc at each antenna), which occurred to a much lesser extent in female littermates (Supplementary figure S2-7). Table 2.1 lists all the sialylated glycoforms accumulated in *Neu1<sup>ΔEx3</sup>* kidney tissues and provides a relative quantitative comparison between WT and *Neu1<sup>ΔEx3</sup>* mice. To analyze sialic acids linkages, we also performed N-glycoprofiling by HILIC-UPLC-FLR-ESI-MS (282) capable to distinguish between 2,3 and 2,6-linked sialic acids (283). These analyses confirmed major increases of oligomannose and sialylated N-glycans in *Neu1<sup>ΔEx3</sup>* mice (Supplementary figure S2-8A) and indicated that the ratio of 2,3 to 2,6-linked sialic acids is similar in WT and in *Neu1<sup>ΔEx3</sup>* mice, as illustrated by the representative extracted ion current for the disialo-biantennary core-fucosylated structure with  $m/z$  1341.0150 (Supplementary figure S2-8B).

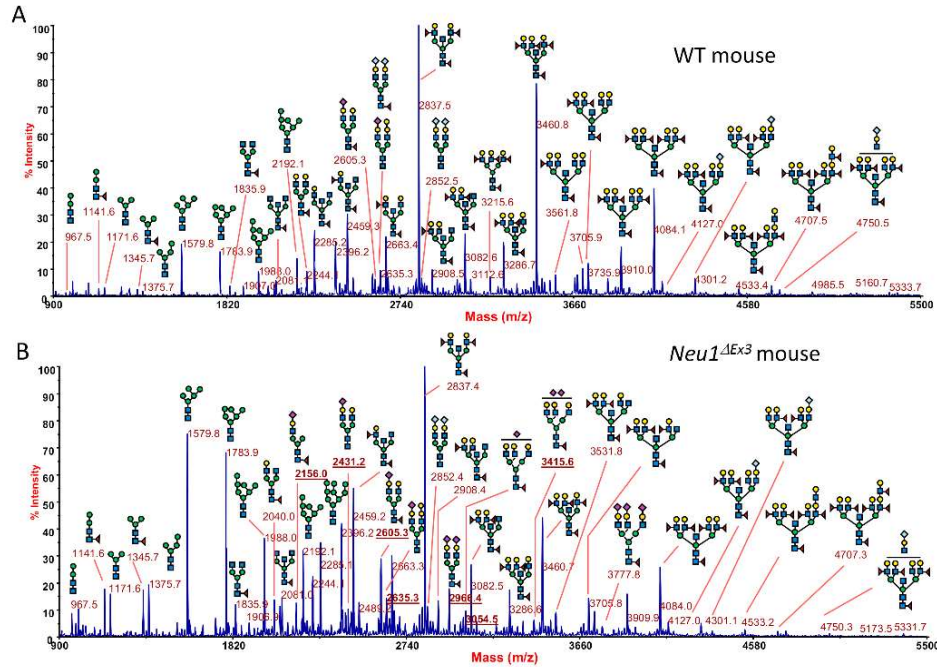


**Figure 2.6: MALDI TOF MS analysis of mouse kidney proteins shows changes in the profile of N-glycans.**

MALDI TOF profiles (mass-range between  $m/z$  900 and 5500) of permethylated N-glycans from kidney tissue glycoproteins representative for samples from WT (A) and *Neu1*<sup>ΔEx3</sup> (B) female mice showing increased amounts of sialylated structures (underlined  $m/z$  values). Structures of the glycan species were corroborated by MS/MS analyses. Species were detected as  $[M+Na]^+$  molecular ions (monoisotopic masses). Graphical representation of glycans is based on the third edition of the Essentials of Glycobiology (284): GlcNAc, blue square; Man, green circle; Gal, yellow circle; Neu5Ac, purple diamond; Neu5Gc, light blue diamond; Fuc, red triangle.

**Table 2.1: Major N-linked sialylated glycans are abnormally abundant in *Neu1*<sup>ΔEx3</sup> mouse kidney tissues.**

<i>m/z</i>	Composition	WT (n.3) Relative area mean ± SD	<i>Neu1</i> <sup>ΔEx3</sup> (n.4) Relative area mean ± SD	<i>p</i> -value
1981.98	NeuAc <sub>1</sub> Gal <sub>1</sub> Man <sub>3</sub> GlcNAc <sub>3</sub>	0.024 ± 0.008	0.232 ± 0.093	<b>1.11E-06</b>
2156.07	NeuAc <sub>1</sub> Gal <sub>1</sub> Man <sub>3</sub> GlcNAc <sub>3</sub> Fuc <sub>1</sub>	0.050 ± 0.015	0.478 ± 0.244	<b>2.40E-05</b>

2390.18	NeuAc <sub>1</sub> Gal <sub>1</sub> Man <sub>5</sub> GlcNAc <sub>3</sub>	0.066 ± 0.022	0.212 ± 0.107	<b><u>4.06E-04</u></b>
2401.20	NeuAc <sub>1</sub> Gal <sub>1</sub> Man <sub>3</sub> GlcNAc <sub>4</sub> Fuc <sub>1</sub>	0.130 ± 0.038	0.379 ± 0.218	<b><u>1.66E-03</u></b>
2431.21	NeuAc <sub>1</sub> Gal <sub>2</sub> Man <sub>3</sub> GlcNAc <sub>4</sub>	0.183 ± 0.042	0.424 ± 0.231	<b><u>3.15E-03</u></b>
2605.30	NeuAc <sub>1</sub> Gal <sub>2</sub> Man <sub>3</sub> GlcNAc <sub>4</sub> Fuc <sub>1</sub>	0.408 ± 0.076	0.982 ± 0.517	<b><u>1.96E-03</u></b>
2635.31	NeuAc <sub>1</sub> Gal <sub>3</sub> Man <sub>3</sub> GlcNAc <sub>4</sub>	0.620 ± 0.118	0.671 ± 0.333	3.31E-01
2809.40	NeuAc <sub>1</sub> Gal <sub>3</sub> Man <sub>3</sub> GlcNAc <sub>4</sub> Fuc <sub>1</sub>	0.312 ± 0.098	0.438 ± 0.304	1.25E-01
2966.47	NeuAc <sub>2</sub> Gal <sub>2</sub> Man <sub>3</sub> GlcNAc <sub>4</sub> Fuc <sub>1</sub>	0.218 ± 0.040	0.728 ± 0.313	<b><u>5.91E-05</u></b>
3054.52	NeuAc <sub>1</sub> Gal <sub>3</sub> Man <sub>3</sub> GlcNAc <sub>5</sub> Fuc <sub>1</sub>	0.337 ± 0.027	0.376 ± 0.213	2.93E-01
3415.70	NeuAc <sub>2</sub> Gal <sub>3</sub> Man <sub>3</sub> GlcNAc <sub>5</sub> Fuc <sub>1</sub>	0.101 ± 0.023	0.222 ± 0.181	<b><u>3.11E-02</u></b>
3776.87	NeuAc <sub>3</sub> Gal <sub>3</sub> Man <sub>3</sub> GlcNAc <sub>5</sub> Fuc <sub>1</sub>	0.085 ± 0.024	0.175 ± 0.123	<b><u>2.17E-02</u></b>
Total sialylated structures		2.534 ± 0.269	5.318 ± 2.566	<b><u>2.25E-03</u></b>

### 2.2.5 Aberrant glycosylation and trafficking of endocytic receptor megalin in kidney cells of *Neu1<sup>ΔEx3</sup>* mice

An endocytic receptor megalin (lipoprotein receptor-related protein 2, LRP2), responsible for the uptake of numerous urinary metabolites, is one of the main glycoproteins on apical membranes of proximal tubules. This protein bears multiple O-linked and N-linked glycans with terminal β-galactose residues, which are essential for the intracellular stability of LRP receptors (285). Glycosylation defects of megalin are known to affect its function and expression, leading to kidney dysfunction and proteinuria (286).

Since the presence of albumin in the urine of *Neu1<sup>ΔEx3</sup>* mice suggested a reabsorption defect potentially related to deficiencies of megalin expression or processing, we analyzed levels of megalin in kidney tissues by immunoblotting and observed drastically decreased levels of megalin in tissues of *Neu1<sup>ΔEx3</sup>* compared to WT mice (Figure 2.7A). To understand

whether reduced renal levels of megalin in *Neu1<sup>ΔEx3</sup>* mice are associated with changes in glycosylation, we performed PNA and SNA lectin blots and determined significantly increased affinity of megalin band for SNA consistent with oversialylation, while PNA labeling of the protein was not changed. However, when we repeated PNA blot with the samples pretreated with endoglycosidase PNGaseF to remove N-linked glycans, we observed that megalin immunoreactive protein bands in WT kidney extracts, either untreated or treated with PNGaseF, were equally stained with PNA. These results are consistent with O-linked glycans with terminal β-galactose residues being the major glycoform recognized by PNA on megalin in murine kidneys (Figure 2.7B). In contrast, in *Neu1<sup>ΔEx3</sup>* kidney extracts, the megalin band was not stained with PNA after PNGaseF treatment, suggesting that the β-galactose residues on O-linked glycans were now masked by sialylation (Figure 2.7B). In the untreated samples from WT kidney, the megalin band was recognized by RCA-1, and the labeling intensity was further increased after the treatment with *Arthrobacter ureafaciens* sialidase. In the samples from *Neu1<sup>ΔEx3</sup>* kidney, the megalin band was recognized by RCA-1 only in sialidase-treated samples consistent with oversialylation of N-linked glycan chains (Figure 2.7C).

To confirm this further, we conducted the analysis of proximal tubule in kidney tissues of WT and *Neu1<sup>ΔEx3</sup>* mice, co-stained with anti-megalín antibodies and either SNA (for sialic acid) or PNA (for galactose), by high-resolution SP8-DLS confocal microscopy (Figure 2.7D). 3D confocal images rendered with the LasX program showed the proximity of the SNA signals and anti-megalín antibodies in the *Neu1<sup>ΔEx3</sup>* tissues, indicating that megalín was sialylated (Figure 2.7D). In contrast, in WT tissues, colocalization was not observed for anti-megalín antibodies and SNA, suggesting that megalín was mainly present in its asialo form. In addition, analysis of tissues labeled with RCA-1 or PNA lectins and anti-megalín antibodies showed a reduced intensity of RCA-1 and PNA labeling co-localizing with megalín in proximal tubules of *Neu1<sup>ΔEx3</sup>* mice compared with WT mice which was restored by sialidase treatment (Figure 2.7E).

We further used high-resolution SP8-DLS confocal microscopy to analyze tissues labeled for megalín and the lysosomal marker LAMP1 and found a drastic difference in localization of megalín in proximal tubules of WT and *Neu1<sup>ΔEx3</sup>* mice. In the WT mice kidney, the majority of megalín was, as expected, found on the apical membranes of proximal tubules. In contrast, in the *Neu1<sup>ΔEx3</sup>* mice kidney, most of megalín protein was found inside LAMP1-positive luminal structures, indicating its trafficking to enlarged lysosomes (Figure 2.7F). Finally, immunoblot analysis of urine samples from *Neu1<sup>ΔEx3</sup>* mice revealed high levels of

megalín as well as of low molecular weight proteins that are known to be reabsorbed via binding to megalín:  $\beta$ 2-microglobulin ( $\beta$ 2-MG), and vitamin D-binding protein (DBP). In contrast, and as expected, urine samples from WT mice did not contain any of these proteins. This suggests that megalín sheds off apical membranes of the proximal tubule cells and that this results in defective reabsorption of low molecular weight proteins (Figure 2.7G). We further tested if megalín deficiency and increased urinary secretion of DBP was associated with altered levels of 25-OH vitamin D by measuring its levels in blood plasma and urine with ELISA. We found no significant difference in 25-OH vitamin D between *Neu1* KO and WT mice in plasma, however, urinary levels were significantly increased in *Neu1<sup>ΔEx3</sup>* compared to WT mice (Figure 2.7G).

To test whether other endocytic receptors and solute carriers, present at the apical membrane of proximal tubules, are also reduced in the *Neu1<sup>ΔEx3</sup>* mice kidney, we have searched our proteomics data for the proteins associated with the corresponding GO terms and identified several proteins decreased or absent in kidney of *Neu1<sup>ΔEx3</sup>* mice (Supplementary figure S2-4, Supplementary table S2-3). This list of proteins included a megalín-binding endocytic receptor cubilín (*Cubn*), Sodium/glucose cotransporter 2 (*Sglt2*), Solute carrier family 22 member 6 (*Slc22a6*, kidney-specific organic transport protein 1), Solute carrier family 22 member 12 (*Slc22a12*, Urate anion exchanger 1), Solute carrier family 22 member 2 (*Slc22a2*, Organic cation transporter 2), and Prostaglandin E2 receptor EP2. Proteomic analysis also confirmed the reduction of megalín (*Lrp-2*) in the *Neu1<sup>ΔEx3</sup>* mice kidney (Supplementary table S2-3). The reduction of cubilín and SGLT2 on the apical surface of proximal renal tubule of *Neu1<sup>ΔEx3</sup>* mice was further directly confirmed by immunofluorescent microscopy and immunoblotting (Figure 2.7J and K).

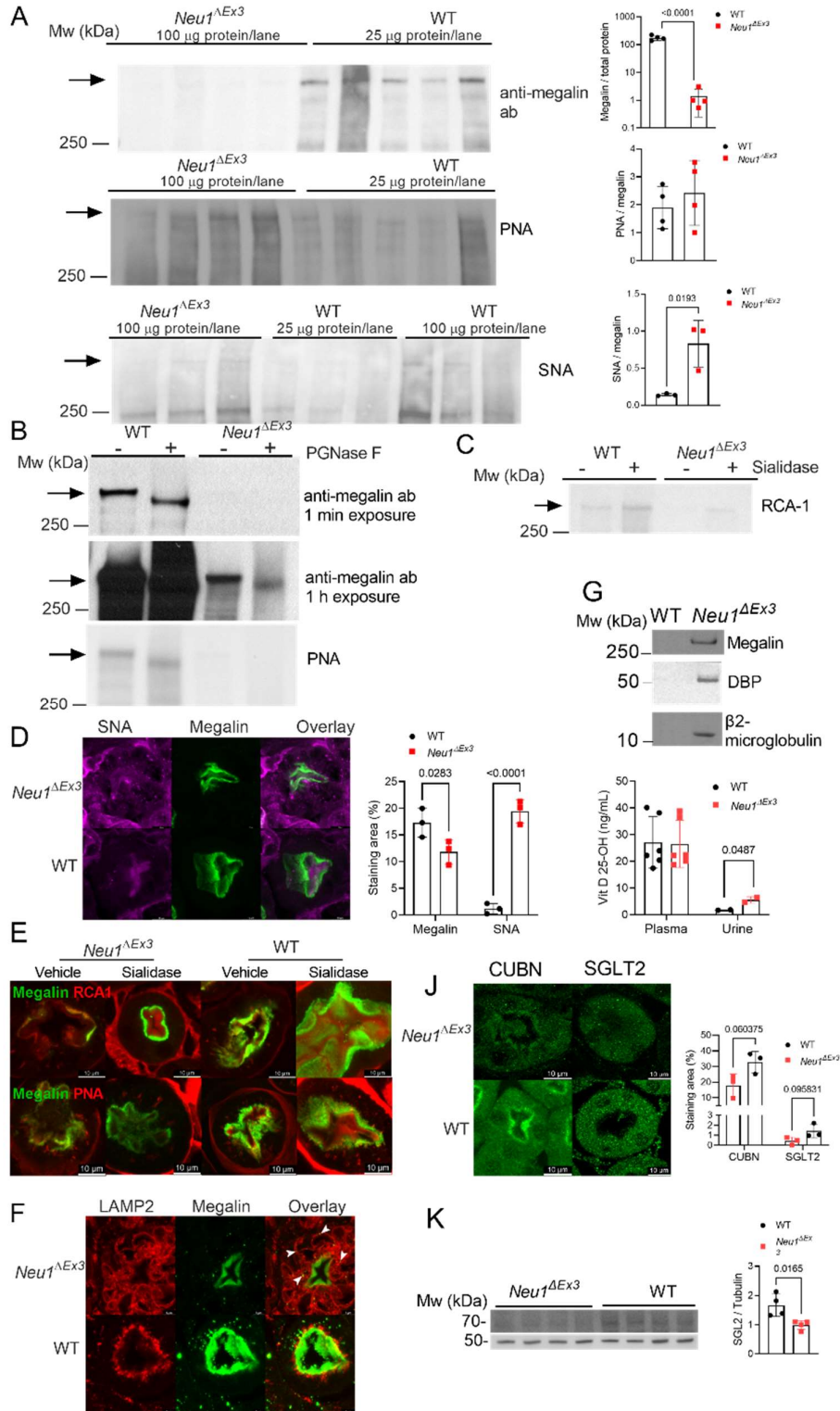


**Figure 2.7: Aberrant glycosylation of megalin affects its abundance and trafficking in the kidney of *Neu1*<sup>ΔEx3</sup> mice.**

(A) Immunoblot shows reduction of megalin in *Neu1<sup>ΔEx3</sup>* mouse kidney. Lectin blots show that megalin affinity to SNA significantly increases, suggestive of protein hypersialylation. 100 or 25 μg of kidney protein extract from *Neu1<sup>ΔEx3</sup>* and WT mice were analyzed. Arrows mark the megalin position. (B) In the WT kidney, megalin shows equal intensity of PNA staining, before and after PNGaseF treatment, suggesting that the protein contains mainly O-linked glycans with terminal galactose residues. In *Neu1<sup>ΔEx3</sup>* kidney, the PNGaseF-treated protein does not show affinity to PNA, suggesting the absence of glycans with terminal galactose. (C) Megalin in WT kidney is recognised by RCA-1 specific for N-linked glycans with terminal galactose residues. In *Neu1<sup>ΔEx3</sup>* kidney, megalin is recognized by RCA-1 only after treatment with bacterial sialidase, consistent with oversialylation masking galactose residues. (D) In proximal renal tubules of *Neu1<sup>ΔEx3</sup>* kidney megalin co-localizes with SNA suggesting its hypersialylation. 3-D images were acquired using SP8-DLS high-resolution confocal microscope, and colocalization of megalin and SNA analyzed by LasX software (Supplemental videos 1 and 2). (E) RCA-1 colocalizes with megalin in WT but not in *Neu1<sup>ΔEx3</sup>* kidney. RCA-1 and PNA staining is increased after sialidase treatment. (F) In proximal tubules of WT kidney, megalin is found on the apical membrane; in *Neu1<sup>ΔEx3</sup>* kidney, it is found inside enlarged LAMP1+ lysosomes (white arrows and Supplemental videos 3 and 4). (G) Megalin, β2-microglobulin (β2-MG), vitamin D-binding protein (DBP) and 25-OH vitamin D are detected in urine of *Neu1<sup>ΔEx3</sup>* mice. (J) Cubilin (CUBN) and solute-carrier SGLT2 show a trend towards reduction on the apical surface of the proximal tubules of *Neu1<sup>ΔEx3</sup>* kidney. (K) Immunoblotting confirms reduction of SGLT2 protein in *Neu1<sup>ΔEx3</sup>* kidney homogenates. Fluorescence and band intensities were quantified with ImageJ software. Individual data, means and SD (n=3) are shown. P values were calculated using unpaired multiple t-test.

### 2.3 Methods

The constitutive KO NEU1 mouse model (*Neu1<sup>ΔEx3</sup>*) was previously described (32). *Neu1<sup>ΔEx3</sup>* homozygous mice were compared with appropriate age- and sex-matched WT control littermates. To generate *Neu1<sup>Cx3cr1ΔEx3</sup>* strain, a mononuclear phagocyte system-specific *Neu1* KO model, previously reported *Neu1<sup>ENSMUSE141558</sup>* strain (32), was interbred with the *B6.Cg-Tg(Pgk1-flpo)10Sykr/J* line (The Jackson Laboratory, stock 011065). This cross resulted in the removal of FRT-flanked *LacZ/BactPNeo* cassette and normal expression of the *Neu1* gene in the *Neu1<sup>loxPEx3</sup>* strain. The *Neu1<sup>Cx3cr1ΔEx3</sup>* strain was obtained by crossing *Neu1<sup>loxPEx3</sup>* strain with the B6J.B6N(Cg)-Cx3cr1tm1.1(cre)Jung/J strain (The Jackson Laboratory, stock 025524), expressing the Cre recombinase under the control of the *Cx3cr1* (chemokine C-X3-C motif

receptor 1) gene promoter. *Neu1*<sup>Cx3cr1ΔEx3</sup> homozygous mice were compared with appropriate age- and sex-matched *Neu1*<sup>loxPEx3</sup> littermates. All mice were housed under 12 h/12 h light - dark cycles with *ad libitum* access to a normal rodent chow and water. NEU1-deficient mice were euthanized on a humane basis due to urinary retention, following the advice of a veterinarian who was examining mice daily for the signs of a distorted bladder and inability to urinate. Lysosomal enzymes were assayed using corresponding fluorogenic 4-methylumbelliferyl substrates as previously described (199, 276). Relative expression of *Neu1*, *Neu2*, *Neu3* and *Neu4* in kidneys was determined by quantitative RT-PCR using previously described primers (32). Urine was collected in metabolic cages and analyzed with a urine dipstick, SDS PAGE or immunoblot. Analysis of kidney protein N-glycosylation by MALDI MS and glycosylation by lectin blotting was conducted essentially as described with or without PNGaseF treatment (282, 287). For the analysis of kidney tissues and bones by histochemistry, lectin histochemistry, immunohistochemistry and transmission electron microscopy (TEM), mice were anaesthetized with sodium pentobarbital and fixed by intracardiac perfusion with 4% paraformaldehyde (histochemistry) or glutaraldehyde (TEM), and their tissues processed essentially as described (287, 288). Semiquantitative analysis of kidney proteins by LC-MS/MS was performed as described (289). The data were visualized with Scaffold 5.2.2, with protein threshold set at 1% false discovery rate (FDR) with a minimum of 2 peptides identified at FDR of 0.1%. Bone analysis by Micro-CT was performed as described previously (290).

For complete methods, see *Supplemental Data Materials and Methods*.

## 2.4 Discussion

During the process of blood filtration through the kidney, water, solutes and proteins pass through the filtration membrane, followed by recovery of proteins in the proximal renal tubule in so-called renal protein reabsorption process. The process of reabsorption ensures that albumin, low molecular weight proteins (LMWP), bicarbonate, glucose, phosphate, amino acids, and other key nutrients are recovered by the organism and not lost with the urine. Reclamation of albumin and LMWP is mainly mediated by two endocytosis receptors, megalin (also known as Low Density Lipoprotein Receptor-related Protein 2, or LRP2), and Cubilin (CUBN), forming a complex at the apical membranes of epithelia (291). LRP2/CUBN receptors are found on the surface of epithelial cells in most tissues (reviewed by (261)), but are most highly expressed in proximal convoluted tubules (292, 293). Both proteins belong to the class of scavenger receptors that recognize and bind multiple ligands including vitamins, carrier proteins, enzymes and hormones (261). Patients with various forms of Fanconi

renotubular syndrome secrete low molecular weight proteins (such as vitamin D-binding protein (DBP), retinol-binding protein and  $\beta$ 2-microglobulin) in the urine because of proximal tubular dysfunction (294, 295). Megalin-null mice have high perinatal mortality rate due to impaired renal function, respiratory complications, and holoprosencephaly (264), suggesting that the protein also plays important roles in embryonic development.

Our results demonstrate that NEU1 plays a crucial role in maintaining normal glycosylation and trafficking of megalin, essential for proper renal reabsorption process. The constitutive *Neu1* KO mice develop kidney dysfunction resulting in low molecular weight proteinuria, glucosuria and elevated UACR. These abnormalities coincide with urinary retention that most likely occurs due to acute outflow tract obstruction and requires euthanasia of the animals. *Neu1*-null males show accelerated development of urinary retention and low molecular weight proteinuria when compared with females.

The documentation of glucosuria in *Neu1*-null animals is intriguing because it could be due to abnormal function of the sodium-glucose cotransporter SGLT2, which our study shows to be reduced in the proximal tubules of *Neu1* KO mice. In the context of normal SGLT1 and SGLT2 functions, glucosuria will occur when serum glucose concentration is higher than the maximal glucose reabsorption capacity of the kidney (or renal glucose transport maximum, TmG). Given that *CathA*<sup>S190-Neo</sup> mice (galactosialidosis model), which have ~90% reduction in tissue NEU1 activity, develop type 2 diabetes (211, 212), we sought to document if hyperglycemia was also observed in *Neu1*-null mice. While *Neu1*-null mice did indeed have higher serum glucose than WT animals, the levels observed are not high enough to cause glucosuria (296). Thus, glucosuria observed in *Neu1*-null mice most likely occurs due to abnormal glucose reabsorption at the proximal tubule. While recent data (297) reveal that SGLT2 possesses an O-linked glycan and two predicted N-linked glycans, the impact of SGLT2 glycosylation on its targeting and/or ability to transport glucose has not yet been investigated.

The other notable finding documented in the urine samples of both *Neu1*-deficient strains is the low urinary pH (5.0 vs. 6.5 for controls) despite exposure to similar mouse chow and environmental conditions. These data suggest that both *Neu1*-deficient strains must have much higher acid loads when compared to WT, and that tubular acid-base regulation at the proximal tubule (via bicarbonate reabsorption) and the distal tubule (via H<sup>+</sup> secretion) are intact. We plan to address the etiology of the acid load in future studies.

Similar symptoms of kidney dysfunction and urinary retention, although attenuated with average lifespan of 5 months in males and 8 months in females, were also observed in the

conditional *Neu1<sup>Cx3cr1ΔEx3</sup>* mice, where we attempted to deplete NEU1 specifically in the phagocytic mononuclear cells. Further analysis, however, revealed that NEU1 was reduced to below detection levels in all studied tissues of *Neu1<sup>Cx3cr1ΔEx3</sup>* mice with an exception of liver and brain. These results suggest that inactivation of the *Neu1* gene occurs in majority of cell types, and not only in mononuclear phagocytic cells, which is consistent with the previous data, showing that the expression of *Cx3cr1* is not limited to immune cells, but happens in a wide variety of tissues and organs (298). However, we also cannot exclude that NEU1 is mainly produced by tissue macrophages, followed by its exocytosis (possibly as a part of extracellularly vesicles) and uptake by other types of cells such as glomerular cells and the cells of proximal and distal convoluted tubules of the kidney. Experiments aimed at understanding if the longer survival of *Neu1<sup>Cx3cr1ΔEx3</sup>* mice occurs because of the slightly higher NEU1 residual levels in all tissues or is due to the retained NEU1 activity in the brain neurons are currently underway in our lab.

Our further analyses revealed multiple structural abnormalities in the kidney tissues of both *Neu1<sup>ΔEx3</sup>* and *Neu1<sup>Cx3cr1ΔEx3</sup>* strains, including reduced density of nephrons associated with renal fibrosis, macrophage infiltration, enlarged lysosomes containing storage materials in the proximal and distal convoluted tubules and podocytes, mitochondrial defects and effaced podocyte foot processes. These pathological changes, also reported for the kidney of sialidosis patients and for another mouse model of sialidosis (106), are thought to be caused by disruption of NEU1-mediated lysosomal catabolism of glycoproteins and sialylated oligosaccharides and their storage in lysosomes of affected tissues. Indeed, our results demonstrate that the kidney cells of *Neu1* KO mice display a specific phenotype consisting of autophagy block, and mTORC1 hyperactivation, common for the cells with a pronounced lysosomal storage in multiple lysosomal diseases including Gaucher, Pompe, and NPC1 (15, 299-303). This increased activity coincides with reduced lysosomal mTORC1 (LAMTOR/Ragulator) activity against TFEB due to the structural changes within the LAMTOR complex, leading to TFEB translocation to the nuclei, drastically increased lysosomal biogenesis, and induction of multiple lysosomal proteins and enzymes. At the same time, we could not confirm a previous report describing hypersialylation of LAMP-1 in NEU1-deficient cells presumably leading to its prolonged half-life and increased lysosomal exocytosis (304).

Since previous results from our lab and others demonstrated that NEU1 is also present on the cell surface, where it is involved in trimming sialic acid residues from glycan chains of glycoproteins, we have analyzed whether protein sialylation is increased in the kidney of NEU1

deficient mice. We found increased affinity of kidney tissues of *Neu1<sup>ΔEx3</sup>* mice to sialic acid-specific lectins and reduced affinity to galactose-specific lectins, suggestive of significantly increased sialylation. This was further confirmed by the analysis of kidney protein N-glycome that revealed remarkable increases in disialo- and trisialo-biantennary N-glycans in *Neu1<sup>ΔEx3</sup>* mice.

Notably, differences in sialylation of kidney proteins were sex-specific; male *Neu1<sup>ΔEx3</sup>* mice, in general, had increased amounts of N-glycans and, also, displayed specific structures, such as a biantennary disialo-glycoform bearing one Neu5Gc at each antenna, which were found only in traces in the tissues of female mice. Together with previous reports by Reiding et al. and Han et al. (305, 306), this is one of the few observations of sex-linked differences in glycan profiles. It will be important to explore if these sex-specific abnormalities are also recapitulated in human patients (307).

Importantly, we found higher average NEU1 activity levels in the kidneys of WT male as compared with female mice (~5 nmol/h mg vs ~3 nmol/h mg), while the NEU1 levels in other tissues are similar in mice of both sexes. These data, together with the increased levels of sialoglycans in NEU1-deficient male mice compared to females, allow us to speculate that males are more dependent on NEU1 action to ensure a proper glycosylation of kidney proteins. Thus, in a situation when NEU1 is completely or partially depleted, *Neu1<sup>ΔEx3</sup>* as well as *Neu1<sup>Cx3cr1ΔEx3</sup>* male mice show drastic changes in glycosylation associated with (and perhaps causing) their significantly reduced survival compared to females. While no normal comparison of sialidosis severity between male and female patients has ever been conducted, a recent study reported faster disease progression in a male compared to a female sibling (78).

Megalyn is hypersialylated in *Neu1*-null mice. This was confirmed by both lectin blotting and IHC coupled with high-resolution fluorescent confocal microscopy. These studies demonstrated that in kidney of *Neu1<sup>ΔEx3</sup>* mice, megalyn is intensely stained with SNA, and not as avidly bound by PNA as in WT. Moreover, both methods revealed that levels of megalyn were drastically reduced in *Neu1*-null mice and, instead of being localized to the apical membranes of proximal convoluted tubules, the protein was trapped in enlarged lysosomes. Megalyn was also detected in the urine of *Neu1<sup>ΔEx3</sup>* mice, indicating its shedding from apical membranes. Although further studies are required to understand the causal relation between megalyn hypersialylation and its impaired trafficking, it is tempting to speculate that megalyn is one of the proteins targeted to apical membranes via galactose-specific lectin in a carbohydrate-dependent manner (for example, via binding to galectin-3) (308). In this case, the

presence of sialic acid residues would mask interactions of O-linked galactose residues with galectins, resulting in megalin relocation to lysosomes. Aberrant glycosylation of megalin occurs in the kidney of mice deficient in *Galnt11*, which encodes a member of the large glycosyltransferase family responsible for initiating mucin-type O-glycosylation of secreted and membrane-bound proteins (286). This results in age-related progressive loss of megalin from proximal renal tubules and impairment of reabsorption of low molecular weight proteins such as  $\alpha$ 1-microglobulin ( $\alpha$ 1-M), retinol binding protein (RBP), and vitamin D-binding protein (DBP) (286). In our study, substrates of megalin,  $\beta$ 2-microglobulin and DBP, were present only in the urine of *Neu1*-null mice, demonstrating that reduced levels of megalin or/and its hypersialylation is also associated with reabsorption defects. Hypoproteinemia, which could be indicative of poor recovery of urinary proteins has been previously reported for the *Neu1* KO mice generated by another group (106). Interestingly, the same group also reported a similar phenotype for a galactosialidosis model (*Ctsa/PPCA*-null mouse) with a secondary deficiency of NEU1 (309). In our galactosialidosis model, *CathA*<sup>S190A-Neo</sup> mouse, the kidneys are normal (310), suggesting that just 10% of the residual NEU1 activity is sufficient to protect mice from a severe kidney damage.

Since megalin-cubilin endocytic system plays a modulating role in vitamin D metabolism, it was plausible to propose that deficiency of this complex and increased urinary secretion of DBP could contribute to bone dysplasia through lower vitamin D levels. Indeed, *Neu1*<sup>ΔEx3</sup> mice demonstrate a bone phenotype that may potentially be explained by a bone mineralization defect or bone formation and resorption anomalies. 25-OH vitamin D levels are significantly increased in the urine of *Neu1*<sup>ΔEx3</sup> mice, suggesting that they are losing it through urinary secretion. At the same time, vitamin D is not deficient in plasma. Thus, further studies involving complete bone histomorphometry analyses with dynamic parameters (bone formation and resorption) are required to address this question.

Together, our results identify NEU1 as an important regulator of glycosylation of kidney proteins, including megalin, and, thus, a key element of the reabsorption process. It is tempting to speculate that desialylation of O-linked glycans may be important for transport and function of other critical proximal tubule receptors and solute carriers found to be deficient in the kidney of *Neu1* KO mice, including the sodium-glucose cotransporter SGLT2 (297), which has important clinical relevance (311). Our findings also yield insights into the pathophysiology of nephrosialidosis and describe a unique model of kidney disease that implicates both glomerular and tubular defects.

## 2.5 References

15. Brown, R.A., et al., *mTOR hyperactivity mediates lysosomal dysfunction in Gaucher's disease iPSC-neuronal cells*. *Dis Model Mech*, 2019. **12**(10).
32. Pan, X., et al., *Neuraminidases 3 and 4 regulate neuronal function by catabolizing brain gangliosides*. *FASEB J*, 2017. **31**(8): p. 3467-3483.
75. Seyrantepe, V., et al., *Molecular pathology of NEU1 gene in sialidosis*. *Hum Mutat*, 2003. **22**(5): p. 343-52.
78. Arora, V., et al., *Sialidosis type II: Expansion of phenotypic spectrum and identification of a common mutation in seven patients*. *Mol Genet Metab Rep*, 2020. **22**: p. 100561.
79. Aylsworth, A.S., et al., *A severe infantile sialidosis: clinical, biochemical, and microscopic features*. *J Pediatr*, 1980. **96**(4): p. 662-8.
80. Chen, W., et al., *Histological studies of renal biopsy in a boy with nephrosialidosis*. *Ultrastruct Pathol*, 2011. **35**(4): p. 168-71.
83. Kelly, T.E. and G. Graetz, *Isolated acid neuraminidase deficiency: a distinct lysosomal storage disease*. *Am J Med Genet*, 1977. **1**(1): p. 31-46.
91. Lowden, J.A. and J.S. O'Brien, *Sialidosis: a review of human neuraminidase deficiency*. *Am J Hum Genet*, 1979. **31**(1): p. 1-18.
106. de Geest, N., et al., *Systemic and neurologic abnormalities distinguish the lysosomal disorders sialidosis and galactosialidosis in mice*. *Hum Mol Genet*, 2002. **11**(12): p. 1455-64.
135. Reily, C., et al., *Glycosylation in health and disease*. *Nat Rev Nephrol*, 2019. **15**(6): p. 346-366.
181. Varki, A., *Sialic acids in human health and disease*. *Trends Mol Med*, 2008. **14**(8): p. 351-60.
185. Charest, P.M. and J. Roth, *Localization of sialic acid in kidney glomeruli: regionalization in the podocyte plasma membrane and loss in experimental nephrosis*. *Proc Natl Acad Sci U S A*, 1985. **82**(24): p. 8508-12.
199. Smutova, V., et al., *Structural basis for substrate specificity of mammalian neuraminidases*. *PLoS One*, 2014. **9**(9): p. e106320.
201. Pshezhetsky, A.V. and M. Ashmarina, *Keeping it trim: roles of neuraminidases in CNS function*. *Glycoconj J*, 2018. **35**(4): p. 375-386.
211. Dridi, L., et al., *Positive regulation of insulin signaling by neuraminidase 1*. *Diabetes*, 2013. **62**(7): p. 2338-46.
212. Fougerat, A., et al., *Neuraminidase 1 activates insulin receptor and reverses insulin resistance in obese mice*. *Mol Metab*, 2018. **12**: p. 76-88.
233. Mohos, S.C. and L. Skoza, *Glomerular sialoprotein*. *Science*, 1969. **164**(3887): p. 1519-21.
234. Klein, P.J., et al., *Thomsen-Friedenreich antigen in haemolytic-uraemic syndrome*. *Lancet*, 1977. **2**(8046): p. 1024-5.
235. Lemyre, E., et al., *Clinical spectrum of infantile free sialic acid storage disease*. *Am J Med Genet*, 1999. **82**(5): p. 385-91.
236. Coats, M.T., et al., *Exposure of Thomsen-Friedenreich antigen in Streptococcus pneumoniae infection is dependent on pneumococcal neuraminidase A*. *Microb Pathog*, 2011. **50**(6): p. 343-9.
237. Pawluczyk, I.Z., et al., *Sialic acid supplementation ameliorates puromycin aminonucleoside nephrosis in rats*. *Lab Invest*, 2015. **95**(9): p. 1019-28.
238. Firth, J.D., *Effect of polycations on the function of the isolated perfused rat kidney*. *Clin Sci (Lond)*, 1990. **79**(6): p. 591-8.
239. Niculovic, K.M., et al., *Podocyte-Specific Sialylation-Deficient Mice Serve as a Model for Human FSGS*. *J Am Soc Nephrol*, 2019. **30**(6): p. 1021-1035.
240. Alexander, W.S., et al., *Thrombocytopenia and kidney disease in mice with a mutation in the C1galt1 gene*. *Proc Natl Acad Sci U S A*, 2006. **103**(44): p. 16442-7.
241. MacArthur, D.G., et al., *Guidelines for investigating causality of sequence variants in human disease*. *Nature*, 2014. **508**(7497): p. 469-76.

242. Martin, L.T., et al., *Genetically altered mice with different sialyltransferase deficiencies show tissue-specific alterations in sialylation and sialic acid 9-O-acetylation*. J Biol Chem, 2002. **277**(36): p. 32930-8.
243. Galeano, B., et al., *Mutation in the key enzyme of sialic acid biosynthesis causes severe glomerular proteinuria and is rescued by N-acetylmannosamine*. J Clin Invest, 2007. **117**(6): p. 1585-94.
244. Kakani, S., et al., *The Gne M712T mouse as a model for human glomerulopathy*. Am J Pathol, 2012. **180**(4): p. 1431-40.
245. Yu, A., et al., *Changes in the Expression of Renal Brush Border Membrane N-Glycome in Model Rats with Chronic Kidney Diseases*. Biomolecules, 2021. **11**(11).
246. Kashtan, C.E., et al., *Proteinuria in a child with sialidosis: case report and histological studies*. Pediatr Nephrol, 1989. **3**(2): p. 166-74.
247. Toyooka, K., et al., *Nephrosialidosis: ultrastructural and lectin histochemical study*. Acta Neuropathol, 1993. **86**(2): p. 198-205.
261. Christensen, E.I. and H. Birn, *Megalin and cubilin: multifunctional endocytic receptors*. Nat Rev Mol Cell Biol, 2002. **3**(4): p. 256-66.
264. Willnow, T.E., et al., *Defective forebrain development in mice lacking gp330/megalin*. Proc Natl Acad Sci U S A, 1996. **93**(16): p. 8460-4.
270. Pshezhetsky, A.V. and A. Hinek, *Where catabolism meets signalling: neuraminidase 1 as a modulator of cell receptors*. Glycoconj J, 2011. **28**(7): p. 441-52.
273. Wuttke, M., et al., *A catalog of genetic loci associated with kidney function from analyses of a million individuals*. Nat Genet, 2019. **51**(6): p. 957-972.
274. Stanzick, K.J., et al., *Discovery and prioritization of variants and genes for kidney function in >1.2 million individuals*. Nat Commun, 2021. **12**(1): p. 4350.
275. Nakanishi, H., *Neuronal and microglial cathepsins in aging and age-related diseases*. Ageing Res Rev, 2003. **2**(4): p. 367-81.
276. Guo, T., et al., *Selective Inhibitors of Human Neuraminidase 3*. J Med Chem, 2018. **61**(5): p. 1990-2008.
277. Kundra, R. and S. Kornfeld, *Asparagine-linked oligosaccharides protect Lamp-1 and Lamp-2 from intracellular proteolysis*. J Biol Chem, 1999. **274**(43): p. 31039-46.
278. Huang da, W., B.T. Sherman, and R.A. Lempicki, *Bioinformatics enrichment tools: paths toward the comprehensive functional analysis of large gene lists*. Nucleic Acids Res, 2009. **37**(1): p. 1-13.
279. Tan, A., et al., *Past, present, and future perspectives of transcription factor EB (TFEB): mechanisms of regulation and association with disease*. Cell Death Differ, 2022. **29**(8): p. 1433-1449.
280. Settembre, C., et al., *A block of autophagy in lysosomal storage disorders*. Hum Mol Genet, 2008. **17**(1): p. 119-29.
281. Xia, B., et al., *Oligosaccharide analysis in urine by maldi-tof mass spectrometry for the diagnosis of lysosomal storage diseases*. Clin Chem, 2013. **59**(9): p. 1357-68.
282. Messina, A., et al., *HILIC-UPLC-MS for high throughput and isomeric N-glycan separation and characterization in Congenital Disorders Glycosylation and human diseases*. Glycoconj J, 2021. **38**(2): p. 201-211.
283. Peng, W., et al., *MS-based glycomics: An analytical tool to assess nervous system diseases*. Front Neurosci, 2022. **16**: p. 1000179.
284. Varki, A., et al., *Essentials of Glycobiology, Fourth Edition*, in *Essentials of Glycobiology*, A. Varki, et al., Editors. 2022: Cold Spring Harbor (NY).
285. Kozarsky, K., D. Kingsley, and M. Krieger, *Use of a mutant cell line to study the kinetics and function of O-linked glycosylation of low density lipoprotein receptors*. Proc Natl Acad Sci U S A, 1988. **85**(12): p. 4335-9.

286. Tian, E., et al., *Galnt11 regulates kidney function by glycosylating the endocytosis receptor megalin to modulate ligand binding*. Proc Natl Acad Sci U S A, 2019. **116**(50): p. 25196-25202.
287. Da Silva, A., et al., *N-acetylneuraminase pyruvate lyase controls sialylation of muscle glycoproteins essential for muscle regeneration and function*. Sci Adv, 2023. **9**(26): p. eade6308.
288. Mazon, M., et al., *Deletion of the Fanconi Anemia C Gene in Mice Leads to Skeletal Anomalies and Defective Bone Mineralization and Microarchitecture*. J Bone Miner Res, 2018. **33**(11): p. 2007-2020.
289. Para, C., et al., *Early defects in mucopolysaccharidosis type IIIC disrupt excitatory synaptic transmission*. JCI Insight, 2021. **6**(15).
290. Pan, X., et al., *Glucosamine amends CNS pathology in mucopolysaccharidosis IIIC mouse expressing misfolded HGSNAT*. J Exp Med, 2022. **219**(8).
291. Morales, C.R., et al., *Low density lipoprotein receptor-related protein-2 expression in efferent duct and epididymal epithelia: evidence in rats for its in vivo role in endocytosis of apolipoprotein J/clusterin*. Biol Reprod, 1996. **55**(3): p. 676-83.
292. Kerjaschki, D. and M.G. Farquhar, *The pathogenic antigen of Heymann nephritis is a membrane glycoprotein of the renal proximal tubule brush border*. Proceedings of the National Academy of Sciences of the United States of America, 1982. **79**(18): p. 5557-5561.
293. Sahali, D., et al., *Comparative immunochemistry and ontogeny of two closely related coated pit proteins. The 280-kd target of teratogenic antibodies and the 330-kd target of nephritogenic antibodies*. Am J Pathol, 1993. **142**(5): p. 1654-67.
294. Storm, T., et al., *Renal phenotypic investigations of megalin-deficient patients: novel insights into tubular proteinuria and albumin filtration\**. Nephrology Dialysis Transplantation, 2012. **28**(3): p. 585-591.
295. Muller, D., et al., *Holoprosencephaly and low molecular weight proteinuria: the human homologue of murine megalin deficiency*. Am J Kidney Dis, 2001. **37**(3): p. 624-8.
296. Vallon, V., et al., *Knockout of Na-glucose transporter SGLT2 attenuates hyperglycemia and glomerular hyperfiltration but not kidney growth or injury in diabetes mellitus*. Am J Physiol Renal Physiol, 2013. **304**(2): p. F156-67.
297. Yang, W., et al., *Mapping the O-glycoproteome using site-specific extraction of O-linked glycopeptides (EXoO)*. Mol Syst Biol, 2018. **14**(11): p. e8486.
298. Lee, M., et al., *Tissue-specific Role of CX3CR1 Expressing Immune Cells and Their Relationships with Human Disease*. Immune Netw, 2018. **18**(1): p. e5.
299. Bartolomeo, R., et al., *mTORC1 hyperactivation arrests bone growth in lysosomal storage disorders by suppressing autophagy*. J Clin Invest, 2017. **127**(10): p. 3717-3729.
300. Shemesh, A., et al., *Suppression of mTORC1 activation in acid-alpha-glucosidase-deficient cells and mice is ameliorated by leucine supplementation*. Am J Physiol Regul Integr Comp Physiol, 2014. **307**(10): p. R1251-9.
301. Pal, R., Y. Xiong, and M. Sardiello, *Abnormal glycogen storage in tuberous sclerosis complex caused by impairment of mTORC1-dependent and -independent signaling pathways*. Proc Natl Acad Sci U S A, 2019. **116**(8): p. 2977-2986.
302. Lim, C.Y., et al., *ER-lysosome contacts enable cholesterol sensing by mTORC1 and drive aberrant growth signalling in Niemann-Pick type C*. Nat Cell Biol, 2019. **21**(10): p. 1206-1218.
303. Du, X., et al., *Akt activation increases cellular cholesterol by promoting the proteasomal degradation of Niemann-Pick C1*. Biochem J, 2015. **471**(2): p. 243-53.
304. Yogalingam, G., et al., *Neuraminidase 1 is a negative regulator of lysosomal exocytosis*. Dev Cell, 2008. **15**(1): p. 74-86.
305. Reiding, K.R., et al., *Murine Plasma N-Glycosylation Traits Associated with Sex and Strain*. J Proteome Res, 2016. **15**(10): p. 3489-3499.

306. Han, J., et al., *Quantitation of sex-specific serum N-glycome changes in expression level during mouse aging based on Bionic Glycome method*. *Exp Gerontol*, 2020. **141**: p. 111098.
307. Van Praet, O., W.S. Argraves, and C.R. Morales, *Co-expression and interaction of cubilin and megalin in the adult male rat reproductive system*. *Mol Reprod Dev*, 2003. **64**(2): p. 129-35.
308. Delacour, D., et al., *Requirement for galectin-3 in apical protein sorting*. *Curr Biol*, 2006. **16**(4): p. 408-14.
309. Zhou, X.Y., et al., *Mouse model for the lysosomal disorder galactosialidosis and correction of the phenotype with overexpressing erythroid precursor cells*. *Genes Dev*, 1995. **9**(21): p. 2623-34.
310. Seyrantepe, V., et al., *Enzymatic activity of lysosomal carboxypeptidase (cathepsin) A is required for proper elastic fiber formation and inactivation of endothelin-1*. *Circulation*, 2008. **117**(15): p. 1973-81.
311. Cowie, M.R. and M. Fisher, *SGLT2 inhibitors: mechanisms of cardiovascular benefit beyond glycaemic control*. *Nat Rev Cardiol*, 2020. **17**(12): p. 761-772.

## 2.6 Supplementary data

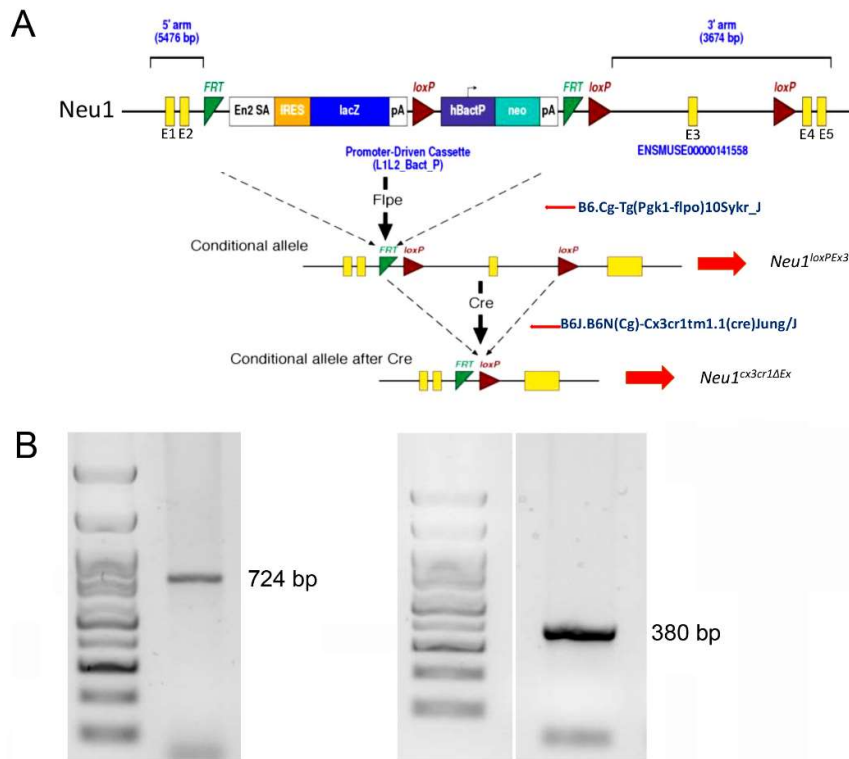


**Figure S 2-1. Generation of *Neu1*<sup>Cx3cr1ΔEx3</sup> mouse strain.**

(A) Scheme showing generation of a conditional *Neu1* KO strain, *Neu1*<sup>Cx3cr1ΔEx3</sup>. Previously described *Neu1*<sup>ENSMUSE141558</sup> strain was interbred with the *B6.Cg-Tg(Pgk1-flpo)10Sykr/J* line (The Jackson Laboratory stock 011065), that expresses the mouse codon-optimized FLP recombinase under the direction of the mouse *Pgk1*, phosphoglycerate kinase 1 promoter. This caused the removal of FRT-flanked *Neo* cassette allowing normal expression of the *Neu1* gene in the resulting *Neu1*<sup>loxPEx3</sup> strain. The *Neu1*<sup>loxPEx3</sup> strain was then crossed with the *B6J.B6N(Cg)-Cx3cr1tm1.1(cre)Jung/J* strain (The Jackson Laboratory stock 025524) expressing the Cre recombinase under the control of the *Cx3cr1* (chemokine C-X3-C motif receptor 1) gene promoter. (B) *Neu1*<sup>Cx3cr1ΔEx3</sup> mice were genotyped by PCR of tail genomic DNA for the presence of *Neu1*<sup>loxPEx3</sup> (724 bp PCR fragment) and *Cx3cr1Cre* (380 bp fragment).

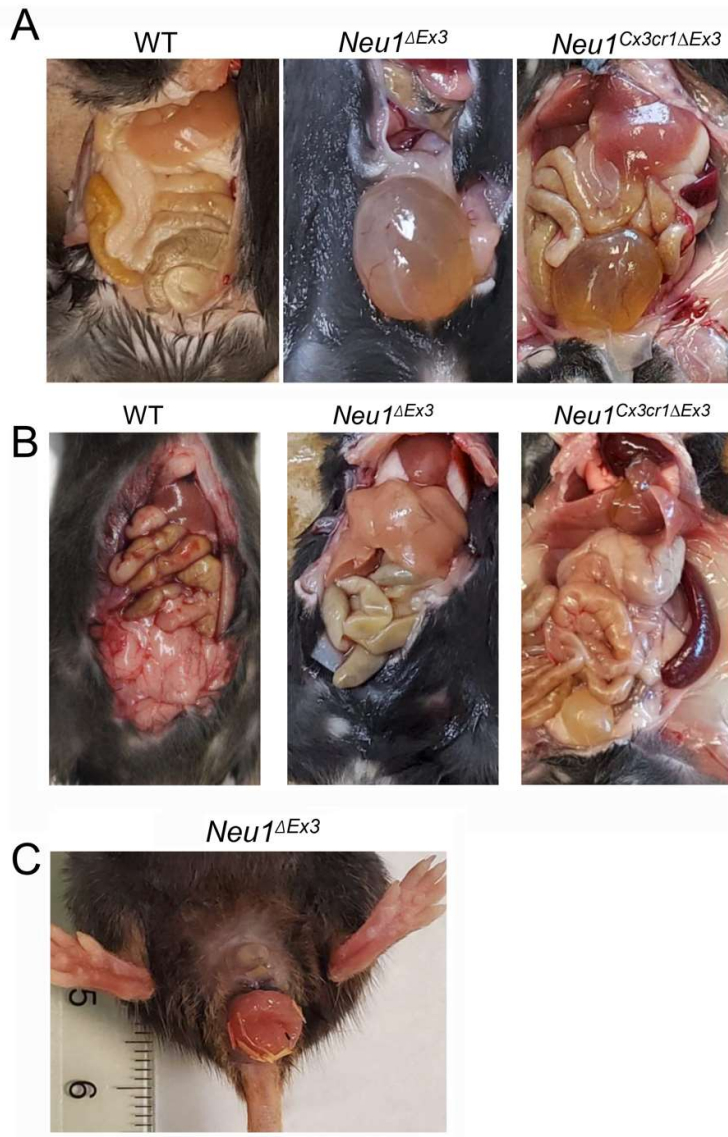


**Figure S 2-2. Necropsy of *Neu1<sup>ΔEx3</sup>* and *Neu1<sup>Cx3cr1ΔEx3</sup>* mice at the terminal stage**

(A) *Neu1<sup>ΔEx3</sup>* and *Neu1<sup>Cx3cr1ΔEx3</sup>* mice at the terminal stage show an inability to urinate causing distention of bladder, not present in the WT mouse. Pictures show representative necropsy images of male 4-month-old *Neu1<sup>ΔEx3</sup>* mouse, 7-month-old *Neu1<sup>Cx3cr1ΔEx3</sup>* mouse and 7-month-old WT mouse. (B) Four-month-old female *Neu1<sup>ΔEx3</sup>* and *Neu1<sup>Cx3cr1ΔEx3</sup>* mice show reduced abdominal fat when compared to WT mouse, accompanied by visibly enlarged liver in *Neu1<sup>ΔEx3</sup>* and enlarged spleen in *Neu1<sup>Cx3cr1ΔEx3</sup>* mouse. (C) Severe rectal prolapse in 6.5-month-old *Neu1<sup>ΔEx3</sup>* female mouse.

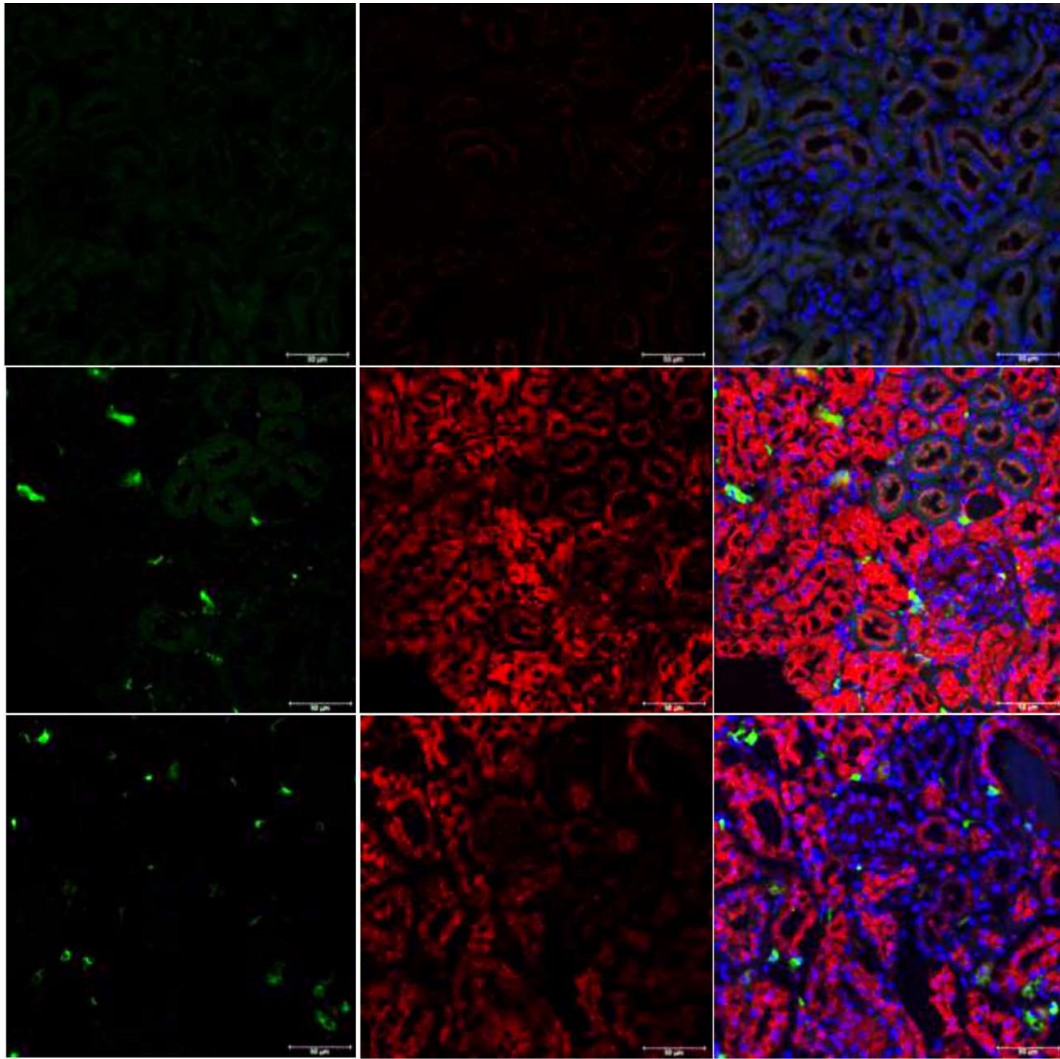


**Figure S 2-3. Infiltration of CD68+ activated macrophages and increased lysosomal biogenesis (LAMP1+ cells) in kidney of 4-month-old *Neu1<sup>ΔEx3</sup>* and *Neu1<sup>Cx3cr1ΔEx3</sup>* mice.**

Panels show representative confocal microscopy images of kidney tissues of 4-month-old *Neu1<sup>ΔEx3</sup>* and *Neu1<sup>Cx3cr1ΔEx3</sup>* mice and their age-matching WT control stained with antibodies against CD68 (green, activated macrophages) and LAMP1 (red, lysosomes). DAPI (blue) was used as a nuclear counterstain.

Graphs show quantification of fluorescence with ImageJ software. Individual data, means and SD obtained for 2 mice per genotypes (3 areas/mouse) are shown. P values were calculated using Nested one-way ANOVA test with a Tukey post hoc test.

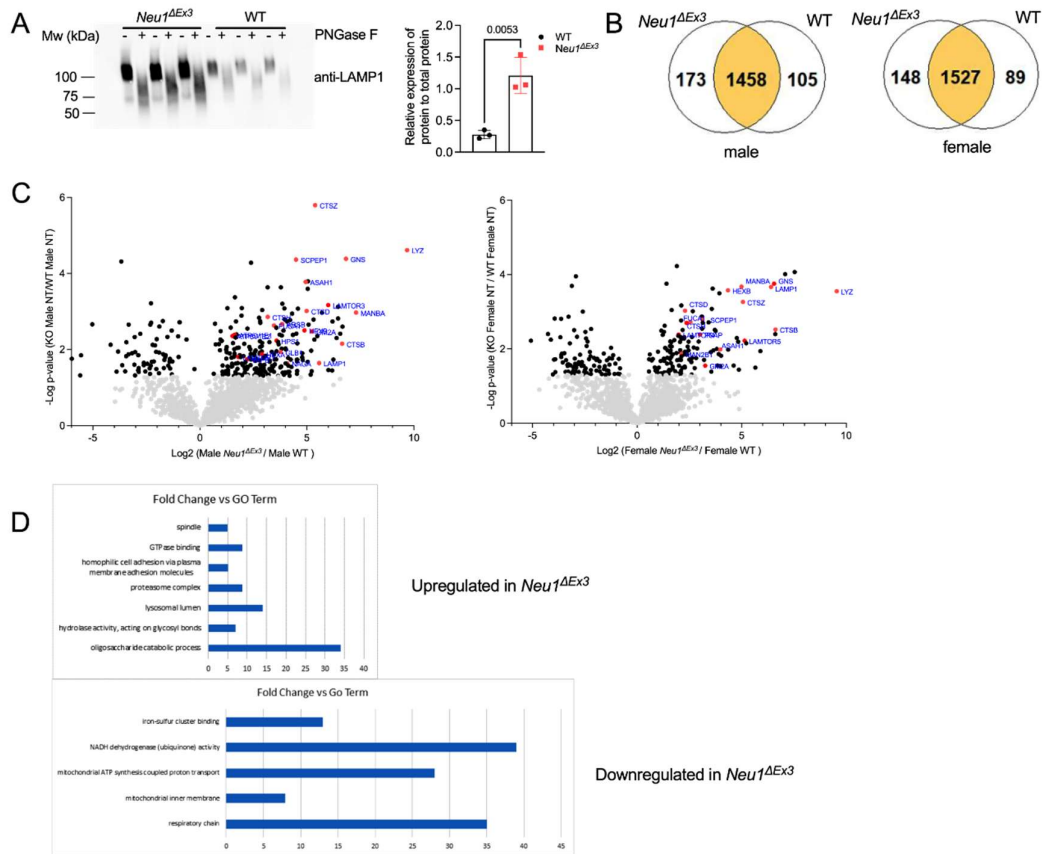


**Figure S 2-4. Semi-quantitative LC-MS/MS analysis of kidney proteins reveals increased levels of lysosomal proteins in male and female 4-month-old *Neu1<sup>ΔEx3</sup>* mice.**

(A) Immunoblot analysis of kidney protein extracts treated or not with PNGaseF demonstrates increased intensity of LAMP-1 immunoreactive band in kidney of *Neu1<sup>ΔEx3</sup>* mice but a similar shift of the LAMP-1 band position after PNGaseF treatment. Graph shows quantification of the band intensity with ImageJ software. Individual results, means and SD are shown (n=3). P values were calculated by one-way ANOVA with Dunn's post hoc test. (B) Total number of proteins identified in kidney of male and female *Neu1<sup>ΔEx3</sup>* and WT mice. (C) Volcano plots of kidney proteins showing differentially regulated proteins that are statistically different in male and female *Neu1<sup>ΔEx3</sup>* and WT mice. Representative lysosomal proteins are shown as red dots and annotated. (D) Gene ontology (GO) terms plotted versus fold changes for protein groups downregulated or upregulated in *Neu1<sup>ΔEx3</sup>* mice in a sex-specific manner.

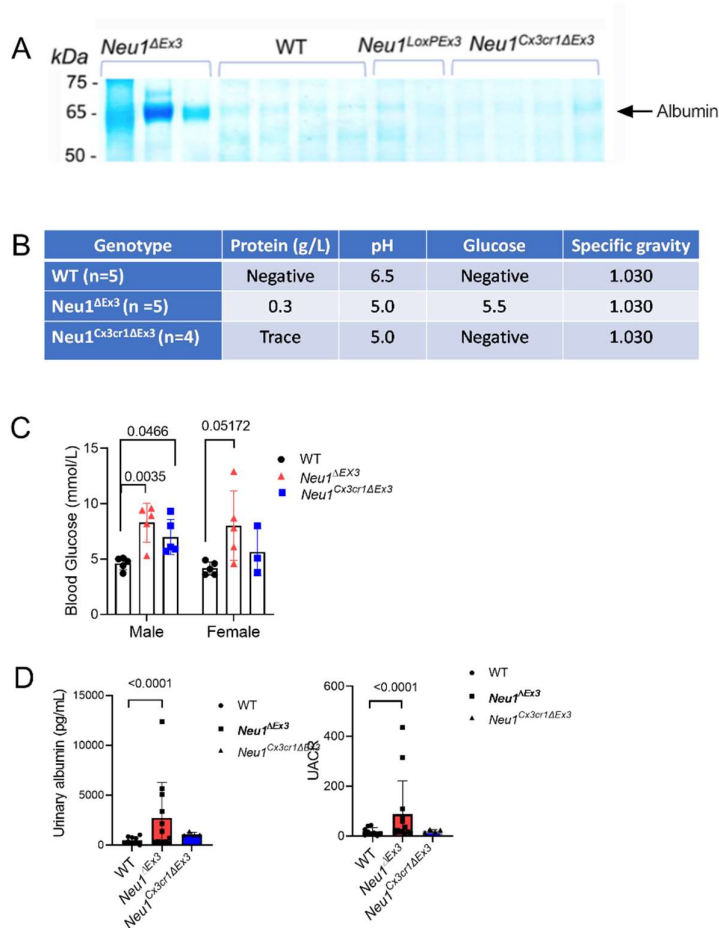


**Figure S 2-5. Four-month-old *Neu1*<sup>ΔEx3</sup> mice develop proteinuria.**

(A) SDS-PAGE analysis of urinary proteins showing a presence of a 65 kDa albumin protein band (arrow) in the urine of 4-month-old *Neu1*<sup>ΔEx3</sup> mice but not of WT or *Neu1*<sup>Cx3cr1ΔEx3</sup> mice. Image shows a representative SDS-PAGE analysis of urine from 3 *Neu1*<sup>ΔEx3</sup>, 4 WT, 2 *Neu1*<sup>LoxPEx3</sup> with normal Neu1 expression and 4 *Neu1*<sup>Cx3cr1ΔEx3</sup> age-matched mice. (B) Urine dipstick (Siemens, Multistix 10 SG) test results showing presence of protein, reduced pH, normal specific gravity, and increased glucose levels in the urine of 4-month-old *Neu1*<sup>ΔEx3</sup> mice. (C) Elevated blood glucose levels were detected in fasted male and female *Neu1*<sup>ΔEx3</sup> mice, and in male *Neu1*<sup>Cx3cr1ΔEx3</sup> mice. (D) ELISA analysis showing reduction of urinary creatinine and a trend for the increase of urinary albumin and urine albumin-to-creatinine ratio (UACR) in 4-month-old *Neu1*<sup>ΔEx3</sup> mice consistent with kidney disfunction. Plasma and urine were collected from 4-month-old and 6-month-old WT (n=9), *Neu1*<sup>ΔEx3</sup> (n=13) and *Neu1*<sup>Cx3cr1ΔEx3</sup> (n=4) mice of both sexes. Levels of plasma and urinary creatinine were quantified by Creatinine kit (Chondrex Inc), and urinary albumin was quantified by ELISA (Abcam).

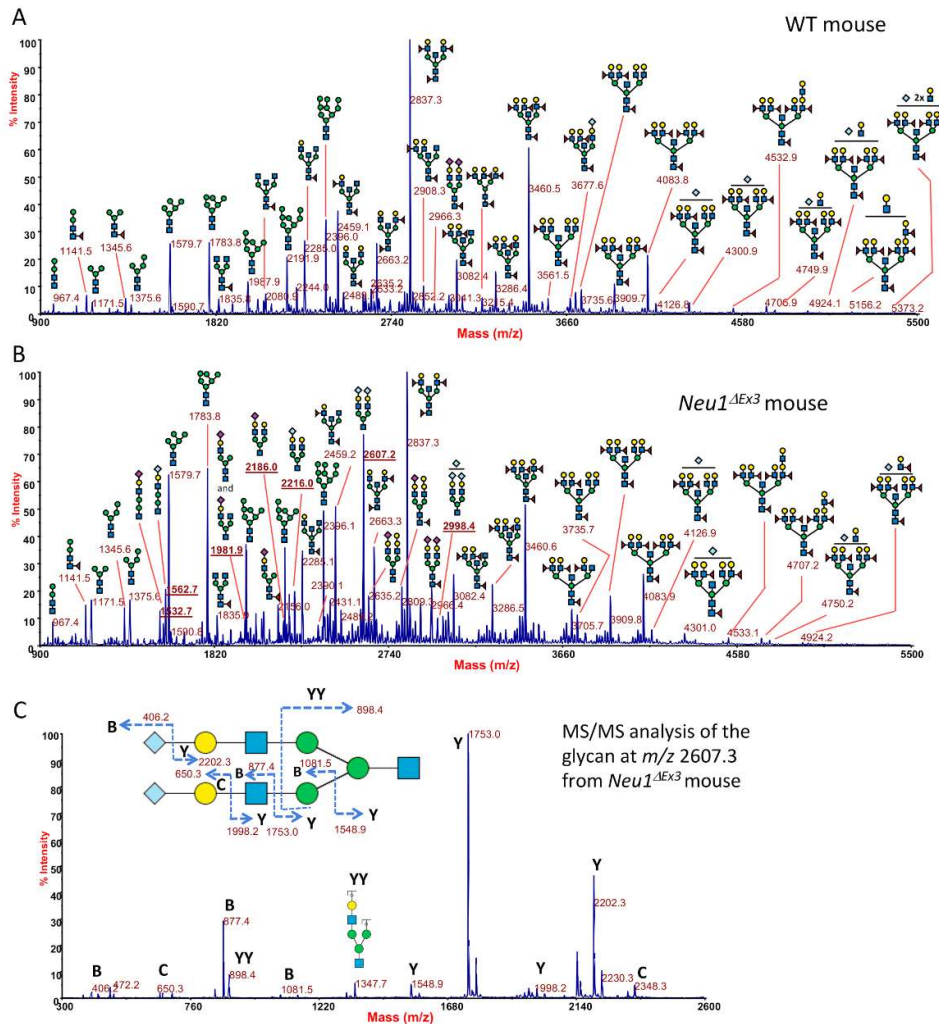


**Figure S 2-6. MALDI mass spectrometry analysis shows the presence of free glycans stored in kidney tissues of 4-month-old *Neu1*<sup>ΔEx3</sup> mice.**

Representative spectra of N-glycans from kidney tissue of **(A)** WT and **(B)** *Neu1*<sup>ΔEx3</sup> mouse. A number of sialylated glycans at *m/z* 1532.7, 1562.7, 1981.9, 2186.0, 2216.0, 2607.2, and 2998.4 (underlined) are present only in *Neu1*<sup>ΔEx3</sup> profiles, and most likely represent free oligosaccharides stored in the lysosomes of kidney tissues and secreted in the urine of NEU1 KO mice. **(C)** MS/MS spectrum of the most abundant species at *m/z* 2607.2, shows the presence of a GlcNAc at the reducing glycan end, instead of the disaccharide GlcNAc-GlcNAc, which is expected to be found in an N-linked glycan released from a glycoprotein or a glycopeptide after digestion with PNGase F. GlcNAc, blue square;

Man, green circle; Gal, yellow circle; Neu5Ac, purple diamond; Neu5Gc, light blue diamond; Fuc, red triangle.

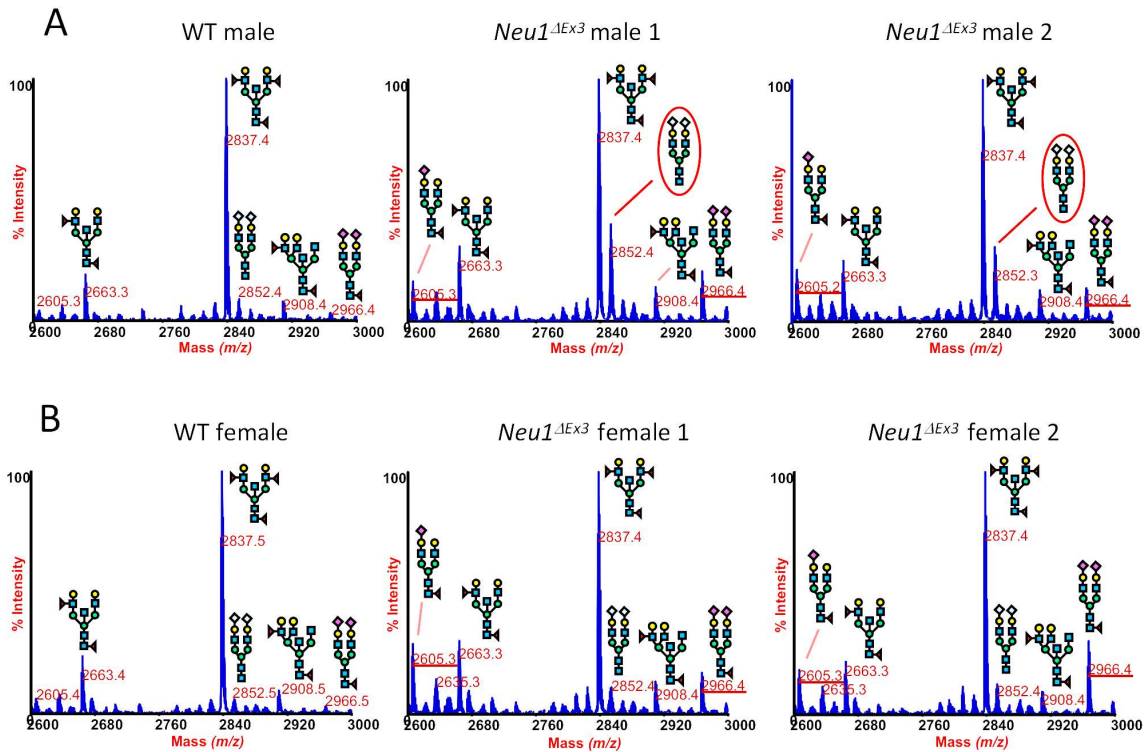


**Figure S 2-7. MALDI MS spectra of N-linked glycans from kidney tissue are sex-specific in *Neu1*<sup>ΔEx3</sup> mice.**

Partial (mass-range between  $m/z$  2600 and 3000) MALDI MS profiles from a 4-month-old male WT mouse and its age-matching male (A) and female (B) *Neu1*<sup>ΔEx3</sup> littermates. Both male and female *Neu1*<sup>ΔEx3</sup> mice show increase in sialylated structures (underlined  $m/z$  values) as compared to WT. Additionally, male *Neu1*<sup>ΔEx3</sup> show an accumulation of the glycoform at  $m/z$  2852.4 (circled in red) not occurring in female *Neu1*<sup>ΔEx3</sup> mice. GlcNAc, blue square; Man, green circle; Gal, yellow circle; Neu5Ac, purple diamond; Neu5Gc, light blue diamond; Fuc, red triangle.

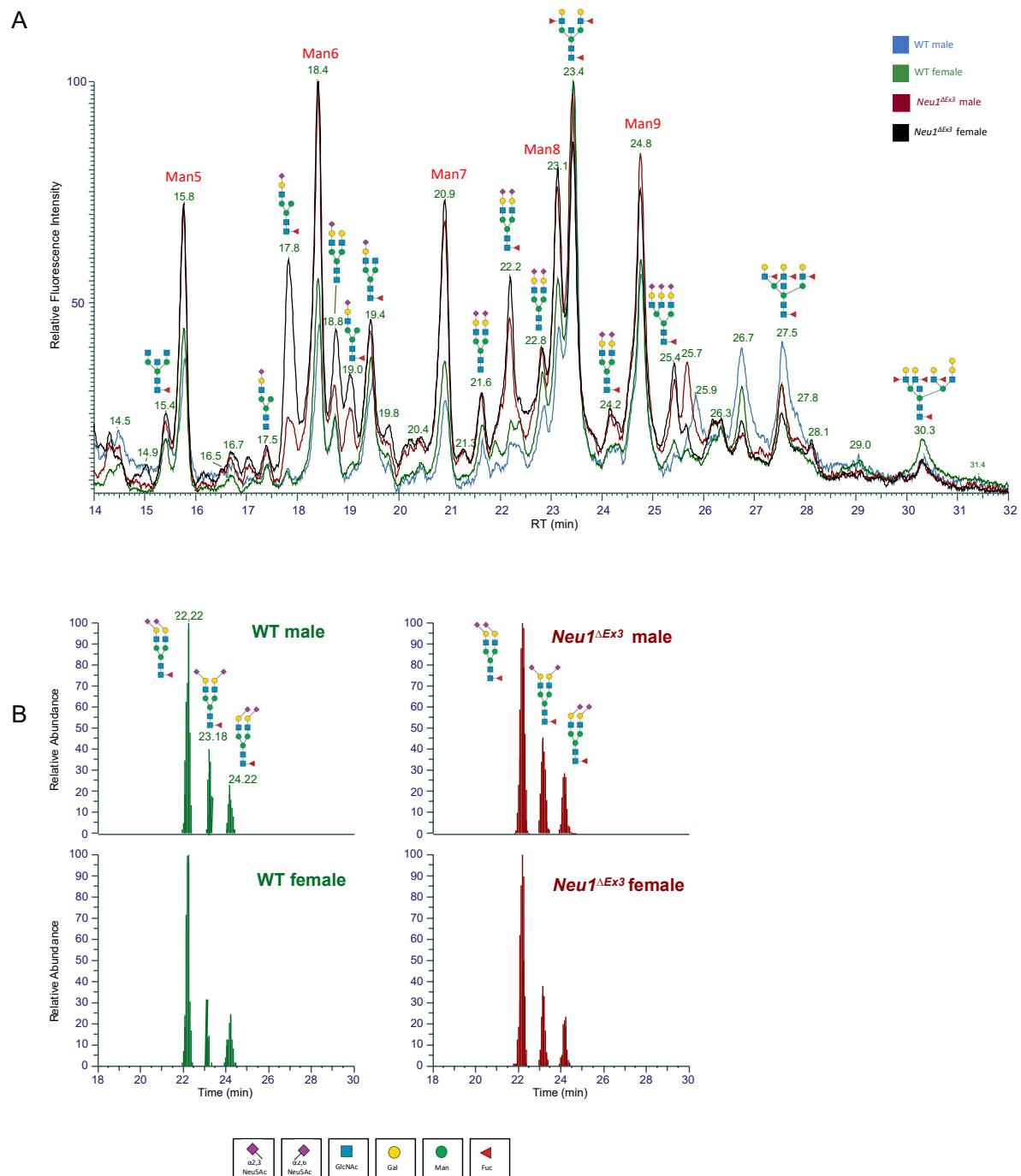


**Figure S 2-8. Analysis of sialic acid linkages in N-glycans by HILIC-UPLC-FLR-ESI-MS.**

(A) Overlaid representative fluorescence (FLR) chromatograms obtained by HILIC-UPLC-FLR-MS of *RapiFluor* labeled kidney protein N-glycans from male and female WT and *Neu1<sup>ΔEx3</sup>*. An increase of oligomannoses and biantennary core fucosylated disialo-glycoform is evident in *Neu1<sup>ΔEx3</sup>* mice of both sexes. The biantennary disialo-glycoform bearing one Neu5Gc at each antenna (retention time 25.7) is much more intense in the *Neu1<sup>ΔEx3</sup>* male mouse.

**(B)** Extracted ion chromatograms of the peak at  $m/z$  1341.0150 ( $\pm 5$ ppm) corresponding to the biantennary core fucosylated disialo-glycoform from four mice (WT and *Neu1* <sup>$\Delta$ Ex3</sup> males and females), showing a separation of glycans containing 2,3 and 2,6-linked sialic acids. Peaks were assigned based on the retention times of similar glyco-isomers from human serum and by comparison of chromatograms of glycans treated or not with a neuraminidase specific for 2,3-linked sialic acid residues.

**Table S 2-1. Bone analyses in WT and Neu1<sup>ΔEx3</sup> mice with micro-CT and histology.**

Parameters/group	WT	Neu1 <sup>ΔEx3</sup>
<b>Micro-Ct (Cortical bone analyses)</b>		
Bone length (mm)	18.4 ± 0.3	16.5 ± 0.3
Bone volume (mm <sup>3</sup> )	1.07 ± 0.03	0.83 ± 0.08
Total volume (mm <sup>3</sup> )	1.44 ± 0.05	1.22 ± 0.06
Bone volume fraction (BVf)	0.75 ± 0.01	0.68 ± 0.05
Bone mineral content (BMC, mg)	1.09 ± 0.02	0.81 ± 0.08
Bone mineral density (BMD, mg/cm <sup>3</sup> )	1015 ± 15	976 ± 11
Cortical thickness (mm)	0.18 ± 0.01	0.16 ± 0.01
<b>Histomorphometry (Trabecular bone analyses)</b>		
Bone volume (BV, mm <sup>2</sup> )	0.14 ± 0.04	0.25 ± 0.03
Tissue volume (TV, mm <sup>2</sup> )	2.33 ± 0.07	2.06 ± 0.02
Bone surface (BS, mm)	6.67 ± 1.68	14.68 ± 0.17
BV/TV	0.08 ± 0.02	0.14 ± 0.01
BS/TV	49.47 ± 4.23	61.50 ± 5.83
Trabecular thickness (Tb.Th, μm)	41.1 ± 3.9	32.8 ± 3.1
Trabecular number (Tb.N, n/mm <sup>2</sup> )	1.4 ± 0.3	3.7 ± 0.04
Trabecular separation (Tb.Sp, μm)	782.3 ± 214.8	240.4 ± 45.9
Growth plate thickness (mm)	0.117 ± 0.053	0.108 ± 0.015
Growth plate thickness (%)	68.4 ± 1.1	49.5 ± 5.7
Growth plate volume (mm <sup>2</sup> )	0.056 ± 0.003	0.049 ± 0.002
Growth plate volume (%)	67.2 ± 1.3	50.4 ± 7.2
Chondrocyte number (n/mm <sup>2</sup> of growth plate)	1310 ± 113	1711 ± 87
Primary spongiosa thickness (μm)	54.1 ± 4.6	113.4 ± 27.5
Primary spongiosa thickness (%)	31.6 ± 1.1	50.5 ± 5.7
Primary spongiosa (mm <sup>2</sup> )	0.027 ± 0.003	0.051 ± 0.016
Primary spongiosa volume (%)	32.8 ± 1.3	49.6 ± 7.2
BV Primary spongiosa (mm <sup>2</sup> )	0.008 ± 0.003	0.025 ± 0.009
BV Primary spongiosa (%)	53.6 ± 10.3	48.6 ± 1.9

**Table S 2-2. Complete list of sialylated free oligosaccharides identified by MS and MS/MS in the water-soluble fraction of protein pellets from *NEU1<sup>ΔEx3</sup>* mouse kidney tissue.**

<i>m/z</i>	Structure	<i>m/z</i>	Structure	<i>m/z</i>	Structure
1240.60		2403.18	 and 	3357.66	
1532.76					
1562.77		2547.26		3447.69	
1981.98		2577.27		3806.88	
2011.99		2607.28		3838.87	 and 
2186.08		2998.46	 and 		
2216.09					
2343.16	 	3056.50			

**Table S 2-3: List of proteins reduced in Neu1<sup>ΔEx3</sup> mice kidney identified by LC-MS/MS.**

List of proteins reduced in <i>Neu1</i> <sup>ΔEx3</sup> kidney of 4-month-old female mice							Exclusive unique peptide counts					
#	Identified Proteins (1841)	Accession Number	Alternate ID	MW	T-Test (p-value): (p < 0.05)	Quantitative Profile	KO1	KO2	KO3	WT1	WT2	WT3
1	Low-density lipoprotein receptor-related protein 2 OS=Mus musculus (Mouse) OX=10090 GN=Lrp2 PE=1 SV=1	A2ARV4	Lrp2	519 kDa	0.01	KO Female NT low, WT Female NT high	106	87	62	159	170	128
2	ATP synthase subunit beta, mitochondrial OS=Mus musculus (Mouse) OX=10090 GN=Atp5f1b PE=1 SV=2	P56480	Atp5f1b	56 kDa	0.0043	KO Female NT low, WT Female NT high	66	66	59	93	96	83
3	Peroxisomal bifunctional enzyme OS=Mus musculus (Mouse) OX=10090 GN=Ehhadh PE=1 SV=4	Q9DBM2	Ehhadh	78 kDa	0.01	KO Female NT low, WT Female NT high	52	41	41	102	108	73

4	ATP synthase subunit alpha, mitochondrial OS=Mus musculus (Mouse) OX=10090 GN=Atp5f1a PE=1 SV=1	Q03265	Atp5f1a	60 kDa	0.038	KO Female NT low, WT Female NT high	51	54	47	80	84	59
5	Catalase OS=Mus musculus (Mouse) OX=10090 GN=Cat PE=1 SV=4	P24270	Cat	60 kDa	0.027	KO Female NT low, WT Female NT high	54	44	43	65	67	61
6	Cluster of Sodium/potassium-transporting ATPase subunit alpha-1 OS=Mus musculus (Mouse) OX=10090 GN=Atp1a1 PE=1 SV=1 (Q8VDN2)	Q8VDN2 [5]	Atp1a1	113 kDa	0.037	KO Female NT low, WT Female NT high	49	32	37	49	55	51
7	Argininosuccinate synthase OS=Mus musculus (Mouse) OX=10090 GN=Ass1 PE=1 SV=1	P16460	Ass1	47 kDa	0.046	KO Female NT low, WT Female NT high	49	42	42	53	57	52
8	Pyruvate carboxylase, mitochondrial OS=Mus musculus (Mouse) OX=10090 GN=Pc PE=1 SV=1	Q05920	Pc	130 kDa	0.029	KO Female NT low, WT Female NT high	52	39	38	62	67	55

9	Glutamate dehydrogenase 1, mitochondrial OS=Mus musculus (Mouse) OX=10090 GN=Glud1 PE=1 SV=1	P26443	Glud1	61 kDa	0.027	KO Female NT low, WT Female NT high	52	47	38	54	53	54
10	Villin-1 OS=Mus musculus (Mouse) OX=10090 GN=Vil1 PE=1 SV=3	Q62468	Vil1	93 kDa	0.019	KO Female NT low, WT Female NT high	39	32	27	44	47	41
11	Sorbitol dehydrogenase OS=Mus musculus (Mouse) OX=10090 GN=Sord PE=1 SV=3	Q64442	Sord	38 kDa	0.035	KO Female NT low, WT Female NT high	35	28	28	45	49	42
12	Cluster of ADP/ATP translocase 2 OS=Mus musculus (Mouse) OX=10090 GN=Slc25a5 PE=1 SV=3 (P51881)	P51881 [2]	Slc25a5	33 kDa	0.0028	KO Female NT low, WT Female NT high	36	30	28	43	42	39
13	Cluster of Aldo-keto reductase family 1 member C21 OS=Mus musculus (Mouse) OX=10090 GN=Akr1c21 PE=1 SV=2 (Q91WR5)	Q91WR5 [3]	Akr1c21	37 kDa	0.013	KO Female NT low, WT Female NT high	22	19	17	30	32	28

14	Glycine N-acyltransferase-like protein Keg1 OS=Mus musculus (Mouse) OX=10090 GN=Keg1 PE=1 SV=1	Q9DCY0	Keg1	34 kDa	0.022	KO Female NT low, WT Female NT high	22	21	18	28	31	26
15	Kynurenine/alpha-aminoadipate aminotransferase, mitochondrial OS=Mus musculus (Mouse) OX=10090 GN=Aadat PE=1 SV=1	Q9WVM8	Aadat	48 kDa	0.032	KO Female NT low, WT Female NT high	44	20	20	57	61	41
16	2-iminobutanoate/2-iminopropanoate deaminase OS=Mus musculus (Mouse) OX=10090 GN=Rida PE=1 SV=3	P52760	Rida	14 kDa	0.021	KO Female NT low, WT Female NT high	29	25	23	39	34	30
17	N-acyl-aromatic-L-amino acid amidohydrolase (carboxylate-forming) OS=Mus musculus (Mouse) OX=10090 GN=Acy3 PE=1 SV=1	Q91XE4	Acy3	35 kDa	0.021	KO Female NT low, WT Female NT high	22	16	15	29	29	24
18	Meprin A subunit alpha OS=Mus musculus (Mouse) OX=10090 GN=Mep1a PE=1 SV=4	P28825	Mep1a	84 kDa	0.027	KO Female NT low, WT Female NT high	15	13	13	27	34	20

19	Glycine amidinotransferase, mitochondrial OS=Mus musculus (Mouse) OX=10090 GN=Gatm PE=1 SV=1	Q9D964	Gatm	48 kDa	0.046	KO Female NT low, WT Female NT high	34	29	21	32	33	30
20	Propionyl-CoA carboxylase alpha chain, mitochondrial OS=Mus musculus (Mouse) OX=10090 GN=Pcca PE=1 SV=2	Q91ZA3	Pcca	80 kDa	0.022	KO Female NT low, WT Female NT high	31	23	24	37	33	31
21	Hydroxyacid oxidase 2 OS=Mus musculus (Mouse) OX=10090 GN=Hao2 PE=1 SV=1	Q9NYQ2	Hao2	39 kDa	0.018	KO Female NT low, WT Female NT high	30	26	23	51	55	38
22	Probable D-lactate dehydrogenase, mitochondrial OS=Mus musculus (Mouse) OX=10090 GN=Ldhd PE=1 SV=1	Q7TNG8	Ldhd	52 kDa	0.0028	KO Female NT low, WT Female NT high	13	14	15	20	21	18
23	Cytochrome b-c1 complex subunit 2, mitochondrial OS=Mus musculus (Mouse) OX=10090 GN=Uqcrc2 PE=1 SV=1	Q9DB77	Uqcrc2	48 kDa	0.037	KO Female NT low, WT Female NT high	24	22	16	35	37	25

24	Cluster of Heat shock 70 kDa protein 1A OS=Mus musculus (Mouse) OX=10090 GN=Hspa1a PE=1 SV=2 (Q61696)	Q61696 [2]	Hspa1a	70 kDa	0.046	KO Female NT low, WT Female NT high	12	8	6	14	10	19
25	Fumarate hydratase, mitochondrial OS=Mus musculus (Mouse) OX=10090 GN=Fh PE=1 SV=3	P97807	Fh	54 kDa	0.00027	KO Female NT low, WT Female NT high	25	23	21	30	30	26
26	Nucleoside diphosphate-linked moiety X motif 19 OS=Mus musculus (Mouse) OX=10090 GN=Nudt19 PE=1 SV=2	P11930	Nudt19	40 kDa	0.0026	KO Female NT low, WT Female NT high	10	8	8	18	21	18
27	Triokinase/FMN cyclase OS=Mus musculus (Mouse) OX=10090 GN=Tkfc PE=1 SV=1	Q8VC30	Tkfc	60 kDa	0.033	KO Female NT low, WT Female NT high	19	9	12	24	26	20
28	Acyl-coenzyme A synthetase ACSM1, mitochondrial OS=Mus musculus (Mouse) OX=10090 GN=Acsm1 PE=1 SV=1	Q91VA0	Acsm1	65 kDa	0.016	KO Female NT low, WT Female NT high	21	14	11	30	33	27

29	Peroxisomal multifunctional enzyme type 2 OS=Mus musculus (Mouse) OX=10090 GN=Hsd17b4 PE=1 SV=3	P51660	Hsd17b4	79 kDa	0.021	KO Female NT low, WT Female NT high	15	9	9	21	17	18
30	Carboxylesterase 1D OS=Mus musculus (Mouse) OX=10090 GN=Ces1d PE=1 SV=1	Q8VCT4	Ces1d	62 kDa	0.00014	KO Female NT low, WT Female NT high	10	12	9	18	19	18
31	NADH-ubiquinone oxidoreductase 75 kDa subunit, mitochondrial OS=Mus musculus (Mouse) OX=10090 GN=Ndufs1 PE=1 SV=2	Q91VD9	Ndufs1	80 kDa	0.0085	KO Female NT low, WT Female NT high	12	14	7	22	28	22
32	Cluster of Carbonyl reductase [NADPH] 1 OS=Mus musculus (Mouse) OX=10090 GN=Cbr1 PE=1 SV=3 (P48758)	P48758 [2]	Cbr1	31 kDa	0.014	KO Female NT low, WT Female NT high	27	23	22	31	31	24
33	Heat shock protein 75 kDa, mitochondrial OS=Mus musculus (Mouse) OX=10090 GN=Trap1 PE=1 SV=1	Q9CQN1	Trap1	80 kDa	0.013	KO Female NT low, WT Female NT high	16	16	12	22	19	22
34	Ketohexokinase OS=Mus musculus (Mouse) OX=10090 GN=Khk PE=1 SV=1	P97328	Khk	33 kDa	0.02	KO Female NT low, WT	15	11	8	21	28	26

						Female NT high						
35	Carboxylesterase 1F OS=Mus musculus (Mouse) OX=10090 GN=Ces1f PE=1 SV=1	Q91WU0	Ces1f	62 kDa	0.035	KO Female NT low, WT Female NT high	6	2	2	5	5	4
36	Valacyclovir hydrolase OS=Mus musculus (Mouse) OX=10090 GN=Bphl PE=1 SV=1	Q8R164	Bphl	33 kDa	0.0039	KO Female NT low, WT Female NT high	16	10	9	18	19	17
37	Cluster of 3-ketoacyl-CoA thiolase A, peroxisomal OS=Mus musculus (Mouse) OX=10090 GN=Acaa1a PE=1 SV=1 (Q921H8)	Q921H8 [2]	Acaa1a	44 kDa	0.048	KO Female NT low, WT Female NT high	18	15	11	21	19	21
38	Peroxisomal carnitine O- octanoyltransferase OS=Mus musculus (Mouse) OX=10090 GN=Crot PE=1 SV=1	Q9DC50	Crot	70 kDa	0.0054	KO Female NT low, WT Female NT high	4	1	0	10	9	12
39	3-hydroxyisobutyrate dehydrogenase, mitochondrial OS=Mus musculus (Mouse) OX=10090 GN=Hibadh PE=1 SV=1	Q99L13	Hibadh	35 kDa	0.033	KO Female NT low, WT Female NT high	15	18	17	22	20	18

40	Phosphate carrier protein, mitochondrial OS=Mus musculus (Mouse) OX=10090 GN=Slc25a3 PE=1 SV=1	Q8VEM8	Slc25a3	40 kDa	0.05	KO Female NT low, WT Female NT high	13	11	9	19	27	14
41	Fumarylacetoacetase OS=Mus musculus (Mouse) OX=10090 GN=Fah PE=1 SV=2	P35505	Fah	46 kDa	0.0091	KO Female NT low, WT Female NT high	17	14	14	25	24	20
42	Cadherin-16 OS=Mus musculus (Mouse) OX=10090 GN=Cdh16 PE=1 SV=1	O88338	Cdh16	90 kDa	0.032	KO Female NT low, WT Female NT high	12	13	7	14	22	15
43	Lipoamide acyltransferase component of branched-chain alpha-keto acid dehydrogenase complex, mitochondrial OS=Mus musculus (Mouse) OX=10090 GN=Dbt PE=1 SV=2	P53395	Dbt	53 kDa	0.018	KO Female NT low, WT Female NT high	12	10	8	17	16	15
44	Succinate dehydrogenase [ubiquinone] iron-sulfur subunit, mitochondrial OS=Mus musculus (Mouse) OX=10090 GN=Sdhb PE=1 SV=1	Q9CQA3	Sdhb	32 kDa	0.038	KO Female NT low, WT Female NT high	14	9	11	17	13	18

45	Electron transfer flavoprotein-ubiquinone oxidoreductase, mitochondrial OS=Mus musculus (Mouse) OX=10090 GN=Etfdh PE=1 SV=1	Q921G7	Etfdh	68 kDa	0.0022	KO Female NT low, WT Female NT high	10	7	7	17	20	15
46	Apoptosis-inducing factor 1, mitochondrial OS=Mus musculus (Mouse) OX=10090 GN=Aifm1 PE=1 SV=1	Q9Z0X1	Aifm1	67 kDa	0.012	KO Female NT low, WT Female NT high	8	10	7	17	20	12
47	Cytochrome c1, heme protein, mitochondrial OS=Mus musculus (Mouse) OX=10090 GN=Cyc1 PE=1 SV=1	Q9D0M3	Cyc1	35 kDa	0.016	KO Female NT low, WT Female NT high	8	8	6	18	17	8
48	NADH dehydrogenase [ubiquinone] flavoprotein 1, mitochondrial OS=Mus musculus (Mouse) OX=10090 GN=Ndufv1 PE=1 SV=1	Q91YT0	Ndufv1	51 kDa	0.025	KO Female NT low, WT Female NT high	11	11	6	15	20	16
49	Alpha-methylacyl-CoA racemase OS=Mus musculus (Mouse) OX=10090 GN=Amacr PE=1 SV=4	O09174	Amacr	42 kDa	0.031	KO Female NT low, WT Female NT high	4	4	4	7	6	10

50	ATP synthase subunit gamma, mitochondrial OS=Mus musculus (Mouse) OX=10090 GN=Atp5f1c PE=1 SV=1	Q91VR2	Atp5f1c	33 kDa	0.0048	KO Female NT low, WT Female NT high	10	7	9	14	14	11
51	Cytochrome c oxidase subunit 2 OS=Mus musculus (Mouse) OX=10090 GN=Mtco2 PE=1 SV=1	P00405	Mtco2	26 kDa	0.042	KO Female NT low, WT Female NT high	10	8	7	11	15	10
52	Secernin-2 OS=Mus musculus (Mouse) OX=10090 GN=Scrn2 PE=1 SV=1	Q8VCA8	Scrn2	47 kDa	0.016	KO Female NT low, WT Female NT high	9	5	5	10	10	10
53	Voltage-dependent anion-selective channel protein 2 OS=Mus musculus (Mouse) OX=10090 GN=Vdac2 PE=1 SV=2	Q60930	Vdac2	32 kDa	0.033	KO Female NT low, WT Female NT high	9	9	7	8	13	9
54	Prohibitin OS=Mus musculus (Mouse) OX=10090 GN=Phb PE=1 SV=1	P67778	Phb	30 kDa	0.0058	KO Female NT low, WT Female NT high	5	6	4	18	15	12

55	3-hydroxyanthranilate 3,4-dioxygenase OS=Mus musculus (Mouse) OX=10090 GN=Haa0 PE=1 SV=1	Q78JT3	Haa0	33 kDa	0.015	KO Female NT low, WT Female NT high	6	6	3	11	8	10
56	ATP-binding cassette sub-family D member 3 OS=Mus musculus (Mouse) OX=10090 GN=Abcd3 PE=1 SV=2	P55096	Abcd3	75 kDa	0.01	KO Female NT low, WT Female NT high	5	1	0	9	12	9
57	NADPH--cytochrome P450 reductase OS=Mus musculus (Mouse) OX=10090 GN=Por PE=1 SV=2	P37040	Por	77 kDa	0.03	KO Female NT low, WT Female NT high	7	4	3	7	11	10
58	Xaa-Pro aminopeptidase 1 OS=Mus musculus (Mouse) OX=10090 GN=Xpnpep1 PE=1 SV=1	Q6P1B1	Xpnpep1	70 kDa	0.038	KO Female NT low, WT Female NT high	7	4	6	9	10	12
59	Complex I assembly factor ACAD9, mitochondrial OS=Mus musculus (Mouse) OX=10090 GN=Acad9 PE=1 SV=2	Q8JZN5	Acad9	69 kDa	0.031	KO Female NT low, WT Female NT high	6	3	3	7	8	6
60	Prohibitin-2 OS=Mus musculus (Mouse) OX=10090 GN=Phb2 PE=1 SV=1	O35129	Phb2	33 kDa	0.031	KO Female NT low, WT	3	6	4	10	10	7

						Female NT high						
61	NADH dehydrogenase [ubiquinone] 1 alpha subcomplex subunit 12 OS=Mus musculus (Mouse) OX=10090 GN=Ndufa12 PE=1 SV=2	Q7TMF3	Ndufa12	17 kDa	0.033	KO Female NT low, WT Female NT high	6	5	4	8	6	5
62	Enoyl-CoA delta isomerase 3, peroxisomal OS=Mus musculus (Mouse) OX=10090 GN=Eci3 PE=1 SV=1	Q78JN3	Eci3	35 kDa	0.022	KO Female NT low, WT Female NT high	3	3	2	5	6	4
63	NADH dehydrogenase [ubiquinone] iron-sulfur protein 3, mitochondrial OS=Mus musculus (Mouse) OX=10090 GN=Ndufs3 PE=1 SV=2	Q9DCT2	Ndufs3	30 kDa	0.042	KO Female NT low, WT Female NT high	3	4	2	10	13	6
64	Cluster of NADPH-dependent 3-ketosteroid reductase Hsd3b4 OS=Mus musculus (Mouse) OX=10090 GN=Hsd3b4 PE=1 SV=3 (Q61767)	Q61767 [2]	Hsd3b4	42 kDa	0.01	KO Female NT low, WT Female NT high	3	1	1	7	9	10
65	Mitochondrial amidoxime reducing component 2 OS=Mus musculus (Mouse) OX=10090 GN=Mtarc2 PE=1 SV=1	Q922Q1	Mtarc2	38 kDa	0.018	KO Female NT low, WT Female NT high	4	2	3	7	8	4

66	Calcium-binding mitochondrial carrier protein Aralar1 OS=Mus musculus (Mouse) OX=10090 GN=Slc25a12 PE=1 SV=1	Q8BH59	Slc25a12	75 kDa	0.023	KO Female NT low, WT Female NT high	0	1	0	4	9	7
67	40S ribosomal protein S14 OS=Mus musculus (Mouse) OX=10090 GN=Rps14 PE=1 SV=3	P62264	Rps14	16 kDa	0.008	KO Female NT low, WT Female NT high	5	3	3	7	5	7
68	Sideroflexin-1 OS=Mus musculus (Mouse) OX=10090 GN=Sfxn1 PE=1 SV=3	Q99JR1	Sfxn1	36 kDa	0.039	KO Female NT low, WT Female NT high	3	1	1	4	7	5
69	EH domain-containing protein 4 OS=Mus musculus (Mouse) OX=10090 GN=Ehd4 PE=1 SV=1	Q9EQP2	Ehd4	61 kDa	0.023	KO Female NT low, WT Female NT high	3	1	1	4	4	3
70	CDGSH iron-sulfur domain-containing protein 1 OS=Mus musculus (Mouse) OX=10090 GN=Cisd1 PE=1 SV=1	Q91WS0	Cisd1	12 kDa	0.0022	KO Female NT low, WT Female NT high	2	3	3	5	5	4

71	Enoyl-[acyl-carrier-protein] reductase, mitochondrial OS=Mus musculus (Mouse) OX=10090 GN=Mecr PE=1 SV=2	Q9DCS3	Mecr	40 kDa	0.015	KO Female NT low, WT Female NT high	2	1	0	5	4	5
72	Sulfide:quinone oxidoreductase, mitochondrial OS=Mus musculus (Mouse) OX=10090 GN=Sqor PE=1 SV=3	Q9R112	Sqor	50 kDa	0.018	KO Female NT low, WT Female NT high	2	1	1	6	4	5
73	Mitochondrial 2-oxoglutarate/malate carrier protein OS=Mus musculus (Mouse) OX=10090 GN=Slc25a11 PE=1 SV=3	Q9CR62	Slc25a11	34 kDa	0.013	KO Female NT low, WT Female NT high	4	3	3	7	9	7
74	Liver carboxylesterase 1 OS=Mus musculus (Mouse) OX=10090 GN=Ces1 PE=1 SV=1	Q8VCC2	Ces1	63 kDa	0.00039	KO Female NT low, WT Female NT high	0	0	0	0	0	0
75	Acyl-coenzyme A amino acid N-acyltransferase 1 OS=Mus musculus (Mouse) OX=10090 GN=Acnat1 PE=1 SV=1	A2AKK5	Acnat1	46 kDa	0.011	KO Female NT low, WT Female NT high	3	0	0	10	9	7
76	NADH dehydrogenase [ubiquinone] 1 alpha subcomplex subunit 5 OS=Mus	Q9CPP6	Ndufa5	13 kDa	0.0072	KO Female NT low, WT	0	1	2	6	5	3

	musculus (Mouse) OX=10090 GN=Ndufa5 PE=1 SV=3					Female NT high						
77	60S ribosomal protein L28 OS=Mus musculus (Mouse) OX=10090 GN=Rpl28 PE=1 SV=2	P41105	Rpl28	16 kDa	0.0031	KO Female NT low, WT Female NT high	2	2	1	4	5	4
78	Actin-related protein 2/3 complex subunit 1A OS=Mus musculus (Mouse) OX=10090 GN=Arpc1a PE=1 SV=1	Q9R0Q6	Arpc1a	42 kDa	0.0053	KO Female NT low, WT Female NT high	1	0	0	2	4	5
79	NADH dehydrogenase [ubiquinone] 1 beta subcomplex subunit 4 OS=Mus musculus (Mouse) OX=10090 GN=Ndufb4 PE=1 SV=3	Q9CQC7	Ndufb4	15 kDa	0.047	KO Female NT low, WT Female NT high	2	3	2	4	3	4
80	Voltage-dependent anion-selective channel protein 3 OS=Mus musculus (Mouse) OX=10090 GN=Vdac3 PE=1 SV=1	Q60931	Vdac3	31 kDa	0.0038	KO Female NT low, WT Female NT high	0	2	0	5	5	3
81	NADH dehydrogenase [ubiquinone] iron- sulfur protein 5 OS=Mus musculus (Mouse) OX=10090 GN=Ndufs5 PE=1 SV=3	Q99LY9	Ndufs5	13 kDa	0.039	KO Female NT low, WT Female NT high	2	2	2	4	3	3

82	Ectonucleoside triphosphate diphosphohydrolase 5 OS=Mus musculus (Mouse) OX=10090 GN=Entpd5 PE=1 SV=1	Q9WUZ9	Entpd5	47 kDa	0.016	KO Female NT low, WT Female NT high	2	1	0	3	4	3
83	NADH dehydrogenase [ubiquinone] 1 beta subcomplex subunit 5, mitochondrial OS=Mus musculus (Mouse) OX=10090 GN=Ndufb5 PE=1 SV=1	Q9CQH3	Ndufb5	22 kDa	0.031	KO Female NT low, WT Female NT high	1	2	0	5	5	3
84	NADH dehydrogenase [ubiquinone] 1 beta subcomplex subunit 8, mitochondrial OS=Mus musculus (Mouse) OX=10090 GN=Ndufb8 PE=1 SV=1	Q9D6J5	Ndufb8	22 kDa	0.021	KO Female NT low, WT Female NT high	0	2	1	2	3	2
85	Mitochondrial pyruvate carrier 2 OS=Mus musculus (Mouse) OX=10090 GN=Mpc2 PE=1 SV=1	Q9D023	Mpc2	14 kDa	0.047	KO Female NT low, WT Female NT high	2	1	1	2	3	3
86	NADH dehydrogenase [ubiquinone] iron-sulfur protein 8, mitochondrial OS=Mus musculus (Mouse) OX=10090 GN=Ndufs8 PE=1 SV=1	Q8K3J1	Ndufs8	24 kDa	0.016	KO Female NT low, WT Female NT high	1	1	1	2	2	3
87	NADH dehydrogenase [ubiquinone] 1 alpha subcomplex subunit 6 OS=Mus	Q9CQZ5	Ndufa6	15 kDa	0.016	KO Female NT low, WT	1	2	1	5	4	3

	musculus (Mouse) OX=10090 GN=Ndufa6 PE=1 SV=1					Female NT high						
88	DnaJ homolog subfamily A member 1 OS=Mus musculus (Mouse) OX=10090 GN=Dnaja1 PE=1 SV=1	P63037	Dnaja1	45 kDa	0.023	KO Female NT low, WT Female NT high	2	0	0	2	2	4
89	Glycine dehydrogenase (decarboxylating), mitochondrial OS=Mus musculus (Mouse) OX=10090 GN=Gldc PE=1 SV=1	Q91W43	Gldc	113 kDa	0.038	KO Female NT low, WT Female NT high	2	0	0	7	8	3
90	Transmembrane emp24 domain- containing protein 10 OS=Mus musculus (Mouse) OX=10090 GN=Tmed10 PE=1 SV=1	Q9D1D4	Tmed10	25 kDa	0.013	KO Female NT low, WT Female NT high	1	2	1	2	4	4
91	NADH dehydrogenase [ubiquinone] 1 alpha subcomplex subunit 2 OS=Mus musculus (Mouse) OX=10090 GN=Ndufa2 PE=1 SV=3	Q9CQ75	Ndufa2	11 kDa	0.016	KO Female NT low, WT Female NT high	1	1	1	2	2	3
92	Solute carrier family 22 member 2 OS=Mus musculus (Mouse) OX=10090 GN=Slc22a2 PE=1 SV=1	O70577	Slc22a2	62 kDa	0.026	KO Female NT low, WT Female NT high	0	0	0	1	2	3

93	4-hydroxyphenylpyruvate dioxygenase OS=Mus musculus (Mouse) OX=10090 GN=Hpd PE=1 SV=3	P49429	Hpd	45 kDa	0.008	KO Female NT low, WT Female NT high	0	0	0	4	3	5
94	Solute carrier family 22 member 12 OS=Mus musculus (Mouse) OX=10090 GN=Slc22a12 PE=1 SV=1	Q8CFZ5	Slc22a12	60 kDa	0.025	KO Female NT low, WT Female NT high	0	0	0	2	3	1
95	Lysine--tRNA ligase OS=Mus musculus (Mouse) OX=10090 GN=Kars1 PE=1 SV=1	Q99MN1	Kars1	68 kDa	0.016	KO Female NT low, WT Female NT high	1	0	1	2	2	2
96	Dehydrogenase/reductase SDR family member 1 OS=Mus musculus (Mouse) OX=10090 GN=Dhrs1 PE=1 SV=1	Q99L04	Dhrs1	34 kDa	0.047	KO Female NT low, WT Female NT high	1	0	0	2	2	1
97	Acyl-coenzyme A thioesterase 8 OS=Mus musculus (Mouse) OX=10090 GN=Acot8 PE=1 SV=1	P58137	Acot8	36 kDa	0.047	KO Female NT low, WT Female NT high	1	0	0	1	2	2

98	Mitochondrial pyruvate carrier 1 OS=Mus musculus (Mouse) OX=10090 GN=Mpc1 PE=1 SV=1	P63030	Mpc1	12 kDa	0.0075	KO Female NT low, WT Female NT high	0	1	0	2	2	2
99	Serine beta-lactamase-like protein LACTB, mitochondrial OS=Mus musculus (Mouse) OX=10090 GN=Lactb PE=1 SV=1	Q9EP89	Lactb	61 kDa	0.026	KO Female NT low, WT Female NT high	0	0	0	2	1	1
100	Vesicular integral-membrane protein VIP36 OS=Mus musculus (Mouse) OX=10090 GN=Lman2 PE=1 SV=2	Q9DBH5	Lman2	40 kDa	0.016	KO Female NT low, WT Female NT high	0	0	0	1	2	1
101	Arginase-2, mitochondrial OS=Mus musculus OX=10090 GN=Arg2 PE=1 SV=1	O08691		60 kDa	0.016	KO Female NT low, WT Female NT high	0	0	0	2	1	1

List of proteins decreased in *Neu1<sup>ΔEx3</sup>* kidney of 4-month-old male mice. Exclusive unique peptide counts

#	Identified Proteins (1841)	Accession Number	Alternate ID	MW	T-Test (p-value) : (p < 0.05)	Quantitative Profile	KO 1	KO 2	KO 3	WT 1	WT 2	WT 3
1	3-hydroxyanthranilate 3,4-dioxygenase OS=Mus musculus (Mouse) OX=10090 GN=Hao PE=1 SV=1	Q78JT3	Hao	33 kDa	0.008 8	KO Male NT low, WT Male NT high	7	6	1	15	18	13
2	60 kDa heat shock protein, mitochondrial OS=Mus musculus (Mouse) OX=10090 GN=Hspd1 PE=1 SV=1	P63038	Hspd1	61 kDa	0.000 49	KO Male NT low, WT Male NT high	65	71	57	85	84	81
3	Acyl carrier protein, mitochondrial OS=Mus musculus (Mouse) OX=10090 GN=Ndufab1 PE=1 SV=1	Q9CR21	Ndufab1	17 kDa	0.015	KO Male NT low, WT Male NT high	2	3	3	10	11	7
4	Acyl-coenzyme A synthetase ACSM3, mitochondrial OS=Mus musculus (Mouse) OX=10090 GN=Acsm3 PE=1 SV=2	Q3UNX5	Acsm3	66 kDa	0.000 21	KO Male NT low, WT Male NT high	7	12	8	38	41	37

5	Acylphosphatase-2 OS=Mus musculus (Mouse) OX=10090 GN=Acyp2 PE=1 SV=2	P56375	Acyp2	12 kDa	0.0075	KO Male NT low, WT Male NT high	1	1	1	3	3	2
6	Adenylate kinase 4, mitochondrial OS=Mus musculus (Mouse) OX=10090 GN=Ak4 PE=1 SV=1	Q9WUR9	Ak4	25 kDa	0.026	KO Male NT low, WT Male NT high	2	5	1	11	7	8
7	Alcohol dehydrogenase 1 OS=Mus musculus (Mouse) OX=10090 GN=Adh1 PE=1 SV=2	P00329	Adh1	40 kDa	0.033	KO Male NT low, WT Male NT high	16	21	15	25	23	29
8	Cluster of Alpha-1-antitrypsin 1-2 OS=Mus musculus (Mouse) OX=10090 GN=Serpina1b PE=1 SV=2 (P22599)	P22599 [5]	Serpina1b	46 kDa	0.00094	KO Male NT low, WT Male NT high	6	7	3	39	15	39
9	Alpha-2-macroglobulin receptor-associated protein OS=Mus musculus (Mouse) OX=10090 GN=Lrpap1 PE=1 SV=1	P55302	Lrpap1	42 kDa	0.042	KO Male NT low, WT Male NT high	7	11	5	26	32	17
10	Aminoacylase-1 OS=Mus musculus (Mouse) OX=10090 GN=Acy1 PE=1 SV=1	Q99JW2	Acy1	46 kDa	0.014	KO Male NT low, WT	6	10	5	17	17	14

						Male NT high						
11	Anionic trypsin-2 OS=Mus musculus (Mouse) OX=10090 GN=Prss2 PE=1 SV=1	P07146	Prss2	26 kDa	0.017	KO Male NT low, WT Male NT high	8	8	7	16	17	16
12	Apolipoprotein A-I OS=Mus musculus (Mouse) OX=10090 GN=Apoa1 PE=1 SV=2	Q00623	Apoa1	31 kDa	0.048	KO Male NT low, WT Male NT high	17	29	23	33	34	31
13	ATP synthase subunit d, mitochondrial OS=Mus musculus (Mouse) OX=10090 GN=Atp5pd PE=1 SV=3	Q9DCX2	Atp5pd	19 kDa	0.016	KO Male NT low, WT Male NT high	13	11	14	27	40	21
14	ATP-dependent Clp protease ATP-binding subunit clpX-like, mitochondrial OS=Mus musculus (Mouse) OX=10090 GN=Clpx PE=1 SV=2	Q9JHS4	Clpx	69 kDa	0.047	KO Male NT low, WT Male NT high	0	1	0	2	1	2
15	Band 4.1-like protein 1 OS=Mus musculus (Mouse) OX=10090 GN=Epb4111 PE=1 SV=2	Q9Z2H5	Epb4111	98 kDa	0.025	KO Male NT low, WT Male NT high	1	1	1	4	4	1

16	Caprin-1 OS=Mus musculus (Mouse) OX=10090 GN=Caprin1 PE=1 SV=2	Q60865	Caprin1	78 kDa	0.042	KO Male NT low, WT Male NT high	2	5	3	8	10	6
17	CDGSH iron-sulfur domain-containing protein 3, mitochondrial OS=Mus musculus (Mouse) OX=10090 GN=Cisd3 PE=1 SV=1	B1AR13	Cisd3	16 kDa	0.007 5	KO Male NT low, WT Male NT high	0	0	0	2	1	2
18	Clusterin OS=Mus musculus (Mouse) OX=10090 GN=Clu PE=1 SV=1	Q06890	Clu	52 kDa	0.035	KO Male NT low, WT Male NT high	3	2	3	11	12	5
19	Cluster of Cysteine sulfinic acid decarboxylase OS=Mus musculus (Mouse) OX=10090 GN=Csad PE=1 SV=1 (Q9DBE0)	Q9DBE0 [2]	Csad	55 kDa	0.027	KO Male NT low, WT Male NT high	8	12	10	18	14	18
20	Cytidine deaminase OS=Mus musculus (Mouse) OX=10090 GN=Cda PE=1 SV=2	P56389	Cda	16 kDa	0.043	KO Male NT low, WT Male NT high	8	12	10	15	22	16

21	Cytochrome b-c1 complex subunit 6, mitochondrial OS=Mus musculus (Mouse) OX=10090 GN=Uqcrh PE=1 SV=2	P99028	Uqcrh	10 kDa	0.0074	KO Male NT low, WT Male NT high	9	10	10	13	19	16
22	Cytochrome b-c1 complex subunit 8 OS=Mus musculus (Mouse) OX=10090 GN=Uqcrq PE=1 SV=3	Q9CQ69	Uqcrq	10 kDa	0.047	KO Male NT low, WT Male NT high	2	2	2	2	3	4
23	Cytochrome b-c1 complex subunit Rieske, mitochondrial OS=Mus musculus (Mouse) OX=10090 GN=Uqcrrs1 PE=1 SV=1	Q9CR68	Uqcrrs1	29 kDa	0.0022	KO Male NT low, WT Male NT high	3	4	2	10	9	8
24	Cytochrome c oxidase subunit 5A, mitochondrial OS=Mus musculus (Mouse) OX=10090 GN=Cox5a PE=1 SV=2	P12787	Cox5a	16 kDa	0.025	KO Male NT low, WT Male NT high	18	17	18	35	38	23
25	Cytochrome c oxidase subunit 6B1 OS=Mus musculus (Mouse) OX=10090 GN=Cox6b1 PE=1 SV=2	P56391	Cox6b1	10 kDa	0.017	KO Male NT low, WT Male NT high	3	4	6	7	8	10
26	Cytochrome c oxidase subunit 7A2, mitochondrial OS=Mus musculus	P48771	Cox7a2	9 kDa	0.04	KO Male NT low, WT	4	4	4	6	5	5

	(Mouse) OX=10090 GN=Cox7a2 PE=1 SV=2					Male NT high						
27	Cytochrome c oxidase subunit NDUFA4 OS=Mus musculus (Mouse) OX=10090 GN=Ndufa4 PE=1 SV=2	Q62425	Ndufa4	9 kDa	0.041	KO Male NT low, WT Male NT high	1	2	1	8	6	2
28	Cluster of Cytochrome c, somatic OS=Mus musculus (Mouse) OX=10090 GN=Cycs PE=1 SV=2 (P62897)	P62897 [2]	Cycs	12 kDa	0.015	KO Male NT low, WT Male NT high	18	18	18	23	26	23
29	D-dopachrome decarboxylase OS=Mus musculus (Mouse) OX=10090 GN=Ddt PE=1 SV=3	O35215	Ddt	13 kDa	0.041	KO Male NT low, WT Male NT high	0	0	1	5	11	5
30	Deaminated glutathione amidase OS=Mus musculus (Mouse) OX=10090 GN=Nit1 PE=1 SV=2	Q8VDK1	Nit1	36 kDa	0.007 2	KO Male NT low, WT Male NT high	5	6	2	10	10	7
31	Dihydrolipoyl dehydrogenase, mitochondrial OS=Mus musculus (Mouse) OX=10090 GN=Did PE=1 SV=2	O08749	Did	54 kDa	0.024	KO Male NT low, WT Male NT high	39	39	39	46	60	50

32	EH domain-containing protein 4 OS=Mus musculus (Mouse) OX=10090 GN=Ehd4 PE=1 SV=1	Q9EQP2	Ehd4	61 kDa	0.047	KO Male NT low, WT Male NT high	1	2	1	3	1	2
33	Electrogenic sodium bicarbonate cotransporter 1 OS=Mus musculus (Mouse) OX=10090 GN=Slc4a4 PE=1 SV=2	O88343	Slc4a4	121 kDa	0.02	KO Male NT low, WT Male NT high	6	8	3	11	12	10
34	Endoplasmic reticulum resident protein 29 OS=Mus musculus (Mouse) OX=10090 GN=Erp29 PE=1 SV=2	P57759	Erp29	29 kDa	0.000 39	KO Male NT low, WT Male NT high	0	0	0	4	4	2
35	Endoribonuclease LACTB2 OS=Mus musculus (Mouse) OX=10090 GN=Lactb2 PE=1 SV=1	Q99KR3	Lactb2	33 kDa	0.02	KO Male NT low, WT Male NT high	19	20	20	25	27	24
36	Enoyl-CoA delta isomerase 3, peroxisomal OS=Mus musculus (Mouse) OX=10090 GN=Eci3 PE=1 SV=1	Q78JN3	Eci3	35 kDa	0.003 3	KO Male NT low, WT Male NT high	3	3	3	3	4	4

37	Eukaryotic translation initiation factor 3 subunit J-A OS=Mus musculus (Mouse) OX=10090 GN=Eif3j1 PE=2 SV=1	Q3UGC7 (+1)	Eif3j1	29 kDa	0.0075	KO Male NT low, WT Male NT high	1	2	2	5	6	4
38	Glutaredoxin-related protein 5, mitochondrial OS=Mus musculus (Mouse) OX=10090 GN=Glr5 PE=1 SV=2	Q80Y14	Glr5	16 kDa	0.039	KO Male NT low, WT Male NT high	5	4	5	7	9	5
39	Glutathione hydrolase 1 proenzyme OS=Mus musculus (Mouse) OX=10090 GN=Ggt1 PE=1 SV=1	Q60928	Ggt1	62 kDa	0.0089	KO Male NT low, WT Male NT high	9	7	12	14	15	20
40	Glycine cleavage system H protein, mitochondrial OS=Mus musculus (Mouse) OX=10090 GN=Gcsh PE=1 SV=2	Q91WK5	Gcsh	19 kDa	0.039	KO Male NT low, WT Male NT high	3	3	2	5	6	5
41	Heat shock protein 105 kDa OS=Mus musculus (Mouse) OX=10090 GN=Hsph1 PE=1 SV=2	Q61699	Hsph1	96 kDa	0.015	KO Male NT low, WT Male NT high	0	2	2	5	5	6

42	Cluster of High mobility group protein B1 OS=Mus musculus (Mouse) OX=10090 GN=Hmgb1 PE=1 SV=2 (P63158)	P63158 [2]	Hmgb1	25 kDa	0.029	KO Male NT low, WT Male NT high	3	1	4	9	11	7
43	Histone H1.0 OS=Mus musculus (Mouse) OX=10090 GN=H1-0 PE=2 SV=4	P10922	H1-0	21 kDa	0.016	KO Male NT low, WT Male NT high	1	0	3	5	4	5
44	Cluster of Histone H1.3 OS=Mus musculus (Mouse) OX=10090 GN=H1-3 PE=1 SV=2 (P43277)	P43277 [3]	H1-3	22 kDa	0.043	KO Male NT low, WT Male NT high	6	0	4	14	9	5
45	Homogentisate 1,2-dioxygenase OS=Mus musculus (Mouse) OX=10090 GN=Hgd PE=1 SV=2	O09173	Hgd	50 kDa	0.014	KO Male NT low, WT Male NT high	20	23	24	30	35	31
46	Kynurenine/alpha-aminoadipate aminotransferase, mitochondrial OS=Mus musculus (Mouse) OX=10090 GN=Aadat PE=1 SV=1	Q9WVM 8	Aadat	48 kDa	0.048	KO Male NT low, WT Male NT high	8	10	9	15	12	20

47	Meprin A subunit alpha OS=Mus musculus (Mouse) OX=10090 GN=Mep1a PE=1 SV=4	P28825	Mep1a	84 kDa	0.021	KO Male NT low, WT Male NT high	21	18	18	29	29	32
48	Meprin A subunit beta OS=Mus musculus (Mouse) OX=10090 GN=Mep1b PE=1 SV=2	Q61847	Mep1b	80 kDa	0.009 9	KO Male NT low, WT Male NT high	10	10	8	18	15	15
49	Mitochondrial fission 1 protein OS=Mus musculus (Mouse) OX=10090 GN=Fis1 PE=1 SV=1	Q9CQ92	Fis1	17 kDa	0.007 5	KO Male NT low, WT Male NT high	1	1	1	2	3	2
50	NADH dehydrogenase [ubiquinone] 1 alpha subcomplex subunit 2 OS=Mus musculus (Mouse) OX=10090 GN=Ndufa2 PE=1 SV=3	Q9CQ75	Ndufa2	11 kDa	0.047	KO Male NT low, WT Male NT high	1	1	1	3	2	2
51	NADH dehydrogenase [ubiquinone] 1 alpha subcomplex subunit 3 OS=Mus musculus (Mouse) OX=10090 GN=Ndufa3 PE=1 SV=1	Q9CQ91	Ndufa3	9 kDa	0.007 5	KO Male NT low, WT Male NT high	0	0	0	1	2	2
52	NADH dehydrogenase [ubiquinone] 1 alpha subcomplex subunit 5 OS=Mus	Q9CPP6	Ndufa5	13 kDa	0.045	KO Male NT low, WT	1	1	1	6	7	3

	musculus (Mouse) OX=10090 GN=Ndufa5 PE=1 SV=3					Male NT high						
53	NADH dehydrogenase [ubiquinone] 1 beta subcomplex subunit 10 OS=Mus musculus (Mouse) OX=10090 GN=Ndufb10 PE=1 SV=3	Q9DCS9	Ndufb1 0	21 kDa	0.025	KO Male NT low, WT Male NT high	4	2	4	5	5	6
54	NADH dehydrogenase [ubiquinone] 1 subunit C2 OS=Mus musculus (Mouse) OX=10090 GN=Ndufc2 PE=1 SV=1	Q9CQ54	Ndufc2	14 kDa	0.014	KO Male NT low, WT Male NT high	2	0	2	4	6	4
55	NADH dehydrogenase [ubiquinone] iron- sulfur protein 4, mitochondrial OS=Mus musculus (Mouse) OX=10090 GN=Ndufs4 PE=1 SV=3	Q9CXZ1	Ndufs4	20 kDa	0.041	KO Male NT low, WT Male NT high	5	2	2	7	6	4
56	NADH dehydrogenase [ubiquinone] iron- sulfur protein 5 OS=Mus musculus (Mouse) OX=10090 GN=Ndufs5 PE=1 SV=3	Q99LY9	Ndufs5	13 kDa	0.039	KO Male NT low, WT Male NT high	1	1	1	3	4	2
57	NADP-dependent malic enzyme OS=Mus musculus (Mouse) OX=10090 GN=Me1 PE=1 SV=2	P06801	Me1	64 kDa	0.004 1	KO Male NT low, WT Male NT high	18	22	15	34	32	34

58	Nascent polypeptide-associated complex subunit alpha, muscle-specific form OS=Mus musculus (Mouse) OX=10090 GN=Naca PE=1 SV=2	P70670	Naca	220 kDa	0.003 1	KO Male NT low, WT Male NT high	4	4	5	6	6	6
59	Nicotinate-nucleotide pyrophosphorylase [carboxylating] OS=Mus musculus (Mouse) OX=10090 GN=Qprt PE=1 SV=1	Q91X91	Qprt	32 kDa	0.05	KO Male NT low, WT Male NT high	4	5	7	11	7	7
60	Nucleophosmin OS=Mus musculus (Mouse) OX=10090 GN=Npm1 PE=1 SV=1	Q61937	Npm1	33 kDa	0.049	KO Male NT low, WT Male NT high	4	4	7	11	10	8
61	Peroxisomal acyl-coenzyme A oxidase 2 OS=Mus musculus (Mouse) OX=10090 GN=Acox2 PE=1 SV=2	Q9QXD1	Acox2	77 kDa	0.046	KO Male NT low, WT Male NT high	5	4	2	11	6	12
62	Peroxisomal acyl-coenzyme A oxidase 3 OS=Mus musculus (Mouse) OX=10090 GN=Acox3 PE=1 SV=2	Q9EPL9	Acox3	78 kDa	0.032	KO Male NT low, WT Male NT high	6	8	1	16	12	22

63	Peroxisomal carnitine O-octanoyltransferase OS=Mus musculus (Mouse) OX=10090 GN=Crot PE=1 SV=1	Q9DC50	Crot	70 kDa	0.0024	KO Male NT low, WT Male NT high	11	15	14	26	26	31
64	Plasminogen activator inhibitor 1 RNA-binding protein OS=Mus musculus (Mouse) OX=10090 GN=Serbp1 PE=1 SV=2	Q9CY58	Serbp1	45 kDa	0.048	KO Male NT low, WT Male NT high	0	0	0	16	24	7
65	Probable D-lactate dehydrogenase, mitochondrial OS=Mus musculus (Mouse) OX=10090 GN=Ldhd PE=1 SV=1	Q7TNG8	Ldhd	52 kDa	0.042	KO Male NT low, WT Male NT high	25	36	20	41	41	53
66	Prohibitin-2 OS=Mus musculus (Mouse) OX=10090 GN=Phb2 PE=1 SV=1	O35129	Phb2	33 kDa	0.011	KO Male NT low, WT Male NT high	1	3	1	6	6	8
67	Proteasome subunit beta type-6 OS=Mus musculus (Mouse) OX=10090 GN=Psm6 PE=1 SV=3	Q60692	Psm6	25 kDa	0.016	KO Male NT low, WT Male NT high	1	1	1	3	1	2
68	Protein 4.1 OS=Mus musculus (Mouse) OX=10090 GN=Epb41 PE=1 SV=2	P48193	Epb41	96 kDa	0.036	KO Male NT low, WT	5	3	2	10	14	6

						Male NT high						
69	Serine/arginine-rich splicing factor 2 OS=Mus musculus (Mouse) OX=10090 GN=Srsf2 PE=1 SV=4	Q62093	Srsf2	25 kDa	0.036	KO Male NT low, WT Male NT high	2	3	4	6	7	2
70	Signal transducing adapter molecule 1 OS=Mus musculus (Mouse) OX=10090 GN=Stam PE=1 SV=3	P70297	Stam	60 kDa	0.047	KO Male NT low, WT Male NT high	0	0	1	1	1	1
71	Transcription factor BTF3 OS=Mus musculus (Mouse) OX=10090 GN=Btf3 PE=1 SV=3	Q64152	Btf3	22 kDa	0.002 2	KO Male NT low, WT Male NT high	0	0	0	2	3	1
72	Ubiquinone biosynthesis protein COQ9, mitochondrial OS=Mus musculus (Mouse) OX=10090 GN=Coq9 PE=1 SV=1	Q8K1Z0	Coq9	35 kDa	0.016	KO Male NT low, WT Male NT high	4	3	4	8	6	10
73	Cluster of Ubiquitin-40S ribosomal protein S27a OS=Mus musculus (Mouse) OX=10090 GN=Rps27a PE=1 SV=2 (P62983)	P62983 [3]	Rps27a	18 kDa	0.007 5	KO Male NT low, WT Male NT high	1	1	2	5	1	3

74	UV excision repair protein RAD23 homolog A OS=Mus musculus (Mouse) OX=10090 GN=Rad23a PE=1 SV=2	P54726	Rad23a	40 kDa	0.019	KO Male NT low, WT Male NT high	0	0	0	2	3	1
75	Cluster of Y-box-binding protein 1 OS=Mus musculus (Mouse) OX=10090 GN=Ybx1 PE=1 SV=3 (P62960)	P62960 [2]	Ybx1	36 kDa	0.021	KO Male NT low, WT Male NT high	7	2	7	8	4	8

## 2.7 Supplementary materials

### Study approval

All animal experiments were approved by the CHU Sainte-Justine Research Ethics Committee and performed in compliance with the Comité Institutionnel des Bonnes Pratiques Animales en Recherche (CIBPAR; approval numbers 2020-2658 and 2022-3452), in accordance with the Canadian Council on Animal Care guidelines.

### Animals

The constitutive KO NEU1 mouse model (*Neu1<sup>ΔEx3</sup>*) was previously described (32). Heterozygous mice were interbred, and litters were genotyped by PCR using genomic DNA extracted from clipped tail tip, as described (32). *Neu1<sup>ΔEx3</sup>* homozygous mice were compared with appropriate age- and sex-matched WT control littermates.

To generate *Neu1<sup>Cx3cr1ΔEx3</sup>* strain, a mononuclear phagocyte system-specific *Neu1* KO model, previously reported *Neu1<sup>ENSMUSE141558</sup>* strain (32), was interbred with the *B6.Cg-Tg(Pgk1-flpo)10Sykr/J* line (The Jackson Laboratory, stock 011065), that expresses the mouse codon-optimized FLP recombinase under the direction of the mouse *Pgk1*, phosphoglycerate kinase 1 promoter. This cross resulted in the removal of FRT-flanked *LacZ/BactPNeo* cassette and normal expression of the *Neu1* gene in the *Neu1<sup>loxPEx3</sup>* strain (Supplementary figure S1A). The *Neu1<sup>loxPEx3</sup>* strain was further crossed with the B6J.B6N(Cg)-Cx3cr1tm1.1(cre)Jung/J strain (The Jackson Laboratory, stock 025524), expressing the Cre recombinase under the control of the *Cx3cr1* (chemokine C-X3-C motif receptor 1) gene promoter. In the *Cx3cr1*-expressing cells of the progeny of *Neu1<sup>loxPEx3</sup>* and B6J.B6N(Cg)-Cx3cr1tm1.1(cre)Jung/J, the exon 3 of the *Neu1* gene was consequently removed, as confirmed by Sanger sequencing. Heterozygous *Neu1<sup>Cx3cr1ΔEx3</sup>* mice were bred to each other, and litters genotyped by PCR using genomic DNA extracted from clipped tail tip as shown in the Supplementary figure S1B. *Neu1<sup>Cx3cr1ΔEx3</sup>* homozygous mice were compared with appropriate age- and sex-matched *Neu1<sup>loxPEx3</sup>* littermates.

All mice were housed in an enriched environment in a poly-carbonate cages under 12 h/12 h light - dark cycles in a temperature- and humidity-controlled room. Mice had *ad libitum* access to a normal rodent chow and water.

### Analysis of mouse phenotype

*Neu1<sup>ΔEx3</sup>* and *Neu1<sup>Cx3cr1ΔEx3</sup>* mice were weighted weekly, from 4 to 17 weeks of age. Survival was measured for 21 male *Neu1<sup>ΔEx3</sup>* and 18 female *Neu1<sup>ΔEx3</sup>* mice siblings, 39 male and 38 female *Neu1<sup>Cx3cr1ΔEx3</sup>* siblings, and for the matching numbers of male and female WT controls.

NEU1-deficient mice were euthanized on a humane basis due to urinary retention following the advice of a veterinarian who was examining mice daily for the signs of a distorted bladder and inability to urinate. After euthanasia, the visceral organs were dissected, and the wet weight of the kidney, liver and spleen was measured and recorded.

### **Lysosomal enzyme assays**

Total acidic  $\alpha$ -neuraminidase,  $\beta$ -galactosidase and  $\beta$ -hexosaminidase activities were measured in tissue homogenates using corresponding fluorogenic 4-methylumbelliferyl substrates as previously described (199). NEU1 activity was measured by supplementing the  $\alpha$ -neuraminidase assay mixture with the specific inhibitor for both NEU3 and NEU4 enzymes, CG17700 (also known as C9-4BPT-DANA), at a final concentration of 125  $\mu$ M as previously described (276). Protein concentration was measured using Pierce BCA protein assay kit (#23225, Thermo Scientific).

### **Quantitative RT-PCR**

Whole kidneys were collected, and RNA extracted using Trizol reagent (Invitrogen) according to manufacturer's protocol. RNA quality was assessed by Nanodrop (Thermo Scientific) and 1  $\mu$ g of RNA was subjected to reverse transcription with QuantiTect Reverse Transcription kit (Qiagen). Analyses were performed in duplicate for each sample using SYBR Green Supermix (Bio-Rad) and previously described primers (32). Relative expression of *Neu1*, *Neu2*, *Neu3* and *Neu4* in kidneys were determined by the  $2^{-\Delta\Delta CT}$  method and normalized to the levels of *RPL32* mRNA.

### **Analysis of urinary proteins**

Urine was collected by housing mice in metabolic cages for 6 h while mice had free access to water. Mouse urine was, first, analyzed with a urine dipstick (Siemens, Multistix 10 SG). Then, urinary proteins were precipitated using trichloroacetic acid (TCA), as previously described (312), with some modifications. Briefly, TCA was added to 50  $\mu$ L of urine at a final concentration of 4%. Samples were mixed by vortexing, incubated on ice for 20 min and centrifuged at 13,000 g for 15 min. Pellets were rinsed with acetone and dried at room temperature. Protein pellets were dissolved in 40  $\mu$ L of 4x Laemmli buffer (#BP-110R, Boston Bioproducts), and pH was adjusted with 5  $\mu$ L of 1 M Tris buffer, pH 8.4. Proteins were denatured by boiling for 5 min, resolved by SDS-PAGE on 8% acrylamide gel and stained with freshly prepared Coomassie brilliant blue for 1 h. Gels were de-stained with 10% acetic acid under gentle agitation overnight at a room temperature. For immunoblots, urine protein

samples were resolved on NuPAGE 3-8% Tris-Acetate gradient gels (Invitrogen, EA03785BOX), transferred to nitrocellulose membranes, blocked with 5% bovine serum albumin (BSA) in phosphate buffered saline (PBS) and hybridized with the following antibodies:

Antigen	Host/Target species	Dilution	Manufacturer, catalogue number
Megalin	Rabbit anti-human	1:1000	Abcam, Ab76969
Vitamin D binding protein (DBP)	Mouse monoclonal	1:500	Santa Cruz, A-5
$\beta_2$ -microglobulin	Mouse monoclonal	1:1000	Santa Cruz, BBM.1

### **Blood glucose measurement**

Animals were kept in cages under fasting conditions for 16 h, with free access to water. Blood, collected from clipped tail tip, was analyzed using a glucometer (Contour Next, Bayer).

### **Analysis of kidney protein glycosylation by lectin blotting**

Whole kidneys were homogenized with 250  $\mu$ L of RIPA buffer (50 mM Tris HCl, 150 mM NaCl, 1% Nonidet P-40, 0.25% Na-deoxycholate, 0.1% SDS, 2 mM EDTA, 1 mM PMSF, pH 7.5), supplemented with protease and phosphatase inhibitor cocktail (Roche), using a sonic dismembrator (Artek Systems Corporation). The homogenate was cleared by centrifugation at 13,000 g for 25 min, and the protein concentration was measured with Pierce BCA protein assay kit (#23225, Thermo Scientific) and adjusted to 0.8  $\mu$ g/ $\mu$ L. Samples were boiled for 5 min and separated by SDS-PAGE on an 8% gel. Blots were transferred to nitrocellulose membrane. After staining with a Pierce™ Reversible Protein Stain Kit for Nitrocellulose Membranes (ThermoFisher Scientific) and blocking with 5% BSA for 1 h at room temperature, membranes were incubated overnight at 4°C with biotinylated peanut agglutinin (1:1000, PNA, Vector Laboratories, Burlington, ON, Canada) or biotinylated *Sambucus nigra* lectin (1:5000, SNA, Vector Laboratories, Burlington, ON, Canada) and, then, exposed to streptavidin-horseradish peroxidase conjugate (1:2000; GE Healthcare Life Sciences, Baie-d’Urfé, QC, Canada). Lectin reactivity was revealed by enhanced chemiluminescence (ECL) using the Pierce™ ECL Western Blotting Substrate (Thermo Fisher Scientific Inc., Rockford, USA). The total intensities of the stained protein bands were quantified by ImageJ software (Rasband, W.S., ImageJ, U.S. National Institutes of Health, Bethesda, Maryland, USA, <https://imagej.net/>)

and normalized for the combined intensity of protein bands stained with Pierce™ Reversible Protein Stain.

Whole kidneys were homogenized in 0.1% Rapigest (Waters Corporation) dissolved in freshly prepared 50 mM ammonium bicarbonate containing 5 mM DTT. Protein concentration was measured with Pierce BCA protein assay kit (#23225, Thermo Scientific), adjusted to 4.1 µg/µL, and resolved on gradient NuPAGE 3-8% Tris-Acetate gels (Invitrogen, EA03785BOX). Proteins were transferred to nitrocellulose membrane, blocked, and stained with antibodies and lectins as listed below.

Antigen	Host/Target species	Dilution	Manufacturer, catalogue number
Megalyn	Rabbit anti-human	1:1000 in 3% milk in TBS, pH 8.4	Abcam, Ab76969
Peanut agglutinin (PNA)	Biotinylated	1:2000	Vectorlabs, B-1075-5
Maackia Amurensis Lectin II (MALII)	Biotinylated	1:1000	Vectorlabs, B-1265-1
Ricinus Commuis Agglutinin I (RCA-1)	Biotinylated	1:1000	Vectorlabs, RCA120
Sambucus Nigra Lectin (SNA)	Biotinylated	1:5000	Vectorlab, B-1305-2

To analyse *N*-linked protein glycans, kidneys were homogenized in 0.1% Rapigest prepared in 50 mM ammonium bicarbonate. The homogenate was cleared by centrifugation at 13000 g for 20 min, supplemented with DTT to a final concentration of 5 mM, and incubated at 60°C for 30 minutes. A 20 µg aliquot of each sample treated or not with peptide *N*-glycosidase F (PNGaseF) (New England Biolabs, P0704L) to remove *N*-linked glycans (313), or *Arthrobacter ureafaciens* bacterial sialidase (Roche #10269611001) to remove sialylations, were resolved on 3-8% gradient NuPAGE Tris-Acetate gel (Invitrogen, EA03785BOX), and transferred to nitrocellulose membrane. The membrane was blocked with 3% milk in 0.05% TBS-Tween 20 for 1 h at a room temperature and hybridized for 2 h at a room temperature with streptavidin (1:5000) or anti-rabbit (1:5000) HPR-conjugated secondary antibody. Signals

were revealed using Pierce™ ECL Western Blotting Substrate (Thermo Fisher Scientific Inc., Rockford, USA).

The following antibodies were used:

Antigen	Host/Target species	Dilution	Manufacturer, catalogue number
Megalyn	Rabbit anti-human	1:1000 in 3% milk in TBS, pH 8.4	Abcam, Ab76969
Peanut agglutinin (PNA)	Biotinylated	1:2000	Vectorlabs, B-1075-5
Sambucus Nigra Lectin (SNA)	Biotinylated	1:5000	Vectorlab, B-1305-2
Ricinus Communis Agglutinin I (RCA-1)	Biotinylated	1:1000	Vectorlabs, RCA120

#### **Analysis of kidney protein N-glycosylation by MALDI MS**

Mouse kidney tissue was homogenized and lysed in a chloroform/methanol/water mixture 4:8:3 (v/v/v) as described previously (314). The protein pellet was separated from the lipid-containing supernatant by centrifugation, cleaned by repeated washes with acetone/water (4:1) at 4°C, dried under a stream of nitrogen and stored at -20°C. An additional cleaning step was performed during the analysis, by resuspending the protein pellet in ddH<sub>2</sub>O, followed by centrifugation. The supernatant, containing free urinary oligosaccharides accumulating as undegraded NEU1 substrates (281), was concentrated and analyzed separately by permethylation and MALDI MS. To accomplish the *N*-linked glycan analysis, the washed protein pellet (~2 mg) was resuspended in 0.2 mL of 0.1% RapiGest™ Surfactant (Waters Corporation, Milford, Massachusetts) in 50 mM NH<sub>4</sub>HCO<sub>3</sub> using an ultrasonic processor equipped with a 2 mm probe (130 Watt, 50% amplitude, 5 min in pulsing mode). The obtained homogenate was incubated at 100 °C for 5 min, followed by reduction in 5 mM dithiothreitol (DTT, Sigma) at 56°C for 30 min and alkylation in 15 mM iodoacetamide (IAA, Sigma) in the dark, at room temperature for 45 min. Glycan chains were cleaved by peptide-N-glycosidase F (PNGase F) (4U, Roche Molecular Biochemicals, Mannheim, Germany) overnight at 37 °C. The released N-glycans were purified, and permethylated by ICH<sub>3</sub> in a DMSO/NaOH slurry as described (315, 316). MALDI TOF and MALDI TOF/TOF analyses of permethylated N-

glycans were performed using 5-chloro-2-mercaptobenzothiazole (CMBT, 10 mg/ml in 80:20 methanol/water, v/v) as a matrix, and acquired on a 4800 proteomic Analyzer (AB Sciex) in positive polarity and in reflector mode (315). Data were analyzed using DataExplorer™ 4.9 software. Glycan structures were assigned based on molecular weight, knowledge of the biosynthetic pathway and MS/MS analyses, using the bioinformatic tools developed by the Consortium for Functional Glycomics (<http://functionalglycomics.org>).

### **Analysis of kidney protein N-glycosylation by HILIC-UPLC-FLR-ESI-MS**

Analysis of protein N-glycosylation by HILIC-UPLC-FLR-ESI-MS was performed as previously described (282). Briefly, enzymatic release and labelling of *N*-glycans was performed using the GlycoWorks™ RapiFluor-MS™ *N*-Glycan kit (Waters Corporation, Milford, MA, USA), per manufacturer's protocol with the exception of deglycosylation reaction time which was extended from 5 to 20 min. *N*-glycans, labeled at the glycosylamine residue of the terminal chitobiose epitope, were separated by an UHPLC Thermo system (Vanquish™ Flex System VF-501-A-02) coupled to an Orbitrap Exploris™ 120 HESI EASY-IC mass spectrometer (Thermo Fisher Scientific Inc., Bremen, Germany) equipped with a Vanquish™ fluorescence detector (VC-D50-A). Samples were separated using a Hydrophilic Interaction Liquid Chromatography (HILIC) column (ACQUITY UPLC Glycan BEH Amide 130 Å, 1.7 µm, 2.1 × 150 mm, Waters Corporation Milford, MA, USA) at a flow rate of 0.4 ml/min at 60 °C, with 200 mM ammonium formate aqueous solution (pH 4.4), as a mobile phase A, and acetonitrile (ACN), as a mobile phase B. The gradient ramped from 25% A to 46 % A in 35 min.

MS analyses were conducted under the following conditions: heater temperature 275 °C, capillary temperature 250 °C, spray voltage 3.3 kV, RF lens 70 %. Spectra were acquired in positive polarity, and resolution was adjusted at 30000 FWHM at 400 m/z. Full scan spectra were acquired in the mass range of 700-2000 m/z using the Automatic Gain Control (AGC) target with Data-Dependent MS2 Analysis (DDA) by higher-energy collision dissociation (HCD) of the four most abundant precursor ions, each with normalized collision energy (NCEs) at 25, 35, and 65 %. Isolation window was set as 0.5 m/z, with Orbitrap MS2 resolution of 15000, automated scan range mode, standard AGC target, and automated maximum injection time. Fluorescence detection was conducted using wavelengths of 265 nm (excitation) and 425 nm (emission) with a sampling rate of 2 Hz. Three technical replicates were performed for each sample and three runs for each analysis with no substantial differences identified for chromatograms and spectra between samples.

## Histochemistry and immunohistochemistry

Animals were deeply anaesthetized with sodium pentobarbital and fixed by intracardiac perfusion with 4% paraformaldehyde prepared in PBS, pH 7.4. Kidneys were removed and immersed in 4% paraformaldehyde in PBS overnight, changed to 70% ethanol before tissue processing. The tissues were dehydrated, cleared for 18 h in the tissue transfer processor (Leica TP1020), embedded in paraffin (Leica EG1160) and stored at 4° C. Kidney tissues were sliced to 5 µm thickness using a microtome (Leica RM2145), placed on glass slides, and dried at 37 °C overnight. For routine H&E staining, samples were first deparaffinized with xylene and rehydrated with ethanol in decreasing concentrations of 100%, 95%, 75% and 60%. Then, the slides were stained with hematoxylin (MHS16, Sigma) and Eosin (Vintage Eosin-Y, StatLab) and mounted with Eukitt Quick-hardening mounting medium (03989, Sigma). For immunostaining, after deparaffinization and rehydration, kidney sections were boiled in 10 mM sodium citrate buffer with 0.05% Tween 20, pH 6.0, for 15 min for antigen retrieval. Tissue sections were blocked for 1 h with 5% BSA and 0.04% Tween 20 at room temperature and stained with Cy3-labeled PNA (1:100, Vector Laboratories) and Cy5-labeled SNA (1:100, Vector Laboratories), diluted in carbo-free blocking solution, for 1 h at room temperature, and mounted with DAPI-containing Prolong Gold Antifade Mounting medium (P36931, ThermoFisher). Slides were analyzed by Axioscan (Zeiss), and images were processed using the ZenBlue Lite program (Zeiss).

For fluorescent confocal microscopy analyses, PFA-fixed kidneys were transferred to a 30% sucrose in PBS, incubated overnight at 4°C, embedded in OCT (Sakura) and kept frozen at -80 °C. OCT-embedded frozen kidney blocks were cut using a cryostat (Leica) to 15 µm thickness, blocked and permeabilized with 1% Triton X-100 in 10% goat serum for 1 h at room temperature. Tissue sections were stained with the following antibodies:

Antigen	Host/Target species	Dilution	Manufacturer, catalogue number
Megalín	Rabbit anti-human	1:200 in 3% milk in PBS, pH 8.4	Abcam, Ab76969
Peanut agglutinin (PNA), Cy3-labeled		1:100	Vectorlabs, CL-1073-1
Sambucus Nigra Lectin (SNA), Cy5-labeled		1:100	Vectorlab, CL-1305-1

Ricinus Communis Agglutinin I (RCA I), Rhodamine-labeled		1:100	Vectorlabs, RL-1082-5
LAMP1	Rat anti-human	1:50	DSHB, H4A3
CD68	Rabbit	1:200	Abcam, Ab125212

Slides were mounted with DAPI-containing Prolong Gold Antifade Mounting medium (P36931, ThermoFisher) and analyzed using SP8-DLS inverted confocal microscope (Leica TCS SP8). Images were processed and quantified using ImageJ.

For nephron quantification, H&E stained 5  $\mu\text{m}$  thick paraffin sections of age and sex matched *Neu1<sup>ΔEx3</sup>* (n=3), *Neu1<sup>Cx3cr1ΔEx3</sup>* (n=3) and WT (n=4) mice were scanned with Axioscan at 40x brightfield. Five 823.53  $\mu\text{m}$  x 912.06  $\mu\text{m}$  regions of kidney cortex were selected at the same positions, and glomeruli were manually counted and normalized (multiplied) by the wet weight of the kidney.

### Transmission Electron Microscopy

Male and female WT, *Neu1<sup>ΔEx3</sup>*, *Neu1<sup>loxPEx3</sup>* and *Neu1<sup>Cx3cr1ΔEx3</sup>* mice were anesthetised with sodium pentobarbital and perfused with PBS and 5% glutaraldehyde in 0.1 M phosphate buffer, pH 7.0. After perfusion, organs were carefully removed and post-fixed by immersion in 5% glutaraldehyde overnight at 4 °C. Kidney samples were trimmed to obtain the cortex regions that were, then, washed with 0.1 M cacodylate buffer, pH 7.4, before secondary fixation with 1% osmium tetroxide and 1.5% potassium ferrocyanide for 2 h. Samples were dehydrated with an ethanol series and propylene oxide, infiltrated with epoxy resin, and, embedded in Durcupan®-Epon® mixture. Semi-thin (1  $\mu\text{m}$  thick) sections were cut, mounted on glass slides, stained with toluidine blue and examined on Leica DMS light microscope to select the sections eventually used for electron microscopy.

The Epon blocks were trimmed, and 100 nm ultrathin sections were cut with an Ultracut E ultramicrotome. Samples were mounted on 200-mesh copper grids, stained with uranyl acetate (Electron Microscopy Sciences) and lead citrate, and examined on a FEI Tecnai G2 Spirit BioTwin 120 kV Cryo-TEM at McGill University Facility for Electron Microscopy Research (FEMR). PCT images were taken at the 4800x magnification, DCT, at 4800x magnification, glomeruli, at 1200x magnification and podocytes, at 13000x magnification.

## **Liquid Chromatography-Mass Spectrometry**

Samples were reconstituted in 50 mM ammonium bicarbonate with 10 mM TCEP [Tris(2-carboxyethyl) phosphine hydrochloride (Thermo Fisher Scientific)], and vortexed for 1 h at 37°C. Chloroacetamide (Sigma-Aldrich) was added for alkylation to a final concentration of 55 mM. Samples were vortexed for another hour at 37°C. One microgram of trypsin was added, and digestion was performed for 8 h at 37°C. Samples were dried down and solubilized in 5% ACN-4% formic acid (FA). Peptides were loaded and separated on a home-made reversed-phase column (150- $\mu$ m i.d. by 200 mm) with a 56-min gradient from 10 to 30% ACN-0.2% FA and a 600-nl/min flow rate on an Easy nLC-1000 connected to an Orbitrap Fusion (Thermo Fisher Scientific, San Jose, CA). Each full MS spectrum acquired at a resolution of 120,000 was followed by tandem-MS (MS-MS) spectra acquisition on the most abundant multiply charged precursor ions for a maximum of 3 s. Tandem-MS experiments were performed using higher energy collision dissociation (HCD) at a collision energy of 27%. The data were processed using PEAKS X (Bioinformatics Solutions, Waterloo, ON) and a Uniprot mouse database. Mass tolerances for precursor and fragment ions were 10 ppm and 0.01 Da, respectively. Fixed modification was carbamidomethyl (C). Variable selected posttranslational modifications were acetylation (N-ter), oxidation (M), deamidation (NQ), and phosphorylation (STY). The data were visualized with Scaffold 5.2.2, showing protein threshold at 1% false discovery rate (FDR) with a minimum of 2 peptides identified at FDR of 0.1%.

## **Bone analysis**

The left tibia bone of each mouse was scanned in a Micro-CT scanner (eXplore Locus, GE Healthcare Canada) with a tube voltage of 80 kVP, current of 450  $\mu$ A, 2000 ms integration time and a resolution of 20  $\mu$ M. Images analysis allowed the evaluation of cortical bone parameters: cortical bone volume, bone mineral density, bone mineral content and thickness using an automatic bone analysis software (eXplore MicroView from GE Healthcare, Canada). The bone specimens were then decalcified using CAL-EX (Cal-Ex™ II Fixative/Decalcifier, Fisher Chemical™) before embedding in paraffin, slicing with a microtome (Thermo Scientific Microm HM 325-2 Manual Microtome) at 4 microns and staining with Masson Trichrome. Static bone histomorphometry measures were assessed on a single section for each animal for three regions: primary spongiosa, growth plate and secondary spongiosa for the trabecular bone parameters (Bioquant Meg IV System; R & Biometrics, TE, USA), using an Olympus BX45 microscope (Olympus, Richmond Hill, ON, Canada). A standardized ROI was used for each measure for all animals.

### **Analysis of 25-hydroxy vitamin D (25-OH) by ELISA**

Mouse 25-hydroxy vitamin D (25-OH) was analyzed in plasma (n=6 per genotype) and urine (n=2 per genotype) of *Neu1<sup>ΔEx3</sup>* and WT mice using an ELISA kit (MyBioSource #MBS263918) as per manufacturer's protocol. Briefly, plasma and urine samples were diluted at 1:5 and assessed for 25-OH in a double antibody sandwiched ELISA technique, and absorbance values were measured with Clariostar (BMG Labtech).

### **Statistics**

Statistical analyses were performed using Prism GraphPad 9.3.0. software (GraphPad Software San Diego, CA). The normality for all data was checked using the D'Agostino & Pearson omnibus normality test. The significance of the difference was determined using t-test when comparing two groups and one-way ANOVA test, followed by a Tukey multiple comparison test, when comparing more than two groups. Two-way ANOVA followed by Bonferroni or a Tukey post hoc test was used for two-factor analysis. A P-value of 0.05 or less was considered significant.

## Link between chapter 2 and chapter 3

In Chapter 2 of this thesis, we described the phenotypic characterization of *Neu1<sup>ΔEx3</sup>* and *Neu1<sup>Cx3cr1ΔEx3</sup>* mice which included systemic pathology such as organomegaly, infertility and short life span. We also documented the ultrastructural abnormalities, fibrosis and inflammation in the kidneys of both mouse models. We demonstrated that the altered glycosylation of megalin causes its mis-trafficking to the lysosomes instead of the epithelial cell surface in PRT and plays a major role in the development of kidney dysfunction which resulted in the loss of essential metabolites and receptors. The renal phenotype in our sialidosis mouse model also has many shared traits with other CKD such as proteinuria, nephron loss and receptors shedding into the urine (317, 318). This confirms our hypothesis that changes in the glycosylation of megalin is a major contributor to the progression of kidney dysfunction in nephrosialidosis. However, sialidosis is an ultra-rare disease which is not currently untreatable. Therefore in Chapter 3, we explored the viability of allogenic HSPC transplant in the *Neu1<sup>ΔEx3</sup>* mouse model. In this pilot study, we tested if the pathology documented in Chapter 2 can be ameliorated by allogenic transplantation of WT HSPC. This experiment was also important to determine the engraftment efficacy in the *Neu1<sup>ΔEx3</sup>* mouse model, as low engraftment due to poor bone marrow retention was previously reported (134). Another goal is to determine the parameters that will be used in future preclinical studies for LV-gene-modified HPSC gene therapy. Hence, we designed a pilot study by modifying a pre-existing protocol for the HSPC transplantation experiment that was developed in our laboratory. In the following chapter, we reported the successful engraftment of WT HSPC transplant in the *Neu1<sup>ΔEx3</sup>* mouse and partial rescue of the brain (behavior analysis) and kidney pathology.

### 3 Allogenic HSPC transplantation of *Neu1*<sup>ΔEx3</sup> mice

#### 3.1 Introduction

There is currently no effective treatment for sialidosis. Enzyme replacement therapy (ERT) has been approved for the treatment of non-neuropathic LSD such as Gaucher disease type I, Pompe disease, Scheie subtype of MPS I, MPS VI, MPS IV, and Fabry disease. However, ERT for neuropathic LSD faced the challenge of passing through the blood-brain barrier (BBB). Therapeutic enzymes for ERT are produced through recombinant technology in cultured human or mammalian cells where the resulting glycoproteins are modified with M6P residues for targeting lysosomes. However, a majority of these recombinant proteins are rapidly cleared in the visceral organs such as the liver, kidney and spleen leaving insufficient distribution to the bone, eye and muscles, hence why these organs show limited response to ERT (110). Additionally, neurological forms of LSD cannot be treated with systemic injections of recombinant enzymes due to the existence of the BBB. An alternate route for delivery of the enzymes to the brain involves intrathecal injection into the subarachnoid space of the spinal cord, a strategy that bypasses the BBB. This approach has been tested in murine models of MPS IIIA and revealed normalization of heparan sulfate storage in the brain and spinal cord (319). At the same time clinical trials for MPS IIIA failed to demonstrate clear clinical benefits and were discontinued (320, 321). Membrane-associated proteins such as NEU1 show additional constraints due to their inability to diffuse between the cells. Moreover, ERT for sialidosis would require the production of two enzymes as NEU1 needs to be in a complex with CTSA to remain stable and catalytically active, which would increase the cost of treatment.

HSPC transplantation currently remains the only method for replenishment of the deficient enzymes to the CNS approved in clinical practice. HSPC transplant allows for the long-term replenishment and self-renewal of progeny cells, but also cross-correction through the secretion of enzymes to clear the accumulation of substrates in all tissues and organs. In addition, HSPC-derived macrophages migrate through the BBB to the CNS, where they can reduce neuroinflammation, eliminate excess storage materials by phagocytosis and become a source of enzyme for astrocytes and neurons. HSPC transplantation is now a clinical method of choice for the neuropathic form of MPS I (Hurler syndrome). The procedure recovers near-normal levels of iduronidase enzyme activity in the majority of visceral tissues, corrects cardiac pathology, and improves neurocognitive development, vision and hearing (322).

In theory, cross-correction of brain cells should solely occur with soluble, secreted lysosomal enzymes. However, WT HSPC transplantation to the model of cystinosis reduced the accumulation of cystine in all tissues, but more importantly, stopped the progression of kidney pathology with long-term preservation of kidney function (272). The mechanism behind the above phenomena is still debated but it may involve a combination of a limited secretion of cysteine transporter cystinosin in the form of exosomes that can be taken up by other cells and reduction of tissue inflammation (including neuroinflammation), but immunocompetent cells derived from the donor HSPCs.

Although allogenic hematopoietic stem cell transplantation has made extraordinary progress in the treatment of genetic diseases, the availability of immuno-compatible donors with optimal human leucocyte antigen (HLA) genotype matching limits its applications. To overcome this, HSPC gene therapy employs ex vivo gene transfer with autologous HSPC, which is transduced with a viral vector carrying the normal gene. This prevents the risk of developing graft-versus-host disease (GVHD) and provides an additional advantage to boost the production of a therapeutic enzyme using strong promoters. Importantly, HSPCs whether gene-modified or not, are capable of self-renewal and establishing a new population of modified cells throughout the lifetime. Lentiviral (LV) mediated gene correction of HSPC transplantation has been proven to correct a neurological LSD, MLD by replenishing with corrected macrophages and microglia that cross-corrected cells through enzyme secretion (271). Further clinical trials showed prevention of disease onset in patients pre-symptomatic at the time of treatment (126, 128). As a result, HSPC-LV therapy for infantile MLD patients (Libmeldy™) has been approved for clinical use in Europe. Clinical trials for presymptomatic MPSIIIA patients are currently in progress in the Manchester Hospital, UK, where the first treated patients showed a supraphysiologic SGSH activity in leucocytes and plasma, as well as >90% reduction of HS levels in biological fluids over the baseline, and the early neurocognitive data are strongly suggestive of neurological correction (Dr. S. Johns, WORLD Symposium on LSD, Orlando, Feb. 2023). Unfortunately, the treatment comes with a high cost (2,000,000 Euro per patient with Libmeldy™) estimated to over-stretch the public healthcare system. These studies also revealed that HSPC transplantation requires a high concentration of transplanted stem cells to ensure fast hematopoietic recovery and a stable outcome.

In the current work, we demonstrate that a pilot study of WT HSPC-transplant in constitutive *Neu1*<sup>ΔEx3</sup> and obtained preliminary data on the amelioration of renal and brain

pathology to determine parameters for further studies with LV-mediated gene therapy in sialidosis mouse model.

## 3.2 Materials and method

### **Study approval**

All animal experiments were approved by the CHU Sainte-Justine Research Ethics Committee and performed in compliance with the Comité Institutionnel des Bonnes Pratiques Animales en Recherche (CIBPAR; approval numbers 2020-2658 and 2022-3452), in accordance with the Canadian Council on Animal Care guidelines.

### **Animals**

The constitutive KO NEU1 mouse model (*Neu1<sup>ΔEx3</sup>*) was previously described (32). Heterozygous mice were interbred, and litters were genotyped by PCR using genomic DNA extracted from clipped tail tip, as described (32).

### **Isolation of HSPC and tail-vein transplantation**

Tibia, femur and iliac bones were dissected and washed 1x with 70% ethanol followed by 3 washes with PBS containing 1% penicillin and streptomycin. Under sterile conditions, bone marrow was flushed with ice-cold SCGM media using 25G syringe and cells were dissociated with pipette and strained through 70 µm nylon mesh strainer and centrifuged at 1500 RPM for 10 min, 4°C. The pellet was resuspended in 10 mL red blood cells (RBC) lysis buffer (155 mM NH<sub>4</sub>Cl, 12 mM NaHCO<sub>3</sub>, 0.1 mM EDTA) for 1 min and 20 mL of ice-cold SCGM media was added. To isolate HSPC pellet, cells were harvested by centrifugation at 1500 RPM for 10 min at 4°C and resuspended in EasySepT Buffer (Stem Cell Technologies). HSPCs were isolated with the EasySep Mouse Hematopoietic Progenitor Cell Isolation Kit (Stem Cell Technologies) according to the manufacturer's instructions and maintained in culture in 10 mL of SCGM media supplemented with 10 ng/ml rmIL-6, 100 ng/ml rmFlt-3L, 100 ng/ml rmTPO and 100 ng/ml rmSCF at 37°C with 5% CO<sub>2</sub>. After overnight incubation, cells concentration of 2 x 10<sup>6</sup> were resuspended in PBS and injected in the tail vein of *Neu1<sup>ΔEx3</sup>* mice. Prior to HSPC transplantation, mice were treated for 5 consecutive days by busulfan (IP, 25 mg/kg each day) and kept in sterile conditions. They were fed irradiated food and treated with Baytril® (enrofloxacin, 50 mg/ml in drinking water) for 15 days.

### **Flow cytometry**

Blood from the mouse mandibular vein (50 µl-100 µl) was collected in EDTA-containing capillary and was stained for 15 minutes in the dark at room temperature with APC labeled anti-mouse CD45.1 Antibody (Biolegend, 1:20) and PE labeled anti-mouse CD45.2 Antibody

(Biolegend, 1:20). Erythrocytes were lysed with RBC lysis buffer (155 mM NH<sub>4</sub>Cl, 12 mM NaHCO<sub>3</sub>, 0.1 mM EDTA) for 10 minutes and white cells were collected by centrifugation for 5 min at 350 g and resuspended in PBS+1% FBS twice. Fluorescence compensation was performed with Anti-Mouse Ig, κ/Negative Control (FBS) Compensation Particles Set (BDTM CompBeads) according to manufacturer's instructions and analysis was performed using BD FACSCanto II instrument.

### **Open field test**

A 30-minute room adjustment period was implemented for each group of mice before the start of open field test. The arena of dimension 45 cm length x 45 cm width x 40 cm height (Open-Field Box Panlab, Harvard Apparatus, Perspex (Plexiglass)) was cleaned with 70% ethanol before the test. The open field test was performed by placing a mouse in the center of the arena. Mouse behavior was video recorded with Logitech C920 camera for 20 minutes and analyzed using the software Smart 3.0 to quantify the number of entries in the center and the total distance travelled.

### **Brain and kidney pathology amelioration.**

WT, *Neu1<sup>ΔEx3</sup>* and *Neu1<sup>ΔEx3</sup>*-HSPC transplanted mice were anaesthetized with sodium pentobarbital and with post-fixing in 4% paraformaldehyde overnight, and solution change to 30% sucrose overnight at 4°C for rehydration. Organs were embedded in OCT and sectioned to 40 μm thickness for brain and 15 μm thickness for kidney, blocked and permeabilized with 1% Triton X-100 in 10% goat serum and stained with the following antibodies: rabbit Anti-Neu1 (Abcam #233119, 1:200), mouse anti-NeuN (Cell signaling #94403, 1:100), rat anti-LAMP1 (DSHB #1D4B, 1:50), LAMP2 (DSHB #H4B4), 1:50, rabbit anti-CD68 (Abcam #Ab125212, 1:200), anti-CD63 (Santa Cruz #Sc-5275), chicken anti-GFAP (Abcam, Ab4674), rabbit anti-megalin (Abcam #Ab76969, 1:100), PNA-cy3 (Vectorlabs #CL-1073-1, 1:100), SNA-cy5 (Vectorlabs #CL-1305-1, 1:100), RCA-1-rhodamine (Vectorlabs #FL-1081-5, 1:100) and MAL II (EY laboratories). Sections were mounted with DAPI-containing Prolong Gold Antifade Mounting medium (P36931, ThermoFisher) and analyzed using SP8-DLS inverted confocal microscope (Leica TCS SP8). Images were processed and quantified using ImageJ.

### **Lysosomal enzyme assays**

Total acidic α-neuraminidase, β-galactosidase and β-hexosaminidase activities were measured in tissue homogenates using corresponding fluorogenic 4-methylumbelliferyl substrates as previously described (199). NEU1 activity was measured by supplementing the α-

neuraminidase assay mixture with the specific inhibitor for both NEU3 and NEU4 enzymes, CG17700 (also known as C9-4BPT-DANA), at a final concentration of 125  $\mu$ M as previously described (276). Protein concentration was measured using Pierce BCA protein assay kit (#23225, Thermo Scientific).

### 3.3 Result

#### 3.3.1 *Neu1<sup>ΔEx3</sup>* mice show high engraftment after allogenic HSPC translocation.

Since allogenic HSPC transplantation is effectively used in clinical practice for patients affected with several lysosomal diseases, such as MPS I, Krabbe disease and cystinosis we decided to test if transplantation of HSPC from a congenic donor mouse expressing a normal level of NEU1 would increase the levels of NEU1 in tissues of *Neu1<sup>ΔEx3</sup>* mice and ameliorate their clinical phenotype. We first isolated HSPC from B6.SJL-Ptprca Pepcb/BoyJ (donor) mouse carrying the differential *Ptprc* pan leucocyte marker CD45.1 (Ly5.1) using EasySep Mouse Hematopoietic Progenitor Cell Isolation kit. Our pilot study (Table 3.1) was conducted using a female 6-weeks-old *Neu1<sup>ΔEx3</sup>* mouse with WT and *Neu1<sup>ΔEx3</sup>* mouse as engraftment controls. A cohort of these mice was transplanted in our laboratory for a separate project and showed engraftment between 75 and 95% (Pan *et al.* manuscript submitted).

The mice were first placed on a myeloablation protocol developed in our laboratory that involves their treatment with busulfan for five consecutive days by daily intraperitoneal injections at a dosage of 25 mg/kg BW. HSPC were collected from six donor mice and transplanted via tail vein injection at a dose of  $2 \times 10^6$  cells resuspended in 100  $\mu$ L of saline per animal. After transplantation mice were housed in sterile conditions with irradiated food and water supplemented by Baytril (Elanco) for 15 days. Mice were monitored daily for signs of adverse reactions for 2 weeks following the transplantation.

6-weeks post-transplantation, mice mandibular blood was collected by cheek vein puncture and analyzed by flow cytometry to verify the engraftment. The engraftment rate assessed by measuring the levels of CD45.1 marker in myeloid cells was 75.3% for the *Neu1<sup>ΔEx3</sup>* mouse (Figure 3.1A and B). However, one WT (HSPC transplanted) mouse died at 3 weeks post-transplantation, while others were kept until the age of 4 months.

**Table 3.1: HSPC transplantation of *Neu1<sup>ΔEx3</sup>* mice.**

Mouse	Age (Weeks)	Gender	Engraftment rate % (% of CD45.1+ cells)
WT (non-transplanted)	12	Female	NA
WT (Transplanted)	12	Female	Died 3-weeks post-transplant

<i>Neu1<sup>ΔEx3</sup></i> (non-transplanted)	12	Female	NA
<i>Neu1<sup>ΔEx3</sup></i> (transplanted)	12	Female	75.3

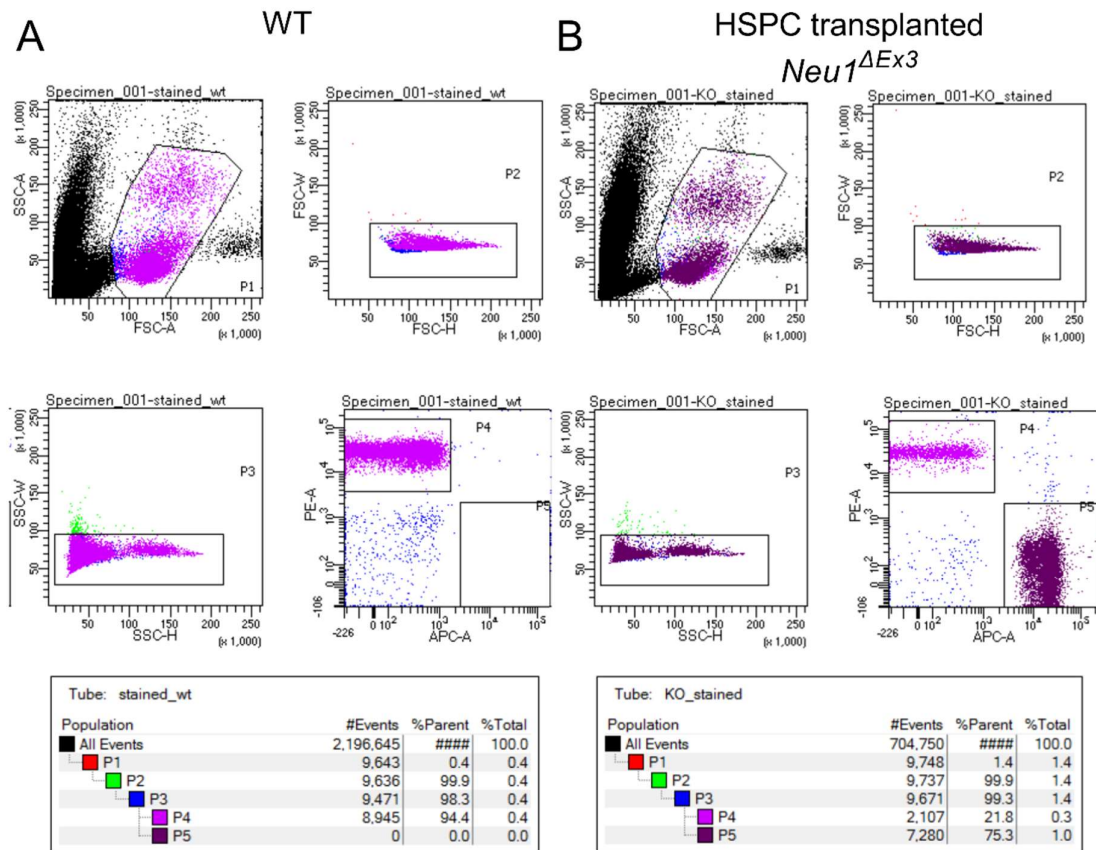


**Figure 3.1: Flow cytometry reveals high % of CD45.1+ myeloid cells in the blood of transplanted *Neu1<sup>ΔEx3</sup>* suggesting effective HSPC engraftment.**

Mice mandibular blood was collected from 12-weeks old non-transplanted WT mice (A), as well as from HSPC transplanted *Neu1<sup>ΔEx3</sup>* (B) and analyzed by flow cytometry with antibodies against CD45.1 marker. 75.3 % of *Neu1<sup>ΔEx3</sup>* transplanted mice are CD45.1+ suggesting high engraftment rate of donor HSPC.

### 3.3.2 Transplanted *Neu1<sup>ΔEx3</sup>* mouse shows improvement of behavior deficits.

At 4 months post-transplantation, the behavior of WT, *Neu1<sup>ΔEx3</sup>* and transplanted *Neu1<sup>ΔEx3</sup>* mice was studied by open field test that assessed locomotor activity and anxiety levels (Figure 3.2A and B). Previously we have documented mobility issues in *Neu1<sup>ΔEx3</sup>* that showed a drastically

reduced number of entries in a Y-maze (less than 10 entries with a median of 35 entries in WT mice) (Supplementary Figure S3-1). As this pilot study used a small number of mice (n=1 of transplanted *Neu1<sup>ΔEx3</sup>*), statistical analysis was not possible. However, we see drastically fewer entries into the center (Figure 3.2A and B) by the *Neu1<sup>ΔEx3</sup>* mouse compared to the transplanted *Neu1<sup>ΔEx3</sup>* mouse and WT. The number of entries in the center crossed by the transplanted *Neu1<sup>ΔEx3</sup>* mouse was still reduced compared to the WT mouse (represented by movement trajectory in Figure 3.2A). The total distance travelled in the arena for the transplanted *Neu1<sup>ΔEx3</sup>* mouse was similar to WT mice, while *Neu1<sup>ΔEx3</sup>* exhibited less exploratory behavior, traveling less than half the distance (Figure 3.2C).

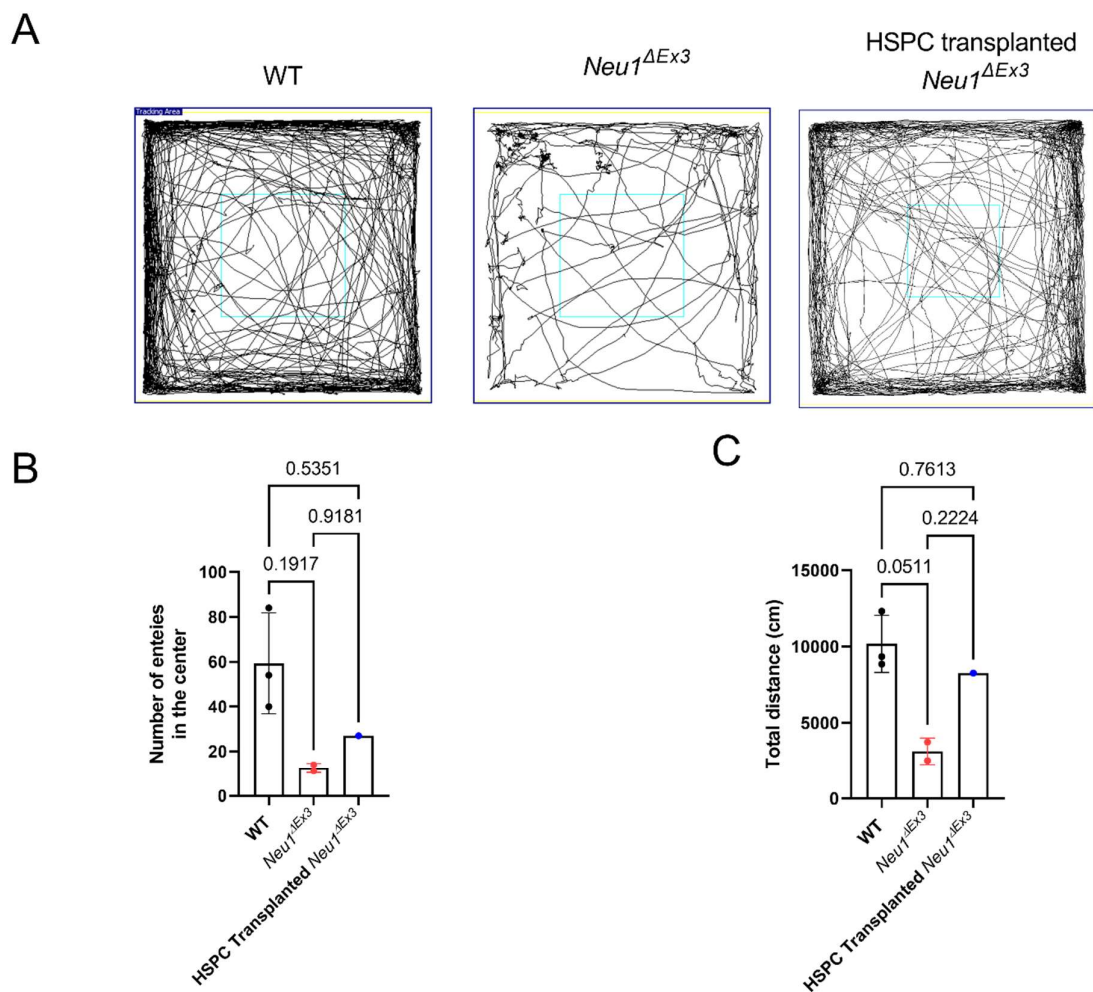


**Figure 3.2: Corrected locomotion in HSPC transplanted *Neu1<sup>ΔEx3</sup>* mouse.**

(A) Trajectory of the exploration of WT, transplanted and non-transplanted *Neu1<sup>ΔEx3</sup>* mice in the open field arena. (B) number of entries into the open field arena and (C) total distance explored by each mouse (in cm) of the open field arena.

3.3.3 *Neu1<sup>ΔEx3</sup>* mouse transplanted with HSPC shows reduced lysosomal biogenesis in multiple tissues compared with untreated mice.

To assess if deficient NEU1 enzyme activity in *Neu1<sup>ΔEx3</sup>* mouse tissues was corrected or partially corrected by transplantation of WT HSPC, we measured total neuraminidase and NEU1 activity in the bone marrow, kidney, liver, spleen, lung and brain tissues of WT, *Neu1<sup>ΔEx3</sup>* and transplanted *Neu1<sup>ΔEx3</sup>* (*Neu1<sup>ΔEx3</sup>* + HSPC) mice (Figure 3.3A). These results indicated that in contrast to non-transplanted mice, tissues of *Neu1<sup>ΔEx3</sup>* + HSPC mouse had measurable levels of NEU1 activity in visceral organ tissues, the highest being detected in the spleen (~10% of the WT level). In contrast, NEU1 levels in the brain and bone marrow were not increased compared to untreated mice.

We also assessed levels of  $\beta$ -galactosidase and  $\beta$ -hexosaminidase enzyme activities in the above tissues since our previous data (see Chapter 3) and published studies indicated that the activities of these lysosomal glycosidases are reliable markers of induced lysosomal biogenesis. In transplanted *Neu1<sup>ΔEx3</sup>* mouse, the level of  $\beta$ -galactosidase and  $\beta$ -hexosaminidase was 2- to 4-fold reduced in all tissues suggesting that increased lysosomal biogenesis was partially rescued by the transplantation of WT HSPC (Figure 3.3B and C). It is tempting to speculate that the levels of NEU1 delivered from the transplant (although not detectable in the total tissue homogenates) were sufficient to reduce the level of lysosomal storage in the HSPC-derived tissue macrophages and perhaps in the adjacent tissue cells, where the enzyme could be delivered by cross-correction. In turn, this could reduce TFEB-mediated overexpression of lysosomal proteins. This hypothesis remains to be verified by direct analysis of soluble oligosaccharides by MALDI TOF MS, as well as mTORC1 activity in the tissues and nuclear TFEB localization as we did in the kidney tissues of untreated mice (see Chapter 2).

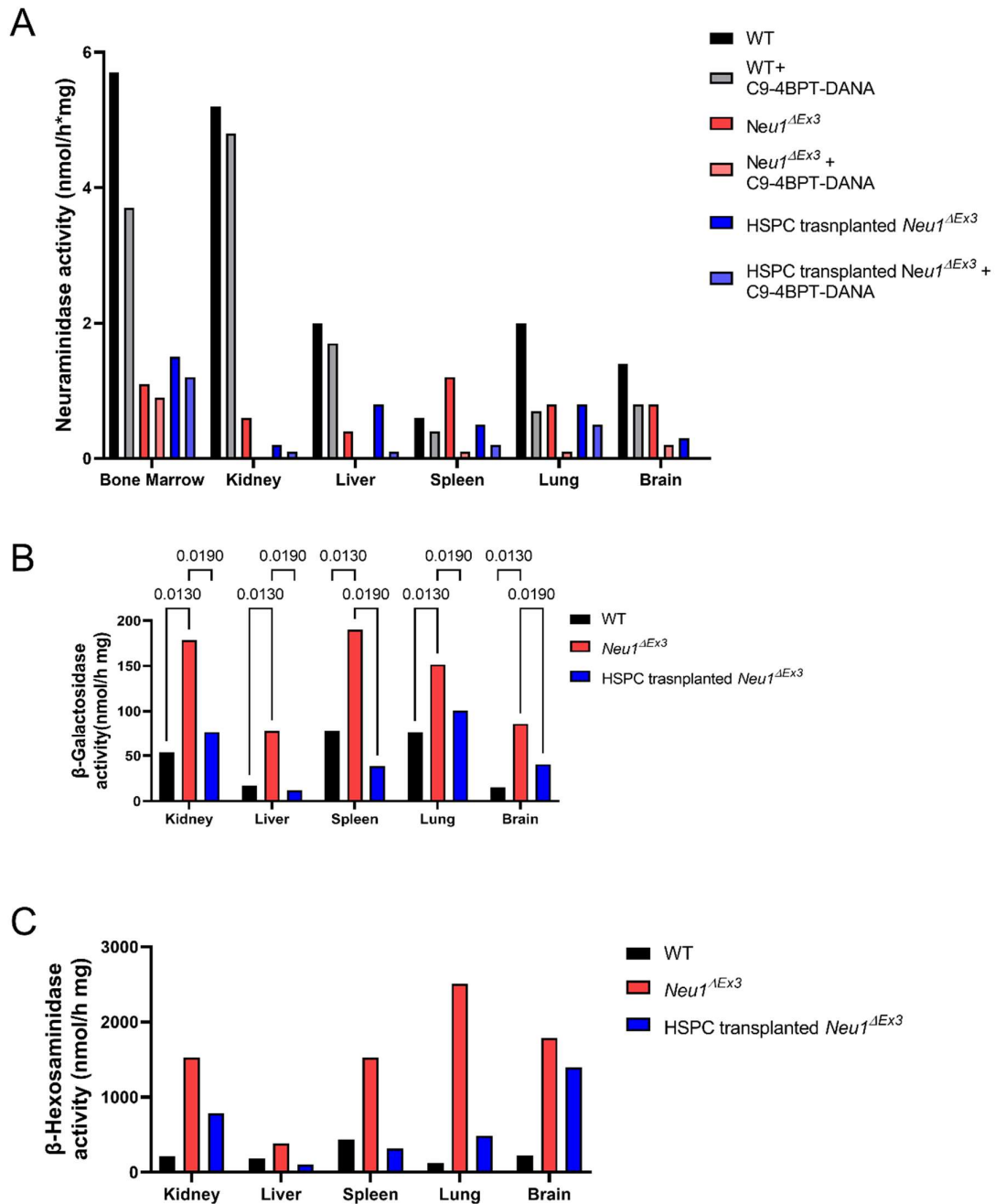


**Figure 3.3: HSPC transplanted *Neu1*<sup>ΔEx3</sup> mouse show partial normalization of increased lysosomal biogenesis in visceral organs.**

(A) Total neuraminidase and NEU1 enzyme activity were measured in visceral tissues and brain of WT, *Neu1*<sup>ΔEx3</sup> and transplanted *Neu1*<sup>ΔEx3</sup> (*Neu1*<sup>ΔEx3</sup> + HSPC) mice. NEU1 activity in tissues of transplanted *Neu1*<sup>ΔEx3</sup> mice showed a trend for increase but remained below 10% of the WT levels. Lysosomal biogenesis was measured in mouse tissues by assessing (B) β-

galactosidase and (C)  $\beta$ -hexosaminidase enzyme activities that showed a trend towards a decrease in visceral tissues but not in the brain.

3.3.4 Reduction of lysosomal storage and protein hypersialylation and rescue of Megalin receptor level and localization in the kidney of HSPC transplanted *Neu1<sup>ΔEx3</sup>* mouse.

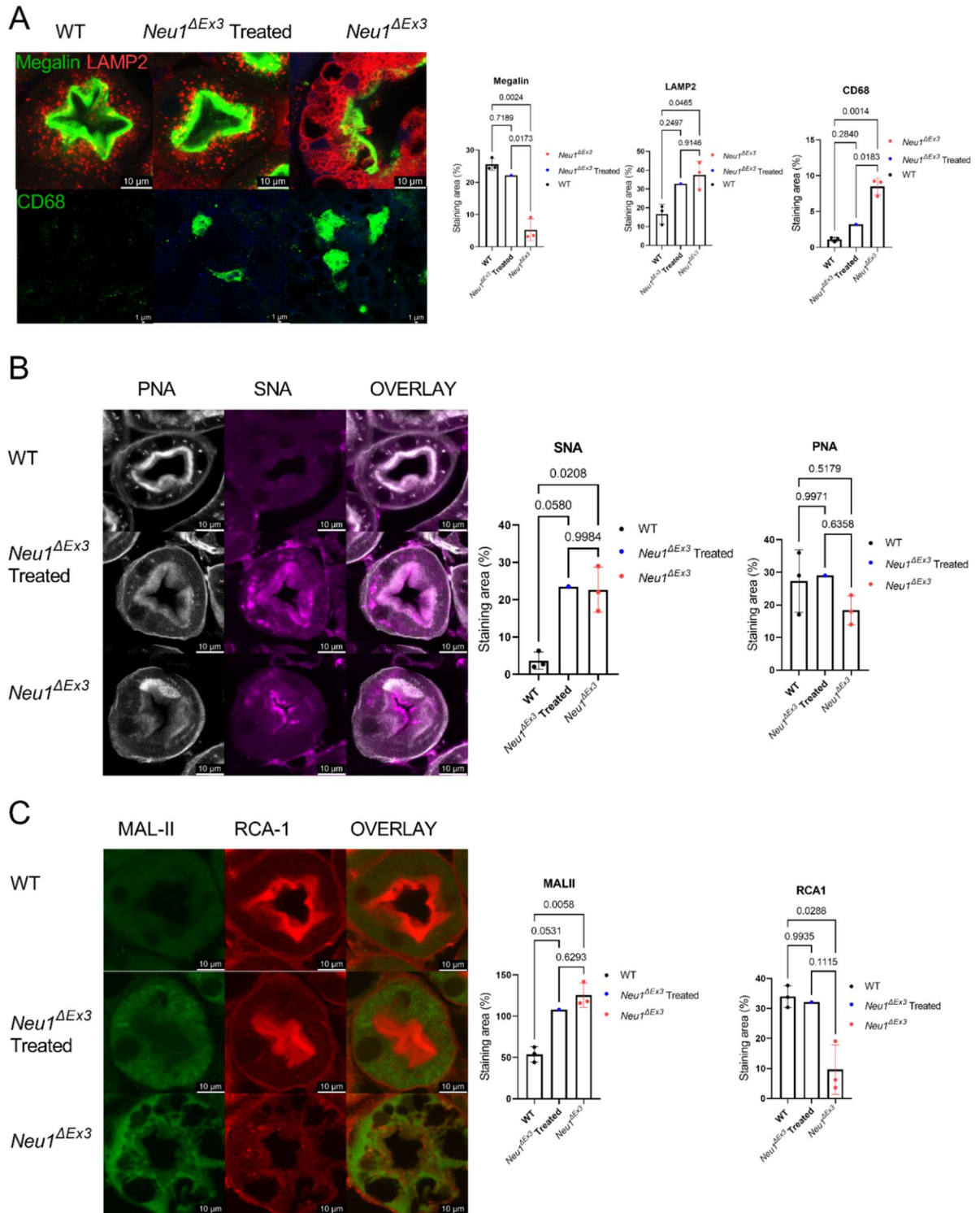


**Figure 3.4: WT HSPC transplantation of *Neu1*<sup>ΔEx3</sup> mouse partially improved pathological alterations in proximal convoluted tubules.**

(A) Epithelial PCT cells in the kidney of HSPC transplanted mice show reduced levels of lysosomal membrane marker LAMP-2 and decreased CD68-positive macrophages compared to those of untreated *Neu1<sup>ΔEx3</sup>* mice. In HSPC-treated *Neu1<sup>ΔEx3</sup>* kidney megalin receptor levels are increased and comparable to WT kidney. Labelling with galactose-specific PNA (B) and RCA-1 (C) lectins is increased at the apical surface of megalin and at the basolateral membrane of the PCT, labelling with sialic acid-specific lectin (B) SNA is unchanged while MALII (C) showed a trend for decrease suggesting a partial rescue of protein hypersialylation.

To assess the levels of lysosomal biogenesis and inflammation we stained the kidney sections with antibodies against a lysosomal membrane marker, LAMP-2 and against an activated macrophage marker, CD68, respectively. In the kidney of HSPC transplanted *Neu1<sup>ΔEx3</sup>* mouse, the level of LAMP2-staining in the cortex was reduced when compared to that in untreated *Neu1<sup>ΔEx3</sup>* mouse (Figure 3.4A). Besides while in the PCT of untreated mice LAMP-2 labeled a limiting membrane of giant vacuoles consistent with enlarged lysosomes containing storage materials, in tissues of both WT and HSPC transplanted *Neu1<sup>ΔEx3</sup>* mouse anti-LAMP-2 antibodies labeled small puncta adjacent to the apical membrane resembling the size and localization of lysosomes (Figure 3.4A). Similarly, in HSPC-transplanted *Neu1<sup>ΔEx3</sup>* mouse we detected a reduced mobilization of inflammatory cells CD68-positive macrophage to the interstitial areas of the cortical kidneys compared to untreated mouse (Figure 3.4A). We further investigated if WT HSPC transplantation could rescue aberrant protein sialylation associated with mistargeting and deficiency of megalin in PCT of *Neu1<sup>ΔEx3</sup>* mice (see Chapter 2). Labelling of kidney sections with anti-megalín antibodies showed drastically increased megalín at the apical surface of the PCTs of HSPC treated compared with untreated *Neu1<sup>ΔEx3</sup>* mouse (Figure 3.4A). We also observed markedly increased labelling of basolateral PRT surface with PNA (Figure 3.4B) and RCA-1 (Figure 3.4C) lectins, though to be specific for terminal  $\beta$ -galactose residues in O-linked and N-linked glycans, respectively, suggesting that the treatment reduces hypersialylation of these glycans unmasking galactose residues. Notably, we also observed increased PNA staining in juxtaposition to the apical side of megalín (Figure 3.4B), consistent with the suggestion, that the treatment also partially restored levels of O-linked glycans with terminal galactose residues attached to megalín receptors. As previously reported, these residues are essential for maintaining function and intracellular localization of the receptor (286). Reduced sialylation of glycoproteins was also consistent with decreased staining throughout the PCT epithelial cells with MALII lectin specific for alpha-2, 6-linked terminal sialic acids (Figure 3.4C). We also detected somewhat reduced staining of the

cytoplasmic puncta of the same cells with alpha-2,3-sialic acid-specific SNA lectin. The biological meaning of this observation remains to be understood.

### 3.3.5 Improvement of CNS pathology in HSPC transplanted *Neu1<sup>ΔEx3</sup>* mouse.

Neuroimmune response manifesting with excessive microastrogliosis has been reported to be a hallmark of brain pathology in sialidosis patients and mouse models (106). To assess if transplantation of WT HSPC resulted in the correction of micro-astrogliosis and other pathological changes in the brain, brain section from WT, as well as untreated and treated *Neu1<sup>ΔEx3</sup>* mice were stained with antibodies against GFAP and CD68, the protein markers for astrocytes and activated microglia cells (Figure 3.5A). There was no reduction in CD68-positive and GFAP-positive cells in the cortex of HSPC transplanted compared to untreated *Neu1<sup>ΔEx3</sup>* mouse. Meanwhile, the labelling for the marker of lysosomal biogenesis/storage, LAMP-1 was similar in both NeuN+ neurons and CD68+ microglia in cortices of *Neu1<sup>ΔEx3</sup>* and HSPC *Neu1<sup>ΔEx3</sup>* mice, indicating that, in contrast to the kidney, the transplantation did not rescue lysosomal storage in the brain (Figure 3.5B). Consistently, levels of NEU1 in the NeuN+ cortical neurons were similar in the tissues of treated and untreated mice (Figure 3.5A). We also did not see a difference in the levels of another marker for lysosomal storage and activation, CD63 (323), in the CD68+ microglia (Figure 3.4A).

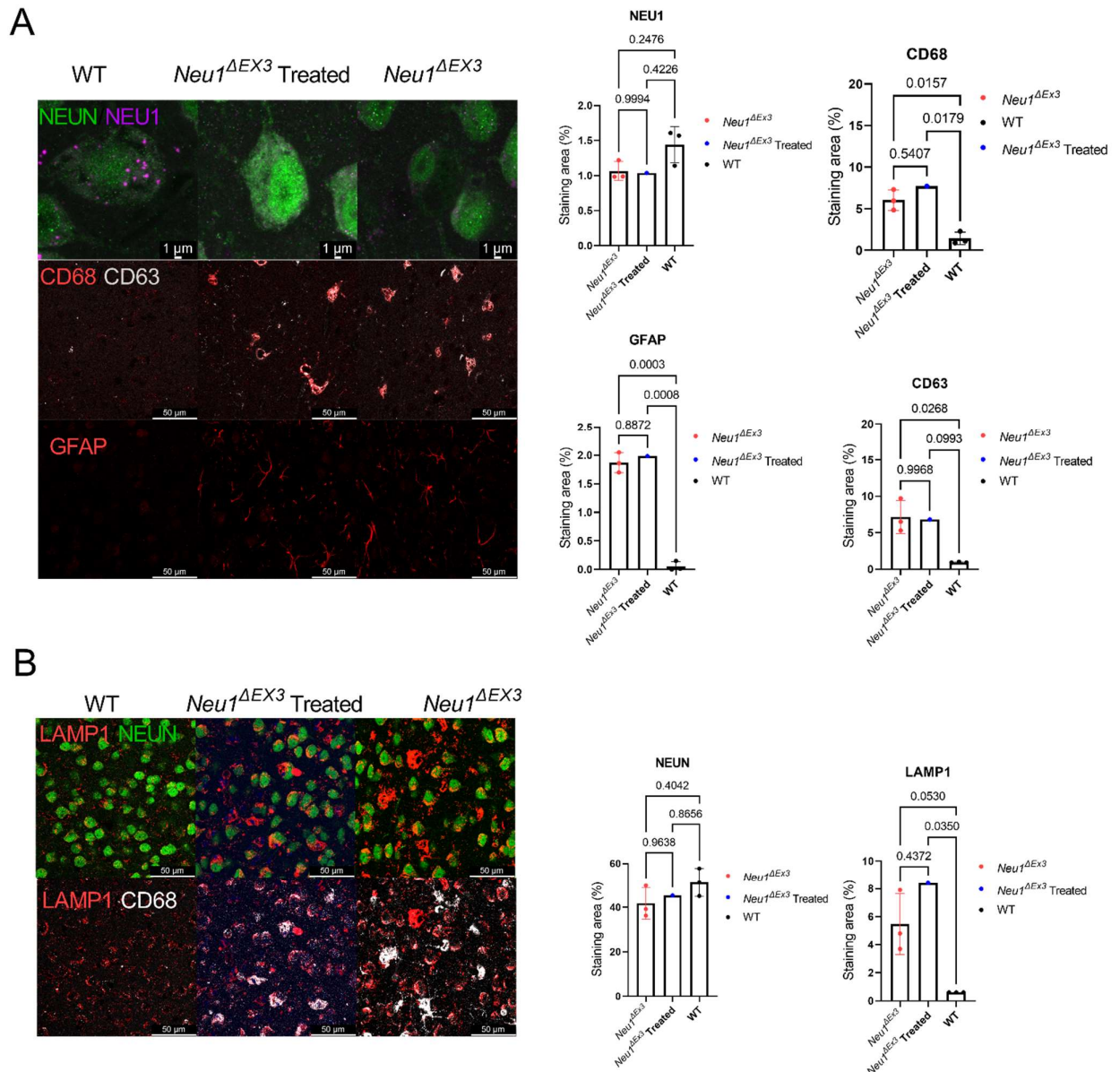


**Figure 3.5: Lysosomal storage and neuroinflammation are not reduced in the brain cortex of HSPC transplanted  $Neu1^{\Delta Ex3}$  mouse.**

(A) Similar levels of GFAP-positive astrocytes, CD68-positive microglial cells with colocalization of inflammatory/lysosomal storage marker CD63 are observed in frontal cortex of HSPC transplanted  $Neu1^{\Delta Ex3}$  mouse and  $Neu1^{\Delta Ex3}$  mouse. Reduced NEU1 levels are observed in NeuN+ neurons in both non-treated and HSPC transplanted  $Neu1^{\Delta Ex3}$  mice compared to those in the WT mouse. (B) Increased LAMP-1 levels are observed in neurons and microglia of both HSPC transplanted and non-transplanted  $Neu1^{\Delta Ex3}$  mouse.

### 3.4 Discussion

In the current study, we attempted to correct kidney and brain pathology in sialidosis type II mice by transplantation of WT HSPC without gene modification. We intended to conduct a pilot study with at least three *Neu1<sup>ΔEx3</sup>* mice, but unfortunately encountered problems with mouse reproduction which did not allow us to have enough homozygous litters. This study had two aims, the first was to determine if HSPC engraftment can be achieved in NEU1-deficient mice in contrast to the results previously reported by another research lab (134). It was hypothesized in the above study that the absence of NEU1 causes hypersialylation of LAMP1 and leads to increased docking of lysosomes at the plasma membrane and exocytosis of serine proteases. In turn this causes the removal of serpins necessary for the mobilization of HSPC to the bone marrow niche. However, we have previously observed that the levels of LAMP1 in our sialidosis mouse model increase as a result of induced lysosomal biogenesis as demonstrated by measuring the activity of lysosomal enzymes, TFEB levels and localization and proteomics analysis (chapter 2). We did not observe a hypersialylation of LAMP1 protein, and at the same time, we also showed that LAMP2+ staining is found throughout the renal PRT cell and does not localize at the plasma membrane. Furthermore, we achieved engraftment of 75.3% of CD45.1+ donor leucocytes in our transplanted *Neu1<sup>ΔEx3</sup>* mouse.

The second aim was to determine if the WT transplant is capable of ameliorating pathology in the kidneys, where we see the most rapid and severe progression of pathology (described in Chapter 2), and the brain which can not be effectively treated by ERT due to the existence of BBB. Although we did not observe a rescue of the deficient NEU1 enzyme activity the kidney and brain, we did observe a partial rescue of aberrant sialylation in the kidney tissue with normalization of PNA lectin staining. We also observed an rescue of megalin levels.

For this pilot study, we harvested HPSC from the WT C57BL/6 strain that carries a differential leucocyte marker CD45.1 (Jackson Laboratory #002014). Although the engraftment rate in our *Neu1<sup>ΔEx3</sup>* mouse achieved 75.3% however, we found only a slight increase of NEU1 enzyme activity in all tested tissues, with no increase in the brain. Despite the negligible increase of NEU1 activity in the kidney tissues of HSPC treated *Neu1<sup>ΔEx3</sup>* mouse, we detected a substantial decrease in lysosomal biogenesis in their PRT 1.5 months post-HSPC transplant. This was evident from a ~2-fold decrease in the activities of lysosomal  $\beta$ -galactosidase and  $\beta$ -hexosaminidase activities in all studied tissues except for the brain compared to untreated *Neu1<sup>ΔEx3</sup>* mouse. This was also consistent with the normalization of increased LAMP-2 staining detected in PCT by immunofluorescence. We speculate that even low levels of HSPC-derived

NEU1 are capable of correcting kidney tissue pathogenesis due to continuous hematopoiesis and successive HSPC self-renewal. This hypothesis is indirectly supported by a previous publication showing that 10% of the residual NEU1 activity is sufficient to maintain normal lysosomal catabolism of glycoconjugates (310). HSPC have a potential to differentiate into both myeloid progenitor or lymphoid progenitor cells which should produce functional copies of NEU1/CTSA wild-type enzymes to multiple tissues for cross-correction. Although NEU1 is a membrane-bound enzyme, there is evidence that it is secreted from the cells and can be found in the biological fluids in the form of extracellular vesicles/exosomes which can cross-correct other cells and tissues (324, 325). Further studies with multiple mice per cohort are required however to determine if the transplant also recovered other signs of kidney pathology such as fibrosis, reduced number of glomeruli, albuminuria and glucosuria.

In LSD, lysosomal storage leads to the onset of inflammation caused by the activation of phagocytic cells and the production of inflammatory cytokines, eventually leading to cell death in the affected tissues. In sialidosis, the brain and the kidney are amongst the most affected tissues both showing infiltration of activated macrophages. Immunostaining of tissue sections revealed a reduction in CD68-positive activated macrophages in the kidney but not in the brain of the HSPC-transplanted mice, which is indicative of partial correction. Additionally, previous work in long-term tracking of HSPC expansion to a different lymphoid lineage has reported early (6-12 months) clonal stability which stabilizes over time (326). Hence, our HSPC transplanted mice might benefit from a longer (> 4 months) period allowing for progenitor cell expansion. On the other hand, we need to take into consideration HSPC clonal exhaustion versus stability given the limited lifespan of mice.

Additionally, the replenishment of HSPC-derived NEU1, although at a marginal level was sufficient to correct the glycosylation defects in the kidneys of *Neu1<sup>ΔEx3</sup>* mouse. Representative confocal images of the PCT showed recovery of PNA/RCA-1 staining specific for galactose and a reducing trend of MALII-staining confirming the removal of excessive terminal sialic acids from the glycans on kidney glycoproteins. More importantly, the correction of protein glycosylation in HSPC-transplanted mice had a positive effect on the trafficking of megalin to the apical surface of the PCT and showed increased expression. Even though *Neu1<sup>ΔEx3</sup>* mice typically developed severe renal pathology at 4 months and were euthanized, the HSPC transplanted *Neu1<sup>ΔEx3</sup>* mouse showed improved mobility and response similar to those of age-matched WT mice and showed no signs of developing urinary retention. These improvements encourage further studies with increased cohort size including mice of both sexes.

In the brain of both HSPC-treated and non-treated *Neu1<sup>ΔEx3</sup>*, we detected astro-microgliosis characterized by elevated numbers of GFAP+ and CD68+ cells, indicative of neuroinflammation. Besides lysosomal storage and increased lysosomal biogenesis were evident in both microglia and neurons by the increased LAMP1 staining. Moreover, the NEU1 does not colocalize with cortical neurons in HSPC transplanted *Neu1<sup>ΔEx3</sup>*.

Additionally, the HSPC transplantation appears to improve the behavior in *Neu1<sup>ΔEx3</sup>* mouse drastically. The sialidosis mice have mobility issues and their movement in the open field arena is severely impaired at the age of 4 months. In our previous behavior study with Y-maze (Supplementary figure S3-1), *Neu1<sup>ΔEx3</sup>* mice of both sexes consistently made less than 10 entries into the arms of the maze within 10 minutes which disqualified this test as a tool for measuring spatial memory. In the current pilot study, the behavioral analysis does not have statistical power as we used only one mouse per group, nevertheless, the total distance travelled in the open field arena for the transplanted *Neu1<sup>ΔEx3</sup>* mouse was similar to that of the WT. This suggests that the treated mouse recovered its mobility, although further studies are necessary to reproduce this result and to determine if this improvement is caused by the rescue of the brain pathology or the absence of urinary retention.

In summary, our data reveal that heterologous HSPC transplantation is achievable in a sialidosis mouse model and leads to the promising correction of kidney and brain pathology. Our results also revealed that transplanted mouse survived longer allowing for a longer post-transplant evaluation. Additionally, our results demonstrate that the WT HSPC cannot effectively correct the NEU1 levels in the brain, but this could be potentially achieved by transplantation of HSPC with lentiviral-mediated supraphysiological NEU1 levels. As this study has already indicated that a marginal increase of NEU1 activity in tissues *Neu1<sup>ΔEx3</sup>* mouse managed to achieve substantial correction of renal pathology, one could expect that increasing the residual activity to 30% of normal may result in a complete recovery. The inclusion of both sexes in the study would further shed light on their response to HSPC transplantation, which is essential knowing that there are sex-based differences in the progression of the disease (78).

### 3.5 References

32. Pan, X., et al., *Neuraminidases 3 and 4 regulate neuronal function by catabolizing brain gangliosides*. *FASEB J*, 2017. **31**(8): p. 3467-3483.
78. Arora, V., et al., *Sialidosis type II: Expansion of phenotypic spectrum and identification of a common mutation in seven patients*. *Mol Genet Metab Rep*, 2020. **22**: p. 100561.
106. de Geest, N., et al., *Systemic and neurologic abnormalities distinguish the lysosomal disorders sialidosis and galactosialidosis in mice*. *Hum Mol Genet*, 2002. **11**(12): p. 1455-64.
110. Concolino, D., F. Deodato, and R. Parini, *Enzyme replacement therapy: efficacy and limitations*. *Ital J Pediatr*, 2018. **44**(Suppl 2): p. 120.
126. Biffi, A., et al., *Lentiviral hematopoietic stem cell gene therapy benefits metachromatic leukodystrophy*. *Science*, 2013. **341**(6148): p. 1233158.
128. Sessa, M., et al., *Lentiviral haemopoietic stem-cell gene therapy in early-onset metachromatic leukodystrophy: an ad-hoc analysis of a non-randomised, open-label, phase 1/2 trial*. *Lancet*, 2016. **388**(10043): p. 476-87.
134. Yogalingam, G., et al., *Neuraminidase 1 Is a Negative Regulator of Lysosomal Exocytosis*. *Developmental Cell*, 2008. **15**(1): p. 74-86.
199. Smutova, V., et al., *Structural basis for substrate specificity of mammalian neuraminidases*. *PLoS One*, 2014. **9**(9): p. e106320.
271. Peterson, C.W., et al., *Autologous, Gene-Modified Hematopoietic Stem and Progenitor Cells Repopulate the Central Nervous System with Distinct Clonal Variants*. *Stem Cell Reports*, 2019. **13**(1): p. 91-104.
272. Syres, K., et al., *Successful treatment of the murine model of cystinosis using bone marrow cell transplantation*. *Blood*, 2009. **114**(12): p. 2542-52.
276. Guo, T., et al., *Selective Inhibitors of Human Neuraminidase 3*. *J Med Chem*, 2018. **61**(5): p. 1990-2008.
281. Xia, B., et al., *Oligosaccharide analysis in urine by maldi-tof mass spectrometry for the diagnosis of lysosomal storage diseases*. *Clin Chem*, 2013. **59**(9): p. 1357-68.
282. Messina, A., et al., *HILIC-UPLC-MS for high throughput and isomeric N-glycan separation and characterization in Congenital Disorders Glycosylation and human diseases*. *Glycoconj J*, 2021. **38**(2): p. 201-211.
286. Tian, E., et al., *Galnt11 regulates kidney function by glycosylating the endocytosis receptor megalin to modulate ligand binding*. *Proc Natl Acad Sci U S A*, 2019. **116**(50): p. 25196-25202.
310. Seyrantepe, V., et al., *Enzymatic activity of lysosomal carboxypeptidase (cathepsin) A is required for proper elastic fiber formation and inactivation of endothelin-1*. *Circulation*, 2008. **117**(15): p. 1973-81.
312. Ngo, A.N., et al., *Optimal Concentration of 2,2,2-Trichloroacetic Acid for Protein Precipitation Based on Response Surface Methodology*. *J Anal Bioanal Tech*, 2014. **5**(4).
313. Biolabs, N.E., *PNGase F Protocol (Non-Denaturing Reaction Conditions) V.2*. 2022.
314. Aoki, K. and M. Tiemeyer, *The glycomics of glycan glucuronylation in Drosophila melanogaster*. *Methods Enzymol*, 2010. **480**: p. 297-321.
315. Palmigiano, A., et al., *CSF N-Glycomics Using MALDI MS Techniques in Alzheimer's Disease*. *Methods Mol Biol*, 2018. **1750**: p. 75-91.
316. Ciucanu, I. and F. Kerek, *A simple and rapid method for the permethylation of carbohydrates*. *Carbohydrate Research*, 1984. **131**(2): p. 209-217.
317. Tian, D., et al., *The effect of A1 adenosine receptor in diabetic megalin loss with caspase-1/IL18 signaling*. *Diabetes Metab Syndr Obes*, 2019. **12**: p. 1583-1596.
318. Charlton, J.R., et al., *Beyond the tubule: pathological variants of LRP2, encoding the megalin receptor, result in glomerular loss and early progressive chronic kidney disease*. *Am J Physiol Renal Physiol*, 2020. **319**(6): p. F988-F999.

319. King, B., et al., *Low-dose, continuous enzyme replacement therapy ameliorates brain pathology in the neurodegenerative lysosomal disorder mucopolysaccharidosis type IIIA*. J Neurochem, 2016. **137**(3): p. 409-22.
320. Wijburg, F.A., et al., *Long-term safety and clinical outcomes of intrathecal heparan-N-sulfatase in patients with Sanfilippo syndrome type A*. Mol Genet Metab, 2021. **134**(4): p. 317-322.
321. Wijburg, F.A., et al., *A multicenter open-label extension study of intrathecal heparan-N-sulfatase in patients with Sanfilippo syndrome type A*. Mol Genet Metab, 2021. **134**(1-2): p. 175-181.
322. Krivit, W., *Allogenic stem cell transplantation for the treatment of lysosomal and peroxisomal metabolic diseases*. Springer Semin Immunopathol, 2004. **26**(1-2): p. 119-32.
323. Guo, M., et al., *Microglial Exosomes in Neurodegenerative Disease*. Front Mol Neurosci, 2021. **14**: p. 630808.
324. Sumida, M., et al., *Rapid Trimming of Cell Surface Polysialic Acid (PolySia) by Exovesicular Sialidase Triggers Release of Preexisting Surface Neurotrophin*. J Biol Chem, 2015. **290**(21): p. 13202-14.
325. Allendorf, D.H. and G.C. Brown, *Neu1 Is Released From Activated Microglia, Stimulating Microglial Phagocytosis and Sensitizing Neurons to Glutamate*. Front Cell Neurosci, 2022. **16**: p. 917884.
326. Kim, S., et al., *Dynamics of HSPC repopulation in nonhuman primates revealed by a decade-long clonal-tracking study*. Cell Stem Cell, 2014. **14**(4): p. 473-85.

### 3.6 Supplementary data

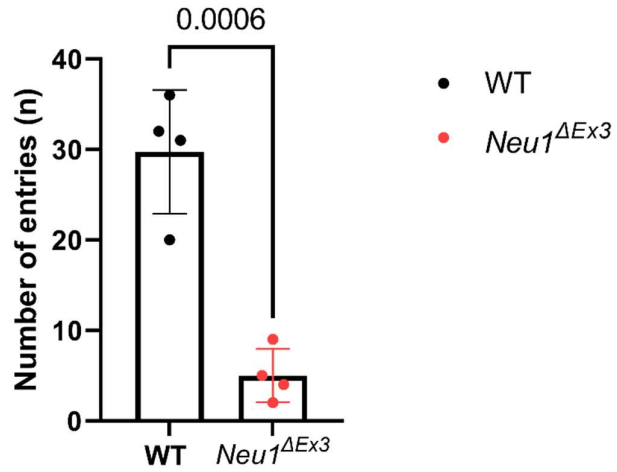


**Figure S 3-1: Y-maze number of arm entries.**

*Neu1*<sup>ΔEx3</sup> mouse showed less tendency to explore at 4-months old as exhibited by the reduced number of arm entries.

## 4 General discussion

In this work, we first characterized two Neu1-deficient mouse models *Neu1<sup>ΔEx3</sup>* and *Neu1<sup>Cx3cr1ΔEx3</sup>* mice to have a better understanding of the systemic pathology and clinical similarities to sialidosis patients. The first manuscript (in Chapter 2) described in detail the pathology of the two Neu1-deficient mouse models, including renal inflammation, fibrosis and ultrastructural abnormalities in the kidneys. In *Neu1<sup>ΔEx3</sup>* mice, we demonstrated the earlier development of kidney dysfunction at the average age of 4 months in male and 6 months in female *Neu1<sup>ΔEx3</sup>* mice. In this study, we described a role of NEU1 in maintaining kidney function where hypersialylation of the endocytic receptor megalin caused mistrafficking of the receptor to the lysosomes instead of recycling to the epithelial cell surface, resulting in the poor tubular reabsorption at the PRT and excessive loss of essential vitamins, solutes, proteins and receptors into the urine. Surprisingly, we found higher average NEU1 activity levels in the kidneys of WT male mice compared to female mice, while NEU1 levels were at similar levels in all other tested tissues in both sexes. This suggests higher NEU1 levels are needed in male mice kidneys to maintain normal function, which is also reflected in the earlier development of renal pathology in male mice compared to female mice. Overall, this study characterized *Neu1<sup>ΔEx3</sup>* mice as a reliable model for studying nephrosialidosis and contributed to further understanding of the underlying mechanisms in the progression of kidney dysfunction in nephrosialidosis.

In Chapter 3, we showed preliminary results of WT HSPC transplantation in *Neu1<sup>ΔEx3</sup>* mouse and the potential of this procedure to rescue the renal and brain pathology associated with NEU1 deficiency. This study aimed to fulfill two goals, first to determine the optimal parameters for conducting HSPC transplantation in *Neu1<sup>ΔEx3</sup>* mice such as the age, the amount of WT HSPC needed for transplantation, and the response of recipient sialidosis mice to the myeloablative regimen and HSPC transplant. Our second goal was to determine the engraftment efficacy and the extent of pathology rescue in HSPC-treated mice, especially in hard-to-penetrate tissues such as the brain and kidney. As such, this work can serve as a pilot study in preparation for a future preclinical study of LV-gene modified-HSPC gene therapy for sialidosis and sets clinical endpoints for amelioration of pathology with allogenic WT HSPC transplant. Our preliminary results demonstrate successful engraftment of WT HSPC in *Neu1<sup>ΔEx3</sup>* mouse, although increase of NEU1 levels were minor in the visceral tissues, brain and bone marrow. However, the treatment was sufficient to rescue renal pathology, showing

reduction of inflammation and lysosomal biogenesis, along with partial correction of the glycosylation of megalin in the PRT. We also showed evidence for increased megalin protein that was correctly localized at the apical surface of the PRT. However, no amelioration of the brain pathology was detected, with high levels of inflammation (astromicrogliosis) and lysosomal biogenesis in both HPSC-treated and non-treated *Neu1<sup>ΔEx3</sup>* mice. Behavior analysis using open field test suggests improved exploratory and locomotor behavior of HPSC-treated mice showing normalization of distance travelled and number of entries to the center. However, additional behavior tests such as Y-maze and novel object recognition would be a better determinant of memory and learning in mice and provide further confirmation of the rescue of neuropathology. Furthermore, this study would benefit from the addition of both sexes to have a better understanding sex-specific responses to the treatment. Especially since sialidosis patients seemed to demonstrate a gender-specific pathology detected both in animal models and patients. This study could also benefit from the testing of HSPC treatment in the conditional *Neu1<sup>Cx3cr1ΔEx3</sup>* mouse model to test whether the majority of tissue NEU1 is expressed by macrophages/microglia. Still, the expression of *Cx3Cr1* is not limited to immune cells, hence the variation of pathology documented in *Neu1<sup>Cx3cr1ΔEx3</sup>* mice makes it an unsuitable strain for this study and requires a generation of a more specific model. Finally, given that HSPC are capable of long-term self-renewal and HSPC-derived progeny stabilizes over time, the HSPC-treated mice would benefit from transplantation at an earlier age (before 6 weeks) with a longer period of clonal expansion for self-replenishment in all tissues.

## Conclusions

In conclusion, the result of my doctoral research demonstrated that NEU1 plays a crucial role in regulating the glycosylation and trafficking of megalin which contributes to severe renal dysfunction in the *Neu1<sup>ΔEx3</sup>* mouse model of sialidosis.

First, we validated the *Neu1<sup>ΔEx3</sup>* mouse strain as a model of type II sialidosis, which very closely recapitulates the clinical phenotypes of human patients, with short life-span, skeletal deformation, organ enlargement and more importantly the early onset and rapidly progressive renal pathology. Due to the rarity of nephrosialidosis, the *Neu1<sup>ΔEx3</sup>* model provides us with the opportunity to study the underlying mechanisms of pathology, furthering our insight into the etiology of renal dysfunction of nephrosialidosis.

Second, we identified alteration of renal protein glycosylation and increase of N-linked sialylation in male *Neu1<sup>ΔEx3</sup>* kidney tissues, which provides insight into the mechanism of rapid sex-specific development of renal pathology in male mice and is a valuable tool for further study of the cellular processes underlying aberrant sialylation of chronic kidney diseases, which are more prevalent in men.

Third, our study showed a unique renal pathophysiology in sialidosis that has not been previously described and suggests that the loss of megalin, other endocytic receptors and solute carriers in the kidney could be a major contributor to the progression of severe nephropathy in nephrosialidosis and other nephropathic LSD with mixed traits of glomerular and tubular nephropathy.

Lastly, our result on allogeneic HSPC transplant in *Neu1<sup>ΔEx3</sup>* mouse showed high engraftment rate and promising signs of correction of kidney and brain (behavioral) pathology suggesting a new direction for treatment of type II sialidosis.

## Master references list

1. Alberts B, et al., *Molecular Biology of the Cell 5th edition*. 2008, Garland Science: New York.
2. Ishida, Y., et al., *A model of lysosomal pH regulation*. J Gen Physiol, 2013. **141**(6): p. 705-20.
3. Braulke, T. and J.S. Bonifacino, *Sorting of lysosomal proteins*. Biochim Biophys Acta, 2009. **1793**(4): p. 605-14.
4. Alberts, B., et al., *Molecular Biology of the Cell*. 5th edition ed. 2008.
5. Canuel, M., et al., *Sortilin mediates the lysosomal targeting of cathepsins D and H*. Biochem Biophys Res Commun, 2008. **373**(2): p. 292-7.
6. Bonifacino, J.S. and L.M. Traub, *Signals for sorting of transmembrane proteins to endosomes and lysosomes*. Annu Rev Biochem, 2003. **72**: p. 395-447.
7. Yang, C. and X. Wang, *Lysosome biogenesis: Regulation and functions*. J Cell Biol, 2021. **220**(6).
8. Hu, Y.B., et al., *The endosomal-lysosomal system: from acidification and cargo sorting to neurodegeneration*. Transl Neurodegener, 2015. **4**: p. 18.
9. Parzych, K.R. and D.J. Klionsky, *An overview of autophagy: morphology, mechanism, and regulation*. Antioxid Redox Signal, 2014. **20**(3): p. 460-73.
10. Hurley, J.H. and L.N. Young, *Mechanisms of Autophagy Initiation*. Annu Rev Biochem, 2017. **86**: p. 225-244.
11. Runwal, G., et al., *LC3-positive structures are prominent in autophagy-deficient cells*. Sci Rep, 2019. **9**(1): p. 10147.
12. Zhang, W., et al., *Regulation of TFEB activity and its potential as a therapeutic target against kidney diseases*. Cell Death Discov, 2020. **6**: p. 32.
13. Napolitano, G. and A. Ballabio, *TFEB at a glance*. J Cell Sci, 2016. **129**(13): p. 2475-81.
14. Palmieri, M., et al., *mTORC1-independent TFEB activation via Akt inhibition promotes cellular clearance in neurodegenerative storage diseases*. Nat Commun, 2017. **8**: p. 14338.
15. Brown, R.A., et al., *mTOR hyperactivity mediates lysosomal dysfunction in Gaucher's disease iPSC-neuronal cells*. Dis Model Mech, 2019. **12**(10).
16. Meikle, P.J., et al., *Prevalence of lysosomal storage disorders*. JAMA, 1999. **281**(3): p. 249-54.
17. Pastores, G.M. and G.H. Maegawa, *Clinical neurogenetics: neuropathic lysosomal storage disorders*. Neurol Clin, 2013. **31**(4): p. 1051-71.
18. Sun, A., *Lysosomal storage disease overview*. Ann Transl Med, 2018. **6**(24): p. 476.
19. Lukong, K.E., et al., *Characterization of the sialidase molecular defects in sialidosis patients suggests the structural organization of the lysosomal multienzyme complex*. Hum Mol Genet, 2000. **9**(7): p. 1075-85.
20. Saftig, P. and J. Klumperman, *Lysosome biogenesis and lysosomal membrane proteins: trafficking meets function*. Nat Rev Mol Cell Biol, 2009. **10**(9): p. 623-35.
21. Sandhoff, K. and K. Harzer, *Gangliosides and gangliosidoses: principles of molecular and metabolic pathogenesis*. J Neurosci, 2013. **33**(25): p. 10195-208.
22. Liu, Y., et al., *Mouse model of GM2 activator deficiency manifests cerebellar pathology and motor impairment*. Proc Natl Acad Sci U S A, 1997. **94**(15): p. 8138-43.
23. Duraes, J., E. Salsano, and M.D.C. Macario, *Adult-Onset Krabbe Disease: The Importance of a Systematic Approach to Brain MRI Findings*. Neurol Clin Pract, 2021. **11**(1): p. e15-e17.
24. Orr, M.E. and S. Oddo, *Autophagic/lysosomal dysfunction in Alzheimer's disease*. Alzheimers Res Ther, 2013. **5**(5): p. 53.
25. Ohmi, K., et al., *Sanfilippo syndrome type B, a lysosomal storage disease, is also a tauopathy*. Proc Natl Acad Sci U S A, 2009. **106**(20): p. 8332-7.
26. Annunziata, I., et al., *Lysosomal NEU1 deficiency affects amyloid precursor protein levels and amyloid-beta secretion via deregulated lysosomal exocytosis*. Nat Commun, 2013. **4**: p. 2734.
27. Wong, K., et al., *Neuropathology provides clues to the pathophysiology of Gaucher disease*. Mol Genet Metab, 2004. **82**(3): p. 192-207.

28. Cullen, V., et al., *Acid beta-glucosidase mutants linked to Gaucher disease, Parkinson disease, and Lewy body dementia alter alpha-synuclein processing*. *Ann Neurol*, 2011. **69**(6): p. 940-53.
29. Sidransky, E., et al., *Multicenter analysis of glucocerebrosidase mutations in Parkinson's disease*. *N Engl J Med*, 2009. **361**(17): p. 1651-61.
30. Clark, L.N., et al., *Mutations in the glucocerebrosidase gene are associated with early-onset Parkinson disease*. *Neurology*, 2007. **69**(12): p. 1270-7.
31. Schnaar, R.L., R. Gerardy-Schahn, and H. Hildebrandt, *Sialic acids in the brain: gangliosides and polysialic acid in nervous system development, stability, disease, and regeneration*. *Physiol Rev*, 2014. **94**(2): p. 461-518.
32. Pan, X., et al., *Neuraminidases 3 and 4 regulate neuronal function by catabolizing brain gangliosides*. *FASEB J*, 2017. **31**(8): p. 3467-3483.
33. Yamano, T., et al., *Pathological study on a severe sialidosis (alpha-neuraminidase deficiency)*. *Acta Neuropathol*, 1986. **71**(3-4): p. 278-84.
34. Ziv, Y., et al., *Immune cells contribute to the maintenance of neurogenesis and spatial learning abilities in adulthood*. *Nat Neurosci*, 2006. **9**(2): p. 268-75.
35. Barrette, B., et al., *Requirement of myeloid cells for axon regeneration*. *J Neurosci*, 2008. **28**(38): p. 9363-76.
36. Leon-Rodriguez, A., et al., *Anxiety-like behavior and microglial activation in the amygdala after acute neuroinflammation induced by microbial neuraminidase*. *Sci Rep*, 2022. **12**(1): p. 11581.
37. Choi, S.S., et al., *Human astrocytes: secretome profiles of cytokines and chemokines*. *PLoS One*, 2014. **9**(4): p. e92325.
38. Vitner, E.B., et al., *Contribution of brain inflammation to neuronal cell death in neuronopathic forms of Gaucher's disease*. *Brain*, 2012. **135**(Pt 6): p. 1724-35.
39. Van Hoecke, L., et al., *Involvement of the Choroid Plexus in the Pathogenesis of Niemann-Pick Disease Type C*. *Front Cell Neurosci*, 2021. **15**: p. 757482.
40. Versele, R., et al., *TNF-alpha and IL-1beta Modulate Blood-Brain Barrier Permeability and Decrease Amyloid-beta Peptide Efflux in a Human Blood-Brain Barrier Model*. *Int J Mol Sci*, 2022. **23**(18).
41. Tansey, M.G., et al., *Inflammation and immune dysfunction in Parkinson disease*. *Nat Rev Immunol*, 2022. **22**(11): p. 657-673.
42. Rozenfeld, P. and S. Feriozzi, *Contribution of inflammatory pathways to Fabry disease pathogenesis*. *Mol Genet Metab*, 2017. **122**(3): p. 19-27.
43. Trauner, D.A., et al., *Neurological impairment in nephropathic cystinosis: motor coordination deficits*. *Pediatr Nephrol*, 2010. **25**(10): p. 2061-6.
44. Zhang, A. and S. Huang, *Progress in pathogenesis of proteinuria*. *Int J Nephrol*, 2012. **2012**: p. 314251.
45. Klootwijk, E.D., et al., *Renal Fanconi syndrome: taking a proximal look at the nephron*. *Nephrol Dial Transplant*, 2015. **30**(9): p. 1456-60.
46. Hara-Chikuma, M., et al., *Impaired acidification in early endosomes of CIC-5 deficient proximal tubule*. *Biochem Biophys Res Commun*, 2005. **329**(3): p. 941-6.
47. Christensen, E.I., et al., *Loss of chloride channel CIC-5 impairs endocytosis by defective trafficking of megalin and cubilin in kidney proximal tubules*. *Proc Natl Acad Sci U S A*, 2003. **100**(14): p. 8472-7.
48. Bhargava, P. and R.G. Schnellmann, *Mitochondrial energetics in the kidney*. *Nat Rev Nephrol*, 2017. **13**(10): p. 629-646.
49. Desmond, M.J., et al., *Tubular proteinuria in mice and humans lacking the intrinsic lysosomal protein SCARB2/Limp-2*. *Am J Physiol Renal Physiol*, 2011. **300**(6): p. F1437-47.
50. Schroder, J., et al., *Deficiency of the tetraspanin CD63 associated with kidney pathology but normal lysosomal function*. *Mol Cell Biol*, 2009. **29**(4): p. 1083-94.

51. Christensen, E.I., et al., *Distribution of alpha-galactosidase A in normal human kidney and renal accumulation and distribution of recombinant alpha-galactosidase A in Fabry mice*. J Am Soc Nephrol, 2007. **18**(3): p. 698-706.
52. Valbuena, C., et al., *Kidney biopsy findings in heterozygous Fabry disease females with early nephropathy*. Virchows Arch, 2008. **453**(4): p. 329-38.
53. Tagawa, A., et al., *Impaired Podocyte Autophagy Exacerbates Proteinuria in Diabetic Nephropathy*. Diabetes, 2016. **65**(3): p. 755-67.
54. Yamahara, K., et al., *Obesity-mediated autophagy insufficiency exacerbates proteinuria-induced tubulointerstitial lesions*. J Am Soc Nephrol, 2013. **24**(11): p. 1769-81.
55. Liu, W.J., et al., *Lysosome restoration to activate podocyte autophagy: a new therapeutic strategy for diabetic kidney disease*. Cell Death Dis, 2019. **10**(11): p. 806.
56. Sansanwal, P. and M.M. Sarwal, *p62/SQSTM1 prominently accumulates in renal proximal tubules in nephropathic cystinosis*. Pediatr Nephrol, 2012. **27**(11): p. 2137-2144.
57. Sansanwal, P., et al., *Mitochondrial autophagy promotes cellular injury in nephropathic cystinosis*. J Am Soc Nephrol, 2010. **21**(2): p. 272-83.
58. Chévrier, M., et al., *Autophagosome maturation is impaired in Fabry disease*. Autophagy, 2010. **6**(5): p. 589-99.
59. Zhang, Q., et al., *Circulating mitochondrial DAMPs cause inflammatory responses to injury*. Nature, 2010. **464**(7285): p. 104-107.
60. Bulow, R.D. and P. Boor, *Extracellular Matrix in Kidney Fibrosis: More Than Just a Scaffold*. J Histochem Cytochem, 2019. **67**(9): p. 643-661.
61. Isaka, Y., *Targeting TGF-beta Signaling in Kidney Fibrosis*. Int J Mol Sci, 2018. **19**(9).
62. Abrahamson, D.R., et al., *Cellular origins of type IV collagen networks in developing glomeruli*. J Am Soc Nephrol, 2009. **20**(7): p. 1471-9.
63. Holderied, A., et al., *Glomerular parietal epithelial cell activation induces collagen secretion and thickening of Bowman's capsule in diabetes*. Lab Invest, 2015. **95**(3): p. 273-82.
64. Canaud, G. and J.V. Bonventre, *Cell cycle arrest and the evolution of chronic kidney disease from acute kidney injury*. Nephrol Dial Transplant, 2015. **30**(4): p. 575-83.
65. Raggi, C., et al., *Dedifferentiation and aberrations of the endolysosomal compartment characterize the early stage of nephropathic cystinosis*. Hum Mol Genet, 2014. **23**(9): p. 2266-78.
66. Berquez, M., et al., *Lysosomal cystine export regulates mTORC1 signaling to guide kidney epithelial cell fate specialization*. Nat Commun, 2023. **14**(1): p. 3994.
67. Iwano, M., et al., *Evidence that fibroblasts derive from epithelium during tissue fibrosis*. J Clin Invest, 2002. **110**(3): p. 341-50.
68. Huang, R., P. Fu, and L. Ma, *Kidney fibrosis: from mechanisms to therapeutic medicines*. Signal Transduct Target Ther, 2023. **8**(1): p. 129.
69. Wickman, L., et al., *Podocyte Depletion in Thin GBM and Alport Syndrome*. PLoS One, 2016. **11**(5): p. e0155255.
70. Cocchiario, P., et al., *The Multifaceted Role of the Lysosomal Protease Cathepsins in Kidney Disease*. Front Cell Dev Biol, 2017. **5**: p. 114.
71. Petermann, I., et al., *Lysosomal, cytoskeletal, and metabolic alterations in cardiomyopathy of cathepsin L knockout mice*. FASEB J, 2006. **20**(8): p. 1266-8.
72. Moles, A., et al., *Cathepsins B and D drive hepatic stellate cell proliferation and promote their fibrogenic potential*. Hepatology, 2009. **49**(4): p. 1297-307.
73. Fox, C., et al., *Inhibition of lysosomal protease cathepsin D reduces renal fibrosis in murine chronic kidney disease*. Sci Rep, 2016. **6**: p. 20101.
74. Bonten, E.J., et al., *Heterodimerization of the sialidase NEU1 with the chaperone protective protein/cathepsin A prevents its premature oligomerization*. J Biol Chem, 2009. **284**(41): p. 28430-28441.

75. Seyrantepe, V., et al., *Molecular pathology of NEU1 gene in sialidosis*. Hum Mutat, 2003. **22**(5): p. 343-52.
76. d'Azzo, A., E. Machado, and I. Annunziata, *Pathogenesis, Emerging therapeutic targets and Treatment in Sialidosis*. Expert Opin Orphan Drugs, 2015. **3**(5): p. 491-504.
77. Tylki-Szymanska, A., A. Ługowska, and B. Czartoryska, *Neuraminidase deficiency presenting as a nephrosialidosis: The first case detected in Poland*. Pediatrics International, 1996. **38**(5): p. 529-532.
78. Arora, V., et al., *Sialidosis type II: Expansion of phenotypic spectrum and identification of a common mutation in seven patients*. Mol Genet Metab Rep, 2020. **22**: p. 100561.
79. Aylsworth, A.S., et al., *A severe infantile sialidosis: clinical, biochemical, and microscopic features*. J Pediatr, 1980. **96**(4): p. 662-8.
80. Chen, W., et al., *Histological studies of renal biopsy in a boy with nephrosialidosis*. Ultrastruct Pathol, 2011. **35**(4): p. 168-71.
81. Maroofian, R., et al., *Parental Whole-Exome Sequencing Enables Sialidosis Type II Diagnosis due to an NEU1 Missense Mutation as an Underlying Cause of Nephrotic Syndrome in the Child*. Kidney Int Rep, 2018. **3**(6): p. 1454-1463.
82. Tazi, K., et al., *Ascites in infantile onset type II Sialidosis*. JIMD Rep, 2022. **63**(4): p. 316-321.
83. Kelly, T.E. and G. Graetz, *Isolated acid neuraminidase deficiency: a distinct lysosomal storage disease*. Am J Med Genet, 1977. **1**(1): p. 31-46.
84. Roth, K.S., et al., *Acid alpha-neuraminidase deficiency: a nephropathic phenotype?* Clin Genet, 1988. **34**(3): p. 185-94.
85. Sperl, W., et al., *Nephrosis in two siblings with infantile sialic acid storage disease*. Eur J Pediatr, 1990. **149**(7): p. 477-82.
86. Sphranger, J., J. Gehler, and M. Cantz, *Mucopolidosis I--a sialidosis*. Am J Med Genet, 1977. **1**(1): p. 21-9.
87. Laver, J., et al., *Infantile lethal neuraminidase deficiency (sialidosis)*. Clin Genet, 1983. **23**(2): p. 97-101.
88. Paschke, E., et al., *Infantile type of sialic acid storage disease with sialuria*. Clin Genet, 1986. **29**(5): p. 417-24.
89. Schiff, M., et al., *Long-term follow-up of metachronous marrow-kidney transplantation in severe type II sialidosis: what does success mean?* Nephrol Dial Transplant, 2005. **20**(11): p. 2563-5.
90. Itoh, K., et al., *Novel missense mutations in the human lysosomal sialidase gene in sialidosis patients and prediction of structural alterations of mutant enzymes*. J Hum Genet, 2002. **47**(1): p. 29-37.
91. Lowden, J.A. and J.S. O'Brien, *Sialidosis: a review of human neuraminidase deficiency*. Am J Hum Genet, 1979. **31**(1): p. 1-18.
92. Lv, R.J., et al., *Clinical and genetic characteristics of type I sialidosis patients in mainland China*. Ann Clin Transl Neurol, 2020. **7**(6): p. 911-923.
93. Emmady, P.D. and A.C. Anilkumar, *EEG Abnormal Waveforms*, in StatPearls. 2023: Treasure Island (FL).
94. Loughman, A., S.C. Bowden, and W.J. D'Souza, *A comprehensive assessment of cognitive function in the common genetic generalized epilepsy syndromes*. Eur J Neurol, 2017. **24**(3): p. 453-460.
95. Urbanski, G., et al., *A Case of Type I Sialidosis With Osteonecrosis Revealing a New Mutation in NEU1*. Journal of Inborn Errors of Metabolism and Screening, 2014. **2**: p. 2326409814543468.
96. Neves Jde, C., et al., *Neuraminidase-1 mediates skeletal muscle regeneration*. Biochim Biophys Acta, 2015. **1852**(9): p. 1755-64.
97. Gupta, A.O., et al., *Hematopoietic cell transplantation for sialidosis type I*. Mol Genet Metab Rep, 2022. **30**: p. 100832.

98. Sekijima, Y., et al., *Clinical and serial MRI findings of a sialidosis type I patient with a novel missense mutation in the NEU1 gene*. Intern Med, 2013. **52**(1): p. 119-24.
99. Lu, C.S., et al., *Cortical damage in the posterior visual pathway in patients with sialidosis type 1*. Brain Imaging Behav, 2017. **11**(1): p. 214-223.
100. Palmeri, S., et al., *Type I sialidosis: a clinical, biochemical and neuroradiological study*. Eur Neurol, 2000. **43**(2): p. 88-94.
101. Palaniyappan, L., et al., *Combined white matter imaging suggests myelination defects in visual processing regions in schizophrenia*. Neuropsychopharmacology, 2013. **38**(9): p. 1808-15.
102. Raz, N. and N. Levin, *Cortical and white matter mapping in the visual system-more than meets the eye: on the importance of functional imaging to understand visual system pathologies*. Front Integr Neurosci, 2014. **8**: p. 68.
103. Amano, N., et al., *Neuropathological findings of an autopsy case of adult beta-galactosidase and neuraminidase deficiency*. Acta Neuropathol, 1983. **61**(3-4): p. 283-90.
104. Mohammad, A.N., et al., *Type 1 sialidosis presenting with ataxia, seizures and myoclonus with no visual involvement*. Mol Genet Metab Rep, 2018. **15**: p. 11-14.
105. Delgado-Zabalza, L., et al., *Targeting parvalbumin-expressing neurons in the substantia nigra pars reticulata restores motor function in parkinsonian mice*. Cell Rep, 2023. **42**(10): p. 113287.
106. de Geest, N., et al., *Systemic and neurologic abnormalities distinguish the lysosomal disorders sialidosis and galactosialidosis in mice*. Hum Mol Genet, 2002. **11**(12): p. 1455-64.
107. Kanaka, C., et al., *Mucocutaneous bleeding, a rare but severe complication in nephrosialidosis*. Eur J Pediatr, 1994. **153**(9): p. 703-4.
108. Andrade-Campos, M., et al., *Diagnosis features of pediatric Gaucher disease patients in the era of enzymatic therapy, a national-base study from the Spanish Registry of Gaucher Disease*. Orphanet J Rare Dis, 2017. **12**(1): p. 84.
109. Lee, C.L., et al., *Fabry Disease and the Effectiveness of Enzyme Replacement Therapy (ERT) in Left Ventricular Hypertrophy (LVH) Improvement: A Review and Meta-Analysis*. Int J Med Sci, 2022. **19**(1): p. 126-131.
110. Concolino, D., F. Deodato, and R. Parini, *Enzyme replacement therapy: efficacy and limitations*. Ital J Pediatr, 2018. **44**(Suppl 2): p. 120.
111. Ditters, I.A.M., et al., *Home-based enzyme replacement therapy in children and adults with Pompe disease; a prospective study*. Orphanet J Rare Dis, 2023. **18**(1): p. 108.
112. Cadaoas, J., et al., *Galactosialidosis: preclinical enzyme replacement therapy in a mouse model of the disease, a proof of concept*. Mol Ther Methods Clin Dev, 2021. **20**: p. 191-203.
113. Sahin, O., et al., *Mucopolysaccharidoses and the blood-brain barrier*. Fluids Barriers CNS, 2022. **19**(1): p. 76.
114. Ben-Zvi, A., et al., *Mfsd2a is critical for the formation and function of the blood-brain barrier*. Nature, 2014. **509**(7501): p. 507-11.
115. Cohen, J.L., et al., *In Utero Enzyme-Replacement Therapy for Infantile-Onset Pompe's Disease*. N Engl J Med, 2022. **387**(23): p. 2150-2158.
116. Fischetto, R., et al., *Substrate reduction therapy with Miglustat in pediatric patients with GM1 type 2 gangliosidosis delays neurological involvement: A multicenter experience*. Mol Genet Genomic Med, 2020. **8**(10): p. e1371.
117. Cox, T., et al., *Novel oral treatment of Gaucher's disease with N-butyldeoxynojirimycin (OGT 918) to decrease substrate biosynthesis*. Lancet, 2000. **355**(9214): p. 1481-5.
118. Krivit, W., et al., *Microglia: the effector cell for reconstitution of the central nervous system following bone marrow transplantation for lysosomal and peroxisomal storage diseases*. Cell Transplant, 1995. **4**(4): p. 385-92.

119. Biffi, A., et al., *Correction of metachromatic leukodystrophy in the mouse model by transplantation of genetically modified hematopoietic stem cells*. J Clin Invest, 2004. **113**(8): p. 1118-29.
120. Masouridi-Levrat, S., F. Simonetta, and Y. Chalandon, *Immunological Basis of Bone Marrow Failure after Allogenic Hematopoietic Stem Cell Transplantation*. Front Immunol, 2016. **7**: p. 362.
121. Cressant, A., et al., *Improved behavior and neuropathology in the mouse model of Sanfilippo type IIIB disease after adeno-associated virus-mediated gene transfer in the striatum*. J Neurosci, 2004. **24**(45): p. 10229-39.
122. Ciron, C., et al., *Gene therapy of the brain in the dog model of Hurler's syndrome*. Ann Neurol, 2006. **60**(2): p. 204-13.
123. Markakis, E.A., et al., *Comparative transduction efficiency of AAV vector serotypes 1-6 in the substantia nigra and striatum of the primate brain*. Mol Ther, 2010. **18**(3): p. 588-93.
124. Sergijenko, A., et al., *Myeloid/Microglial driven autologous hematopoietic stem cell gene therapy corrects a neuronopathic lysosomal disease*. Mol Ther, 2013. **21**(10): p. 1938-49.
125. Wilkinson, F.L., et al., *Busulfan conditioning enhances engraftment of hematopoietic donor-derived cells in the brain compared with irradiation*. Mol Ther, 2013. **21**(4): p. 868-76.
126. Biffi, A., et al., *Lentiviral hematopoietic stem cell gene therapy benefits metachromatic leukodystrophy*. Science, 2013. **341**(6148): p. 1233158.
127. Capotondo, A., et al., *Brain conditioning is instrumental for successful microglia reconstitution following hematopoietic stem cell transplantation*. Proc Natl Acad Sci U S A, 2012. **109**(37): p. 15018-23.
128. Sessa, M., et al., *Lentiviral haemopoietic stem-cell gene therapy in early-onset metachromatic leukodystrophy: an ad-hoc analysis of a non-randomised, open-label, phase 1/2 trial*. Lancet, 2016. **388**(10043): p. 476-87.
129. Cherqui, S., *Cysteamine therapy: a treatment for cystinosis, not a cure*. Kidney Int, 2012. **81**(2): p. 127-9.
130. Harrison, F., et al., *Hematopoietic stem cell gene therapy for the multisystemic lysosomal storage disorder cystinosis*. Mol Ther, 2013. **21**(2): p. 433-44.
131. Wang, D., et al., *Short-term, high dose enzyme replacement therapy in sialidosis mice*. Mol Genet Metab, 2005. **85**(3): p. 181-9.
132. Bonten, E.J., et al., *Targeting macrophages with baculovirus-produced lysosomal enzymes: implications for enzyme replacement therapy of the glycoprotein storage disorder galactosialidosis*. FASEB J, 2004. **18**(9): p. 971-3.
133. Bonten, E.J., et al., *Chaperone-mediated gene therapy with recombinant AAV-PPCA in a new mouse model of type I sialidosis*. Biochim Biophys Acta, 2013. **1832**(10): p. 1784-92.
134. Yogalingam, G., et al., *Neuraminidase 1 Is a Negative Regulator of Lysosomal Exocytosis*. Developmental Cell, 2008. **15**(1): p. 74-86.
135. Reily, C., et al., *Glycosylation in health and disease*. Nat Rev Nephrol, 2019. **15**(6): p. 346-366.
136. Stanley P, M.K., Lewis NE, et al. N-Glycans., *Essentials of Glycobiology 4th edition*, in *Essentials of Glycobiology*, A. Varki, et al., Editors. 2022: Cold Spring Harbor (NY).
137. Zachara NE, A.Y., Boyce M, et al., *Essentials of Glycobiology, Fourth Edition*, in *Essentials of Glycobiology*, A. Varki, et al., Editors. 2022: Cold Spring Harbor (NY).
138. Hart, G.W., M.P. Housley, and C. Slawson, *Cycling of O-linked beta-N-acetylglucosamine on nucleocytoplasmic proteins*. Nature, 2007. **446**(7139): p. 1017-22.
139. Shivatare, S.S., V.S. Shivatare, and C.H. Wong, *Glycoconjugates: Synthesis, Functional Studies, and Therapeutic Developments*. Chem Rev, 2022. **122**(20): p. 15603-15671.
140. Jung, J.U., et al., *The roles of glycosphingolipids in the proliferation and neural differentiation of mouse embryonic stem cells*. Exp Mol Med, 2009. **41**(12): p. 935-45.
141. Cummings RD, S.R., Ozeki Y., *Essentials of Glycobiology, Fourth Edition*, in *Essentials of Glycobiology*, A. Varki, et al., Editors. 2022: Cold Spring Harbor (NY).

142. Sharon, N. and H. Lis, *History of lectins: from hemagglutinins to biological recognition molecules*. *Glycobiology*, 2004. **14**(11): p. 53R-62R.
143. Islam, M.K., et al., *Lectins as potential tools for cancer biomarker discovery from extracellular vesicles*. *Biomarker Research*, 2023. **11**(1): p. 85.
144. Suzuki, Y., *Sialobiology of influenza: molecular mechanism of host range variation of influenza viruses*. *Biol Pharm Bull*, 2005. **28**(3): p. 399-408.
145. Ishikawa, Y., et al., *Expression and diversity of the sialic acid-binding adhesin and its homologs associated with oral streptococcal infection*. *Microbiol Immunol*, 2022. **66**(2): p. 59-66.
146. Gallegos, K.M., et al., *Shiga toxin binding to glycolipids and glycans*. *PLoS One*, 2012. **7**(2): p. e30368.
147. Brown, G.D., J.A. Willment, and L. Whitehead, *C-type lectins in immunity and homeostasis*. *Nat Rev Immunol*, 2018. **18**(6): p. 374-389.
148. Smith, B.A.H. and C.R. Bertozzi, *Author Correction: The clinical impact of glycobiology: targeting selectins, Siglecs and mammalian glycans*. *Nat Rev Drug Discov*, 2021. **20**(3): p. 244.
149. Stanley P, W.M., Lauc G, et al., *Essentials of Glycobiology, Fourth Edition*, in *Essentials of Glycobiology*, A. Varki, et al., Editors. 2022: Cold Spring Harbor (NY).
150. Ferreira, I.G., et al., *Carcinoembryonic antigen is a sialyl Lewis x/a carrier and an E-selectin ligand in non-small cell lung cancer*. *Int J Oncol*, 2019. **55**(5): p. 1033-1048.
151. Julien, S., et al., *Selectin ligand sialyl-Lewis x antigen drives metastasis of hormone-dependent breast cancers*. *Cancer Res*, 2011. **71**(24): p. 7683-93.
152. Dall'Olio, F., M. Pucci, and N. Malagolini, *The Cancer-Associated Antigens Sialyl Lewis(a/x) and Sd(a): Two Opposite Faces of Terminal Glycosylation*. *Cancers (Basel)*, 2021. **13**(21).
153. Kozlov, G. and K. Gehring, *Calnexin cycle - structural features of the ER chaperone system*. *FEBS J*, 2020. **287**(20): p. 4322-4340.
154. Varki, A. and S. Kornfeld, *P-type Lectins*, in *Essentials of Glycobiology*, A. Varki, et al., Editors. 2009: Cold Spring Harbor (NY).
155. Lobsanov, Y.D., et al., *X-ray crystal structure of the human dimeric S-Lac lectin, L-14-II, in complex with lactose at 2.9-Å resolution*. *J Biol Chem*, 1993. **268**(36): p. 27034-8.
156. Nio-Kobayashi, J. and T. Itabashi, *Galectins and Their Ligand Glycoconjugates in the Central Nervous System Under Physiological and Pathological Conditions*. *Front Neuroanat*, 2021. **15**: p. 767330.
157. Pasquini, L.A., et al., *Galectin-3 drives oligodendrocyte differentiation to control myelin integrity and function*. *Cell Death Differ*, 2011. **18**(11): p. 1746-56.
158. Varki, A. and T. Angata, *Siglecs--the major subfamily of I-type lectins*. *Glycobiology*, 2006. **16**(1): p. 1R-27R.
159. York, M.R., et al., *A macrophage marker, Siglec-1, is increased on circulating monocytes in patients with systemic sclerosis and induced by type I interferons and toll-like receptor agonists*. *Arthritis Rheum*, 2007. **56**(3): p. 1010-20.
160. Nitschke, L., et al., *CD22 is a negative regulator of B-cell receptor signalling*. *Curr Biol*, 1997. **7**(2): p. 133-43.
161. Sun, J., et al., *Myelin-associated glycoprotein (Siglec-4) expression is progressively and selectively decreased in the brains of mice lacking complex gangliosides*. *Glycobiology*, 2004. **14**(9): p. 851-7.
162. Hernandez-Caselles, T., et al., *A study of CD33 (SIGLEC-3) antigen expression and function on activated human T and NK cells: two isoforms of CD33 are generated by alternative splicing*. *J Leukoc Biol*, 2006. **79**(1): p. 46-58.
163. Stanczak, M.A., et al., *Self-associated molecular patterns mediate cancer immune evasion by engaging Siglecs on T cells*. *J Clin Invest*, 2018. **128**(11): p. 4912-4923.

164. Hudak, J.E., S.M. Canham, and C.R. Bertozzi, *Glycocalyx engineering reveals a Siglec-based mechanism for NK cell immunoevasion*. *Nat Chem Biol*, 2014. **10**(1): p. 69-75.
165. Varki, A., *Glycan-based interactions involving vertebrate sialic-acid-recognizing proteins*. *Nature*, 2007. **446**(7139): p. 1023-9.
166. Rabelink, T.J. and D. de Zeeuw, *The glycocalyx--linking albuminuria with renal and cardiovascular disease*. *Nat Rev Nephrol*, 2015. **11**(11): p. 667-76.
167. Cohen, M. and A. Varki, *The sialome--far more than the sum of its parts*. *OMICS*, 2010. **14**(4): p. 455-64.
168. Moons, S.J., et al., *Sialic acid glycoengineering using N-acetylmannosamine and sialic acid analogs*. *Glycobiology*, 2019. **29**(6): p. 433-445.
169. Freeze, H.H., G.W. Hart, and R.L. Schnaar, *Glycosylation Precursors*, in *Essentials of Glycobiology*, A. Varki, et al., Editors. 2015, Cold Spring Harbor Laboratory Press

Copyright 2015-2017 by The Consortium of Glycobiology Editors, La Jolla, California. All rights reserved.: Cold Spring Harbor (NY). p. 51-63.

170. Varki, A., R.L. Schnaar, and R. Schauer, *Sialic Acids and Other Nonulosonic Acids*, in *Essentials of Glycobiology*, A. Varki, et al., Editors. 2015, Cold Spring Harbor Laboratory Press

Copyright 2015-2017 by The Consortium of Glycobiology Editors, La Jolla, California. All rights reserved.: Cold Spring Harbor (NY). p. 179-95.

171. Kwon, D.N., et al., *CMP-Neu5Ac Hydroxylase Null Mice as a Model for Studying Metabolic Disorders Caused by the Evolutionary Loss of Neu5Gc in Humans*. *Biomed Res Int*, 2015. **2015**: p. 830315.
172. Varki, A., *Loss of N-glycolylneuraminic acid in humans: Mechanisms, consequences, and implications for hominid evolution*. *Am J Phys Anthropol*, 2001. **Suppl 33**(Suppl): p. 54-69.
173. Domon, B. and C.E. Costello, *A systematic nomenclature for carbohydrate fragmentations in FAB-MS/MS spectra of glycoconjugates*. *Glycoconjugate Journal*, 1988. **5**(4): p. 397-409.
174. Stephenson, R.O., Y. Yamanaka, and J. Rossant, *Disorganized epithelial polarity and excess trophectoderm cell fate in preimplantation embryos lacking E-cadherin*. *Development*, 2010. **137**(20): p. 3383-91.
175. Bergfeld, A.K., et al., *Metabolism of vertebrate amino sugars with N-glycolyl groups: elucidating the intracellular fate of the non-human sialic acid N-glycolylneuraminic acid*. *J Biol Chem*, 2012. **287**(34): p. 28865-81.
176. Akhavan, A., et al., *SEA domain proteolysis determines the functional composition of dystroglycan*. *Faseb j*, 2008. **22**(2): p. 612-21.
177. Knibbs, R.N., et al., *Characterization of the carbohydrate binding specificity of the leucoagglutinating lectin from *Maackia amurensis*. Comparison with other sialic acid-specific lectins*. *J Biol Chem*, 1991. **266**(1): p. 83-8.
178. Shibuya, N., et al., *The elderberry (*Sambucus nigra* L.) bark lectin recognizes the Neu5Ac(alpha 2-6)Gal/GalNAc sequence*. *J Biol Chem*, 1987. **262**(4): p. 1596-601.
179. Bashir, S., et al., *Presentation Mode of Glycans Affect Recognition of Human Serum anti-Neu5Gc IgG Antibodies*. *Bioconjug Chem*, 2019. **30**(1): p. 161-168.
180. Tangvoranuntakul, P., et al., *Human uptake and incorporation of an immunogenic nonhuman dietary sialic acid*. *Proc Natl Acad Sci U S A*, 2003. **100**(21): p. 12045-50.
181. Varki, A., *Sialic acids in human health and disease*. *Trends Mol Med*, 2008. **14**(8): p. 351-60.
182. Jennings, M.P., C.J. Day, and J.M. Atack, *How bacteria utilize sialic acid during interactions with the host: snip, snatch, dispatch, match and attach*. *Microbiology (Reading)*, 2022. **168**(3).
183. Allendorf, D.H., M. Puigdemívol, and G.C. Brown, *Activated microglia desialylate their surface, stimulating complement receptor 3-mediated phagocytosis of neurons*. *Glia*, 2020. **68**(5): p. 989-998.

184. Cioffi, D.L., et al., *Terminal sialic acids are an important determinant of pulmonary endothelial barrier integrity*. Am J Physiol Lung Cell Mol Physiol, 2012. **302**(10): p. L1067-77.
185. Charest, P.M. and J. Roth, *Localization of sialic acid in kidney glomeruli: regionalization in the podocyte plasma membrane and loss in experimental nephrosis*. Proc Natl Acad Sci U S A, 1985. **82**(24): p. 8508-12.
186. Werneburg, S., et al., *Polysialic acid modification of the synaptic cell adhesion molecule SynCAM 1 in human embryonic stem cell-derived oligodendrocyte precursor cells*. Stem Cell Res, 2015. **14**(3): p. 339-46.
187. Mori, A., et al., *Different properties of polysialic acids synthesized by the polysialyltransferases ST8SIA2 and ST8SIA4*. Glycobiology, 2017. **27**(9): p. 834-846.
188. Quartu, M., et al., *Polysialylated-neural cell adhesion molecule (PSA-NCAM) in the human trigeminal ganglion and brainstem at prenatal and adult ages*. BMC Neurosci, 2008. **9**: p. 108.
189. El Maarouf, A. and U. Rutishauser, *Removal of polysialic acid induces aberrant pathways, synaptic vesicle distribution, and terminal arborization of retinotectal axons*. J Comp Neurol, 2003. **460**(2): p. 203-11.
190. Mikkonen, M., et al., *Hippocampal plasticity in Alzheimer's disease: changes in highly polysialylated NCAM immunoreactivity in the hippocampal formation*. Eur J Neurosci, 1999. **11**(5): p. 1754-64.
191. Murray, H.C., et al., *Distribution of PSA-NCAM in normal, Alzheimer's and Parkinson's disease human brain*. Neuroscience, 2016. **330**: p. 359-75.
192. Curreli, S., et al., *Polysialylated neuropilin-2 is expressed on the surface of human dendritic cells and modulates dendritic cell-T lymphocyte interactions*. J Biol Chem, 2007. **282**(42): p. 30346-56.
193. Thiesler, H., J. Beimdiek, and H. Hildebrandt, *Polysialic acid and Siglec-E orchestrate negative feedback regulation of microglia activation*. Cell Mol Life Sci, 2021. **78**(4): p. 1637-1653.
194. Miyagi, T. and K. Yamaguchi, *Mammalian sialidases: physiological and pathological roles in cellular functions*. Glycobiology, 2012. **22**(7): p. 880-96.
195. Lukong, K.E., et al., *Intracellular distribution of lysosomal sialidase is controlled by the internalization signal in its cytoplasmic tail*. J Biol Chem, 2001. **276**(49): p. 46172-81.
196. Miyagi, T. and S. Tsuiki, *Rat-liver lysosomal sialidase. Solubilization, substrate specificity and comparison with the cytosolic sialidase*. Eur J Biochem, 1984. **141**(1): p. 75-81.
197. Zanchetti, G., et al., *Sialidase NEU3 is a peripheral membrane protein localized on the cell surface and in endosomal structures*. Biochem J, 2007. **408**(2): p. 211-9.
198. Seyrantepe, V., et al., *Neu4, a novel human lysosomal lumen sialidase, confers normal phenotype to sialidosis and galactosialidosis cells*. J Biol Chem, 2004. **279**(35): p. 37021-9.
199. Smutova, V., et al., *Structural basis for substrate specificity of mammalian neuraminidases*. PLoS One, 2014. **9**(9): p. e106320.
200. Sandbhor, M.S., et al., *Substrate recognition of the membrane-associated sialidase NEU3 requires a hydrophobic aglycone*. Biochemistry, 2011. **50**(32): p. 6753-62.
201. Pshezhetsky, A.V. and M. Ashmarina, *Keeping it trim: roles of neuraminidases in CNS function*. Glycoconj J, 2018. **35**(4): p. 375-386.
202. Li, Y., et al., *Identifying selective inhibitors against the human cytosolic sialidase NEU2 by substrate specificity studies*. Mol Biosyst, 2011. **7**(4): p. 1060-72.
203. Davies, L.R., et al., *Metabolism of vertebrate amino sugars with N-glycolyl groups: resistance of alpha2-8-linked N-glycolylneuraminic acid to enzymatic cleavage*. J Biol Chem, 2012. **287**(34): p. 28917-31.
204. Pshezhetsky, A.V., et al., *Cloning, expression and chromosomal mapping of human lysosomal sialidase and characterization of mutations in sialidosis*. Nat Genet, 1997. **15**(3): p. 316-20.
205. Carrillo, M.B., et al., *Cloning and characterization of a sialidase from the murine histocompatibility-2 complex: low levels of mRNA and a single amino acid mutation are*

- responsible for reduced sialidase activity in mice carrying the *Neu1a* allele. *Glycobiology*, 1997. **7**(7): p. 975-86.
206. Vinogradova, M.V., et al., *Molecular mechanism of lysosomal sialidase deficiency in galactosialidosis involves its rapid degradation*. *Biochem J*, 1998. **330** ( Pt 2)(Pt 2): p. 641-50.
207. Annunziata, I. and A. d'Azzo, *Galactosialidosis: historic aspects and overview of investigated and emerging treatment options*. *Expert Opin Orphan Drugs*, 2017. **5**(2): p. 131-141.
208. Takahashi, Y., et al., *Urinary oligosaccharide excretion and severity of galactosialidosis and sialidosis*. *Clin Chim Acta*, 1991. **203**(2-3): p. 199-210.
209. Oheda, Y., et al., *Elimination of abnormal sialylglycoproteins in fibroblasts with sialidosis and galactosialidosis by normal gene transfer and enzyme replacement*. *Glycobiology*, 2006. **16**(4): p. 271-80.
210. Ulrich-Bott, B., et al., *Lysosomal sialidase deficiency: increased ganglioside content in autopsy tissues of a sialidosis patient*. *Enzyme*, 1987. **38**(1-4): p. 262-6.
211. Dridi, L., et al., *Positive regulation of insulin signaling by neuraminidase 1*. *Diabetes*, 2013. **62**(7): p. 2338-46.
212. Fougerat, A., et al., *Neuraminidase 1 activates insulin receptor and reverses insulin resistance in obese mice*. *Mol Metab*, 2018. **12**: p. 76-88.
213. Seyrantepe, V., et al., *Regulation of phagocytosis in macrophages by neuraminidase 1*. *J Biol Chem*, 2010. **285**(1): p. 206-15.
214. Liang, F., et al., *Monocyte differentiation up-regulates the expression of the lysosomal sialidase, *Neu1*, and triggers its targeting to the plasma membrane via major histocompatibility complex class II-positive compartments*. *J Biol Chem*, 2006. **281**(37): p. 27526-38.
215. Rottier, R.J., E. Bonten, and A. d'Azzo, *A point mutation in the *neu-1* locus causes the neuraminidase defect in the SM/J mouse*. *Hum Mol Genet*, 1998. **7**(2): p. 313-21.
216. Nan, X., I. Carubelli, and N.M. Stamatou, *Sialidase expression in activated human T lymphocytes influences production of IFN-gamma*. *J Leukoc Biol*, 2007. **81**(1): p. 284-96.
217. Amith, S.R., et al., *Dependence of pathogen molecule-induced toll-like receptor activation and cell function on *Neu1* sialidase*. *Glycoconj J*, 2009. **26**(9): p. 1197-212.
218. Demina, E.P., et al., *Persistent reduction in sialylation of cerebral glycoproteins following postnatal inflammatory exposure*. *J Neuroinflammation*, 2018. **15**(1): p. 336.
219. Miyagi, T., et al., *Molecular cloning and expression of cDNA encoding rat skeletal muscle cytosolic sialidase*. *J Biol Chem*, 1993. **268**(35): p. 26435-40.
220. Miyagi, T. and S. Tsuiki, *Purification and characterization of cytosolic sialidase from rat liver*. *J Biol Chem*, 1985. **260**(11): p. 6710-6.
221. Monti, E., et al., *Cloning and characterization of *NEU2*, a human gene homologous to rodent soluble sialidases*. *Genomics*, 1999. **57**(1): p. 137-43.
222. Oh, M., et al., *Defect in cytosolic *Neu2* sialidase abrogates lipid metabolism and impairs muscle function in vivo*. *Sci Rep*, 2022. **12**(1): p. 3216.
223. Satyavarapu, E.M., S. Nath, and C. Mandal, *Desialylation of *Atg5* by sialidase (*Neu2*) enhances autophagosome formation to induce anchorage-dependent cell death in ovarian cancer cells*. *Cell Death Discov*, 2021. **7**(1): p. 26.
224. Wada, T., et al., *Cloning, expression, and chromosomal mapping of a human ganglioside sialidase*. *Biochem Biophys Res Commun*, 1999. **261**(1): p. 21-7.
225. Li, S.C., et al., *Degradation of *G(M1)* and *G(M2)* by mammalian sialidases*. *Biochem J*, 2001. **360**(Pt 1): p. 233-7.
226. Hasegawa, T., et al., *Molecular cloning of mouse ganglioside sialidase and its increased expression in *Neuro2a* cell differentiation*. *J Biol Chem*, 2000. **275**(11): p. 8007-15.
227. Tagami, S., et al., *Ganglioside *GM3* Participates in the Pathological Conditions of Insulin Resistance\**. *Journal of Biological Chemistry*, 2002. **277**(5): p. 3085-3092.

228. Kabayama, K., et al., *Dissociation of the insulin receptor and caveolin-1 complex by ganglioside GM3 in the state of insulin resistance*. Proceedings of the National Academy of Sciences, 2007. **104**(34): p. 13678-13683.
229. Yamaguchi, K., et al., *Evidence for mitochondrial localization of a novel human sialidase (NEU4)*. Biochem J, 2005. **390**(Pt 1): p. 85-93.
230. Shiozaki, K., et al., *Developmental change of sialidase neu4 expression in murine brain and its involvement in the regulation of neuronal cell differentiation*. J Biol Chem, 2009. **284**(32): p. 21157-64.
231. Seyrantepe, V., et al., *Mice deficient in Neu4 sialidase exhibit abnormal ganglioside catabolism and lysosomal storage*. Hum Mol Genet, 2008. **17**(11): p. 1556-68.
232. Seyrantepe, V., et al., *Mice doubly-deficient in lysosomal hexosaminidase A and neuraminidase 4 show epileptic crises and rapid neuronal loss*. PLoS Genet, 2010. **6**(9): p. e1001118.
233. Mohos, S.C. and L. Skoza, *Glomerular sialoprotein*. Science, 1969. **164**(3887): p. 1519-21.
234. Klein, P.J., et al., *Thomsen-Friedenreich antigen in haemolytic-uraemic syndrome*. Lancet, 1977. **2**(8046): p. 1024-5.
235. Lemyre, E., et al., *Clinical spectrum of infantile free sialic acid storage disease*. Am J Med Genet, 1999. **82**(5): p. 385-91.
236. Coats, M.T., et al., *Exposure of Thomsen-Friedenreich antigen in Streptococcus pneumoniae infection is dependent on pneumococcal neuraminidase A*. Microb Pathog, 2011. **50**(6): p. 343-9.
237. Pawluczyk, I.Z., et al., *Sialic acid supplementation ameliorates puromycin aminonucleoside nephrosis in rats*. Lab Invest, 2015. **95**(9): p. 1019-28.
238. Firth, J.D., *Effect of polycations on the function of the isolated perfused rat kidney*. Clin Sci (Lond), 1990. **79**(6): p. 591-8.
239. Niculovic, K.M., et al., *Podocyte-Specific Sialylation-Deficient Mice Serve as a Model for Human FSGS*. J Am Soc Nephrol, 2019. **30**(6): p. 1021-1035.
240. Alexander, W.S., et al., *Thrombocytopenia and kidney disease in mice with a mutation in the C1galt1 gene*. Proc Natl Acad Sci U S A, 2006. **103**(44): p. 16442-7.
241. MacArthur, D.G., et al., *Guidelines for investigating causality of sequence variants in human disease*. Nature, 2014. **508**(7497): p. 469-76.
242. Martin, L.T., et al., *Genetically altered mice with different sialyltransferase deficiencies show tissue-specific alterations in sialylation and sialic acid 9-O-acetylation*. J Biol Chem, 2002. **277**(36): p. 32930-8.
243. Galeano, B., et al., *Mutation in the key enzyme of sialic acid biosynthesis causes severe glomerular proteinuria and is rescued by N-acetylmannosamine*. J Clin Invest, 2007. **117**(6): p. 1585-94.
244. Kakani, S., et al., *The Gne M712T mouse as a model for human glomerulopathy*. Am J Pathol, 2012. **180**(4): p. 1431-40.
245. Yu, A., et al., *Changes in the Expression of Renal Brush Border Membrane N-Glycome in Model Rats with Chronic Kidney Diseases*. Biomolecules, 2021. **11**(11).
246. Kashtan, C.E., et al., *Proteinuria in a child with sialidosis: case report and histological studies*. Pediatr Nephrol, 1989. **3**(2): p. 166-74.
247. Toyooka, K., et al., *Nephrosialidosis: ultrastructural and lectin histochemical study*. Acta Neuropathol, 1993. **86**(2): p. 198-205.
248. Novak, J., et al., *Aberrant Glycosylation of the IgA1 Molecule in IgA Nephropathy*. Semin Nephrol, 2018. **38**(5): p. 461-476.
249. Martin, C.E. and N. Jones, *Nephrin Signaling in the Podocyte: An Updated View of Signal Regulation at the Slit Diaphragm and Beyond*. Front Endocrinol (Lausanne), 2018. **9**: p. 302.

250. Thomas, H.Y. and A.N. Ford Versypt, *Pathophysiology of mesangial expansion in diabetic nephropathy: mesangial structure, glomerular biomechanics, and biochemical signaling and regulation*. J Biol Eng, 2022. **16**(1): p. 19.
251. Weil, E.J., et al., *Podocyte detachment and reduced glomerular capillary endothelial fenestration promote kidney disease in type 2 diabetic nephropathy*. Kidney Int, 2012. **82**(9): p. 1010-7.
252. Ohmori, T., et al., *Impaired NEPHRIN localization in kidney organoids derived from nephrotic patient iPS cells*. Sci Rep, 2021. **11**(1): p. 3982.
253. Refaeli, I., et al., *Distinct Functional Requirements for Podocalyxin in Immature and Mature Podocytes Reveal Mechanisms of Human Kidney Disease*. Sci Rep, 2020. **10**(1): p. 9419.
254. Li, X., et al., *Nephrin Preserves Podocyte Viability and Glomerular Structure and Function in Adult Kidneys*. J Am Soc Nephrol, 2015. **26**(10): p. 2361-77.
255. Olivetti, G., et al., *Morphometry of the renal corpuscle during normal postnatal growth and compensatory hypertrophy. A light microscope study*. J Cell Biol, 1977. **75**(2 Pt 1): p. 573-85.
256. Ebefors, K., et al., *Mesangial cells from patients with IgA nephropathy have increased susceptibility to galactose-deficient IgA1*. BMC Nephrol, 2016. **17**: p. 40.
257. Borza, D.B., *Glomerular basement membrane heparan sulfate in health and disease: A regulator of local complement activation*. Matrix Biol, 2017. **57-58**: p. 299-310.
258. Zhuo, J.L. and X.C. Li, *Proximal nephron*. Compr Physiol, 2013. **3**(3): p. 1079-123.
259. Curthoys, N.P. and O.W. Moe, *Proximal tubule function and response to acidosis*. Clin J Am Soc Nephrol, 2014. **9**(9): p. 1627-38.
260. Kriz, W. and B. Kaissling, *CHAPTER 20 - Structural Organization of the Mammalian Kidney, in Seldin and Giebisch's The Kidney (Fourth Edition)*, R.J. Alpern and S.C. Hebert, Editors. 2008, Academic Press: San Diego. p. 479-563.
261. Christensen, E.I. and H. Birn, *Megalyn and cubilin: multifunctional endocytic receptors*. Nat Rev Mol Cell Biol, 2002. **3**(4): p. 256-66.
262. Kantarci, S., et al., *Mutations in LRP2, which encodes the multiligand receptor megalin, cause Donnai-Barrow and facio-oculo-acoustico-renal syndromes*. Nat Genet, 2007. **39**(8): p. 957-9.
263. Norden, A.G., et al., *Lysosomal enzymuria is a feature of hereditary Fanconi syndrome and is related to elevated CI-mannose-6-P-receptor excretion*. Nephrol Dial Transplant, 2008. **23**(9): p. 2795-803.
264. Willnow, T.E., et al., *Defective forebrain development in mice lacking gp330/megalyn*. Proc Natl Acad Sci U S A, 1996. **93**(16): p. 8460-4.
265. Magen, D., et al., *A loss-of-function mutation in NaPi-IIa and renal Fanconi's syndrome*. N Engl J Med, 2010. **362**(12): p. 1102-9.
266. Haque, S.K., G. Ariceta, and D. Batlle, *Proximal renal tubular acidosis: a not so rare disorder of multiple etiologies*. Nephrol Dial Transplant, 2012. **27**(12): p. 4273-87.
267. Castaneda-Bueno, M., D.H. Ellison, and G. Gamba, *Molecular mechanisms for the modulation of blood pressure and potassium homeostasis by the distal convoluted tubule*. EMBO Mol Med, 2022. **14**(2): p. e14273.
268. McCormick, J.A. and D.H. Ellison, *Distal convoluted tubule*. Compr Physiol, 2015. **5**(1): p. 45-98.
269. Knoers, N.V. and E.N. Levtchenko, *Gitelman syndrome*. Orphanet J Rare Dis, 2008. **3**: p. 22.
270. Pshezhetsky, A.V. and A. Hinek, *Where catabolism meets signalling: neuraminidase 1 as a modulator of cell receptors*. Glycoconj J, 2011. **28**(7): p. 441-52.
271. Peterson, C.W., et al., *Autologous, Gene-Modified Hematopoietic Stem and Progenitor Cells Repopulate the Central Nervous System with Distinct Clonal Variants*. Stem Cell Reports, 2019. **13**(1): p. 91-104.
272. Syres, K., et al., *Successful treatment of the murine model of cystinosis using bone marrow cell transplantation*. Blood, 2009. **114**(12): p. 2542-52.

273. Wuttke, M., et al., *A catalog of genetic loci associated with kidney function from analyses of a million individuals*. Nat Genet, 2019. **51**(6): p. 957-972.
274. Stanzick, K.J., et al., *Discovery and prioritization of variants and genes for kidney function in >1.2 million individuals*. Nat Commun, 2021. **12**(1): p. 4350.
275. Nakanishi, H., *Neuronal and microglial cathepsins in aging and age-related diseases*. Ageing Res Rev, 2003. **2**(4): p. 367-81.
276. Guo, T., et al., *Selective Inhibitors of Human Neuraminidase 3*. J Med Chem, 2018. **61**(5): p. 1990-2008.
277. Kundra, R. and S. Kornfeld, *Asparagine-linked oligosaccharides protect Lamp-1 and Lamp-2 from intracellular proteolysis*. J Biol Chem, 1999. **274**(43): p. 31039-46.
278. Huang da, W., B.T. Sherman, and R.A. Lempicki, *Bioinformatics enrichment tools: paths toward the comprehensive functional analysis of large gene lists*. Nucleic Acids Res, 2009. **37**(1): p. 1-13.
279. Tan, A., et al., *Past, present, and future perspectives of transcription factor EB (TFEB): mechanisms of regulation and association with disease*. Cell Death Differ, 2022. **29**(8): p. 1433-1449.
280. Settembre, C., et al., *A block of autophagy in lysosomal storage disorders*. Hum Mol Genet, 2008. **17**(1): p. 119-29.
281. Xia, B., et al., *Oligosaccharide analysis in urine by maldi-tof mass spectrometry for the diagnosis of lysosomal storage diseases*. Clin Chem, 2013. **59**(9): p. 1357-68.
282. Messina, A., et al., *HILIC-UPLC-MS for high throughput and isomeric N-glycan separation and characterization in Congenital Disorders Glycosylation and human diseases*. Glycoconj J, 2021. **38**(2): p. 201-211.
283. Peng, W., et al., *MS-based glycomics: An analytical tool to assess nervous system diseases*. Front Neurosci, 2022. **16**: p. 1000179.
284. Varki, A., et al., *Essentials of Glycobiology, Fourth Edition*, in *Essentials of Glycobiology*, A. Varki, et al., Editors. 2022: Cold Spring Harbor (NY).
285. Kozarsky, K., D. Kingsley, and M. Krieger, *Use of a mutant cell line to study the kinetics and function of O-linked glycosylation of low density lipoprotein receptors*. Proc Natl Acad Sci U S A, 1988. **85**(12): p. 4335-9.
286. Tian, E., et al., *Galnt11 regulates kidney function by glycosylating the endocytosis receptor megalin to modulate ligand binding*. Proc Natl Acad Sci U S A, 2019. **116**(50): p. 25196-25202.
287. Da Silva, A., et al., *N-acetylneuraminate pyruvate lyase controls sialylation of muscle glycoproteins essential for muscle regeneration and function*. Sci Adv, 2023. **9**(26): p. eade6308.
288. Mazon, M., et al., *Deletion of the Fanconi Anemia C Gene in Mice Leads to Skeletal Anomalies and Defective Bone Mineralization and Microarchitecture*. J Bone Miner Res, 2018. **33**(11): p. 2007-2020.
289. Para, C., et al., *Early defects in mucopolysaccharidosis type IIIC disrupt excitatory synaptic transmission*. JCI Insight, 2021. **6**(15).
290. Pan, X., et al., *Glucosamine amends CNS pathology in mucopolysaccharidosis IIIC mouse expressing misfolded HGSNAT*. J Exp Med, 2022. **219**(8).
291. Morales, C.R., et al., *Low density lipoprotein receptor-related protein-2 expression in efferent duct and epididymal epithelia: evidence in rats for its in vivo role in endocytosis of apolipoprotein J/clusterin*. Biol Reprod, 1996. **55**(3): p. 676-83.
292. Kerjaschki, D. and M.G. Farquhar, *The pathogenic antigen of Heymann nephritis is a membrane glycoprotein of the renal proximal tubule brush border*. Proceedings of the National Academy of Sciences of the United States of America, 1982. **79**(18): p. 5557-5561.

293. Sahali, D., et al., *Comparative immunochemistry and ontogeny of two closely related coated pit proteins. The 280-kd target of teratogenic antibodies and the 330-kd target of nephritogenic antibodies.* Am J Pathol, 1993. **142**(5): p. 1654-67.
294. Storm, T., et al., *Renal phenotypic investigations of megalin-deficient patients: novel insights into tubular proteinuria and albumin filtration\**. Nephrology Dialysis Transplantation, 2012. **28**(3): p. 585-591.
295. Muller, D., et al., *Holoprosencephaly and low molecular weight proteinuria: the human homologue of murine megalin deficiency.* Am J Kidney Dis, 2001. **37**(3): p. 624-8.
296. Vallon, V., et al., *Knockout of Na-glucose transporter SGLT2 attenuates hyperglycemia and glomerular hyperfiltration but not kidney growth or injury in diabetes mellitus.* Am J Physiol Renal Physiol, 2013. **304**(2): p. F156-67.
297. Yang, W., et al., *Mapping the O-glycoproteome using site-specific extraction of O-linked glycopeptides (EXO).* Mol Syst Biol, 2018. **14**(11): p. e8486.
298. Lee, M., et al., *Tissue-specific Role of CX3CR1 Expressing Immune Cells and Their Relationships with Human Disease.* Immune Netw, 2018. **18**(1): p. e5.
299. Bartolomeo, R., et al., *mTORC1 hyperactivation arrests bone growth in lysosomal storage disorders by suppressing autophagy.* J Clin Invest, 2017. **127**(10): p. 3717-3729.
300. Shemesh, A., et al., *Suppression of mTORC1 activation in acid-alpha-glucosidase-deficient cells and mice is ameliorated by leucine supplementation.* Am J Physiol Regul Integr Comp Physiol, 2014. **307**(10): p. R1251-9.
301. Pal, R., Y. Xiong, and M. Sardiello, *Abnormal glycogen storage in tuberous sclerosis complex caused by impairment of mTORC1-dependent and -independent signaling pathways.* Proc Natl Acad Sci U S A, 2019. **116**(8): p. 2977-2986.
302. Lim, C.Y., et al., *ER-lysosome contacts enable cholesterol sensing by mTORC1 and drive aberrant growth signalling in Niemann-Pick type C.* Nat Cell Biol, 2019. **21**(10): p. 1206-1218.
303. Du, X., et al., *Akt activation increases cellular cholesterol by promoting the proteasomal degradation of Niemann-Pick C1.* Biochem J, 2015. **471**(2): p. 243-53.
304. Yogalingam, G., et al., *Neuraminidase 1 is a negative regulator of lysosomal exocytosis.* Dev Cell, 2008. **15**(1): p. 74-86.
305. Reiding, K.R., et al., *Murine Plasma N-Glycosylation Traits Associated with Sex and Strain.* J Proteome Res, 2016. **15**(10): p. 3489-3499.
306. Han, J., et al., *Quantitation of sex-specific serum N-glycome changes in expression level during mouse aging based on Bionic Glycome method.* Exp Gerontol, 2020. **141**: p. 111098.
307. Van Praet, O., W.S. Argraves, and C.R. Morales, *Co-expression and interaction of cubilin and megalin in the adult male rat reproductive system.* Mol Reprod Dev, 2003. **64**(2): p. 129-35.
308. Delacour, D., et al., *Requirement for galectin-3 in apical protein sorting.* Curr Biol, 2006. **16**(4): p. 408-14.
309. Zhou, X.Y., et al., *Mouse model for the lysosomal disorder galactosialidosis and correction of the phenotype with overexpressing erythroid precursor cells.* Genes Dev, 1995. **9**(21): p. 2623-34.
310. Seyrantepe, V., et al., *Enzymatic activity of lysosomal carboxypeptidase (cathepsin) A is required for proper elastic fiber formation and inactivation of endothelin-1.* Circulation, 2008. **117**(15): p. 1973-81.
311. Cowie, M.R. and M. Fisher, *SGLT2 inhibitors: mechanisms of cardiovascular benefit beyond glycaemic control.* Nat Rev Cardiol, 2020. **17**(12): p. 761-772.
312. Ngo, A.N., et al., *Optimal Concentration of 2,2,2-Trichloroacetic Acid for Protein Precipitation Based on Response Surface Methodology.* J Anal Bioanal Tech, 2014. **5**(4).
313. Biolabs, N.E., *PNGase F Protocol (Non-Denaturing Reaction Conditions) V.2.* 2022.
314. Aoki, K. and M. Tiemeyer, *The glycomics of glycan glucuronylation in Drosophila melanogaster.* Methods Enzymol, 2010. **480**: p. 297-321.

315. Palmigiano, A., et al., *CSF N-Glycomics Using MALDI MS Techniques in Alzheimer's Disease*. *Methods Mol Biol*, 2018. **1750**: p. 75-91.
316. Ciucanu, I. and F. Kerek, *A simple and rapid method for the permethylation of carbohydrates*. *Carbohydrate Research*, 1984. **131**(2): p. 209-217.
317. Tian, D., et al., *The effect of A1 adenosine receptor in diabetic megalin loss with caspase-1/IL18 signaling*. *Diabetes Metab Syndr Obes*, 2019. **12**: p. 1583-1596.
318. Charlton, J.R., et al., *Beyond the tubule: pathological variants of LRP2, encoding the megalin receptor, result in glomerular loss and early progressive chronic kidney disease*. *Am J Physiol Renal Physiol*, 2020. **319**(6): p. F988-F999.
319. King, B., et al., *Low-dose, continuous enzyme replacement therapy ameliorates brain pathology in the neurodegenerative lysosomal disorder mucopolysaccharidosis type IIIA*. *J Neurochem*, 2016. **137**(3): p. 409-22.
320. Wijburg, F.A., et al., *Long-term safety and clinical outcomes of intrathecal heparan-N-sulfatase in patients with Sanfilippo syndrome type A*. *Mol Genet Metab*, 2021. **134**(4): p. 317-322.
321. Wijburg, F.A., et al., *A multicenter open-label extension study of intrathecal heparan-N-sulfatase in patients with Sanfilippo syndrome type A*. *Mol Genet Metab*, 2021. **134**(1-2): p. 175-181.
322. Krivit, W., *Allogenic stem cell transplantation for the treatment of lysosomal and peroxisomal metabolic diseases*. *Springer Semin Immunopathol*, 2004. **26**(1-2): p. 119-32.
323. Guo, M., et al., *Microglial Exosomes in Neurodegenerative Disease*. *Front Mol Neurosci*, 2021. **14**: p. 630808.
324. Sumida, M., et al., *Rapid Trimming of Cell Surface Polysialic Acid (PolySia) by Exovesicular Sialidase Triggers Release of Preexisting Surface Neurotrophin*. *J Biol Chem*, 2015. **290**(21): p. 13202-14.
325. Allendorf, D.H. and G.C. Brown, *Neu1 Is Released From Activated Microglia, Stimulating Microglial Phagocytosis and Sensitizing Neurons to Glutamate*. *Front Cell Neurosci*, 2022. **16**: p. 917884.
326. Kim, S., et al., *Dynamics of HSPC repopulation in nonhuman primates revealed by a decade-long clonal-tracking study*. *Cell Stem Cell*, 2014. **14**(4): p. 473-85.